Institute of Parallel and Distributed Systems

University of Stuttgart
Universitätsstraße 38
D–70569 Stuttgart

Masterarbeit

Investigation of Multistability-affected Period-incrementing and Period-adding Structures in a Model of a Power Converter with Symmetry

Fabian Weik

Course of Study:	Informatik
Examiner:	Prof. Dr. Holger Schwarz
Supervisor:	Prof. Dr. Viktor Avrutin
Commenced:	March 1, 2023
Completed:	September 1, 2023

Abstract

Although the established theory of non-linear dynamical systems is effective at describing physical systems and phenomena, the theory has been developed with a focus on smooth systems, limiting its applicability in certain areas. This limitation becomes apparent when modeling piecewise-smooth systems such as electrical systems that contain at least one switching element or mechanical systems with collisions. This thesis deals with a model of a DC/AC power converter that is piecewise-smooth, discontinuous, and has a certain symmetry. The definition of this model is exceptionally complex, and the model exhibits an unusual period-incrementing structure that is affected by multistability. This thesis identifies the characteristics of the model that lead to this unusual bifurcation structure by constructing an archetypal model that exhibits the same bifurcation behavior. It follows a description of the dynamics of the archetypal model and an explanation of the bifurcation structure using the description of the dynamics. Additionally, this thesis demonstrates that the proposed archetypal model can exhibit behavior leading to bifurcation structures that are related to period-adding structures. The resulting bifurcation structures behave unexpectedly, and this behavior is explained by leveraging the symmetry present in both the archetypal and the original model. Using the symmetry present, the mathematical rules governing the resulting bifurcation structures are derived from the rules governing classical period-adding structures.

Contents

List of Figures

Algorithms and program code

Acronyms

PA period-adding. 19

PAL period-adding-like. 75

PI period-incrementing. 21

PWS piecewise smooth. 15

1 Introduction

Non-linear dynamical systems are ubiquitous in nature. And their study has gained popularity in recent decades. The study of non-linear systems is very effective at explaining a wide range of physical phenomena such as fluid dynamics and weather patterns [BBCK08]. Scientists in this field focus mostly on qualitative changes in the behavior of the systems under parameter variations, so-called bifurcations [Sim10].

However, most of the developed theory of non-linear dynamical systems relies heavily on the smoothness of the model functions. Several real-world applications of dynamical systems are not only non-linear but also piecewise smooth (PWS) or even PWS and discontinuous as well. Although the study of non-linear dynamical systems is still quite young, the study of PWS dynamical systems is even younger. The area has seen a recent surge in interest due to the fact that all electrical systems with switching behavior are inherently PWS, many even PWS discontinuous [Sim10]. Non-smoothness introduces phenomena that do not occur in smooth systems. The class of border collision bifurcations is one of the new bifurcation classes. It is the only class of bifurcations encountered in this thesis.

This thesis focuses on the simplification of an existing model of a DC/AC power converter. The existing model is PWS and discontinuous due to the switching behavior of the power converter. It is highly complex due to a high number of implicit equations and exhibits behavior that leads to an unusual bifurcation structure. The goal of this thesis is to explain the unusual bifurcation structure in the existing model using the simplified model.

Since the topic of this thesis focuses on non-linear dynamics more than computer science, the next chapter will introduce the fundamental concepts and ideas required for the rest of the thesis.

2 State of the Art

This chapter is a brief introduction to the theory of non-linear dynamical systems, as well as PWS and even PWS discontinuous dynamical systems. It also introduces the model that is considered within the scope of this thesis.

2.1 Non-linear Dynamical Systems

Dynamical systems can either be time-continuous or time-discrete. In this thesis, only time-discrete dynamical systems, also called maps, are considered. The time evolution of the state of such a system results from an iterative application of the model function governing the dynamics of the system, i.e. $x_{n+1} = f(x_n)$. Depending on the properties of the model function f, one can distinguish between smooth, PWS continuous, and PWS discontinuous dynamical systems.

This thesis primarily investigates invariant sets. Next, two types of invariant sets are defined, fixed points and cycles.

Definition 2.1 (Fixed Point)
Let $x_{n+1} = f(x_n)$ be a time-discrete non-linear dynamical system where the model function is $f : X \to X$. Then $x \in X$ is a fixed point, if $f(x) = x$.

Definition 2.2 (Iterate Function)
Let $f : X \to X$ be the model function of a time-discrete non-linear dynamical system. Then f^k is the k-th iterate of this function, defined recursively by $f^k(x) = f\left(f^{k-1}(x)\right)$ and $f^1(x) = f(x)$. This means, the function is applied k times.

Definition 2.3 (Cycle)
Let $f : X \to X$ be the model function of a time-discrete non-linear dynamical system. Then the sequence of k points $O_k = \{x_i \mid 0 \leq i < k\}$ is a k-cycle if it satisfies the following conditions.

$$\forall 1 \leq i < k : \quad f(x_i) = x_{i+1} \quad \wedge \quad f(x_{k-1}) = x_0 \tag{2.1}$$

If $x_0 \neq x_i$ for $1 \leq i < k$, then k is the prime period of O_k.

Each point x_i of a k-cycle O_k satisfies $f^k(x_i) = x_i$.

Definition 2.4 (Stability)
Let $f : X \to X$ be the model function of a time-discrete non-linear dynamical system where X is one-dimensional. A fixed point x^* is stable, if $|f'(x^*)| < 1$. Similarly, a k-cycle $O_k = \{x_i \mid 0 \leq i < k\}$ is stable, if the following condition is true for all $0 \leq i < k$.

$$\left| \frac{d}{dx} f^k(x) \bigg|_{x=x_i} \right| < 1 \tag{2.2}$$

Note that the derivative of f^k evaluated at any point x_i of the k-cycle O_k takes the same value. That value being the product of the derivative of the function f evaluated at all points x_i.

$$\frac{d}{dx} f^k(x) \Big|_{x=x_i} = \prod_{j=0}^{k-1} \left(\frac{d}{dx} f(x) \Big|_{x=x_j} \right) \tag{2.3}$$

This thesis only covers stable cycles. Stable cycles have the property that different points of the state space that are not necessarily part of the cycle will eventually end up in the cycle. The set of those points is called the basin of attraction of the cycle.

Definition 2.5 (Basin of Attraction of a Cycle)
Let $f : X \to X$ be the model function of a non-linear dynamical system. Let O_k be a stable cycle in that system. Then the basin of attraction of this cycle is

$$\{x \in X \mid \exists n > 0 : \ f^n(x) \in O_k\} \tag{2.4}$$

Definition 2.6 (Bifurcation)
A bifurcation is a qualitative change of the state space topology of a model under an infinitesimal small parameter variation.

Meaning for example that solutions to the model function or its iterate (fixed points and cycles) disappear or appear under a very small change to parameters. The only bifurcations that are important in this thesis are introduced in the next section. That section covers PWS dynamical systems.

2.2 PWS Dynamical Systems

Initially, the theory of non-linear dynamical systems was developed for smooth dynamical systems only. Hence, several results can't be applied to PWS dynamical systems. But smooth systems are not fit to model several engineering applications, since such systems often undergo sudden changes. For example, a model of an electrical circuit can't be smooth as soon as the circuit has a single switching element, such as a transistor [ZM03]. The model investigated in this thesis describes such a switching electrical circuit that converts power from AC to DC.

In PWS dynamical systems, bifurcations are possible that do not occur in smooth dynamical systems. Even more so in PWS discontinuous dynamical systems, which this thesis focuses on. While the theory for continuous-time 1D PWS discontinuous dynamical systems is quite complete, the theory for time-discrete 1D PWS discontinuous dynamical systems in is further behind [Sim16]. Also while in smooth dynamical systems and PWS continuous dynamical systems bifurcations can be generalized and described using normal forms, this is not possible for PWS discontinuous dynamical systems. The reason for this is that many bifurcations, especially border collision bifurcations which are introduced shortly, are necessarily global in PWS discontinuous maps and normal forms only work for local bifurcations [AGST19]. The advantage of normal forms is that these models neglect all non-essential parameter effects for the description of the bifurcation phenomenon at hand. Furthermore, one can prove that the neglected parameter effects are indeed non-essential for the bifurcation phenomenon. For the model considered in this thesis, such a proof can not

be provided. Nevertheless, this thesis follows a similar approach as it identifies essential and neglects non-essential parameters and parameter effects for the bifurcation structure. But rather than on rigorous proofs, it relies on numerical evidence. The resulting model is called an archetypal model.

The bifurcations covered in this thesis all belong to the previously mentioned class of border collision bifurcations.

Definition 2.7 (Border Collision)
A border collision is a point in the parameter space, where an invariant set (e.g a fixed point or a cycle) collides with a border of the model function in the state space.

Note that the points of the state space, where the model function is not smooth are called borders.

Definition 2.8 (Border Collision Bifurcation)
A border collision bifurcation is a border collision that also causes a qualitative change in the state space topology.

Since model functions of PWS dynamical systems consist of multiple branches, cycles in such systems can be described using symbolic sequences. This allows the differentiation between different cycles even if they have the same period.

Definition 2.9 (Symbolic Sequence)
Let $f : X \to X$ be the model function of a PWS dynamical system that is divided into n partitions $I_j \subset X$ where $0 \leq j < n$. Let the set of symbols associated with each partition I_j be $\{S_j\}_{0 \leq j < n}$. The symbolic sequence $S_f(O_k)$ of a cycle $O_k = \{x_i \mid 0 \leq i < k\}$ is defined in the following way.

$$S_f(O_k) = (o(x_0), o(x_1), \ldots, o(x_{k-1})) \tag{2.5}$$

Where the function o provides a symbol for every point of the cycle. It is defined as $o(x) = S_j$ if $x \in S_j$ for all $0 \leq j < n$ [GAK14].

For example, a k-cycle in a PWS dynamical system divided into two partitions $I_0 = \{x \mid x < 0\}$ and $I_1 = \{x \mid x > 0\}$ with symbols $S_0 = \mathcal{L}$ and $S_1 = \mathcal{R}$ that has one point $x_0 \in I_0$ and $k - 1$ points $x_j \in I_1,\ 1 \leq j < k$ is associated with the symbolic sequence $\mathcal{L}\mathcal{R}^{k-1}$.

Now a class of bifurcation structures that this thesis covers towards the end in Chapter 7 is introduced. Bifurcation structures belonging to this class called period-adding (PA) structures can be found in many PWS dynamical systems.

Period-adding structures are named like this because in such structures, between a parameter region with a cycle of period a and another parameter region with a cycle of period b, there is a parameter region with a cycle of period $a + b$.

An even more compact way to differentiate between multiple cycles that have the same period are rotation number. Here, they are used to describe the structure of PA structures.

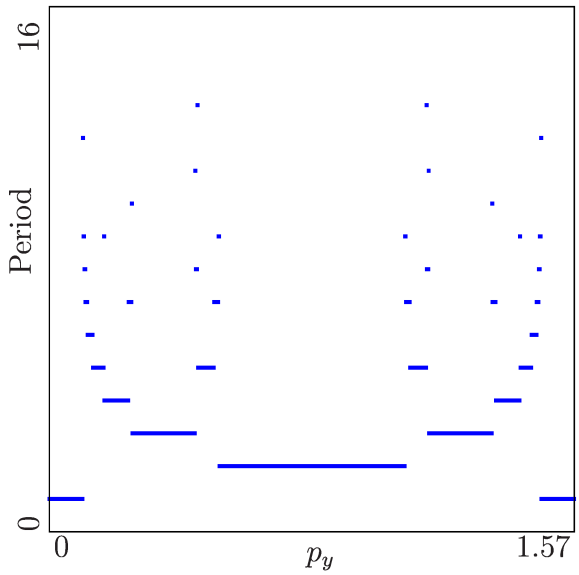

Figure 2.1: 1D scan of periods associated with parameter regions of a PA structure between two parameter regions that are associated with the fixed points $\mathcal{L}$ and $\mathcal{R}$.

Definition 2.10 (Rotation Numbers — Keener)
Let σ be a cycle of a PWS dynamical system $x_{n+1} = f(x_n)$ with two branches, $\mathcal{L}$ and $\mathcal{R}$. Then the rotation number $\rho(\sigma)$ of this cycle is defined as the ratio of number of letters $\mathcal{L}$ in the symbolic sequence of the cycle divided by the period of the cycle σ [Kee80].

$$\rho(\sigma) = \frac{|\sigma|_{\mathcal{L}}}{|\sigma|} \tag{2.6}$$

The rotation numbers of cycles associated with the parameter regions in a PA structure are organized in a Farey-tree. A Farey-tree has two "root nodes" and the child node of two nodes is the Farey-sum of the parent nodes [GAK14].

Definition 2.11 (Farey-sum)
The Farey-sum $a \oplus b$ of two fractions $a = \frac{a_1}{a_2}$ and $b = \frac{b_1}{b_2}$ is defined in the following way.

$$a \oplus b = \frac{a_1}{a_2} \oplus \frac{b_1}{b_2} = \frac{a_1 + b_1}{a_2 + b_2} \tag{2.7}$$

Figure 2.2a shows such a Farey-tree showing the rotation numbers of a PA structure between two parameter regions associated with the fixed points $\mathcal{L}$ and $\mathcal{R}$. If we replace the content of the nodes with the symbolic sequences of the cycles associated with the parameter regions in the PA structure, we get the tree shown in Figure 2.2b. Instead of Farey-addition, here the child node of two parent nodes is the concatenation of the symbolic sequences in the parent nodes. Together with Theorem 2.1, this explains why the tree in Figure 2.2a is a Farey-tree [GAK14].

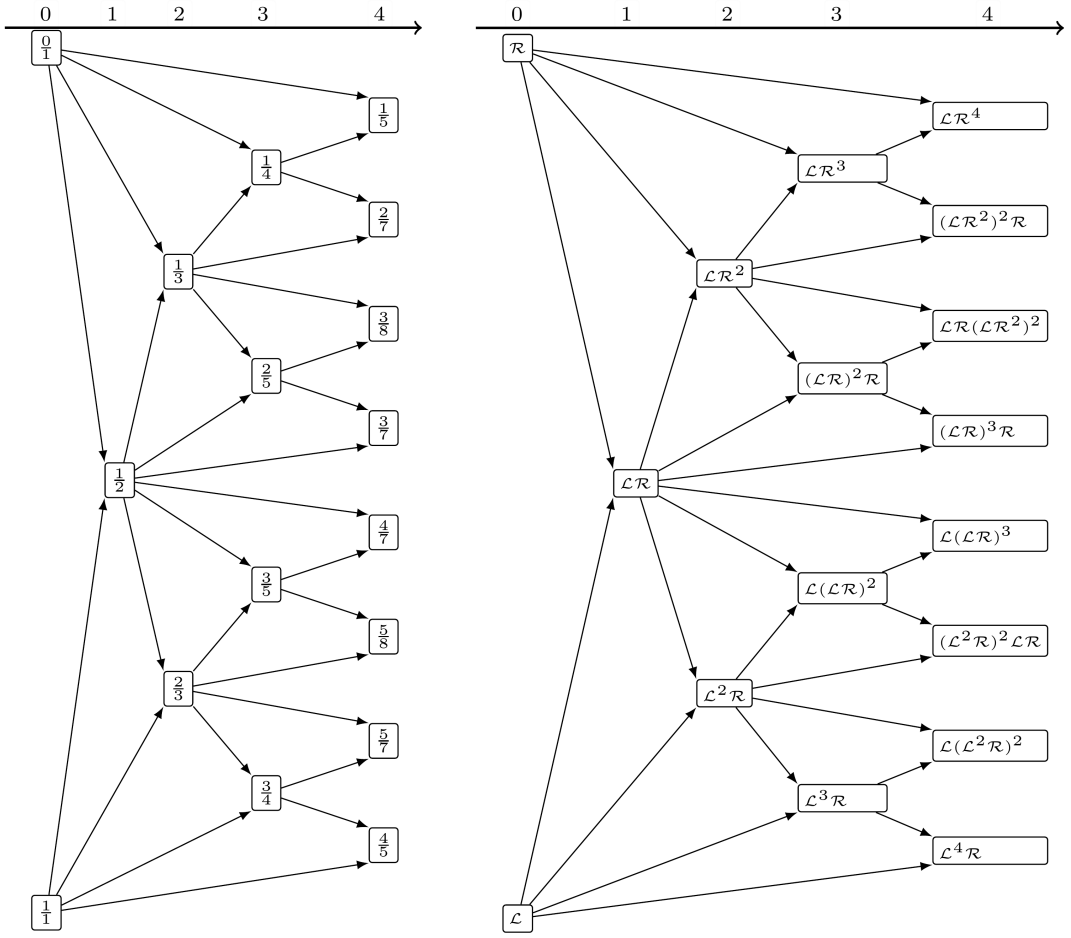

(a) Rotation Numbers **(b)** Symbolic Sequences

Figure 2.2: Farey-trees of a PA structure between two parameter regions that are associated with the fixed points $\mathcal{L}$ and $\mathcal{R}$ (a) Shows the rotation numbers while (b) shows the symbolic sequences of the cycles that are associated with the parameter regions in this structure.

Theorem 2.1 (Rotation Numbers of Concatenated Cycles)
The rotation number of the concatenation of two cycles $\rho(\sigma\varrho)$ is the Farey-sum of the rotation numbers of both cycles, $\rho(\sigma) \oplus \rho(\varrho)$.

Proof

$$\rho(\sigma\varrho) = \frac{|\sigma\varrho|_{\mathcal{L}}}{|\sigma\varrho|} = \frac{|\sigma|_{\mathcal{L}} + |\varrho|_{\mathcal{L}}}{|\sigma| + |\varrho|} = \frac{|\sigma|_{\mathcal{L}}}{|\sigma|} \oplus \frac{|\varrho|_{\mathcal{L}}}{|\varrho|} = \rho(\sigma) \oplus \rho(\varrho)$$

■

Another class of bifurcation structures that also occurs in PWS discontinuous maps is the class of period-incrementing (PI) structures. As the name suggests, here the periods increment from one parameter region to the next [GAK17]. Here, no example scan of the periods associated with the parameter regions in such a PI structure is provided, as we will see an example shortly in the investigated system.

2.3 Investigated Dynamical System

As mentioned before, this thesis considers a complex dynamical system. It is referred to as the original model from now on. This section gives a definition of the model and some properties. Furthermore, it showcases the unusual bifurcation structure this model exhibits. This bifurcation structure is the core motivation for this thesis.

2.3.1 Model Origin

The original model describes the behavior of a DC/AC power converter with hysteresis control. In continuous-time, the converter is described by a differential equation. The differential equation indicates the rate of change of the output of the power converter based on the current output and the current time. Here, the current time is given as a phase since the converter tries to output alternating current that follows a sine wave. The converter switches to achieve its goal. This switching causes discontinuities in the model function.

From this time-continuous model, one can derive a time-discrete model. This model maps a phase at which the converter switches to the phase at which the converter will switch the next time. It is also PWS and discontinuous like the time-continuous model from which it is derived. The next subsection gives an in-depth definition of this map.

2.3.2 Model Definition

The model was defined by Zhusubaliyev and was preliminarily investigated by Akyüz in his thesis "*Investigation of Bifurcation Phenomena in a Model of Power Converter with Hysteresis*" [Aky22]. As mentioned before, we skip the time-continuous model and only focus on the time-discrete one. It is defined as the map $\theta_{n-1} = F(\theta_n) \mod 2\pi$ where F is defined by the following equations.

$$F(\theta) = \begin{cases} F_1(\theta) & \text{if } q \cdot \cos(\theta) > 0 \\ F_2(\theta) & \text{if } q \cdot \cos(\theta) < 0 \end{cases} \tag{2.8}$$

where F_1 and F_2 are given by

$$F_1(\theta) = \begin{cases} \theta + z_{L_+} + z_1 & \text{if } z_{L_+} < z_{L_0} \\ \theta + z_{L_0} + z_2 & \text{if } z_{L_+} > z_{L_0} \end{cases} \tag{2.9a}$$

$$F_2(\theta) = \begin{cases} \theta + z_{R_+} + z_3 & \text{if } z_{R_+} < z_{R_0} \\ \theta + z_{R_0} + z_4 & \text{if } z_{R_+} > z_{R_0} \end{cases} \tag{2.9b}$$

The values for the parameters $z_{L_+}, z_{L_0}, z_{R_+}, z_{R_0}, z_1, z_2, z_3$, and z_4 are the smallest positive solutions to the implicit equations Equations (2.10a) to (2.10h).

$$(q \cdot \cos(\theta) + \mu \cdot \chi) \cdot e^{\lambda \cdot z_{L_+}} = q \cdot \cos(\theta + z_{L_+}) + \chi \tag{2.10a}$$

$$(q \cdot \cos(\theta) + \mu \cdot \chi) \cdot e^{\lambda \cdot z_{L_0}} = q \cdot \cos(\theta + z_{L_0}) - \chi \tag{2.10b}$$

$$(q \cdot \cos(\theta) - \mu \cdot \chi) \cdot e^{\lambda \cdot z_{R_+}} = q \cdot \cos(\theta + z_{R_+}) - \chi \tag{2.10c}$$

$$(q \cdot \cos(\theta) - \mu \cdot \chi) \cdot e^{\lambda \cdot z_{R_0}} = q \cdot \cos(\theta + z_{R_0}) + \chi \tag{2.10d}$$

$$(q \cdot \cos(\theta + z_{L_+}) + \chi + 1) \cdot e^{\lambda \cdot z_1} - 1 = q \cdot \cos(\theta + z_{L_+} + z_1) + \mu \cdot \chi \tag{2.10e}$$

$$(q \cdot \cos(\theta + z_{L_0} + z_2) - \chi - 1) \cdot e^{\lambda \cdot z_2} + 1 = q \cdot \cos(\theta + z_{L_0} + z_2) - \mu \cdot \chi \tag{2.10f}$$

$$(q \cdot \cos(\theta + z_{R_+}) + \chi + 1) \cdot e^{\lambda \cdot z_3} - 1 = q \cdot \cos(\theta + z_{L_+} + z_1) + \mu \cdot \chi \tag{2.10g}$$

$$(q \cdot \cos(\theta + z_{R_0} + z_4) - \chi - 1) \cdot e^{\lambda \cdot z_4} + 1 = q \cdot \cos(\theta + z_{R_0} + z_2) - \mu \cdot \chi \tag{2.10h}$$

The values for χ, λ, μ, and q come from the parameters of the model. The parameters are $\chi_0, E_0, \beta, f, L, R, V_m$, and μ. μ is directly applied in the equations above, while χ, λ, and q are computed from multiple parameters. The values of χ, λ, and q are given by the following Equations (2.11a) to (2.11c).

$$\chi = \frac{R \cdot \chi_0}{\beta \cdot E_0} \tag{2.11a}$$

$$\lambda = \frac{-R}{L \cdot 2 \cdot \pi \cdot f} \tag{2.11b}$$

$$q = \frac{R \cdot V_m}{\beta \cdot E_0} \tag{2.11c}$$

2.3.3 Model Dynamics

The aforementioned interesting dynamics of the original model occur for the fixed parameters $\beta = 1, f = 150, L = 4.2 \cdot 10^{-3}, R = 2, V_m = 5$, and $\mu = 0.5$. The parameters E_0 and χ_0 are varied in the ranges $[14, 28]$ and $[0.1, 0.65]$, respectively. Scanning this parameter plane for the period of stable cycles results in Figure 2.3.

The colors in the 2D scan in Figure 2.3 indicate the period of the stable cycle in those regions. Brighter colors correspond to higher periods and some periods are annotated with numbers in the top right area of the picture. There are long parameter regions that are associated with the same period that get narrower at some points. As we will see shortly, those are actually chains of different parameter regions associated with the same period. One can see that the period of the chain to the right of another chain is two higher than the period associated with the previous chain. This makes the structure a PI structure. Points A, B and C are in the parameter region, which has stable cycles with the period 12. The parameter regions differ in another way, the cycles in these regions are associated with different symbolic sequences. As mentioned before, it describes on which branches of the model function the points of the cycle exist. Shortly some cobweb diagrams are used to illustrate the difference between the parameter regions that belong to the same chain of parameter regions associated with the same period.

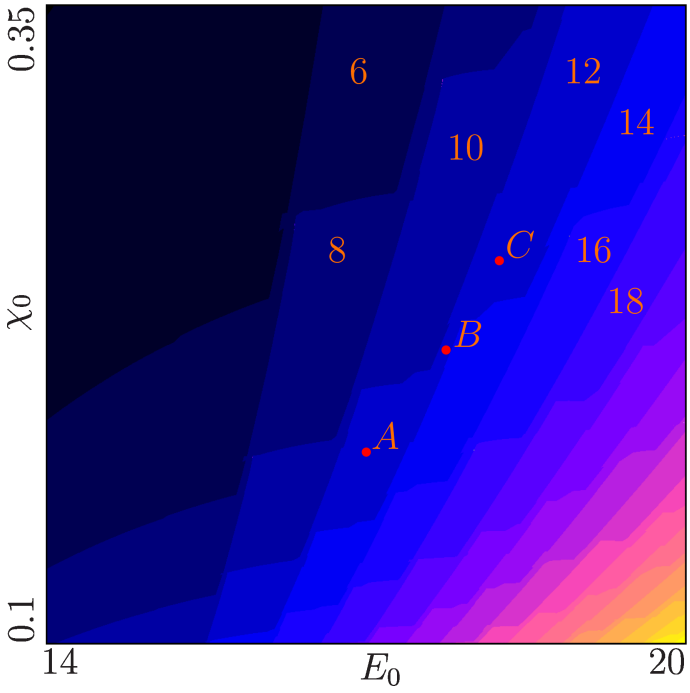

Figure 2.3: 2D scan of the periods associated with parameter regions in the original model. The parameters $\beta = 1$, $f = 150$, $L = 4.2 \cdot 10^{-3}$, $R = 2$, $V_m = 5$, and $\mu = 0.5$ are fixed. The parameters E_0 and χ_0 are varied in the ranges $[14, 28]$ and $[0.1, 0.65]$. The three points A, B, and C mark the parameter values for the cobweb diagrams in Figure 2.4. The numbers in the picture indicate the period of the corresponding chain of parameter regions.

Akyüz pointed out a symmetry in the original model. Equation (2.12) describes this symmetry [Aky22].

$$F(\theta + \pi) \equiv F(\theta) + \pi \mod 2\pi \tag{2.12}$$

This means that the shapes of the branches $F_{\mathcal{A}}$ and F_C are identical. The branch F_C is exactly π to the right of $F_{\mathcal{A}}$ and its values are π larger. The same is true for the branches $F_{\mathcal{B}}$ and $F_{\mathcal{D}}$. It follows that if x is a part of a cycle in the original model, the point $x + \pi$ belongs to a cycle as well. Therefore, only the two following cases are possible:

(A) The points x and $x + \pi$ belong to the same cycle. This cycle is therefore symmetric, and such cycles are referred to as "type A" cycles in this thesis. Such cycles must have an even period because there are as many points on the intervals $I_{\mathcal{A}}$ and $I_{\mathcal{B}}$ as there are on the intervals I_C and $I_{\mathcal{D}}$.

(B) The points x and $x + \pi$ belong to different cycles. Then there are at least 2 coexisting cycles with the same period. This is not obvious and therefore proven below. Such cycles are referred to as "type B" cycles in this thesis.

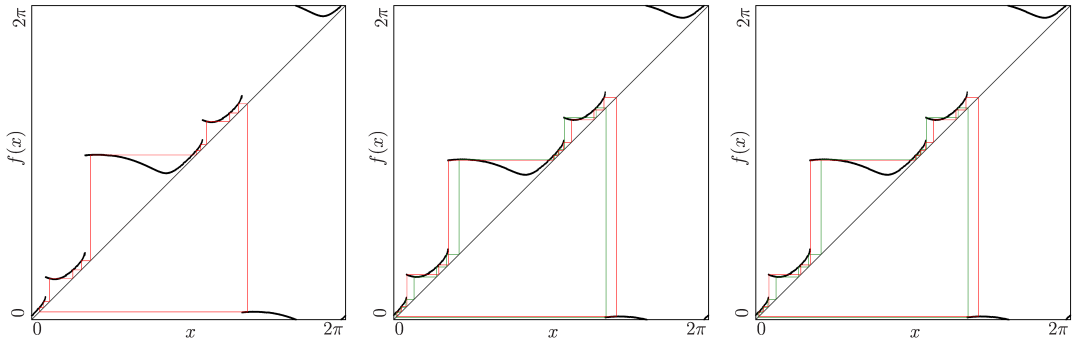

(a) A **(b)** B **(c)** C

Figure 2.4: Cobweb diagrams at three parameter values in the original model. The parameters $\beta = 1$, $f = 150$, $L = 4.2 \cdot 10^{-3}$, $R = 2$, $V_m = 5$, and $\mu = 0.5$ are fixed. The parameter values of E_0 and χ_0 are different in every diagram and are marked with points in Figure 2.3. (a) shows the cycle $O_{\mathcal{A}^3\mathcal{B}^3\mathcal{C}^3\mathcal{D}^3}$ at the point A where $E_0 = 17$ and $\chi_0 = 0.175$, (b) shows the two coexisting twin cycles $O_{\mathcal{A}^3\mathcal{B}^3\mathcal{C}^2\mathcal{D}^4}$ shown in green and $O_{\mathcal{A}^2\mathcal{B}^4\mathcal{C}^3\mathcal{D}^3}$ shown in red at the point B where $E_0 = 17.75$ and $\chi_0 = 0.215$, and (c) shows the cycle $O_{\mathcal{A}^2\mathcal{B}^4\mathcal{C}^2\mathcal{D}^4}$ at the point C where $E_0 = 18.25$, $\chi_0 = 0.25$.

Proof (At Least Two Coexisting "Type B" Cycles)
Let $O_k = \{x_i \mid 0 \leq i < k\}$ be a k-cycle of the original model where $x_i + \pi \notin O_k$ for some $0 \leq i < k$. It follows that $x_i + \pi \notin O_k$ for any $x_i \in O_k$.

Then there is a second cycle $O'_k = \{x_i + \pi \mid x_i \in O_k\}$. This cycle O'_k is completely disjunct from the first cycle O_k per definition. Therefore, there are at least two coexisting cycles $O_k \neq O'_k$ with the same period.

■

Figure 2.4 shows the cobweb diagrams at points A and C. Both parameter regions have only one stable cycle of period 12. This thesis follows the convention that the branch with the smallest positive boundaries is called branch $\mathcal{A}$. And the next branch is called branch $\mathcal{B}$ and so on. The stable cycle at point A has the symbolic sequence $\mathcal{A}^3\mathcal{B}^3\mathcal{C}^3\mathcal{D}^3$ and the cycle at point C has the symbolic sequence $\mathcal{A}^2\mathcal{B}^4\mathcal{C}^2\mathcal{D}^4$. So both cycles are symmetric and therefore "type A" cycles. We call the parameter regions associated with "type A" cycles "type A" parameter regions.

Figure 2.4b shows the cobweb diagram at point B. By looking closely, one can see that there are 2 coexisting cycles in this cobweb diagram. One cycle has the symbolic sequence $\mathcal{A}^3\mathcal{B}^3\mathcal{C}^2\mathcal{D}^4$ shown in green, while the other one has the symbolic sequence $\mathcal{A}^2\mathcal{B}^4\mathcal{C}^3\mathcal{D}^3$ shown in green. Both cycles are asymmetric and therefore "type B" cycles. And they are similar to each other in the way that $O_{\mathcal{A}^3\mathcal{B}^3\mathcal{C}^2\mathcal{D}^4}$ behaves on the branches $\mathcal{A}$ and $\mathcal{B}$ like $O_{\mathcal{A}^2\mathcal{B}^4\mathcal{C}^3\mathcal{D}^3}$ on the branches $\mathcal{C}$ and $\mathcal{D}$ and vice versa. One can think of the cycles being equivalent by shifting them by π in either direction. This agrees with the rules for "type B" cycles outlined above. These cycles also behave similarly to both the cycles at points A and C. The cycle $O_{\mathcal{A}^3\mathcal{B}^3\mathcal{C}^2\mathcal{D}^4}$ behaves like the cycle $O_{\mathcal{A}^3\mathcal{B}^3\mathcal{C}^3\mathcal{D}^3}$ at point A on its left half, while it behaves like the cycle $O_{\mathcal{A}^2\mathcal{B}^4\mathcal{C}^2\mathcal{D}^4}$ at point C on its right half. The same is true for the cycle $O_{\mathcal{A}^2\mathcal{B}^4\mathcal{C}^3\mathcal{D}^3}$ but reversed since it is the other cycle shifted by π. Similarly to "type A" parameter regions, we call this parameter region a "type B" parameter region.

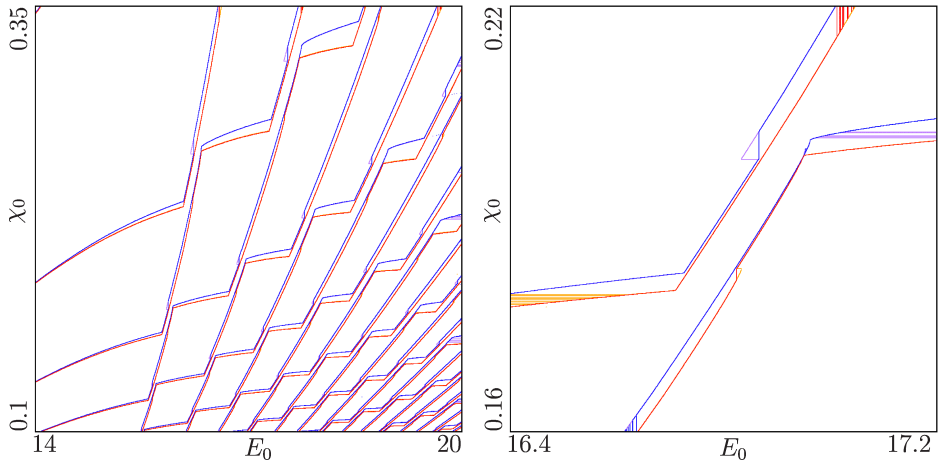

(a) Overview **(b)** Zoomed In

Figure 2.5: 2D scans of the boundaries of parameter regions associated with different periods in the original model. The parameters $\beta = 1$, $f = 150$, $L = 4.2 \cdot 10^{-3}$, $R = 2$, $V_m = 5$, and $\mu = 0.5$ are fixed. The parameters E_0 and χ_0 are varied in different ranges. (a) shows the ranges $[14, 28]$ and $[0.1, 0.65]$, (b) shows a magnified version with the ranges $[16.4, 17.2]$ and $[0.16, 0.22]$.

This behavior is peculiar. To summarize, we have chains of parameter regions associated with the same period. The type of the parameter regions alternates between "type A" and "type B". When the stable cycle in one "type A" parameter region is $O_{\mathcal{A}^a \mathcal{B}^b C^a \mathcal{D}^b}$, the stable cycle in the next "type A" parameter region is $O_{\mathcal{A}^c \mathcal{B}^d C^c \mathcal{D}^d}$ with $c = a - 1$ and $d = b + 1$. The "type B" parameter region in between two "type A" parameter regions of a chain with cycles $O_{\mathcal{A}^a \mathcal{B}^b C^c \mathcal{D}^d}$ and $O_{\mathcal{A}^c \mathcal{B}^d C^a \mathcal{D}^b}$, has the two cycles $O_{\mathcal{A}^x \mathcal{B}^y C^{x-1} \mathcal{D}^{y+1}}$ and $O_{\mathcal{A}^{x-1} \mathcal{B}^{y+1} C^x \mathcal{D}^y}$. Also, there is not only one chain, but many chains next to each other where the period increases by two from one chain to the next.

2.3.4 Overlapping Periods

The chains of parameter regions with the same period overlap. We can see this in Figure 2.5, which shows the boundaries of parameter regions with the same period. Therefore, we can only see the boundaries of the chains and not all boundaries of the single parameter regions that make up the chain. For Figure 2.5a, the fixed and varied parameters are the same as in previous 2D scans like Figure 2.3. For the zoomed-in version Figure 2.5b, the fixed parameters are the same but the varied parameters E_0 and χ_0 are now in the ranges $[16.4, 17.2]$ and $[0.16, 0.22]$, respectively.

Figure 2.6 shows the boundaries of parameter regions with different symbolic sequences. The fixed parameters and varied parameters are the same as in Figure 2.5b. This allows us to see the boundaries of the individual parameter regions that make up the chains. And one can see that the "type A" and "type B" parameter regions of the same chain also overlap. Akyüz found in his thesis that there are 3 coexisting cycles in such an overlap. One of the cycles is from the "type A" parameter region and the other 2 cycles are from the "type B" parameter region.

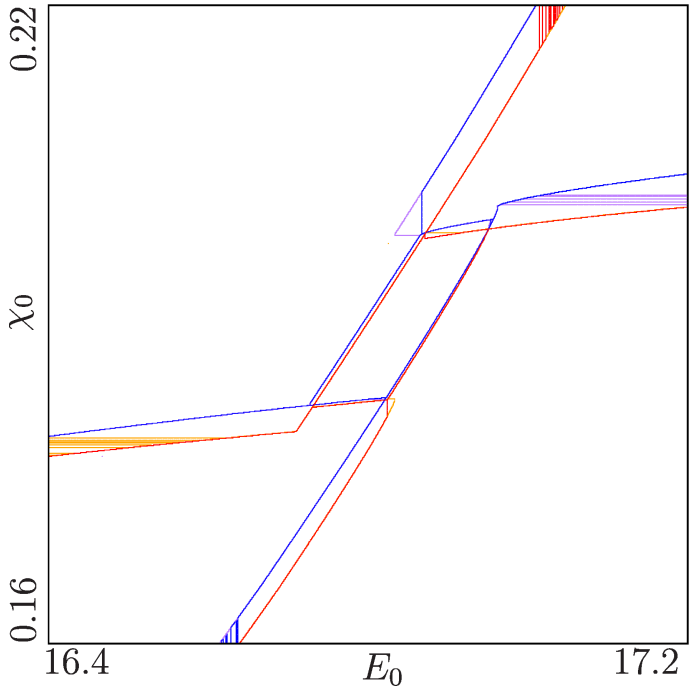

Figure 2.6: 2D scan of the boundaries of parameter regions associated with different symbolic sequences in the original model. The parameters $\beta = 1$, $f = 150$, $L = 4.2 \cdot 10^{-3}$, $R = 2$, $V_m = 5$, and $\mu = 0.5$ are fixed. The parameter ranges of E_0 and χ_0 are the same as in Figure 2.5b, $[16.4, 17.2]$ and $[0.16, 0.22]$. Here, we can see the boundaries of "type B" parameter regions as they have different symbolic sequences as the neighboring "type A" parameter regions of the same chain.

The scans in this subsection are computed in the following way. The program scans in 4 directions, from top to bottom shown in red, from bottom to top shown in blue, from left to right shown in yellow, and finally right to left shown in purple. While scanning, it keeps track of the cycle it converged to last and marks the point, at which it loses the cycle. This way, we can see where different parameter regions with cycles of different period overlap.

This also causes some errors in the diagrams, unfortunately. When a scan starts in a parameter region where multiple cycles of different periods coexist, the cycle it sees at the first parameter point is determined by chance. So for example, two rows that scan from left to right and start in a parameter region where multiple stable cycles coexist might disagree on the period. We can see this happening with the yellow lines in the lower left area of Figure 2.6.

3 Approach

The definition of the original model is highly complicated since it contains many implicit equations. Existing algorithms can simulate the original model, so it is possible to investigate and explain the PI structure. However, due to the repeated use of implicit equations, it is difficult to conclude which effects the parameters have on the model function and which characteristics of the model function lead to the observed PI structure. In this case, the PI structure consists of chains of alternating "type A" and "type B" parameter regions associated with the same period next to one another, where the periods increase by two. A simplified model showing the same PI structure would help to explain the PI structure in the original model. It is also helpful for explaining similar PI structures that might turn up in other dynamical systems.

As mentioned before, this is usually achieved using normal forms. These models neglect all non-essential parameters for the bifurcation structure, and one can prove that the neglected parameters are indeed non-essential for the bifurcation structure. But this is impossible for bifurcation structures in PWS discontinuous dynamical systems with border collision bifurcations. Instead, this thesis constructs an archetypal model. This model is constructed by identifying essential and neglecting non-essential parameters and parameter effects for the bifurcation structure. Using this approach, the PI structure in the archetypal model is explained rigorously. However, the claim that the archetypal model thoroughly describes the behavior of the original model, and therefore the PI structure in the original model, is only supported by numerical evidence.

This model is constructed by analyzing and emulating the original model function. The original model is analyzed for its characteristics. Both the shape of the model function and the effects of its parameters on that shape are important. Then different models are constructed that each share some characteristics with the original model, starting with the most prominent characteristics. The constructed models are analyzed with the goal of finding behavior that is similar or hints at similar behavior as the original model. If a model exhibits promising behavior, it is used as a basis for adding more characteristics identified in the original model. This is a process of trial and error but also analysis and educated guesses. It continues until an archetypal model for the PI structure in the original model is found.

The archetypal model is then thoroughly investigated, and the results are used to explain the PI structure in the archetypal model. Also, the capacity of the archetypal model to emulate the original model is validated using the investigation results. Finally, it is investigated whether this archetypal model exhibits other bifurcation structures at different parameter values.

4 Task Definition

The first task of this thesis is to develop an archetypal model for the observed bifurcation structure in the original model. This task consists of two subtasks. First, the characteristics of the original model have to be identified. Then different models with similar characteristics have to be constructed and analyzed. Chapter 3 outlines the details of both these tasks, and Chapter 5 documents the execution. The result will be the archetypal model for the PI structure observed in the original model and also the characteristics that are identified to be important for this structure.

The next task is to investigate the PI structure in the archetypal model. This is done for two reasons. First, the PI structure has to be explained. Secondly, the capacity of the archetypal model to emulate the behavior of the original model has to be validated. Both is achieved with numerical evidence that results from the investigation of the PI structure in the archetypal model and the characteristics that lead to the PI structure identified by the first task. Chapter 6 covers this task.

The last task is to find out which other bifurcation structures may occur in the archetypal model, and which kinds of changes to the model function are required for this. Chapter 7 covers this task.

5 Setup

This chapter is about the first task. Specifically, it is concerned with finding an archetypal model that exhibits the same behavior as the original model. First, it analyzes the original model and identifies its characteristics. After that, it lists different constructed models with different characteristics similar to the characteristics of the original model function. The behavior of these constructed models is analyzed as outlined in Chapter 3.

5.1 Characteristics

This section analyzes the original model function and identifies its characteristics. The first kind of characteristics are the number and shapes of the branches of the model function. The second kind are the effects that the parameters have on the model function.

5.1.1 Function Shape

This section is concerned with the overall shape and number of branches of the original model function.

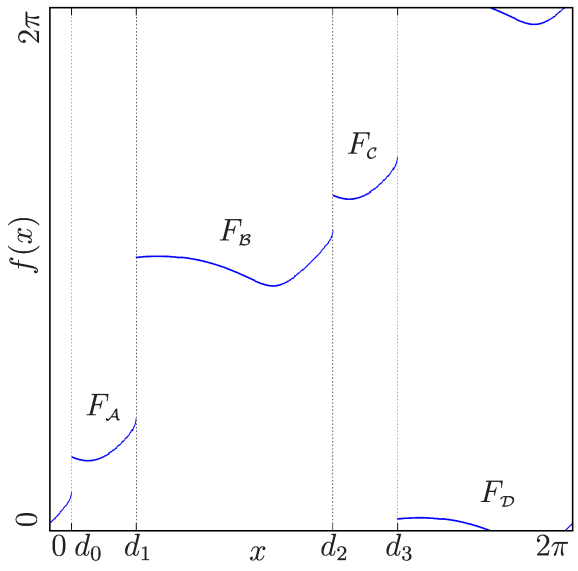

Figure 5.1: The shape of the original model function with the parameter values $E_0 = 15$ and $\chi_0 = 0.2$.

Figure 5.1 shows the shape of the original model function. One can immediately see that the model function has 4 branches. This is also evident from the model definition given in Section 2.3.2. Also, we know from Section 2.3.3 that the model has the symmetry described by Equation (2.12). So the branches $F_{\mathcal{A}}$ and $F_{\mathcal{C}}$ are identical. The same is true for the branches $F_{\mathcal{B}}$ and $F_{\mathcal{D}}$.

There are no fixed points in the parameter regions that this thesis is concerned with. That means, the function is always larger than the bisector $y = x$. Also, for the most part the slope of the function is not steep. Meaning that the absolute value of the model functions derivative is below 1 for a majority of the state space. A model where the absolute value of the derivative of its model function is below 1 for the whole state space is called contractive. In such a model, every fixed point and cycle is stable.

5.1.2 Parameter Effects

This section is concerned with the other types of characteristics, the effects of the parameters of the model on the shape of the model function. First, it analyzes the combined parameter effects along a chain of parameter regions assocoated with cycles the same period. After that, it analyzes the isolated effects of the single parameters and decomposes the combined effects into the isolated effects.

5.1.3 Combined Effects of Parameters

To replicate the dynamics seen in the model, it is helpful to know, how the model changes along the chains of parameter regions that are associated with cycles of the same period. This section therefore analyzes the model function at different points in different chains. Figure 5.2a indicates the points used for this analysis. Figure 5.2b shows, how the model function changes along the chain of parameter regions associated with cycles of period 12. In the figure, there are three functions F^{A_12}, F^{B_12}, and F^{C_12}. The function $F^{A_{12}}$ is the model function with the parameters $E_0 = 15.9, \chi_0 = 0.11$. These parameter values are marked with the point A_{12} in Figure 5.2a. The function $F^{B_{12}}$ is the model function with the parameters $E_0 = 17.07, \chi_0 = 0.182$. And the function $F^{C_{12}}$ is the model function with the parameters $E_0 = 18.5, \chi_0 = 0.27$. The parameter values are marked accordingly in Figure 5.2a.

The most notable changes are the following.

(i) The values of the whole branches $F_{\mathcal{A}}$ and $F_{\mathcal{C}}$ get larger. This change is most notable at the left borders of the branches. The values on the left sides of the branches are affected more by this change than the values on the right sides.

(ii) The values on the left sides of the branches $F_{\mathcal{B}}$ and $F_{\mathcal{D}}$ get smaller while the values on the right sides are not affected much.

(iii) The local minima of the branches $F_{\mathcal{B}}$ and $F_{\mathcal{D}}$ move to the left, and their values get smaller.

One smaller change is that the border between branches $F_{\mathcal{B}}$ and $F_{\mathcal{C}}$ moves left. Note that the same change happens to the border between the branches $F_{\mathcal{D}}$ and $F_{\mathcal{A}}$ due to the symmetry of the function.

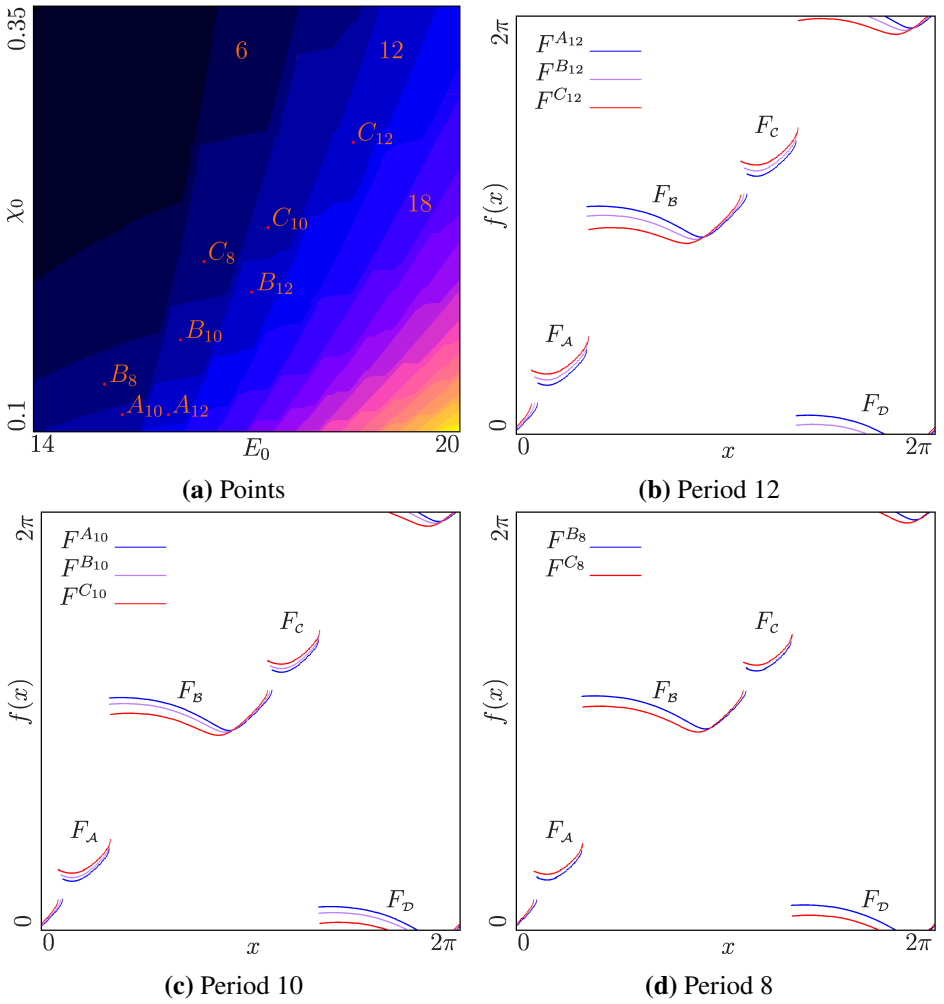

(a) Points **(b)** Period 12

(c) Period 10 **(d)** Period 8

Figure 5.2: The effects of the parameters on the original model function illustrated by plotting the model function at different parameter values. The parameters $\beta = 1, f = 150, L = 4.2 \cdot 10^{-3}, R = 2, V_m = 5$, and $\mu = 0.5$ are fixed. (a) shows a 2D scan of the periods associated with parameter regions in the original model. The parameters E_0 and χ_0 are varied in the ranges $[14, 20]$ and $[0.1, 0.35]$. The points in this scan mark the parameter values used for plotting the model function in (b), (c), and (d). (b) shows the evolution of the shape of the model function along the chain of parameter regions associated with the period 12. The function $F^{A_{12}}$ is the model function with the parameter values at the point A_{12} where $E_0 = 15.9$ and $\chi_0 = 0.11$, $F^{B_{12}}$ at the point B_{12} where $E_0 = 17.07$ and $\chi_0 = 0.182$, and $F^{C_{12}}$ at the point C_{12} where $E_0 = 18.5$ and $\chi_0 = 0.27$. (c) shows the evolution of the shape of the model function along the chain of parameter regions associated with the period 10. Here, $F^{A_{10}}$ is the model function with the parameters at the point A_{10} where $E_0 = 15.25$ and $\chi_0 = 0.11$, $F^{B_{10}}$ at the point B_{10} where $E_0 = 16.07$ and $\chi_0 = 0.154$, and $F^{C_{10}}$ at the point C_{10} where $E_0 = 17.3$ and $\chi_0 = 0.22$. And (d) shows the evolution of the shape of the model function along the chain of parameter regions associated with the period 8. Here, F^{B_8} is the model function with the parameter values at the point B_8 where $E_0 = 15$ and $\chi_0 = 0.128$, and F^{C_8} at the point C_8 where $E_0 = 16.4$ and $\chi_0 = 0.2$.

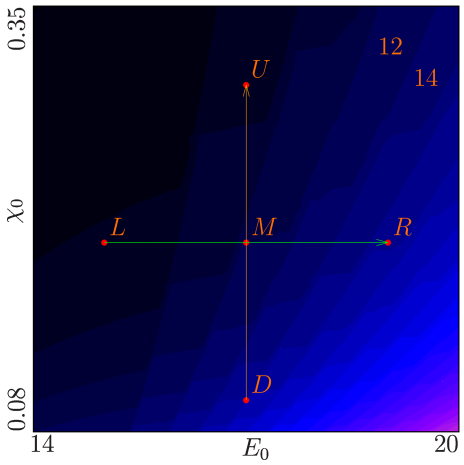

Figure 5.3: 2D scan of the periods associated with parameter regions in the original model. The parameters $\beta = 1$, $f = 150$, $L = 4.2 \cdot 10^{-3}$, $R = 2$, $V_m = 5$, and $\mu = 0.5$ are fixed. The parameters E_0 and χ_0 are varied in the ranges $[14, 20]$ and $[0.08, 0.35]$. It illustrates the parameter ranges used to analyze the isolated effects of the parameters E_0 and χ_0 on the original model function. The green arrow indicates the parameter range used to analyze the effects of the parameter E_0, while the orange arrow indicates the parameter range used to analyze the effects of the parameter χ_0 on the original model function. The points L, M, R, D, and U mark the parameter values used for the cobweb diagrams in Figure 5.4.

The same effects can be observed in the chains of parameter regions associated with cycles of periods 10 and 8, respectively. For the chain of parameter regions associated with cycles of period 10, the model function is plotted in Figure 5.2c at the three points A_{10}, B_{10}, and C_{10} marked in Figure 5.2a. Again, the values of the whole branches $F_{\mathcal{A}}$ and $F_{\mathcal{C}}$ are larger in $F^{C_{10}}$ than they are in $F^{A_{10}}$. And the values on the left sides of the branches $F_{\mathcal{B}}$ and $F_{\mathcal{D}}$ are smaller in $F^{C_{10}}$ than they are in $F^{A_{10}}$. Also, the local minima on those branches move left and down. For the chain of parameter regions associated with cycles of period 8, the model function is plotted in Figure 5.2d at the two points B_8 and C_8 marked in Figure 5.2a. And the values of the branches undergo the same changes again from the model function F^{B_8} to F^{C_8}.

5.1.4 Individual Effects of Parameters

The effects of the parameters described above, always include a change in both parameters E_0 and χ_0. To reproduce the bifurcation structures, it is important to know which effects on the function each parameter has individually. This section focuses on the isolated effects of each parameter by fixing one of the parameters and only varying the other one and observing the effects of this parameter on the shape of the model function.

For the effects of the parameter E_0, $\chi_0 = 0.2$ is fixed and E_0 is varied in the parameter range $[15, 19]$. This is marked as the green arrow in Figure 5.3. As before, the model function is plotted at three parameter values in one figure. The functions are visualized in Figure 5.4a. F^L is the model function with $E_0 = 15$, F^M is the model function with $E_0 = 17$, and F^R is the model function

with $E_0 = 17$. $\chi_0 = 0.2$ is the same for all functions F^L, F^M, and F^R. The parameter values are marked with the points L, M, and R in Figure 5.3. One can see that they are all on the green arrow mentioned before. The following changes can be observed.

(i) The values on the left sides of the branches $F_{\mathcal{B}}$ and $F_{\mathcal{D}}$ get smaller while the values on the right sides are not affected much.

(ii) The local minima of the branches $F_{\mathcal{B}}$ and $F_{\mathcal{D}}$ move left, and their values get smaller.

(iii) The border between the branches $F_{\mathcal{A}}$ and $F_{\mathcal{B}}$ moves to the right. The same is true for the border between the branches F_C and $F_{\mathcal{D}}$ because of the symmetry in the original model.

(iv) The values at the right borders of branches $F_{\mathcal{A}}$ and F_C get larger. This is caused by the border between branches $F_{\mathcal{A}}$ and F_B moving to the right.

For the effects of the parameter χ_0, $E_0 = 17$ is fixed and χ_0 is varied in the parameter range $[0.125, 0.3]$. This parameter range is marked with an orange arrow in Figure 5.3. Again, the model function is plotted at three parameter values in one figure. The functions are visualized in Figure 5.4b. F^D is the model function with $\chi_0 = 0.1$, F^M is the model function with $\chi_0 = 0.2$, and F^U is the model function with $\chi_0 = 0.3$. $E_0 = 15$ is the same for all functions F^D, F^M, and F^U. The parameter values are marked with the points D, M, and U in Figure 5.3. One can see that they are all on the orange arrow mentioned before. The following pronounced changes can be observed.

(i) The values of the whole branches $F_{\mathcal{A}}$ and F_C get larger.

(ii) The border between the branches $F_{\mathcal{A}}$ and $F_{\mathcal{B}}$ moves to the left. The same is true for the border between the branches F_C and $F_{\mathcal{D}}$.

Two other smaller changes that can be observed are the following.

(i) The values on the right sides of the branches $F_{\mathcal{B}}$ and $F_{\mathcal{D}}$ get larger. This includes the values of the local minima on these branches.

(ii) The border between the branches $F_{\mathcal{B}}$ and F_C moves to the left. The same is true for the border between the branches $F_{\mathcal{D}}$ and $F_{\mathcal{A}}$.

5.1.5 Decomposition of Combined Effects

This section considers the decomposition of the combined parameter effects listed in Section 5.1.3 into the effects of the isolated parameter effects listed in Section 5.1.4 and traces each effect back to its cause. This is important, because some of the isolated parameter effects cancel out when the parameters are both varied as we will see later in this section. For this, this section introduces a notation for the effects. The effect of the values on the left side of a branch changing is denoted L, for the right side it is R, and for the whole branch it is W The subscript indicates, which branch the change affects, and the superscript indicates, whether the values get larger + or smaller −. The effect of changing a local minimum is denoted as Mi. The meaning of the subscript stays the same as above, but the superscript also can include L for movement to the left and R for movement to the right. Finally, the effect of moving borders is denoted as B. The subscript now includes the two symbols of branches to which the border belongs and the superscript now has only L or R. For

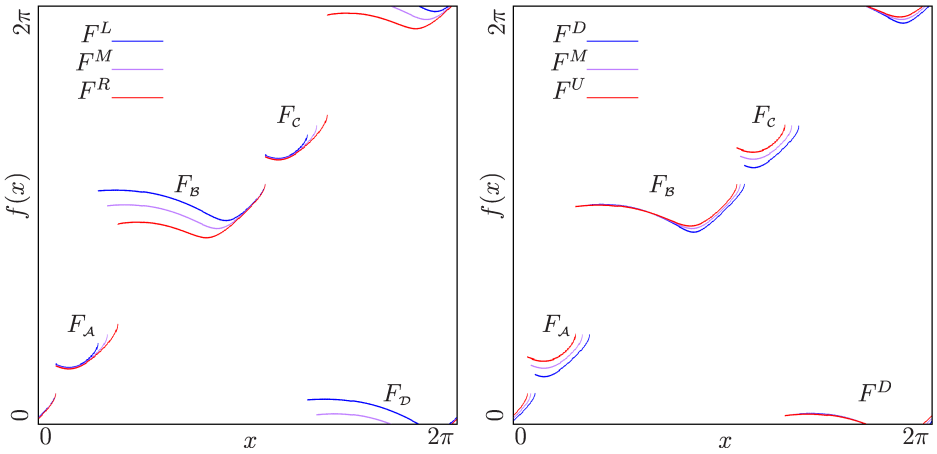

(a) E_0 **(b)** χ_0

Figure 5.4: The isolated effects of the parameters E_0 and χ_0 on the original model function. The parameter values used for plotting the functions are marked with points in Figure 5.3. (a) shows the evolution of the shape of the model function for different parameter values of E_0 while $\chi_0 = 0.2$ is fixed. The function F^L is the model function with the parameter values at the point L where $E_0 = 15$, F^M is at the point M where $E_0 = 17$, and F^R is at the point R where $E_0 = 19$. (b) shows the evolution of the shape of the model function for different parameter values of χ_0 while $E_0 = 17$ is fixed. The function F^D is the model function with the parameter values at the point D where $\chi_0 = 0.1$, F^M is at the point M where $\chi_0 = 0.2$, and F^U is at the point U where $\chi_0 = 0.3$.

brevity, one does not write redundant branch names, so changes happening to branch $F_{\mathcal{A}}$ are also happening to branch F_C. For borders, changes to the border between branches $F_{\mathcal{A}}$ and $F_{\mathcal{B}}$ are also happening to the border between branches F_C and $F_{\mathcal{D}}$ and so on.

Table 5.1 lists all observed effects along the chains of parameter regions associated with cycles of the same period and their decomposition into effects of the single parameters. The first part of the table includes all major changes observed in Section 5.1.3. The second part includes the minor change one can observe of the borders between the branches $f_{\mathcal{B}}$ and f_C moving to the left. The second part also includes the changes observed in Section 5.1.4 that cancel out. From this table we can see that E_0 causes the effects on the branches $F_{\mathcal{B}}$ and $F_{\mathcal{D}}$, while χ_0 causes the changes to the branches $F_{\mathcal{A}}$ and F_C, as well as the minor movement of the borders between the branches $F_{\mathcal{B}}$ and F_C. Note again that the change to the border of branches $F_{\mathcal{B}}$ and F_C also applies for the border between branches $F_{\mathcal{D}}$ and $F_{\mathcal{A}}$.

Combined	E_0	χ_0	Comment
$\mathrm{L}^-_{\mathcal{B}}$	$\mathrm{L}^-_{\mathcal{B}}$	0	Only E_0 causes this
$\mathrm{Mi}^{L-}_{\mathcal{B}}$	$\mathrm{Mi}^{L-}_{\mathcal{B}}$	$-\mathrm{Mi}^+_{\mathcal{B}}$	E_0 and χ_0 have opposing effects, the effect of E_0 is stronger
$\mathrm{W}^+_{\mathcal{A}}$	0	$\mathrm{W}^+_{\mathcal{A}}$	Only χ_0 causes this
$\mathrm{B}^L_{\mathcal{B}C}$	0	$\mathrm{B}^L_{\mathcal{B}C}$	Only χ_0 causes this
0	$\mathrm{B}^R_{\mathcal{A}\mathcal{B}}$	$-\mathrm{B}^L_{\mathcal{A}\mathcal{B}}$	E_0 and χ_0 have opposing effects, they cancel out

Table 5.1: Decomposition of the combined parameter effects along chains of parameter regions with the same period as displayed in Figure 5.2. Each effect is traced back to the effects of changing the parameters E_0 and χ_0 alone as displayed in Figure 5.4.

5.2 Piecewise-quadratic Model

In this section, the first model with similar characteristics to the original model is constructed. This chapter only includes the constructed models on the "good" path. Appendix A lists other models that are not included in this chapter.

This first model has 4 branches that are all quadratic. Hence, it is called the piecewise-quadratic model. In the original model, the branches $F_{\mathcal{B}}$ and $F_{\mathcal{D}}$ are shaped more like cubic functions, but to keep the number of parameters reasonable, this model assumes only quadratic branches. The model also has the same symmetry as the original model, and it is included explicitly in the model definition. The state space of all constructed models is $[0, 1)$ instead of $[0, 2\pi)$ as in the original model.

5.2.1 Model Definition

The model is defined as the map $x_{n+1} = f(x_n) \mod 1$. Where f is given by the following set of equations.

$$f(x) = \begin{cases} g(x) & \text{if } x < \frac{1}{2} \\ g(x - \frac{1}{2}) + \frac{1}{2} & \text{else} \end{cases} \tag{5.1}$$

$$g(x) = \begin{cases} g_L(x) = a_L \cdot x^2 + b_L \cdot x + c_L & \text{if } x < \frac{1}{4} \\ g_R(x) = a_R \cdot x^2 + b_R \cdot x + c_R & \text{else} \end{cases} \tag{5.2}$$

Equation (5.1) explicitly states the discontinuity at 0 and $\frac{1}{2}$. It also explicitly states the symmetry of the model. Each half of the model is then governed by Equation (5.2). Here all the 6 parameters a_L, a_R, b_L, b_R, c_L, and c_R act. This equation also explicitly states the border at $\frac{1}{4}$. And in combination with the explicit symmetry in Equation (5.1), the border at $\frac{3}{4}$ follows.

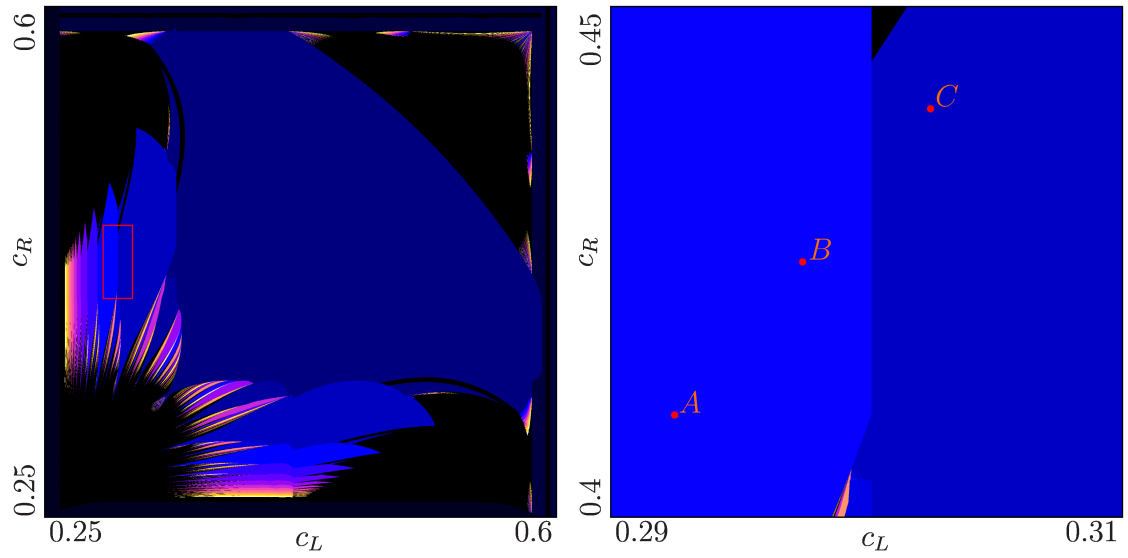

(a) Full **(b)** Zoomed

Figure 5.5: 2D scans of the periods associated with parameter regions in the piecewise quadratic model with centered parabola-shaped branches The parameters $a_L = a_R = 6$, $b_L = -\frac{3}{2}$, and $b_R = -\frac{9}{2}$ are fixed. The parameters c_L and c_R are varied in different ranges. (a) shows the full structure with the parameters being varied in the range $[0.25, 0.6]$ each, (b) shows the ranges marked with a red rectangle in (a), $[0.29, 0.31]$ and $[0.4, 0.45]$. The marked points in (b) are the parameter values that are used for the cobweb diagrams in Figure 5.6

5.2.2 Centered Parabola-shaped Branches

This section examines the piecewise-quadratic model with the centered parabola-shaped branches, see the functions in Figure 5.6. To center the parabola-shaped branches, the parameter values $a_L = a_R = 6$, $b_L = -\frac{3}{2}$, and $b_R = -\frac{9}{2}$ are chosen and only the parameters c_L and c_R are varied. Both varied parameters are in the ranges $[0.25, 0.6]$.

This emulates the effect that χ_0 has on the branches $F_{\mathcal{A}}$ and F_C. Increasing c_L increases the values of the branches $f_{\mathcal{A}}$ and f_C. The effects of E_0 on branches $F_{\mathcal{B}}$ and $F_{\mathcal{D}}$ are lowering the values of the function on the left sides of the branches, moving the local minima of the branches to the left, and reducing the value of the function at the minima. Decreasing c_R does not have the same effects on the branches $f_{\mathcal{B}}$ and $f_{\mathcal{D}}$ but rather lowers the values of the function for the whole branches. Figure 5.5a shows 2D scans of the periods associated with parameter regions in this model.

A phenomenon like in the original model can not be found here. But something very similar happens at the border of these wing-shaped parameter regions. Figure 5.6 shows the cobweb diagrams at the points marked in Figure 5.5b. At point A, there is one stable cycle with period 8. This cycle is depicted in Figure 5.6a and its symbolic sequence is $\mathcal{A}^3BC^3\mathcal{D}$. Point B is in a parameter region, where 2 stable cycles coexist. One can not see this in the 2D scans in Figure 5.5a, since it only ever picks up on one cycle. Figure 5.6b shows the coexisting cycles at this border. The symbolic sequences of the two coexisting cycles are $\mathcal{A}^3BC^3\mathcal{D}$ and $\mathcal{A}^2\mathcal{B}C^2\mathcal{D}$. In contrast to the original model, the cycle that existed before in Figure 5.6a with the symbolic sequence $\mathcal{A}^3BC^3\mathcal{D}$ still exists

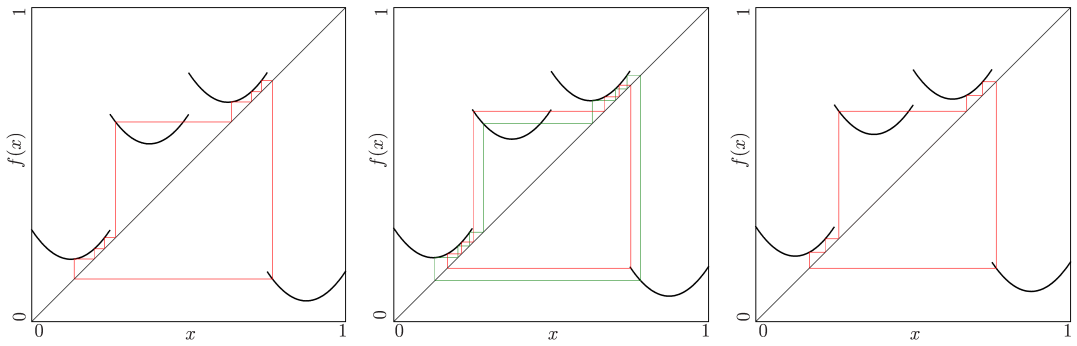

(a) A **(b)** B **(c)** C

Figure 5.6: Cobweb diagrams at three parameter values in the piecewise-quadratic model with centered parabola-shaped branches. The parameters $a_L = a_R = 6$, $b_L = -\frac{3}{2}$, and $b_R = -\frac{9}{2}$ are fixed. The parameters c_L and c_R are different in every diagram and their values are marked with points in Figure 5.5b. (a) shows the cycle $O_{\mathcal{A}^3\mathcal{B}C^3\mathcal{D}}$ at the point A where $c_L = 0.2925$ and $c_R = 0.41$, (b) shows the two coexisting cycles $O_{\mathcal{A}^3\mathcal{B}C^3\mathcal{D}}$ shown in green and $O_{\mathcal{A}^2\mathcal{B}C^2\mathcal{D}}$ shown in red at the point B where $c_L = 0.2975$ and $c_R = 0.425$, and (c) shows the cycle $O_{\mathcal{A}^2\mathcal{B}C^2\mathcal{D}}$ at the point C where $c_L = 0.3025$ and $c_R = 0.44$.

alongside the new cycle with the symbolic sequence $\mathcal{A}^2\mathcal{B}C^2\mathcal{D}$. At point C, there is again only one stable cycle. It has the period 6 and the symbolic sequence $\mathcal{A}^2\mathcal{B}C^2\mathcal{D}$. Therefore, this is the cycle that coexisted with the cycle with the symbolic sequence $\mathcal{A}^3BC^3\mathcal{D}$ at point C.

This is different from the dynamics in the original model in two ways. First, the cycles before and after the parameter region of coexistence have different periods. And second, the cycles existing outside the parameter region of coexistence still exist inside the parameter region of coexistence. In the original model, the cycles existing outside the parameter region of coexistence would disappear at the boundaries and new cycles would emerge inside this parameter region. Here, one simply observes two overlapping parameter regions which is something different from the original model.

5.2.3 Shifted Parabola-shaped Branches

The choice of centering the parabola-shaped branches was not ideal. When looking at the original model function, one can see that the parabolas are not centered. All branches are more shifted to the left. To imitate this shape better, the parameters are set to $b_L = -\frac{1}{2}$ and $b_R = -\frac{7}{2}$ in this section. All other fixed parameters are the same as in the previous section, Section 5.2.2. The parameters c_L and c_R are varied in the intervals $[0.08, 0.525]$ and $[0.825, 1.275]$, respectively.

With the newly chosen fixed parameter values, this model imitates the shape of the original model function better. And it perfectly emulates the effects of χ_0 on the branches $F_{\mathcal{A}}$ and F_C of the original model function still, as described in the previous section. But it also still does not emulate the effects of the parameter E_0 on the branches $F_{\mathcal{B}}$ and $F_{\mathcal{D}}$ of the original model function.

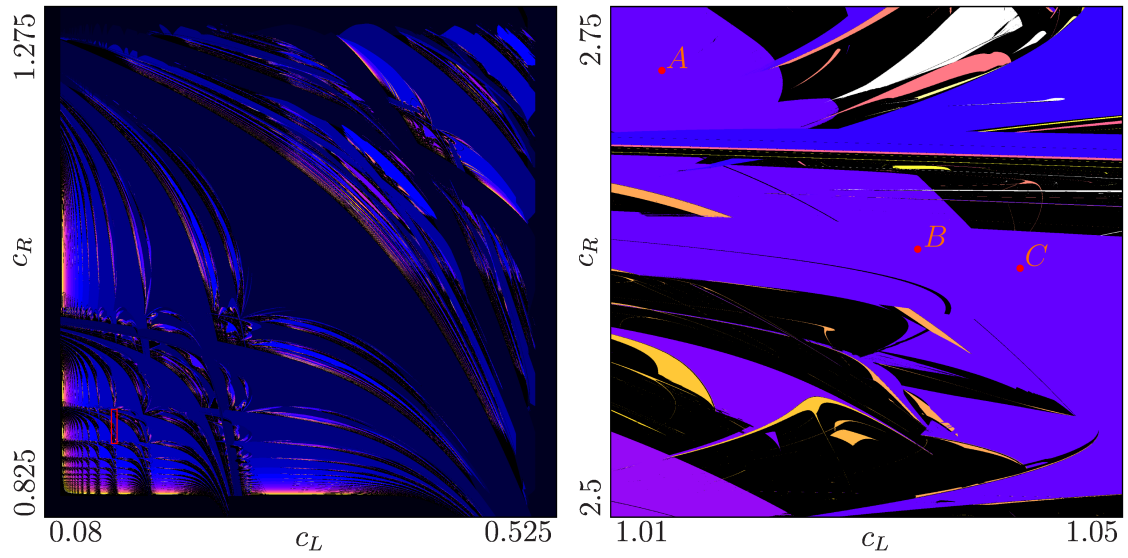

(a) Full **(b)** Zoomed

Figure 5.7: 2D scans of the periods associated with parameter regions in the piecewise-quadratic model with shifted parabola-shaped branches. The parameters $a_L = a_R = 6$, $b_L = -\frac{1}{2}$, and $b_R = -\frac{7}{2}$ are fixed. The parameters c_L and c_R are varied in different ranges. (a) shows the full structure with the parameters being varied in the ranges $[0.08, 0.525]$ and $[0.825, 1.275]$, (b) shows a magnified version with the parameters being varied in the ranges $[1.01, 1.05]$ and $[2.5, 2.75]$. These parameter ranges are marked with a red rectangle in (a). The points in (b) mark the parameter values for the cobweb diagrams in Figure 5.8

Figure 5.7a shows a 2D scan of the periods associated with the parameter regions in this parameter range. The structure seen in this figure repeats infinitely in all directions. An interesting parameter range is marked with a red rectangle. In this parameter range, two wing-shaped parameter regions associated with the same period connect. In the previous section this was not the case and that was one reason for rejecting that model. Figure 5.7b shows a 2D scan of the periods associated with the parameter regions in this parameter range. The points indicate the parameter values used for the analysis with cobweb diagrams.

Figure 5.8 shows all the cobweb diagrams of the model at with the parameter values marked in Figure 5.7b. The cobweb at point A is shown in Figure 5.8a. One can see that it has period 12 and its symbolic sequence is $\mathcal{A}^4\mathcal{B}^2\mathcal{C}^4\mathcal{D}^2$. The cycle at point C also has period 12. Its cobweb diagram is shown in Figure 5.8c, and one can see that its symbolic sequence is $\mathcal{A}^3\mathcal{B}^3\mathcal{C}^3\mathcal{D}^3$.

From point A to point C, one point of the cycle on the branch $f_{\mathcal{A}}$ moved to the branch $f_{\mathcal{B}}$. The same thing happened to a point of the cycle on the branch f_C, it moved to the branch $f_{\mathcal{D}}$. This is similar to what happens in the original model along a chain of parameter regions with the same period. And in between both points, there is a parameter region where 2 cycles coexist. This is shown in Figure 5.8b, which depicts the cycles at point C. But unfortunately, the coexisting cycles are the same cycles that exist at point A and point C, $O_{\mathcal{A}^4\mathcal{B}^2\mathcal{C}^4\mathcal{D}^2}$ and $O_{\mathcal{A}^3\mathcal{B}^3\mathcal{C}^3\mathcal{D}^3}$. Similarly to the previous experiment, we merely observe two parameter regions with stable cycles overlapping, see Section 5.2.2.

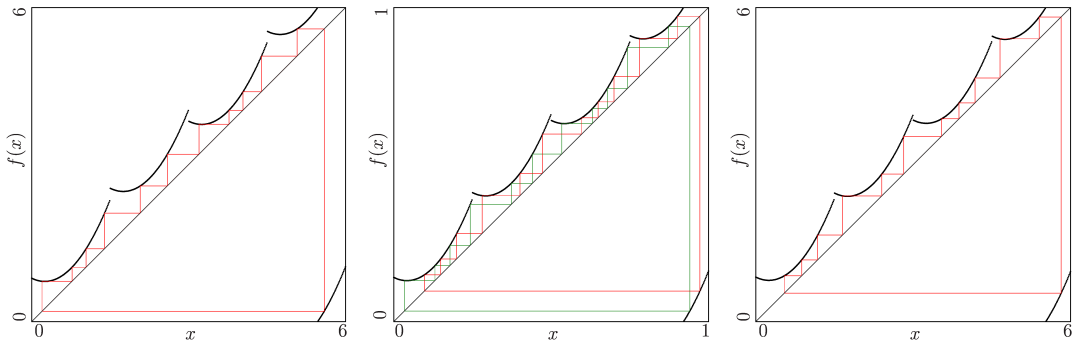

(a) A **(b)** B **(c)** C

Figure 5.8: Cobweb diagrams at three parameter values of c_L and c_R in the piecewise-quadratic model with shifted parabola-shaped branches. The parameters $a_L = a_R = 6$, $b_L = -\frac{1}{2}$, and $b_R = -\frac{7}{2}$ are fixed. The parameters c_L and c_R are different in every diagram and their values are marked with points in Figure 5.7b. (a) shows the cycle $O_{\mathcal{A}^3\mathcal{B}^3C^3\mathcal{D}^3}$ at point A where $c_L = 0.1385$ and $c_R = 0.925$, (b) shows the two coexisting cycles $O_{\mathcal{A}^3\mathcal{B}^3C^3\mathcal{D}^3}$ shown in green and $O_{\mathcal{A}^4\mathcal{B}^2C^4\mathcal{D}^2}$ shown in red at point C where $c_L = 0.141$ and $c_R = 0.911$, and (c) shows the cycle $O_{\mathcal{A}^4\mathcal{B}^2C^4\mathcal{D}^2}$ where $c_L = 0.142$ and $c_R = 0.9095$.

5.3 Piecewise-quadratic Model with Composite Parameters

Previously in Section 5.2, the only varied parameters were c_L and c_R. Changing the parameter c_L emulates the effects of χ_0 on the branches $F_{\mathcal{A}}$ and F_C of the original model function well. But changing c_R does not emulate the effects of E_0 on the branches $F_{\mathcal{B}}$ and $F_{\mathcal{D}}$ very well. This section introduces composite parameters that directly influence the characteristics of the branches $F_{\mathcal{B}}$ and F_D. And the values of the parameters a_R, b_R, and c_R are not directly changed but calculated from those composite parameters.

5.3.1 Composite Parameter Definitions

The composite parameters are $g_R\left(\frac{1}{4}\right)$ for the value at the left border of branches $f_{\mathcal{B}}$ and $f_{\mathcal{D}}$, $g_R\left(\frac{1}{2}\right)$ for the value at the right border of the branches, and finally $\frac{d}{dx}g_R(x)\big|_{x=\frac{1}{2}}$ for the slope of the branches at the right border. The composite parameter $\frac{d}{dx}g_R(x)\big|_{x=\frac{1}{2}} = 1.2$ is fixed. This way, the steepest slope is 1.2 which is just above 1. Therefore, most of the function is still contractive. Also, the composite parameter $g_R\left(\frac{1}{2}\right) = \frac{1}{2} + \epsilon$ is fixed with $\epsilon = \frac{1}{40}$ to have the value at the right border of the branches $f_{\mathcal{B}}$ and $f_{\mathcal{D}}$ just above the bisector $y = x$. The only composite parameter that is not fixed yet is $g_R\left(\frac{1}{4}\right)$, the value of the model function at the left border of the branches $f_{\mathcal{B}}$ and $f_{\mathcal{D}}$. This composite parameter is varied.

$$g_R\left(\frac{1}{4}\right) = a_R \cdot \left(\frac{1}{4}\right)^2 + b_R \cdot \left(\frac{1}{4}\right) + c_R = \frac{a_R}{16} + \frac{b_R}{4} + c_R \tag{5.3a}$$

$$g_R\left(\frac{1}{2}\right) = a_R \cdot \left(\frac{1}{2}\right)^2 + b_R \cdot \left(\frac{1}{2}\right) + c_R = \frac{a_R}{4} + \frac{b_R}{2} + c_R \tag{5.3b}$$

$$\frac{d}{dx} g_R(x)\Big|_{x=\frac{1}{2}} = 2 \cdot a_R \cdot \left(\frac{1}{2}\right) + b_R \tag{5.3c}$$

Equations (5.3a) to (5.3a) are the values of the composite parameters $g_R\left(\frac{1}{4}\right), g_R\left(\frac{1}{2}\right)$, and $\frac{d}{dx} g_R(x)\big|_{x=\frac{1}{2}}$. This is a system of equations that need to be solved for the parameters a_R, b_R, and c_R. To compute the parameters, one can write the system of equations as a matrix and invert it. The matrix and its inverse are in Equation (5.4).

$$\begin{pmatrix} \frac{1}{16} & \frac{1}{4} & 1 \\ \frac{1}{4} & \frac{1}{2} & 1 \\ 1 & 1 & 0 \end{pmatrix}^{-1} = \begin{pmatrix} 16 & -16 & 4 \\ -16 & 16 & -3 \\ 4 & -3 & \frac{1}{2} \end{pmatrix} \tag{5.4}$$

Hence, the equations for the parameters a_R, b_R, and c_R in dependence of the composite parameters $g_R\left(\frac{1}{4}\right), g_R\left(\frac{1}{2}\right)$, and $\frac{d}{dx} g_R(x)\big|_{x=\frac{1}{2}}$ are Equations (5.5) to (5.7).

$$a_R = 16 \cdot g_R\left(\frac{1}{4}\right) - 16 \cdot g_R\left(\frac{1}{2}\right) + 4 \cdot \frac{d}{dx} g_R(x)\Big|_{x=\frac{1}{2}} \tag{5.5}$$

$$b_R = -16 \cdot g_R\left(\frac{1}{4}\right) + 16 \cdot g_R\left(\frac{1}{2}\right) - 3 \cdot \frac{d}{dx} g_R(x)\Big|_{x=\frac{1}{2}} \tag{5.6}$$

$$c_R = 4 \cdot g_R\left(\frac{1}{4}\right) - 3 \cdot g_R\left(\frac{1}{2}\right) + \frac{1}{2} \cdot \frac{d}{dx} g_R(x)\Big|_{x=\frac{1}{2}} \tag{5.7}$$

5.3.2 Steep Parabola-shaped Branches $f_{\mathcal{A}}$ and f_C

The values of the composite parameters $g_R\left(\frac{1}{4}\right)$ and $\frac{d}{dx} g_R(x)\big|_{x=\frac{1}{2}}$ are fixed as described previously in Section 5.3.1. In this section, the values of the parameters of the function g_L are set to $a_L = 8$ and $b_L = -1$ to get steep, shifted parabola-shaped branches $f_{\mathcal{A}}$ and $f_{\mathcal{D}}$, as one can see in the cobweb diagrams in Figure 5.10. Scanning the periods for reasonable values of the parameters α and β results in Figure 5.9. The reasonable values for $\alpha = g_R\left(\frac{1}{4}\right)$ are larger than $\frac{1}{4}$ to keep the parabola above the bisector $y = x$ and smaller than $\frac{1}{2}$ to keep the value of the model function at the left borders of the branches $f_{\mathcal{B}}$ and $f_{\mathcal{D}}$ below the value of the model function at the right borders. For the specified values of a_L and b_L, the reasonable values for $\beta = c_L$ are smaller than 0.22 to not map the points directly onto the branch f_C from the branch $f_{\mathcal{A}}$. To keep the parabola above the bisector $y = x$, the values for β should also be larger than 0.12.

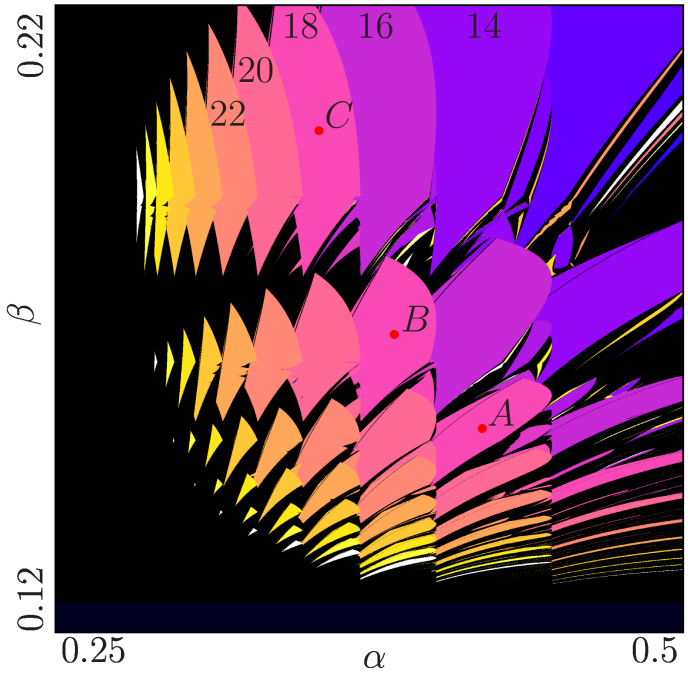

Figure 5.9: 2D scan of the periods associated with parameter regions in the piecewise-quadratic model with composite parameters and steep branches $f_{\mathcal{A}}$ and f_C. The parameters $a_L = 8, b_L = -1, g_R\left(\frac{1}{2}\right) = \frac{1}{2} + \frac{1}{40}$, and $\frac{d}{dx} g_R(x)\big|_{x=\frac{1}{2}} = 1.2$ are fixed. The parameters $\alpha = g_R\left(\frac{1}{4}\right)$ and $\beta = c_L$ are varied in the ranges $[0.25, 0.5]$ and $[0.12, 0.22]$. The points A, B, and C mark the parameter values used for the cobweb diagrams in Figure 5.10. Also, the numbers at the top indicate the period associated with the corresponding parameter regions.

With the newly chosen fixed parameters and the new composite parameters, this model imitates the shape of the original model function well still. The parameter c_L is also still varied and this emulates the effects of χ_0 on the branches $F_{\mathcal{A}}$ and F_C of the original model function well, as described in the previous section, Section 5.2. The other varied parameter is the composite parameter $g_R\left(\frac{1}{4}\right)$. Varying the parameter α is a major improvement for emulating the effects of E_0 on the branches $F_{\mathcal{B}}$ and $F_{\mathcal{D}}$ of the original model function. Increasing α primarily increases the values of the model function on the left sides of the branches $f_{\mathcal{B}}$ and $f_{\mathcal{D}}$ and keeps the values on the right sides the same. It also moves the local minima of those branches to the left and decreases the value of the model function at those points, just as the parameter E_0 did to the original model function.

Figure 5.9 shows a 2D scan of the periods associated with parameter regions in the specified parameter range for α and β. At the top, some periods are annotated. One can see that in the scan there are sequences of parameter regions that are associated with the same period. These sequences are next to each other, where each sequence is associated with a period that is two higher than the period associated with the parameter region sequence to the right of it. This is similar to the PI that can be observed in the original model, as described in Section 2.3.3. One difference is that the sequences in the original model were connected and formed chains.

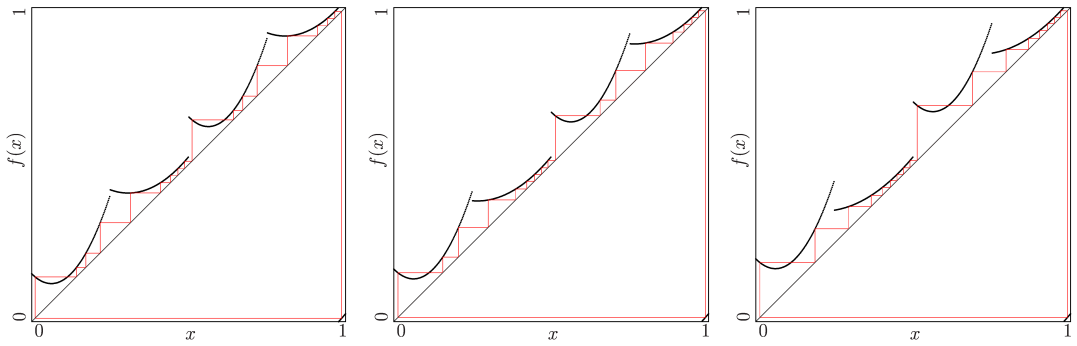

(a) A **(b)** B **(c)** C

Figure 5.10: Cobweb diagrams at three parameter values in the piecewise-quadratic model with composite parameters and steep branches. The $a_L = 8, b_L = -1, g_R\left(\frac{1}{2}\right) = \frac{1}{2} + \frac{1}{40}$, and $\frac{d}{dx} g_R(x)\big|_{x=\frac{1}{2}} = 1 + \frac{1}{5}$ are fixed. The parameters $\alpha = g_R\left(\frac{1}{2}\right)$ and $\beta = c_L$ are different in every diagram and their values are marked with points in Figure 5.9. (a) shows the cycle $O_{\mathcal{A}^4\mathcal{B}^5\mathcal{C}^4\mathcal{D}^5}$ at the point A where $\alpha = 0.42$ and $\beta = 0.1525$, (b) shows the cycle $O_{\mathcal{A}^3\mathcal{B}^6\mathcal{D}^3\mathcal{C}^6}$ at the point B where $\alpha = 0.385$ and $\beta = 0.1675$, and (c) shows the cycle $O_{\mathcal{A}^2\mathcal{B}^7\mathcal{C}^2\mathcal{D}^7}$ at the point C where $\alpha = 0.385$ and $\beta = 0.1675$.

Figure 5.10 shows cobweb diagrams for different parameter values along the sequence of parameter regions associated with the period 18. These parameter values are marked with points in Figure 5.9. Figure 5.10a shows the cycle at the point A with the symbolic sequence $\mathcal{A}^4\mathcal{B}^5\mathcal{C}^4\mathcal{D}^5$. Figure 5.10b shows the cycle at the point B with the symbolic sequence $\mathcal{A}^3\mathcal{B}^6\mathcal{C}^3\mathcal{D}^6$. Notice that the cycle at point B has one point less on the branches $f_{\mathcal{A}}$ and $f_{\mathcal{C}}$ each than the cycle at point A, while it has one point more on the branches $f_{\mathcal{B}}$ and $f_{\mathcal{D}}$ each. It is as if two points, one of each of the branches $f_{\mathcal{A}}$ and $f_{\mathcal{C}}$, moved to the next branch from one parameter region of the sequence to the next. Figure 5.10c shows the cycle at the point B with the symbolic sequence $\mathcal{A}^2\mathcal{B}^7\mathcal{C}^3\mathcal{D}^7$. Again, two points, one of each of the branches $f_{\mathcal{A}}$ and $f_{\mathcal{C}}$, moved to the next branch from the parameter region with point B to the parameter region with the point C. This is also very similar to the behavior of the original model, where two points, one of each of the branches $F_{\mathcal{A}}$ and $F_{\mathcal{C}}$, moved to the next branch each along the chain of parameter regions associated with the same period, as described in Section 2.3.3. Besides that the sequences of parameter region associated with the same period are not connected here, there is another difference to the behavior of the original model. In the original model there are “type B” parameter regions between the “type A” parameter regions of a chain of parameter regions with the same period. To reiterate, “type A” parameter regions are associated with a single symmetric cycle. These are the parameter regions, one can observe in this case also. Between two “type A” parameter regions there is a parameter region that is associated with two coexisting asymmetrical twin cycles, called “type B” parameter region. These “type B” parameter regions are missing in this case.

5.3.3 Shallow Parabola-shaped Branches $f_{\mathcal{A}}$ and f_C

To close the gaps in between the parameter regions in the sequences, the parameters of the function g_L that governs the shape of the branches $f_{\mathcal{A}}$ and f_C is adjusted. The new fixed parameter values are $a_L = 4$ and $b_L = -\frac{1}{2}$. And the other fixed parameters stay the same as in the previous section.

One can see in Figure 5.10 that the shape of the branches $f_{\mathcal{A}}$ and f_C is very steep. This is different from the branches $F_{\mathcal{A}}$ and F_C in the original model that were more shallow. The new fixed parameter values of a_L and b_L also cause the shape of the branches $f_{\mathcal{A}}$ and f_C to be more shallow. One can see this in the cobweb diagrams in Figure 5.12. The varied parameters are the same as in the previous section and therefore the parameter effects of E_0 and χ_0 on the original model function are emulated well. This was thoroughly described in the previous section, Section 5.3.2.

Figure 5.11 shows 2D scans of periods associated with parameter regions in this model. It shows 2 different versions of scans in the same parameter range, $\alpha \in [0.275, 0.35]$ and $\beta \in [0.15, 0.1875]$. The first scan in Figure 5.11a shows the periods of the model as we have seen it also in the previous sections. The second scan in Figure 5.11b shows the periods of the same model but halved. This reveals "type B" parameter regions as they are associated with higher periods than the "type A" parameter regions of the same chains in the halved model. The reason for this is covered in-depth in Section 7.3.2, but for now only the fact that it reveals "type B" parameter regions is important.

We can see in Figure 5.11a that the gap between the "type A" parameter regions of a sequence of parameter regions associated with the same period closed. Also, there are sections of the chains where they get narrower, for example at point C. In the original model one can observe the same narrowing of the chains. These narrower sections are "type B" parameter regions in the original model.

Figure 5.11b reveals "type B" parameter regions in the quadratic model with composite parameters. We can see that "type A" and "type B" parameter regions alternate in the chains of parameter regions associated with the same period. Also, the "type B" parameter regions are at the narrower sections of the chains. This is exactly the same behavior one can observe in the original model when examining the types of the parameter regions making up the chains and their arrangement.

The period the chains are associated with also still increments in neighboring chains as was observed in the last section, Section 5.3.2. Therefore, this structure is similar to the PI structure one can observe in the original model when looking at the periods associated with parameter regions and their types. But this is not the only characteristic of cycles. Therefore, the symbolic sequences of the cycles associated with the parameter regions making up the chains are analyzed next.

Figure 5.12 contains the cobweb diagrams for the cycles at the parameter values that are marked with points A, B, and C in Figure 5.11. This chain of parameter regions is associated with the period 30, therefore all the cycles shown here also have the period 30. The symbolic sequence of the cycle at point A is $\mathcal{A}^7\mathcal{B}^8\mathcal{C}^7\mathcal{D}^8$. It is a symmetric cycle and therefore the parameter region is of "type A". The symbolic sequence of the cycle at point C is $\mathcal{A}^6\mathcal{B}^9\mathcal{C}^6\mathcal{D}^9$. It is also a symmetric cycle and this parameter region is also of "type A". The parameter region with point C is the next "type A" parameter region after the parameter region with point A in the chain. And just like in the original model, one point of each of the branches $f_{\mathcal{A}}$ and f_C moved to the next branch.

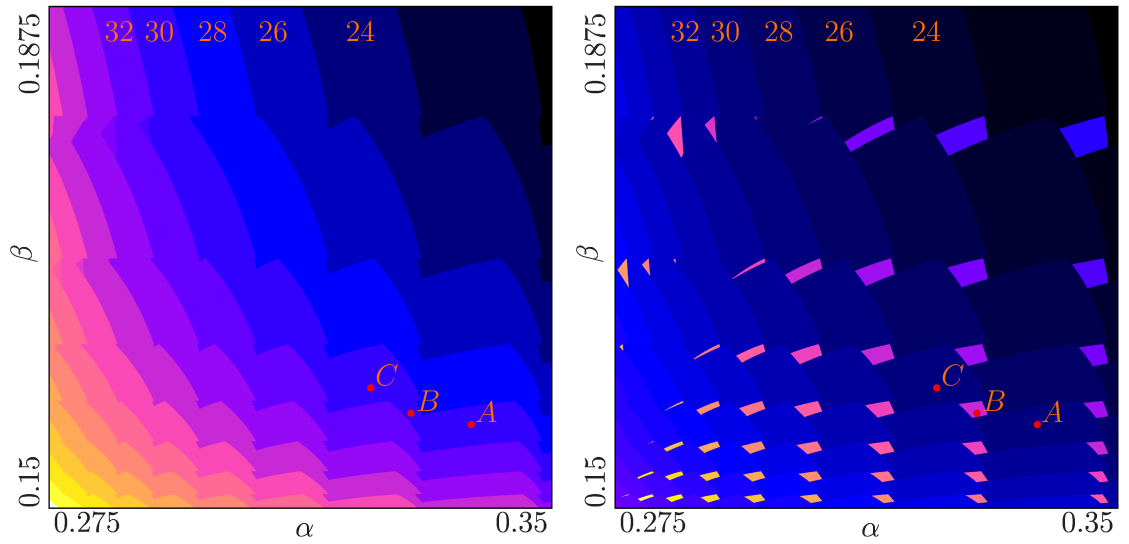

(a) Model **(b)** Halved model

Figure 5.11: 2D scan of the periods associated with parameter regions in the piecewise-quadratic model with composite parameters and shallow branches $f_{\mathcal{A}}$ and f_C. The parameters $a_L = 4, b_L = -\frac{1}{2}, g_R\left(\frac{1}{2}\right) = \frac{1}{2} + \frac{1}{40}$, and $\frac{d}{dx} g_R(x)\big|_{x=\frac{1}{2}} = 1.2$ are fixed. The parameters $\alpha = g_R\left(\frac{1}{4}\right)$ and $\beta = c_L$ are varied in the ranges $[0.275, 0.35]$ and $[0.15, 0.1875]$. The points A, B, and C mark the parameter values used for the cobweb diagrams in Figure 5.10. Also, the numbers at the top indicate the period associated with the corresponding parameter regions. (a) shows the scan for the model as defined above, while (b) shows the scan for the halved model where we can see "type B" parameter regions as they have higher periods than the "type A" parameter regions of the same chain.

Between those two "type A" parameter regions there is a narrower "type B" parameter region with the same period. It is marked with the point C. At this point, there are 2 coexisting cycles with the period 30. Their symbolic sequences are $\mathcal{A}^7\mathcal{B}^8C^6\mathcal{D}^9$ and $\mathcal{A}^6\mathcal{B}^9C^7\mathcal{D}^8$, respectively. This is exactly the same behavior that one can observe in the original model. Between two "type A" parameter regions with the cycles $O_{\mathcal{A}^a\mathcal{B}^bC^c\mathcal{D}^d}$ and $O_{\mathcal{A}^c\mathcal{B}^dC^c\mathcal{D}^d}$ there is a "type B" parameter region with the two coexisting cycles $O_{\mathcal{A}^a\mathcal{B}^bC^c\mathcal{D}^d}$ and $O_{\mathcal{A}^c\mathcal{B}^dC^c\mathcal{D}^d}$. Where $c = a - 1$ and $d = b + 1$.

Therefore, the bifurcation structure in this model fulfills all criteria, although it is mirrored. In the PI structure in the original model, the periods increased from left to right, here they increase from right to left. Also, the chains start in the lower left corner and go towards to the upper right corner, here they start in the lower right corner and go towards the upper left corner. But the model can still be simplified. The branches $f_{\mathcal{B}}$ and $f_{\mathcal{D}}$ are only increasing and almost linear. One can observe this in the cobweb diagrams in Figure 5.12.

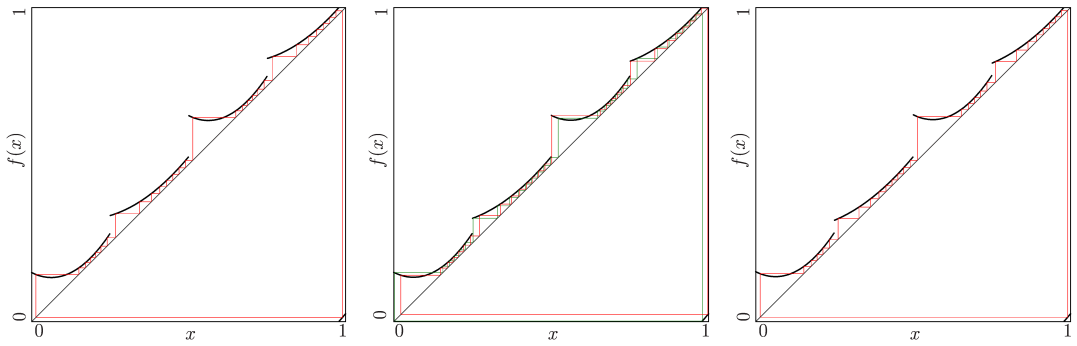

(a) A **(b)** B **(c)** C

Figure 5.12: Cobweb diagrams at three parameter values in the piecewise-quadratic model with composite parameters and shallow branches. The parameters $a_L = 4, b_L = -\frac{1}{2}, g_R\left(\frac{1}{2}\right) = \frac{1}{2} + \frac{1}{40}$, and $\frac{d}{dx} g_R(x)\big|_{x=\frac{1}{2}} = 1.2$ are fixed. The parameters $\alpha = g_R\left(\frac{1}{4}\right)$ and $\beta = c_L$ are different in every diagram and their values are marked with points in Figure 5.11. (a) shows the cycle $O_{\mathcal{A}^7\mathcal{B}^8C^7\mathcal{D}^8}$ the at point A where $\alpha = 0.338$ and $\beta = 0.15625$, (b) shows the two coexisting cycles $O_{\mathcal{A}^7\mathcal{B}^8C^7\mathcal{D}^8}$ shown in green and $O_{\mathcal{A}^6\mathcal{B}^9C^6\mathcal{D}^9}$ shown in red at the point $B$where $\alpha = 0.329$ and $\beta = 0.1571$, and (c) shows the cycle $O_{\mathcal{A}^6\mathcal{B}^9C^6\mathcal{D}^9}$ at the point $C$where $\alpha = 0.323$ and $\beta = 0.159$.

5.4 Archetypal Model

This section introduces the result of this chapter, the archetypal model. It is the model of the last section slightly modified. The branches $f_{\mathcal{B}}$ and $f_{\mathcal{D}}$ are replaced with linear branches and the parameter α is negated in order to mirror the bifurcation structure along the α axis.

5.4.1 Model Definition

The archetypal model is defined as the map $x_{n+1} = f(x_n) \mod 1$ where f is given by the following set of equations.

$$f(x) = \begin{cases} g(x) & \text{if } x < \frac{1}{2} \\ g(x - \frac{1}{2}) + \frac{1}{2} & \text{else} \end{cases} \tag{5.8}$$

$$g(x) = \begin{cases} g_L(x) = a_L \cdot x^2 + b_L \cdot x + c_L & \text{if } x < \frac{1}{4} \\ g_R(x) = b_R \cdot x + c_R & \text{else} \end{cases} \tag{5.9}$$

5.4.2 Parameters

Since the function g_R is now linear, only two composite parameters are necessary to control the shape of the branches $f_{\mathcal{B}}$ and $f_{\mathcal{D}}$. The chosen composite parameters are $g_R\left(\frac{1}{4}\right)$ and $g_R\left(\frac{1}{2}\right)$ and the composite parameter $\frac{d}{dx}g_R(x)\big|_{x=\frac{1}{2}}$ used in the previous sections is not used. As before, the value of the composite parameter $g_R\left(\frac{1}{2}\right) = \frac{1}{2} + \frac{1}{40}$ is fixed to be just above the bisector $y = x$, and the composite parameter $g_R\left(\frac{1}{4}\right)$ is varied.

$$g_R\left(\frac{1}{4}\right) = \frac{b_R}{4} + c_R \tag{5.10a}$$

$$g_R\left(\frac{1}{2}\right) = \frac{b_R}{2} + c_R \tag{5.10b}$$

Equations (5.10a) and (5.10b) are the equations for the values of $g_R\left(\frac{1}{4}\right)$ and $g_R\left(\frac{1}{2}\right)$. This is a system of equations that needs to be solved for the parameters b_R and c_R. As before, this is achieved by writing the system of equations as a matrix and computing the inverse matrix. Equation (5.11) demonstrates this.

$$\begin{pmatrix} \frac{1}{4} & 1 \\ \frac{1}{2} & 1 \end{pmatrix}^{-1} = \begin{pmatrix} -4 & 4 \\ 2 & -1 \end{pmatrix} \tag{5.11}$$

Hence, the equations for b_R and c_R in dependence of the composite parameters $g_R\left(\frac{1}{4}\right)$ and $g_R\left(\frac{1}{4}\right)$ are Equations (5.12) and (5.13).

$$b_R = -4 \cdot g_R\left(\frac{1}{4}\right) + 4 \cdot g_R\left(\frac{1}{2}\right) \tag{5.12}$$

$$c_R = 2 \cdot g_R\left(\frac{1}{4}\right) - 1 \cdot g_R\left(\frac{1}{2}\right) \tag{5.13}$$

As mentioned before, the parameter α is given a negative sign to mirror the PI structure. So $\alpha = -g_R\left(\frac{1}{4}\right)$ in the archetypal model. All parameters are listed in Table 5.2 a for better overview.

Model Parameter	Value
a_L	4
b_L	$-\frac{1}{2}$
c_L	β
b_R	$4 \cdot g_R\left(\frac{1}{2}\right) - 4 \cdot g_R\left(\frac{1}{4}\right)$
c_R	$2 \cdot g_R\left(\frac{1}{4}\right) - g_R\left(\frac{1}{2}\right)$
$g_R\left(\frac{1}{4}\right)$	$-\alpha$
$g_R\left(\frac{1}{2}\right)$	$\frac{1}{2} + \frac{1}{40}$

Table 5.2: Overview of the parameter values of all parameters of the archetypal model with the composite parameters $g_R\left(\frac{1}{4}\right)$ and $g_R\left(\frac{1}{2}\right)$. In the top part, there are all parameters of the function g_L, and in the bottom part are the parameters of the function g_R.

5.4.3 Parameter Effects

The effects of the defined parameters on the model function are straightforward and can be read directly from the previous section. In summary, the parameter α changes the values of the model function on the left sides of the branches $f_{\mathcal{B}}$ and $f_{\mathcal{D}}$. Where a lower value of α means a higher value of the model function in those regions, because the parameter has negative sign. In the previously defined notation, this is written as $\mathrm{L}^{-}_{\mathcal{B}}$. This notation is defined in Section 5.1.2. The parameter β changes the values of the model function on the whole branches $f_{\mathcal{A}}$ and f_C. A higher β means higher values, and it is written as $\mathrm{W}^{+}_{\mathcal{A}}$.

Figure 5.13 illustrates these parameter effects. Both figures show the model function for three parameter values, where either α or β is fixed, and the other parameter is varied. The model functions are labeled according to the value of the variable parameter, f^L for the lowest value, f^M for the middle value, and f^H for the highest value. Figure 5.13a illustrates the effect of α. One can see, how the values of the model function at the left borders of branches $f_{\mathcal{B}}$ and $f_{\mathcal{D}}$ are smaller for higher values of α. Figure 5.13b illustrates the effect of β. Here one can see, how the values of the model function for the whole branches $f_{\mathcal{A}}$ and f_C increase for larger values of β.

Table 5.3 lists the effects of parameters α and β in a table, like also done for the original model in Section 5.1.2. Additionally, the parameter effects of the parameters in the original model are listed for comparison. This gives a nice overview of which characteristics of the original model function are necessary for the observed bifurcation structure. Especially it shows, which parameter effects are not necessary. For example, the effect $\mathrm{Mi}^{L^-}_{\mathcal{B}}$ cannot even be fabricated in this model since branches $f_{\mathcal{B}}$ and $f_{\mathcal{D}}$ are linear and do not have a local minimum. Also, the effect $\mathrm{B}^{L}_{\mathcal{B}C}$, which is the movement of the borders between branches $f_{\mathcal{B}}$ and f_C (and $f_{\mathcal{D}}$ and $f_{\mathcal{A}}$ respectively), is not necessary.

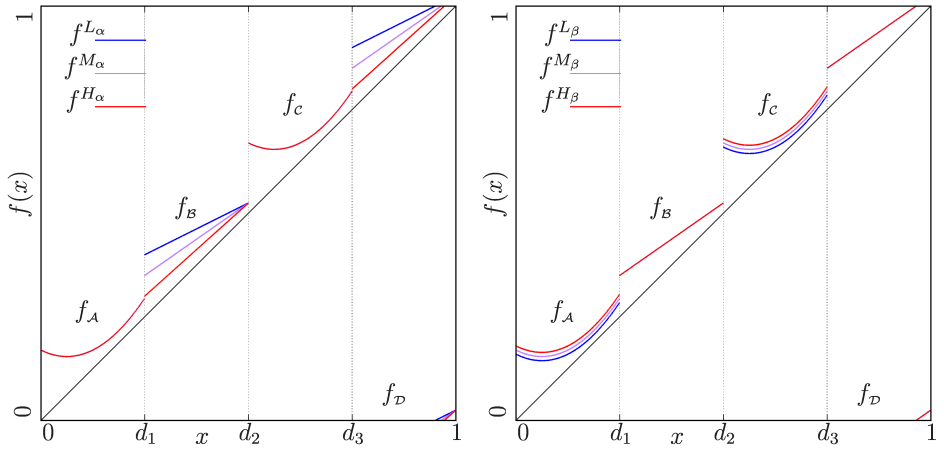

(a) α **(b)** β

Figure 5.13: The isolated effects of the parameters $\alpha = g_R\left(\frac{1}{4}\right)$ and $\beta = c_L$ on the archetypal model function. (a) shows the evolution of the shape of the model function for different values of α while $\beta = 0.17$ is fixed. The function $f^{L\alpha}$ is the model function with $\alpha = -0.4$, f^{M_α} with $\alpha = -0.35$, and f^{H_α} with $\alpha = -0.3$. (b) shows the evolution of the shape of the model function for different values of β while $\alpha = -0.35$ is fixed. The function f^{L_β} is the model function with $\beta = 0.16$, f^{M_β} with $\beta = 0.17$, and f^{H_β} with $\beta = 0.18$.

Combined	E_0	χ_0	α	β
$\mathrm{L}^-_{\mathcal{B}}$	$\mathrm{L}^-_{\mathcal{B}}$		$\mathrm{L}^-_{\mathcal{B}}$	
$\mathrm{Mi}^{L-}_{\mathcal{B}}$	$\mathrm{Mi}^{L-}_{\mathcal{B}}$	$-\mathrm{Mi}^+_{\mathcal{B}}$		
$\mathrm{W}^+_{\mathcal{A}}$		$\mathrm{W}^+_{\mathcal{A}}$		$\mathrm{W}^+_{\mathcal{A}}$
$\mathrm{B}^L_{\mathcal{B}C}$		$\mathrm{B}^L_{\mathcal{B}C}$		
	$\mathrm{B}^R_{\mathcal{A}\mathcal{B}}$	$-\mathrm{B}^L_{\mathcal{A}\mathcal{B}}$		

Table 5.3: Table comparing the effects of the parameters E_0 and χ_0 on the original model function and the effects of α and β on the archetypal model function. Each effect of the parameters E_0 and χ_0 as listed in Table 5.1 is also listed here. If α or β cause the same effect, it is also listed in the respective column.

5.4.4 Behavior

Figure 5.14 shows the 2D scans of the periods associated with parameter regions in the archetypal model. As before, Figure 5.14b shows the halved model to indicate "type B" parameter regions. The structure is not very different from the previous constructed model in Section 5.3.3. There are still chains of parameter regions associated with the same period next to each other with the period increasing by two for each chain. And the types of the parameter regions in each chain alternate between "type A" and "type B". Now the "type B" parameter regions are even more prominent in the chains for larger values of β. This was not the case in the previous model with four quadratic branches.

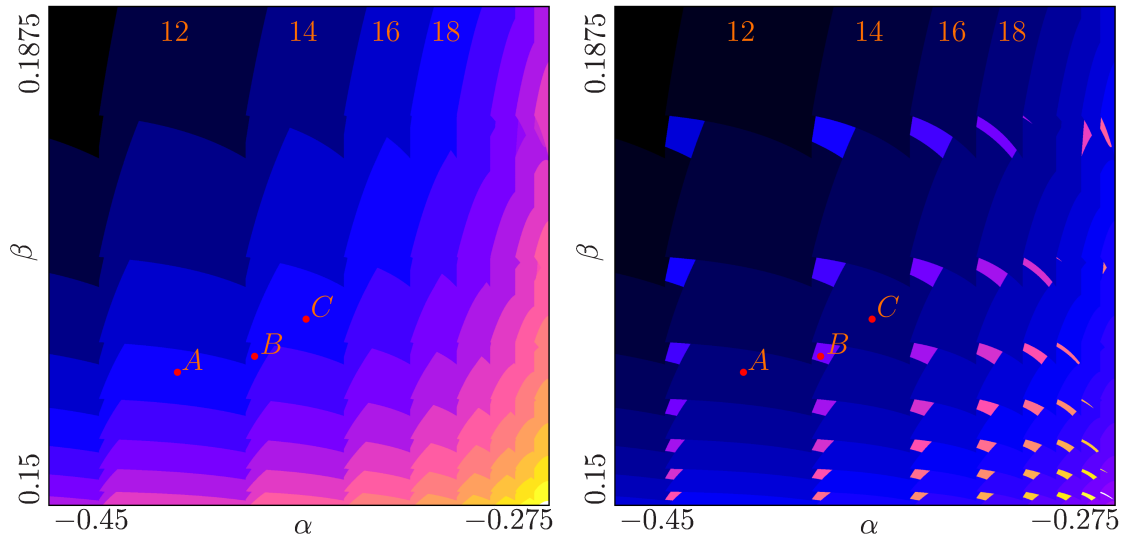

(a) Model **(b)** Halved Model

Figure 5.14: 2D scans of the periods associated with parameter regions in the archetypal model. The parameters $a_L = 4, b_L = -\frac{1}{2}$, and $g_R\left(\frac{1}{2}\right) = \frac{1}{2} + \frac{1}{40}$ are fixed. The parameters $\alpha = -g_R\left(\frac{1}{4}\right)$ and $\beta = c_L$ are varied in the ranges $[-0.45, -0.275]$ and $[0.15, 0.1875]$, respectively. The points A, B, and C mark the parameter values used for the cobweb diagrams in Figure 5.15. (a) shows the scan for the model as defined above, while (b) shows the scan for the halved model where we can see "type B" parameter regions as they have higher periods than the "type A" parameter regions of the same chain.

Figure 5.15 shows cobweb diagrams at the parameter values that are marked with points in Figure 5.14, as also done in previous sections of this chapter. Here, the model also behaves like the original model with the symbolic sequence of the cycle at the point A being $\mathcal{A}^6\mathcal{B}^3\mathcal{C}^6\mathcal{D}^3$, at the point C being $\mathcal{A}^5\mathcal{B}^4\mathcal{C}^5\mathcal{D}^4$, and in between both parameter regions associated with each cycle, two coexisting cycles with the symbolic sequences $\mathcal{A}^6\mathcal{B}^3\mathcal{C}^5\mathcal{D}^4$ and $\mathcal{A}^5\mathcal{B}^4\mathcal{C}^6\mathcal{D}^3$ at the point C. The next chapter covers the behavior of the archetypal model in-depth.

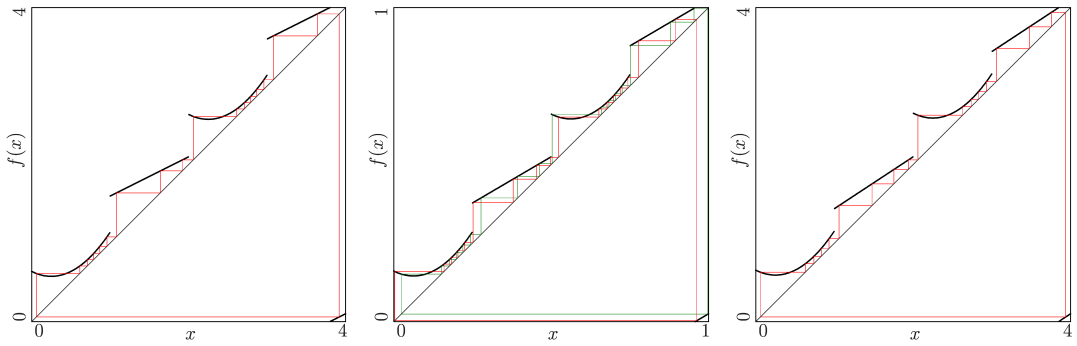

(a) A **(b)** B **(c)** C

Figure 5.15: Cobweb diagrams at three parameter values in the archetypal model. The parameters $a_L = 4, b_L = -\frac{1}{2}$, and $g_R\left(\frac{1}{2}\right) = \frac{1}{2} + \frac{1}{40}$ are fixed. The parameters $\alpha = -g_R\left(\frac{1}{4}\right)$ and $\beta = c_L$ are different in every diagram and their values are marked with point in Figure 5.14. (a) shows the cycle $O_{\mathcal{A}^6\mathcal{B}^3\mathcal{C}^6\mathcal{D}^3}$ the at point $A$where $\alpha = -0.4$ and $\beta = 0.16$, (b) shows the two coexisting cycles $O_{\mathcal{A}^6\mathcal{B}^3\mathcal{C}^5\mathcal{D}^4}$ (green) and $O_{\mathcal{A}^5\mathcal{B}^4\mathcal{C}^6\mathcal{D}^3}$ (red) at the point $B$where $\alpha = -0.378$ and $\beta = 0.1612$, and (c) shows the cycle $O_{\mathcal{A}^5\mathcal{B}^4\mathcal{C}^5\mathcal{D}^4}$ at the point $C$where $\alpha = -0.36$ and $\beta = 0.164$.

6 Dynamics of the Archetypal Model

This chapter analyzes the dynamics of the archetypal model that was defined in the last chapter in Section 5.4.1. Its purpose is to confirm that this model really shows the same bifurcation structure as the original model. The first section, Section 6.1, is an overview of the overall dynamics of the archetypal model. The section after that, Section 6.2, takes an in-depth look at the bifurcations at the boundaries of the different parameter regions. And finally, Section 6.2 explores all the possible coexistence scenarios in the archetypal model.

6.1 Model Dynamics

As already hinted at in Section 5.4.4, the dynamics of this archetypal model are similar to the dynamics of the original model. This section examines the behavior more thoroughly. Figure 6.1 displays 2D scans showing the periods of the stable cycles associated with parameter regions in the archetypal model with fixed parameters $a_L = 4, b_L = -\frac{1}{2}$, and $g_R\left(\frac{1}{2}\right) = \frac{1}{2} + \frac{1}{40}$. The parameters $\alpha = -g_R\left(\frac{1}{4}\right)$ and $\beta = c_R$ are varied in the ranges $[-0.55, -0.275]$ and $[0.15, 0.1875]$, respectively. As before in Figures 5.11 and 5.14, the first scan, Figure 6.1a, shows the periods associated with parameter regions in the archetypal model and the second scan, Figure 6.1b, shows the periods associated with parameter regions in the halved archetypal model. It was preliminarily defined in Section 5.3 and Section 7.3.2 defines it formally.

As in [Aky22], this section examines the chain of parameter regions associated with stable cycles of period 16. The parameter regions are marked with the points A_{16} to G_{16} in Figure 6.1. Figures 6.2a to 6.2c shows cobweb diagrams for the points A_{16}, B_{16}, and C_{16}. The parameter region containing A_{16} is denoted $\mathcal{P}_{\mathcal{A}^7\mathcal{B}\mathcal{C}^7\mathcal{D}}$ since it only associated with the stable cycle $\mathcal{O}_{\mathcal{A}^7\mathcal{B}\mathcal{C}^7\mathcal{D}}$. Figure 2.4a shows the cobweb diagram of this cycle. The parameter region, therefore, is a "type A" parameter region associated with only one stable cycle of period 16. The next parameter region contains the point B_{16} and is associated with two stable cycles $\mathcal{O}_{\mathcal{A}^7\mathcal{B}\mathcal{C}^6\mathcal{D}^2}$ and $\mathcal{O}_{\mathcal{A}^6\mathcal{B}^2\mathcal{C}^7\mathcal{D}}$. Figure 2.4b shows the cobweb diagram of these two cycles. The parameter region containing these cycles is denoted $\mathcal{P}_{\mathcal{A}^7\mathcal{B}\mathcal{C}^6\mathcal{D}^2,\mathcal{A}^6\mathcal{B}^2\mathcal{C}^7\mathcal{D}}$. By the same logic, the parameter region marked with point C_{16} is denoted $\mathcal{P}_{\mathcal{A}^6\mathcal{B}^2\mathcal{C}^6\mathcal{D}^2}$. Figure 6.2c shows the cobweb diagram of that cycle.

Thus far these parameter regions follow the rules laid out in [Aky22] and listed again in Section 2.3.3. The first parameter region has the stable cycle $\mathcal{O}_{\mathcal{A}^{\frac{P}{2}-1}\mathcal{B}\mathcal{C}^{\frac{P}{2}-1}\mathcal{D}}$ where $P = 16$ is the period. It is a "type A" parameter region and the next parameter region is of "type B", as the rules require. This parameter region has the stable cycles $\mathcal{O}_{\mathcal{A}^{\frac{P}{2}-1}\mathcal{B}\mathcal{C}^{\frac{P}{2}-2}\mathcal{D}^2}$ and $\mathcal{O}_{\mathcal{A}^{\frac{P}{2}-2}\mathcal{B}^2\mathcal{C}^{\frac{P}{2}-1}\mathcal{D}}$. This also agrees with the rules. The next parameter region is of "type A" again and has the stable cycle $\mathcal{O}_{A^{\frac{P}{2}-1}\mathcal{B}^2\mathcal{C}^{\frac{P}{2}-2}\mathcal{D}^2}$

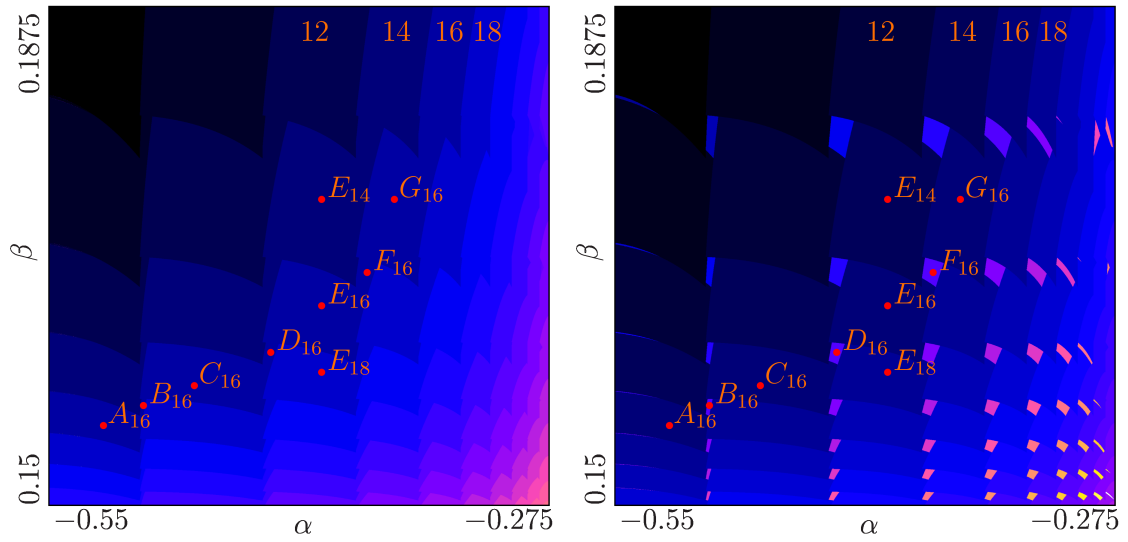

(a) Model **(b)** Halved Model

Figure 6.1: 2D scans of the periods associated with parameter regions in the archetypal model. The parameters $a_L = 4, b_L = -\frac{1}{2}$, and $g_R\left(\frac{1}{2}\right) = \frac{1}{2} + \frac{1}{40}$ are fixed. The parameters $\alpha = -g_R\left(\frac{1}{4}\right)$ and $\beta = c_L$ are varied in the ranges $[-0.55, -0.275]$ and $[0.15, 0.1875]$. The points $A_{16}, B_{16}, C_{16}, D_{16}, E_{16}$, and F_{16} mark the parameter values used for the cobweb diagrams in Figure 6.2. (a) shows the scan for the archetypal model as defined above, while (b) shows the scan of the halved archetypal model where we can see "type B" parameter regions.

as expected by the rules. This chain continues to abide by the rules as can be seen in the cobweb diagrams of points D_{16}, E_{16}, and F_{16} in Figures 6.2d to 6.2f. The corresponding parameter regions are $\mathcal{P}_{\mathcal{A}^6\mathcal{B}^2\mathcal{C}^5\mathcal{D}^3,\mathcal{A}^5\mathcal{B}^3\mathcal{C}^6\mathcal{D}^2}$, $\mathcal{P}_{\mathcal{A}^5\mathcal{B}^3\mathcal{C}^5\mathcal{D}^3}$, and $\mathcal{P}_{\mathcal{A}^5\mathcal{B}^3\mathcal{C}^4\mathcal{D}^4,\mathcal{A}^4\mathcal{B}^4\mathcal{C}^5\mathcal{D}^3}$ respectively.

The stable cycle in the parameter region marked with point E_{14} has period 14. This agrees with the rule that the neighboring chains differ in their periods by 2. Its symbolic sequence is $\mathcal{A}^4\mathcal{B}^3\mathcal{C}^4\mathcal{D}^3$ and its cobweb diagram can be seen in Figure 6.2h. Similarly, the cycle associated with the parameter regions marked with E_{16} has period 16. Its symbolic sequence is $\mathcal{A}^6\mathcal{B}^3\mathcal{C}^6\mathcal{D}^3$ and its cobweb diagram can be seen in Figure 6.2e. So the cycles in the "type A" regions directly above another "type A" parameter region with stable cycle $O_{\mathcal{A}^a\mathcal{B}^b\mathcal{C}^a\mathcal{D}^b}$ has the stable cycle $O_{\mathcal{A}^{a-1}\mathcal{B}^b\mathcal{C}^{a-1}\mathcal{D}^b}$.

The regularities of symbolic sequences associated with "type A" parameter regions that are neighboring horizontally is explored next. The parameter region with point C_{16} is directly left of the parameter region with point E_{18}. It has the stable cycle $O_{\mathcal{A}^6\mathcal{B}^2\mathcal{C}^6\mathcal{D}^2}$, while the parameter region with point E_{18} has the stable cycle $O_{\mathcal{A}16\mathcal{B}^3\mathcal{C}^6\mathcal{D}^3}$. Similarly, the stable cycle in the parameter region marked with point G_{16} which is directly right of the parameter region marked with point E_{14} that has the stable cycle $O_{\mathcal{A}^4\mathcal{B}^4\mathcal{C}^4\mathcal{D}^4}$, has the stable cycle $O_{\mathcal{A}^4\mathcal{B}^3\mathcal{C}^4\mathcal{D}^3}$. Therefore, the cycles in the "type A" regions directly left of another "type A" parameter region with stable cycle $O_{\mathcal{A}^a\mathcal{B}^b\mathcal{C}^a\mathcal{D}^b}$ has the stable cycle $O_{\mathcal{A}^a\mathcal{B}^{b-1}\mathcal{C}^a\mathcal{D}^{b-1}}$. Figures 6.2g to 6.2i show the cobweb diagrams of the archetypal model at the points G_{16}, E_{14}, and E_{18}.

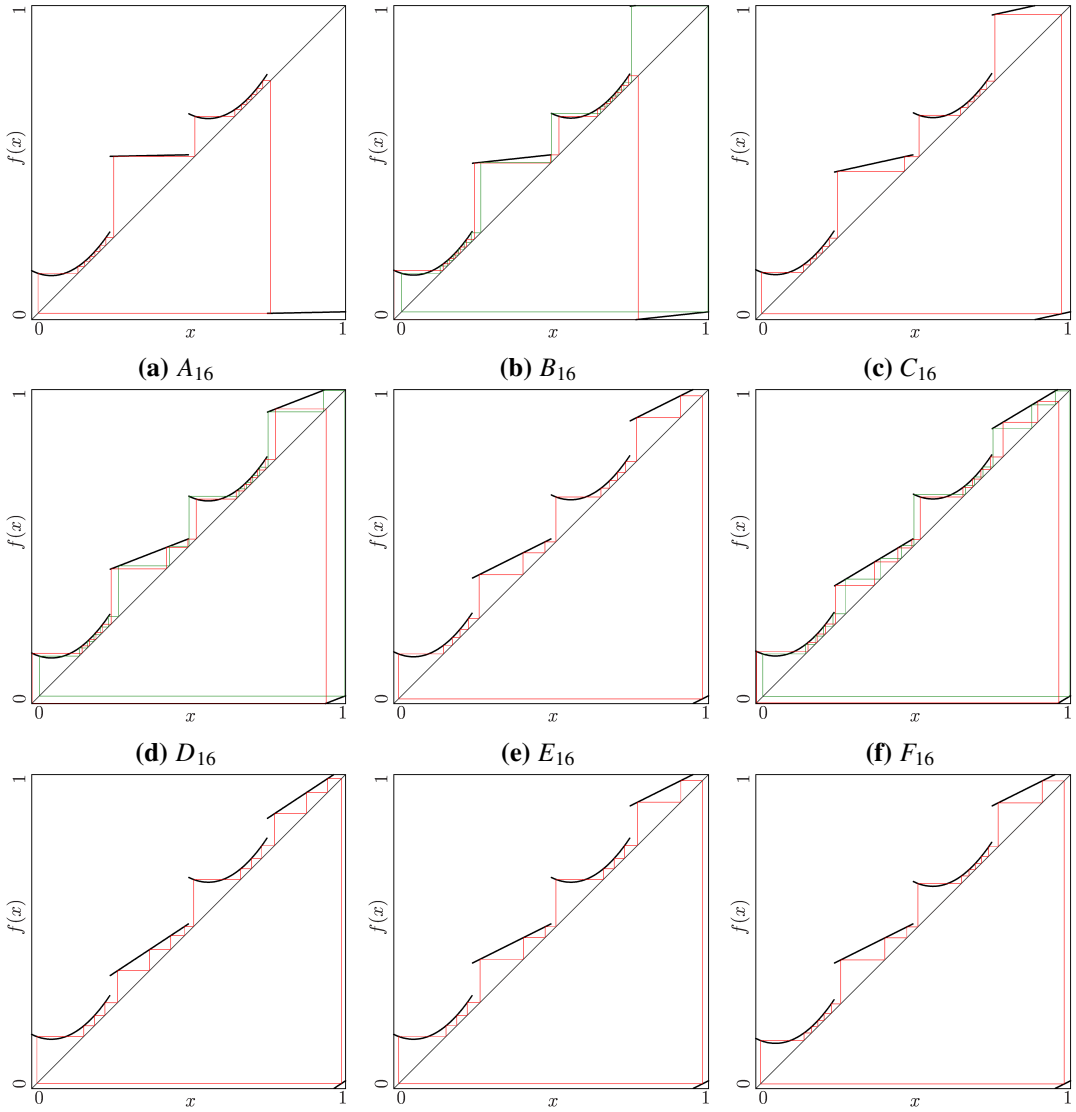

(a) A_{16} **(b)** B_{16} **(c)** C_{16}

(d) D_{16} **(e)** E_{16} **(f)** F_{16}

(g) G_{16} **(h)** E_{14} **(i)** E_{18}

Figure 6.2: Cobweb diagrams at nine parameter values in the archetypal model. The parameters $a_L = 4, b_L = -\frac{1}{2}$, and $g_R\left(\frac{1}{2}\right) = \frac{1}{2} + \frac{1}{40}$ are fixed. The parameters $\alpha = -g_R\left(\frac{1}{4}\right)$ and $\beta = c_L$ are different in every diagram and their values are marked with points in Figure 6.1. (a) shows the cycle $O_{\mathcal{A}^7\mathcal{B}^1C^7\mathcal{D}^1}$ at the point A_{16} where $\alpha = -0.52$ and $\beta = 0.156$, (b) shows the two coexisting cycles $O_{\mathcal{A}^7\mathcal{B}^1C^6\mathcal{D}^2}$ shown in green and $O_{\mathcal{A}^6\mathcal{B}^2C^7\mathcal{D}^1}$ shown in red at the point B_{16} where $\alpha = -0.498$ and $\beta = 0.1575$, (c) shows the cycle $O_{\mathcal{A}^6\mathcal{B}^2C^6\mathcal{D}^2}$ at the point C_{16} where $\alpha = -0.47$ and $\beta = 0.159$, (d) shows the cycle $O_{\mathcal{A}^6\mathcal{B}^2C^6\mathcal{D}^2}$ at the point D_{16} where $\alpha = -0.428$ and $\beta = 0.1615$, (e) shows the two coexisting cycles $O_{\mathcal{A}^6\mathcal{B}^2C^5\mathcal{D}^3}$ shown in green and $O_{\mathcal{A}^5\mathcal{B}^3C^6\mathcal{D}^2}$ shown in red at the point E_{16} where $\alpha = -0.4$ and $\beta = 0.165$, (f) shows the cycle $O_{\mathcal{A}^5\mathcal{B}^3C^5\mathcal{D}^3}$ at the point C_{16} where $\alpha = -0.367$ and $\beta = 0.173$, (g) shows the cycle $O_{\mathcal{A}^5\mathcal{B}^3C^5\mathcal{D}^3}$ at the point G_{16} where $\alpha = -0.36$ and $\beta = 0.173$, (h) shows the cycle $O_{\mathcal{A}^4\mathcal{B}^3C^4\mathcal{D}^3}$ at the point E_{14} where $\alpha = -0.4$ and $\beta = 0.173$, and (i) shows the cycle $O_{\mathcal{A}^6\mathcal{B}^3C^6\mathcal{D}^3}$ at the point E_{18} where $\alpha = -0.4$ and $\beta = 0.16$.

These regularities of horizontally and vertically neighboring "type A" parameter regions make sense. From Section 5.4.3 we know that the effect of increasing α is that the values of the model function get smaller on the left sides of the branches $f_{\mathcal{B}}$ and $f_{\mathcal{D}}$. This leads to a narrower canal between the branches $f_{\mathcal{B}}$ and $f_{\mathcal{D}}$ and the bisector $x = y$. Cycles thus have more points on these branches. This explains why the cycles associated with the "type A" parameter region to the right of another "type A" parameter region have one point more on each of the branches $f_{\mathcal{B}}$ and $f_{\mathcal{D}}$. Similarly, we know from Section 5.4.3 that the effect of decreasing β is that the values of the model function get smaller on the whole branches $f_{\mathcal{A}}$ and f_C. This leads to a narrower canal between the branches $f_{\mathcal{A}}$ and f_C and the bisector $x = y$. This explains why the cycles associated with the "type A" parameter region below another "type A" parameter region have one point more on each of the branches $f_{\mathcal{A}}$ and f_C.

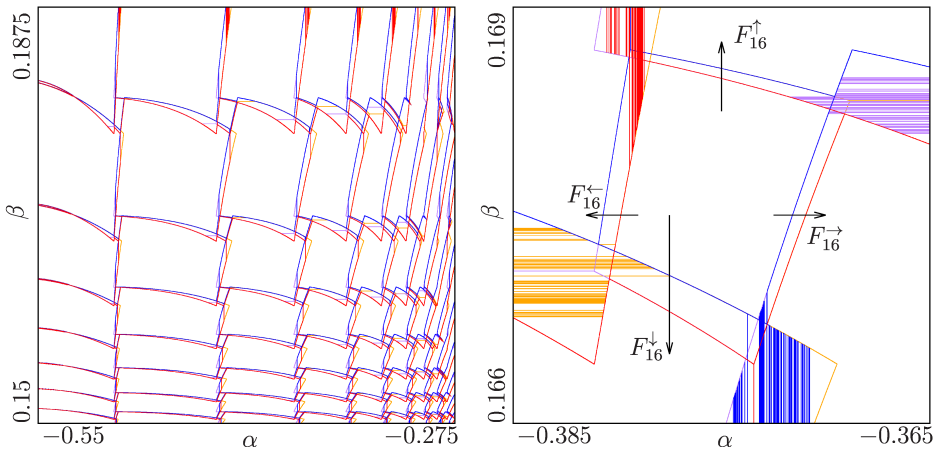

(a) Full **(b)** Zoomed-in

Figure 6.3: 2D scans of the boundaries of parameter regions with different symbolic sequences in the archetypal model. The parameters $a_L = 4, b_L = -\frac{1}{2}$, and $g_R\left(\frac{1}{2}\right) = \frac{1}{2} + \frac{1}{40}$ are fixed. The parameters $\alpha = -g_R\left(\frac{1}{4}\right)$ and $\beta = c_L$ are varied in different ranges. (a) shows full version with the parameters being varied in the ranges $[-0.55, -0.275]$ and $[0.15, 0.1875]$. (b) shows the zoomed-in version with the parameters being varied in the ranges $[-0.385, -0.365]$ and $[0.166, 0.169]$. It focuses on the "type B" parameter region marked with point F_{16} in Figure 6.1. Its boundaries are marked with $F_{16}^{\uparrow}, F_{16}^{\downarrow}, F_{16}^{\leftarrow}$, and $F_{16}^{\rightarrow}$.

6.2 Bifurcations

This section explores the bifurcations that happen at the borders of "type A" and "type B" parameter regions, respectively. Figure 6.3a shows the borders of the parameter regions in full. Figure 6.3b is a zoomed-in version that pictures the parameter region that contains the point F_{16} of Figure 6.1. It is a "type B" parameter region with the stable cycles $O_{\mathcal{A}^5\mathcal{B}^3C^4\mathcal{D}^4}$ and $O_{\mathcal{A}^4\mathcal{B}^4C^5\mathcal{D}^3}$. Every one of its boundaries has a "type A" parameter region on the other side. Therefore, this section only describes the four boundaries of this "type B" parameter region in depth to cover all the boundaries of both "type A" and "type B" parameter regions.

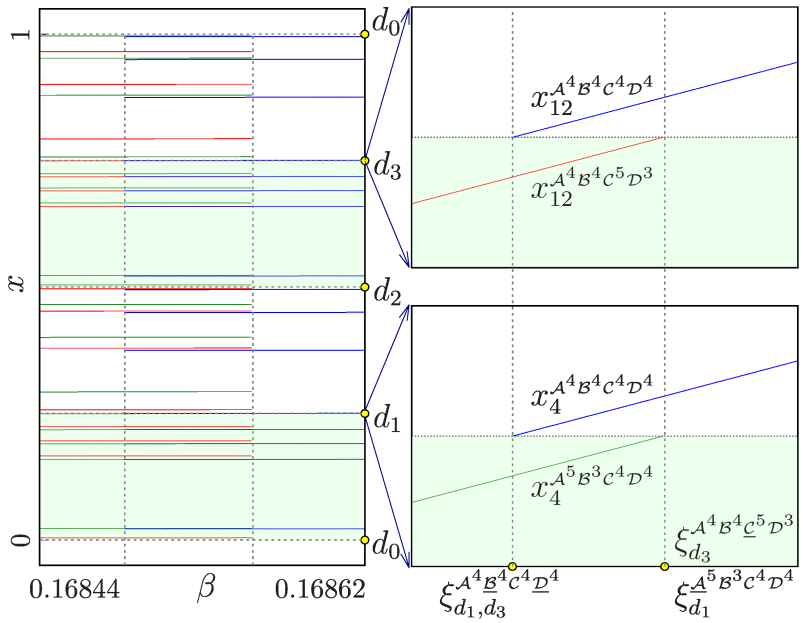

Figure 6.4: 1D bifurcation diagram at the boundary $F_{16}^{\uparrow}$ in the archetypal model. The parameters $a_L = 4, b_L = -\frac{1}{2}, g_R\left(\frac{1}{2}\right) = \frac{1}{2} + \frac{1}{40}$, and $\alpha = -g_R\left(\frac{1}{4}\right) = -0.375$ are fixed. The parameter $\beta = c_L$ is varied in the range $[0.16844, 0.16862]$ marked with an arrow in Figure 6.3b. On the left, the whole state space is pictured while the right side enhances the area of the state space around the borders involved in the pictured border collision bifurcations.

The boundaries of the parameter region containing F_{16} are named $F_{16}^{\uparrow}$ for the upper boundary, $F_{16}^{\downarrow}$ for the lower boundary, $F_{16}^{\leftarrow}$ for the left boundary, and finally $F_{16}^{\rightarrow}$ for the right boundary. These boundaries are also marked with arrows in Figure 6.3b. The first boundary that is covered is $F_{16}^{\uparrow}$.

6.2.1 The Boundary $F_{16}^{\uparrow}$

Figure 6.4 shows the bifurcation diagram of the first considered boundary, $F_{16}^{\uparrow}$. To better differentiate between the two coexisting "type B" cycles of the parameter region marked with point F_{16}, they are plotted in different colors. The cycle $O_{\mathcal{A}^5\mathcal{B}^3\mathcal{C}^4\mathcal{D}^4}$ is shown in green and its twin cycle $O_{\mathcal{A}^4\mathcal{B}^4\mathcal{C}^5\mathcal{D}^3}$ is shown in red. One can see that the cycle $O_{\mathcal{A}^5\mathcal{B}^3\mathcal{C}^4\mathcal{D}^4}$ shown in green collides with the border d_1 when it vanishes. To be more precise, the point $x_4^{\mathcal{A}^5\mathcal{B}^3\mathcal{C}^4\mathcal{D}^4}$ which is the 5th point of the cycle $O_{\mathcal{A}^5\mathcal{B}^3\mathcal{C}^4\mathcal{D}^4}$ collides with the border d_1. This is a border collision bifurcation, and it is denoted as $\xi_{d_1}^{\underline{\mathcal{A}}^5\mathcal{B}^3\mathcal{C}^4\mathcal{D}^4}$.

The lower index of ξ indicates the border of the model function that is involved in the bifurcation. The upper index of ξ indicates two things. First, the object that collides with the border of the model function. In our case this is the cycle $O_{\mathcal{A}^5\mathcal{B}^3\mathcal{C}^4\mathcal{D}^4}$. Second, the underlined symbol indicates the branch of the model function, the colliding point of the cycle belongs to. Together with the information which border is involved in the border collision bifurcation, one can determine which point of the cycle collided with the border. For example, we know that a point of the cycle on

branch $f_{\mathcal{A}}$ collides with the border d_1, which is the right border of the branch $f_{\mathcal{A}}$. Since there are 5 points on branch $f_{\mathcal{A}}$, we can derive that the point $x_4^{\mathcal{A}^5\mathcal{B}^3C^4\mathcal{D}^4}$ is involved in the border collision bifurcation.

A similar thing that happens to cycle $O_{\mathcal{A}^5\mathcal{B}^3C^4\mathcal{D}^4}$ shown in green in Figure 6.4 happens to its twin cycle $O_{\mathcal{A}^4\mathcal{B}^4C^5\mathcal{D}^3}$ red but shifted by $\frac{1}{2}$ in the state space because of the symmetry in the model. Here, the point $x_{12}^{A^4\mathcal{B}^4C^5\mathcal{D}^3}$ collides with the border d_3 and the bifurcation is denoted as $\xi_{d_3}^{A^4\mathcal{B}^4\underline{C}^5\mathcal{D}^3}$. In both cases, the cycles collide from the left side of the border.

The "type A" parameter region above is $\mathcal{P}_{\mathcal{A}^4\mathcal{B}^4C^4\mathcal{D}^4}$. The cycle $O_{\mathcal{A}^4\mathcal{B}^4C^4\mathcal{D}^4}$ shown in blue, which is stable in that parameter region, collides with the same borders the "type B" cycles collide with, d_1 and d_3. But here, two points of the same cycle collide with two different borders at the same parameter values. Point $x_4^{A^4\mathcal{B}^4C^4\mathcal{D}^4}$ collides with the border d_1 while point $x_{12}^{A^4\mathcal{B}^4C^4\mathcal{D}^4}$ collides with d_3. Both collisions happen from the right side of the borders. So one point of the cycle on the branch $f_{\mathcal{B}}$ collides with d_1 and one point on the branch $f_{\mathcal{D}}$ collides with d_3. This is unusual for border collision bifurcations but is explained by the symmetry of both the cycle and the model function. The bifurcation is denoted as $\xi_{d_1,d_3}^{\mathcal{A}^4\underline{\mathcal{B}}^4C^4\underline{\mathcal{D}}^4}$.

6.2.2 The Boundary $F_{16}^{\downarrow}$

At the lower boundary $F_{16}^{\downarrow}$, the two cycles $O_{\mathcal{A}^5\mathcal{B}^3C^4\mathcal{D}^4}$ and $O_{\mathcal{A}^4\mathcal{B}^4C^5\mathcal{D}^3}$ also collide with the borders d_1 and d_3, this time from the right side of the borders. But while the cycle $O_{\mathcal{A}^5\mathcal{B}^5C^4\mathcal{D}^4}$ shown in green collides with the border d_1 at the upper boundary, here it collides with the border d_3. To be more precise, the point $x_{12}^{\mathcal{A}^5\mathcal{B}^3C^4\mathcal{D}^4}$ collides with the border d_3. Meaning one point on the branch $f_{\mathcal{D}}$ collides with the border d_3. This border collision bifurcation is written as $\xi_{d_3}^{\mathcal{A}^5\mathcal{B}^3C^4\underline{\mathcal{D}}^4}$. Similarly, the point $x_4^{\mathcal{A}^4\mathcal{B}^4C^5\mathcal{D}^3}$ of the cycle $O_{\mathcal{A}^4\mathcal{B}^4C^5\mathcal{D}^3}$ shown in red now collides with the border d_1 from the right side of the border. Meaning that one point of branch $f_{\mathcal{B}}$ collides with the border d_1. This border collision bifurcation is written as $\xi_{d_1}^{\mathcal{A}^4\underline{\mathcal{B}}^4C^5\mathcal{D}^3}$.

The "type A" parameter region below the "type B" parameter region is $\mathcal{P}_{\mathcal{A}^5\mathcal{B}^3C^5\mathcal{D}^3}$. The cycle $\mathcal{P}_{\mathcal{A}^5\mathcal{B}^3C^5\mathcal{D}^3}$ shown in blue collides with the same borders as the "type B" cycles, just like before at the upper boundary $F_{16}^{\uparrow}$. Again, two points of this cycle collide with two different borders, d_1 and d_2, at the same parameter values. But here they collide from the left side. The point colliding with d_1 is $x_4^{A^5\mathcal{B}^3C^5\mathcal{D}^3}$ and the point colliding with d_3 is $x_{12}^{A^5\mathcal{B}^3C^5\mathcal{D}^3}$. So one point on the branch $f_{\mathcal{A}}$ collides with the border d_1 and one point on the branch f_C collides with the border d_3. This bifurcation is written as $\xi_{d_1,d_3}^{\underline{\mathcal{A}}^5\mathcal{B}^3\underline{C}^5\mathcal{D}^3}$.

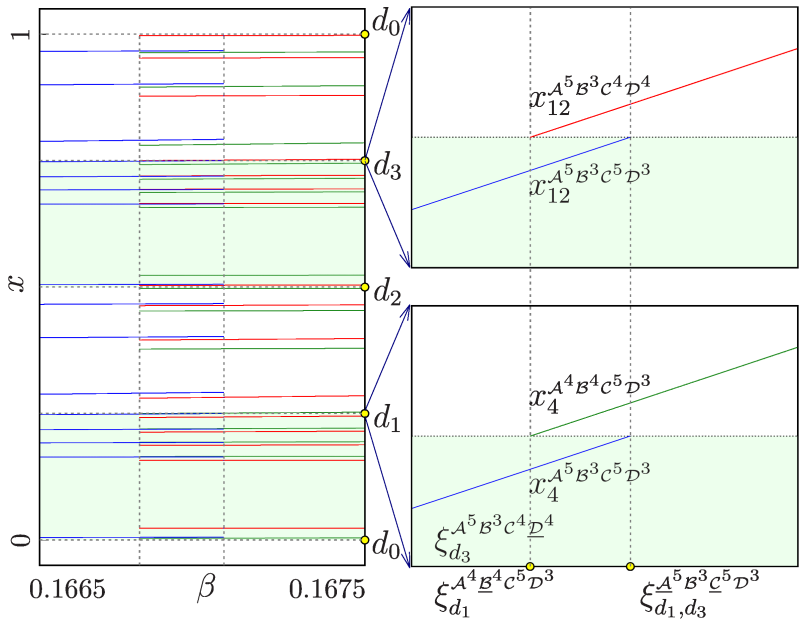

Figure 6.5: 1D bifurcation diagram at the boundary $F_{16}^{\downarrow}$ in the archetypal model. The parameters $a_L = 4, b_L = -\frac{1}{2}, g_R\left(\frac{1}{2}\right) = \frac{1}{2} + \frac{1}{40}$, and $\alpha = -g_R\left(\frac{1}{4}\right) = -0.3775$ are fixed. The parameter $\beta = c_L$ is varied in the range $[0.1665, 0.1675]$ marked with the arrow $F_{16}^{\downarrow}$ in Figure 6.3b. On the left, the whole state space is pictured while the right side enhances the area of the state space around the borders involved in the pictured border collision bifurcations.

6.2.3 The Boundary $F_{16}^{\leftarrow}$

The next examined boundaries are the horizontal boundaries of the same parameter region. At the left boundary $F_{16}^{\leftarrow}$, the two cycles $O_{\mathcal{A}^5\mathcal{B}^3\mathcal{C}^4\mathcal{D}^4}$ shown in green in Figure 6.6 and $O_{\mathcal{A}^4\mathcal{B}^4\mathcal{C}^5\mathcal{D}^3}$ shown in red collide with the borders d_1 and d_2 from the right. These are different borders than the borders involved in the border collision bifurcations at the vertical boundaries $F_{16}^{\uparrow}$ and $F_{16}^{\downarrow}$. The point $x_7^{\mathcal{A}^4\mathcal{B}^4\mathcal{B}^5\mathcal{D}^3}$, which is on branch $f_{\mathcal{B}}$, collides with d_2 while the point $x_{15}^{\mathcal{A}^5\mathcal{B}^3\mathcal{C}^4\mathcal{D}^4}$, which is on branch $f_{\mathcal{D}}$, collides with the border d_0. These bifurcations are written $\xi_{d_0}^{\mathcal{A}^5\underline{\mathcal{B}}^3\mathcal{C}^4\mathcal{D}^4}$ and $\xi_{d_2}^{\mathcal{A}^4\mathcal{B}^4\mathcal{C}^5\underline{\mathcal{D}}^3}$ respectively.

The parameter region left to the "type B" parameter region is $\mathcal{P}_{\mathcal{A}^4\mathcal{B}^3\mathcal{C}^4\mathcal{D}^3}$. As before with the vertical boundaries $F_{16}^{\uparrow}$ and $F_{16}^{\downarrow}$, the cycle of the neighboring "type A" parameter region collides with the same borders as the "type B" cycles but from the opposite direction. The point $x_0^{\mathcal{A}^4\mathcal{B}^3\mathcal{C}^4\mathcal{D}^3}$, which is on branch $f_{\mathcal{A}}$, collides with the border d_0 while the point $x_7^{\mathcal{A}^4\mathcal{B}^3\mathcal{C}^4\mathcal{D}^3}$, which is on branch f_C, collides with the border d_2. This bifurcation is denoted as $\xi_{d_0,d_2}^{\mathcal{A}^4\mathcal{B}^3\mathcal{C}^4\mathcal{D}^3}$.

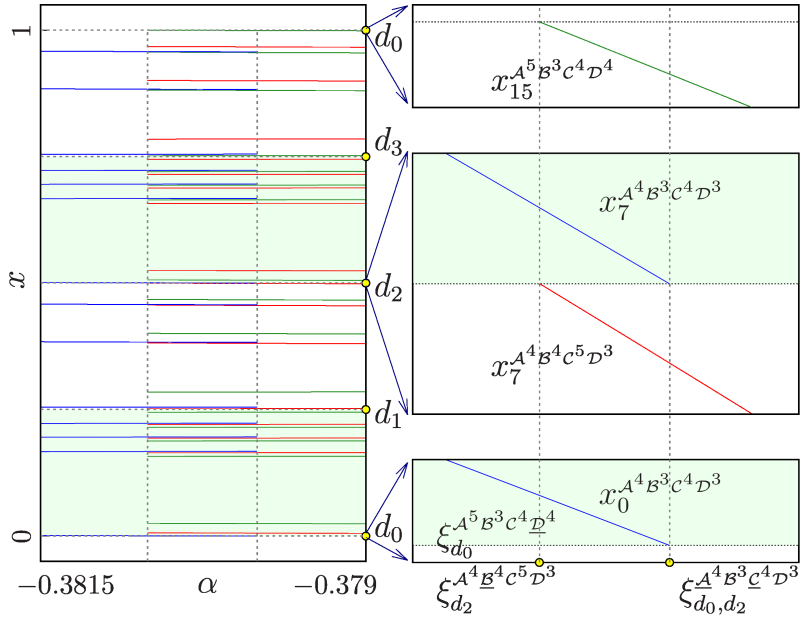

Figure 6.6: 1D bifurcation diagram at the boundary $F_{16}^{\leftarrow}$ in the archetypal model. The parameters $a_L = 4, b_L = -\frac{1}{2}, g_R\left(\frac{1}{2}\right) = \frac{1}{2} + \frac{1}{40}$, and $\beta = c_L = 0.1675$ are fixed. The parameter $\alpha = -g_R\left(\frac{1}{4}\right)$ is varied in the range $[-0.3815, -0.379]$ marked with the arrow $F_{16}^{\leftarrow}$ in Figure 6.3b. On the left, the whole state space is pictured while the right side enhances the area of the state space around the borders involved in the pictured border collision bifurcations.

6.2.4 The Boundary $F_{16}^{\rightarrow}$

At the right boundary $F_{16}^{\rightarrow}$, the two cycles $O_{\mathcal{A}^5\mathcal{B}^3\mathcal{C}^4\mathcal{D}^4}$ shown in green in Figure 6.7 and $O_{\mathcal{A}^4\mathcal{B}^4\mathcal{C}^5\mathcal{D}^3}$ shown in red collide with the borders d_0 and d_2 from left of the borders. The first point of cycle $O_{A^4B^4C^5\mathcal{D}^3}$ shown in green $x_0^{\mathcal{A}^4\mathcal{B}^4\mathcal{C}^5\mathcal{D}^3}$ collides with the border d_0, while the point $x_8^{\mathcal{A}^5\mathcal{B}^3\mathcal{C}^4\mathcal{D}^4}$ of its twin cycle $O_{\mathcal{A}^5\mathcal{B}^3\mathcal{C}^4\mathcal{D}^4}$ shown in red collides with the border d_2. This means that one point of the cycle $O_{\mathcal{A}^4\mathcal{B}^4\mathcal{C}^5\mathcal{D}^3}$ shown in green on the branch $f_{\mathcal{A}}$ collides with the border d_0 and one point of the cycle $O_{\mathcal{A}^5\mathcal{B}^3\mathcal{C}^4\mathcal{D}^4}$ shown in red on the branch f_C collides with the border d_2. The bifurcations are written as $\xi_{d_2}^{\mathcal{A}^5\mathcal{B}^3\underline{\mathcal{C}}^4\mathcal{D}^4}$ and $\xi_{d_0}^{\underline{\mathcal{A}}^4\mathcal{B}^4\mathcal{C}^5\mathcal{D}^3}$, respectively.

The "type A" parameter region right of this parameter region is $\mathcal{P}_{\mathcal{A}^5\mathcal{B}^4\mathcal{C}^5\mathcal{D}^4}$. Here again collides the "type A" cycle with the same borders as the "type B" cycles but from the opposite direction. In this case, two of the points of the cycle $O_{\mathcal{A}^5\mathcal{B}^4\mathcal{C}^5\mathcal{D}^4}$ shown in blue collide with the borders d_0 and d_1 at the same parameter value from left of the borders. To be more precise, the point $x_{17}^{\mathcal{A}^5\mathcal{B}^4\mathcal{C}^5\mathcal{D}^4}$, which is on the branch $f_{\mathcal{D}}$, collides with the border d_0 while the point $x_8^{\mathcal{A}^5\mathcal{B}^4\mathcal{C}^5\mathcal{D}^4}$, which is on the branch $f_{\mathcal{B}}$, collides with the border d_2. This bifurcation is written as $\xi_{d_0,d_2}^{\mathcal{A}^5\underline{\mathcal{B}}^4\mathcal{C}^5\underline{\mathcal{D}}^4}$.

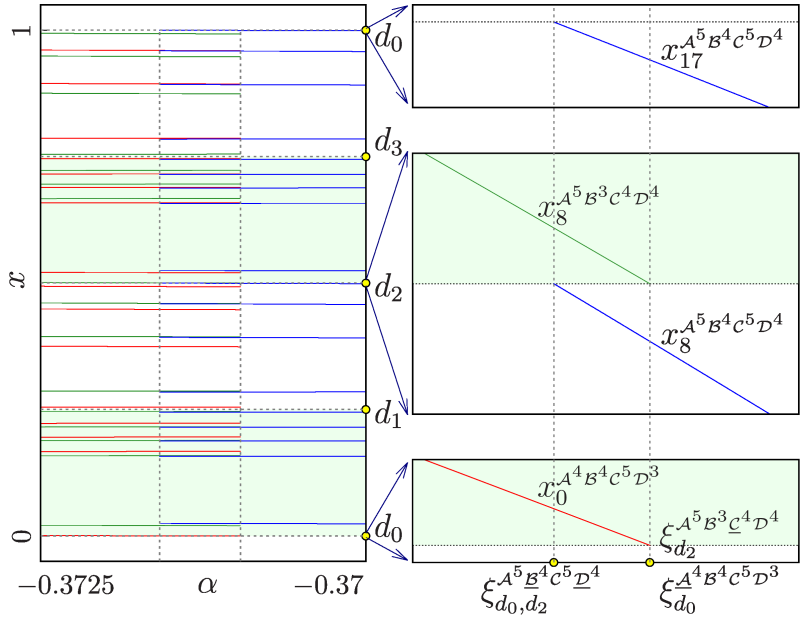

Figure 6.7: 1D bifurcation diagram at the boundary $F_{16}^{\rightarrow}$ in the archetypal model. The parameters $a_L = 4, b_L = -\frac{1}{2}, g_R\left(\frac{1}{2}\right) = \frac{1}{2} + \frac{1}{40}$, and $\beta = c_L = 0.1675$ are fixed. The parameter $\alpha = -g_R\left(\frac{1}{4}\right)$ is varied in the range $[-0.3725, -0.37]$ marked with the arrow $F_{16}^{\rightarrow}$ in Figure 6.3b. On the left, the whole state space is pictured while the right side enhances the area of the state space around the borders involved in the pictured border collision bifurcations.

6.2.5 Summary of Rules for Bifurcations

In the previous sections, the bifurcations occurring at the boundaries of the considered "type B" boundary are distributed on many pages. So it is hard to see regularities in the border collision bifurcations. Also, the bifurcations of the neighboring "type A" parameter regions are in another order — they are paired with the border collision bifurcation of the "type B" parameter region in the opposite direction. This makes it even harder to see the regularities. Thus, this section generalizes and summarizes the rules for the bifurcations at the boundaries of either type of parameter region.

"Type A" Parameter Regions

Let the stable cycle in a "type A" parameter region be $O_{\mathcal{A}^a\mathcal{B}^b\mathcal{C}^a\mathcal{D}^b}$. Then the border collision bifurcations occurring at the boundaries of this parameter region are given by the following rules.

(i) At the upper boundary there is the bifurcation $\xi_{d_1,d_3}^{\underline{\mathcal{A}}^a\mathcal{B}^b\underline{\mathcal{C}}^a\mathcal{D}^b}$.

(ii) At the lower boundary there is the bifurcation $\xi_{d_1,d_3}^{\mathcal{A}^a\underline{\mathcal{B}}^b\mathcal{C}^a\underline{\mathcal{D}}^b}$.

(iii) At the left boundary there is the bifurcation $\xi_{d_0,d_2}^{\mathcal{A}^a\underline{\mathcal{B}}^b\mathcal{C}^a\underline{\mathcal{D}}^b}$.

(iv) At the right boundary there is the bifurcation $\xi_{d_0,d_2}^{\underline{\mathcal{A}}^a\mathcal{B}^b\underline{\mathcal{C}}^a\mathcal{D}^b}$.

"Type B" Parameter Regions

Let the stable cycles in the "type B" parameter region be $O_{\mathcal{A}^a\mathcal{B}^b\mathcal{C}^c\mathcal{D}^d}$ and $O_{\mathcal{A}^c\mathcal{B}^d\mathcal{C}^a\mathcal{D}^b}$, where $c = a - 1$ and $d = b + 1$. Then the border collision bifurcations at the boundaries of this parameter region are given by the following rules.

(i) At the upper boundary there are the bifurcations $\xi_{d_1}^{\underline{\mathcal{A}}^a\mathcal{B}^b\mathcal{C}^c\mathcal{D}^d}$ and $\xi_{d_3}^{\mathcal{A}^c\mathcal{B}^d\underline{\mathcal{C}}^a\mathcal{D}^b}$.

(ii) At the lower boundary there are the bifurcations $\xi_{d_3}^{\mathcal{A}^a\mathcal{B}^b\mathcal{C}^c\underline{\mathcal{D}}^d}$ and $\xi_{d_1}^{\mathcal{A}^c\underline{\mathcal{B}}^d\mathcal{C}^a\mathcal{D}^b}$.

(iii) At the left boundary there are the bifurcations $\xi_{d_0}^{\mathcal{A}^a\mathcal{B}^b\mathcal{C}^c\underline{\mathcal{D}}^d}$ and $\xi_{d_2}^{\mathcal{A}^c\underline{\mathcal{B}}^d\mathcal{C}^a\mathcal{D}^b}$.

(iv) At the right boundary there are the bifurcations $\xi_{d_2}^{\mathcal{A}^a\mathcal{B}^b\underline{\mathcal{C}}^c\mathcal{D}^d}$ and $\xi_{d_0}^{\underline{\mathcal{A}}^c\mathcal{B}^d\mathcal{C}^a\mathcal{D}^b}$.

These rules agree with the rules for border collision bifurcations laid out by Akyüz [Aky22].

At the corners of the parameter regions where two boundaries meet, the border collision bifurcations of both boundaries all happen at the same time. This is called a codimension-2 point, since two bifurcations happen to one cycle at the same time. For example, in the upper right corner of a "type B" parameter region, the cycle $O_{\mathcal{A}^a\mathcal{B}^b\mathcal{C}^c\mathcal{D}^d}$ undergoes the bifurcations $\xi_{d_1}^{\underline{\mathcal{A}}^a\mathcal{B}^b\mathcal{C}^c\mathcal{D}^d}$ and $\xi_{d_2}^{\mathcal{A}^a\mathcal{B}^b\underline{\mathcal{C}}^c\mathcal{D}^b}$, while its twin cycle $O_{\mathcal{A}^c\mathcal{B}^d\mathcal{C}^a\mathcal{D}^b}$ undergoes the bifurcations $\xi_{d_3}^{\mathcal{A}^c\mathcal{B}^d\underline{\mathcal{C}}^a\mathcal{D}^b}$ and $\xi_{d_0}^{\underline{\mathcal{A}}^c\mathcal{B}^d\mathcal{C}^a\mathcal{D}^b}$.

Regularities in the Occurrence of Codimension-1 Bifurcations

The border collision bifurcation rules show some regularities. At each boundary, two borders are involved in the border collision bifurcations. Furthermore, the borders involved and the branches the colliding points belong to depend on the direction of the boundary and are the same for both "type A" and "type B" parameter regions. Note that while in the "type A" parameter region one cycle collides with both borders at the same time, in the "type B" parameter regions each of the coexisting cycles collides with one of the borders each. For example, at the upper boundary of a "type A" parameter region, the points on branches $f_{\mathcal{A}}$ and f_C of the cycle $O_{\mathcal{A}^a\mathcal{B}^b\mathcal{C}^a\mathcal{D}^b}$ collide with

both the borders d_1 and d_3, respectively. On the other hand, at the upper boundary of a "type B" parameter region, the point on the branch $f_{\mathcal{A}}$ of the cycle $O_{\mathcal{A}^a\mathcal{B}^b\mathcal{C}^c\mathcal{D}^d}$ collides with the border d_1, while the point on the branch $f_{\mathcal{C}}$ of the cycle $O_{\mathcal{A}^c\mathcal{B}^d\mathcal{C}^a\mathcal{D}^b}$ collides with the border d_3. This causes the same symbols being underlined for both types of parameter regions depending on the direction of the boundary.

All vertical boundaries involve the borders d_1 and d_3. And the cycles collide with the borders from the left at the upper boundaries while they collide with the borders from the right at the lower boundaries. Where the cycles swap which border they collide with in "type B" parameter regions. For example, at the upper boundary of a "type B" parameter region, the cycle $O_{\mathcal{A}^a\mathcal{B}^b\mathcal{C}^c\mathcal{D}^d}$ collides with the border d_1 from the left side. While the same cycle collides with the border d_3 from the right side at the lower boundary.

Similarly, all horizontal boundaries involve the borders d_0 and d_2. And the cycles collide with the borders from the left at the left boundaries while they collide with the borders from the right at the right boundaries. Where the cycles swap which border they collide with in "type B" parameter regions. For example, at the left boundary of a "type B" parameter region, the cycle $O_{\mathcal{A}^a\mathcal{B}^b\mathcal{C}^c\mathcal{D}^d}$ collides with the border d_0 from the left. While the same cycle collides with the border d_2 from the right at the right boundary.

Regularities in the Occurrence of Codimension-2 Bifurcations

From these regularities we can extrapolate the regularities of the codimension-2 border collision bifurcations at each corner of the parameter regions. Since the border collision bifurcations at the vertical boundaries each involve the borders d_1 and d_3 and the horizontal border collision bifurcations each involve the borders d_0 and d_2, the codimension-2 border collision bifurcation at each corner of a parameter region involves all four borders. For "type A" parameter regions, the single cycle $O_{\mathcal{A}^a\mathcal{B}^b\mathcal{C}^a\mathcal{D}^b}$ collides with all four borders at all four corners of the parameter region. And for "type B" parameter regions, the border collisions distribute evenly across both coexisting twin cycles $O_{\mathcal{A}^a\mathcal{B}^b\mathcal{C}^c\mathcal{D}^d}$ and $O_{\mathcal{A}^c\mathcal{B}^d\mathcal{C}^a\mathcal{D}^b}$. So each twin cycle collides with two borders at the same time.

The four codimension-2 border collision bifurcations for a "type A" parameter region with the cycle $O_{\mathcal{A}^a\mathcal{B}^b\mathcal{C}^a\mathcal{D}^b}$ are the following.

(i) In the upper left corner there are the bifurcations $\xi_{d_1,d_3}^{\underline{\mathcal{A}}^a\mathcal{B}^b\underline{\mathcal{C}}^a\mathcal{D}^b}$ and $\xi_{d_0,d_2}^{\mathcal{A}^a\underline{\mathcal{B}}^b\mathcal{C}^a\underline{\mathcal{D}}^b}$.

(ii) In the upper right corner there are the bifurcations $\xi_{d_1,d_3}^{\underline{\mathcal{A}}^a\mathcal{B}^b\underline{\mathcal{C}}^a\mathcal{D}^b}$ and $\xi_{d_0,d_2}^{\underline{\mathcal{A}}^a\mathcal{B}^b\underline{\mathcal{C}}^a\mathcal{D}^b}$.

(iii) In the lower right corner there are the bifurcations $\xi_{d_1,d_3}^{\mathcal{A}^a\underline{\mathcal{B}}^b\mathcal{C}^a\underline{\mathcal{D}}^b}$ and $\xi_{d_0,d_2}^{\underline{\mathcal{A}}^a\mathcal{B}^b\underline{\mathcal{C}}^a\mathcal{D}^b}$.

(iv) In the lower left corner there are the bifurcations $\xi_{d_1,d_3}^{\mathcal{A}^a\underline{\mathcal{B}}^b\mathcal{C}^a\underline{\mathcal{D}}^b}$ and $\xi_{d_0,d_2}^{\mathcal{A}^a\underline{\mathcal{B}}^b\mathcal{C}^a\underline{\mathcal{D}}^b}$.

The four codimension-2 border collision bifurcations for a "type B" parameter region with the twin cycles $O_{\mathcal{A}^a\mathcal{B}^b\mathcal{C}^c\mathcal{D}^d}$ and $O_{\mathcal{A}^c\mathcal{B}^d\mathcal{C}^a\mathcal{D}^b}$ with $c = a - 1$ and $d = b + 1$ are the following.

(i) In the upper left corner there are the bifurcations $\xi_{d_1}^{\overline{\mathcal{A}^a\mathcal{B}^b\mathcal{C}^c\mathcal{D}^d}}$ and $\xi_{d_0}^{\mathcal{A}^a\mathcal{B}^b\mathcal{C}^c\underline{\mathcal{D}^d}}$ for the cycle $O_{\mathcal{A}^a\mathcal{B}^b\mathcal{C}^c\mathcal{D}^d}$ and $\xi_{d_3}^{\mathcal{A}^c\mathcal{B}^d\underline{\mathcal{C}^a}\mathcal{D}^b}$ and $\xi_{d_2}^{\mathcal{A}^c\underline{\mathcal{B}^d}\mathcal{C}^a\mathcal{D}^b}$ for its twin cycle $O_{\mathcal{A}^c\mathcal{B}^d\mathcal{C}^a\mathcal{D}^b}$.

(ii) In the upper right corner there are the bifurcations $\xi_{d_1}^{\overline{\mathcal{A}^a\mathcal{B}^b\mathcal{C}^c\mathcal{D}^d}}$ and $\xi_{d_2}^{\mathcal{A}^a\mathcal{B}^b\underline{\mathcal{C}^c}\mathcal{D}^d}$ for the cycle $O_{\mathcal{A}^a\mathcal{B}^b\mathcal{C}^c\mathcal{D}^d}$ and $\xi_{d_3}^{\mathcal{A}^c\mathcal{B}^d\underline{\mathcal{C}^a}\mathcal{D}^b}$ and $\xi_{d_0}^{\overline{\mathcal{A}^c\mathcal{B}^d\mathcal{C}^a\mathcal{D}^b}}$ for its twin cycle $O_{\mathcal{A}^c\mathcal{B}^d\mathcal{C}^a\mathcal{D}^b}$.

(iii) In the lower right corner there are the bifurcations $\xi_{d_3}^{\mathcal{A}^a\mathcal{B}^b\mathcal{C}^c\underline{\mathcal{D}^d}}$ and $\xi_{d_2}^{\mathcal{A}^a\mathcal{B}^b\underline{\mathcal{C}^c}\mathcal{D}^d}$ for the cycle $O_{\mathcal{A}^a\mathcal{B}^b\mathcal{C}^c\mathcal{D}^d}$ and $\xi_{d_1}^{\mathcal{A}^c\underline{\mathcal{B}^d}\mathcal{C}^a\mathcal{D}^b}$ and $\xi_{d_0}^{\overline{\mathcal{A}^c\mathcal{B}^d\mathcal{C}^a\mathcal{D}^b}}$ for its twin cycle $O_{\mathcal{A}^c\mathcal{B}^d\mathcal{C}^a\mathcal{D}^b}$.

(iv) In the lower left corner there are the bifurcations $\xi_{d_3}^{\mathcal{A}^a\mathcal{B}^b\mathcal{C}^c\underline{\mathcal{D}^d}}$ and $\xi_{d_0}^{\mathcal{A}^a\mathcal{B}^b\mathcal{C}^c\underline{\mathcal{D}^d}}$ for the cycle $O_{\mathcal{A}^a\mathcal{B}^b\mathcal{C}^c\mathcal{D}^d}$ and $\xi_{d_1}^{\mathcal{A}^c\underline{\mathcal{B}^d}\mathcal{C}^a\mathcal{D}^b}$ and $\xi_{d_2}^{\mathcal{A}^c\underline{\mathcal{B}^d}\mathcal{C}^a\mathcal{D}^b}$ for its twin cycle $O_{\mathcal{A}^c\mathcal{B}^d\mathcal{C}^a\mathcal{D}^b}$.

Again, the direction from which the cycles collide with them depend solely on the position of the corner of the parameter region and not the type of the parameter region. For the upper left corners, the cycles collide from the left at all borders, and for the lower right corner, the cycles collide from the right at all borders. For the lower left and upper right corners, the cycles collide at the borders d_0 and d_2 from one side and at the borders d_1 and d_3 from the opposite direction. In the case of the lower left corner, the cycles collide with the d_0 and d_2 from the left and with the borders d_1 and d_3 from the right. In the case of the upper right corner, the cycles collide with the d_0 and d_2 from the right and with the borders d_1 and d_3 from the left.

Also, we can see how the border collisions distribute across the two twin cycles of "type B" parameter regions. Each cycle is involved in a border collision bifurcation with one border of each set of borders, $\{d_0, d_2\}$ and $\{d_1, d_3\}$. This makes sense, since at each corner each cycle collides with one border of the set $\{d_0, d_2\}$ at vertical boundaries and with one border of the set $\{d_1, d_3\}$ at horizontal boundaries. At the corners, a horizontal border collision bifurcation is combined with a vertical border collision bifurcation and therefore each cycle collides with one border of each set at each corner.

6.3 Coexistence Scenarios

The previous section investigated the bifurcations at the boundaries of "type A" and "type B" parameter regions. There, one can see that there is a space between the border collision bifurcations of the "type B" cycles and the border collision bifurcation of the "type A" cycle where all three cycles coexist at each boundary of the "type B" parameter region. Figure 6.8b illustrates this overlap again, the overlapping regions are marked with the points J, R, S, and T. In Figure 6.8a, one can see that "type A" parameter regions can also overlap with each other. Here, the overlapping regions are marked with M, N, O, and P. One previously not considered case is that there can also be an overlap of two "type A" parameter regions and one "type B" parameter region. This can be seen in Figure 6.8b and is marked with points V, W, X, and Y.

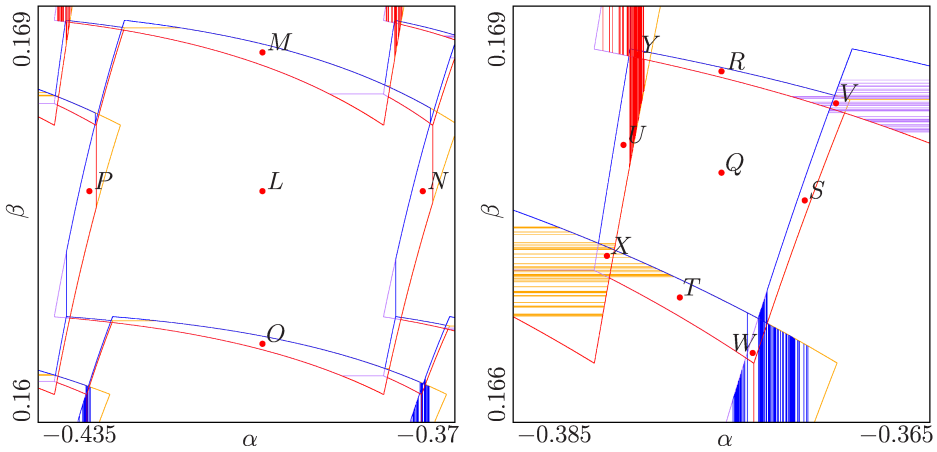

(a) Parameter region E_{16} **(b)** Parameter region F_{16}

Figure 6.8: Magnified 2D scans of the boundaries of parameter regions with different symbolic sequences in the archetypal model. The parameters $a_L = 4, b_L = -\frac{1}{2}$, and $g_R\left(\frac{1}{2}\right) = \frac{1}{2} + \frac{1}{40}$ are fixed. The parameters $\alpha = -g_R\left(\frac{1}{4}\right)$ and $\beta = c_L$ are varied in different ranges. (a) shows the "type A" parameter region marked with the point E_{16} in Figure 6.1. The parameters are varied in the ranges $[-0.435, -0.37]$ and $[0.16, 0.169]$. At the point L there is only one "type A" cycle, while the points M, N, O, and P mark locations with two coexisting "type A" cycles. (b) shows the "type B" parameter region marked with the point F_{16} in Figure 6.1. The parameters are varied in the ranges $[-0.385, -0.365]$ and $[0.166, 0.169]$. At the point Q there are two coexisting "type B" twin cycles, while the points R, S, T, and U mark locations with two coexisting "type B" twin cycles and one "type A" cycle. And the points V, W, X, and Y mark locations with two coexisting "type B" twin cycles and two "type A" cycles.

Each coexistence scenario is covered in the following. The first considered scenario is the simplest one where only one "type A" cycle exists on its own.

6.3.1 Only One "Type A" Cycle

As mentioned above, the most simple case of coexistence in this model is the existence of a stable "type A" cycle on its own. This is the case at the point L in Figure 6.8a. Here, only the stable cycle $O_{\mathcal{A}^5\mathcal{B}^3\mathcal{C}^5\mathcal{D}^3}$ exists.

For this case there is no extra cobweb diagram in this section, since there are already many cobweb diagrams of single "type A" cycles in the previous section, Section 6.1. For example in Figures 6.2a, 6.2c, 6.2e and 6.2g to 6.2i. And the basin of attraction is the whole state space.

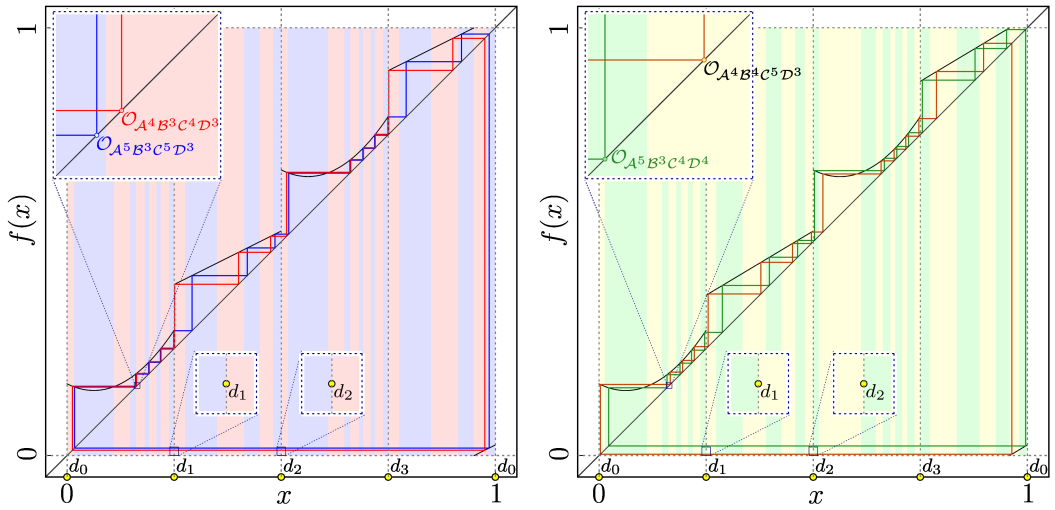

(a) M **(b)** Q

Figure 6.9: Cobweb diagrams at two parameter values in the archetypal model showing coexistence of two stable cycles and their basins of attraction. The parameters $a_L = 4, b_L = -\frac{1}{2}$, and $g_R\left(\frac{1}{2}\right) = \frac{1}{2} + \frac{1}{40}$ are fixed. The parameters $\alpha = -g_R\left(\frac{1}{4}\right)$ and $\beta = c_L$ are differed in every diagram and are marked with points in Figure 6.8. (a) shows the cycles at the point M where $\alpha = -0.4$ and $\beta = 0.168$. Here, two "type A" cycles coexist. (b) shows the cycles at the point Q where $\alpha = -0.375$ and $\beta = 0.1678$. Here, two "type B" twin cycles coexist.

6.3.2 Two "Type A" Cycles

As mentioned at the beginning of Section 6.3, "type A" parameter regions can overlap. This causes the coexistence of two "type A" cycles. It can happen in four different ways. Assuming the stable cycle of the parameter region in the middle is $O_{\mathcal{A}^a\mathcal{B}^b\mathcal{C}^a\mathcal{D}^b}$, it can overlap with parameter regions, where either one of the following cycles is stable (i) $O_{\mathcal{A}^{a-1}\mathcal{B}^b\mathcal{C}^{a-1}\mathcal{D}^b}$, (ii) $O_{\mathcal{A}^a\mathcal{B}^{b+1}\mathcal{C}^a\mathcal{D}^{b+1}}$, (iii) $O_{\mathcal{A}^{a+1}\mathcal{B}^b\mathcal{C}^{a+1}\mathcal{D}^b}$, and (iv) $O_{\mathcal{A}^a\mathcal{B}^{b-1}\mathcal{C}^a\mathcal{D}^{b-1}}$. For the specific case pictured in Figure 6.8a, this results in the following coexistence scenarios.

(i) $\mathcal{A}^5\mathcal{B}^3\mathcal{C}^5\mathcal{D}^3$ and $\mathcal{A}^4\mathcal{B}^3\mathcal{C}^4\mathcal{D}^3$, marked with M in Figure 6.8a,

(ii) $\mathcal{A}^5\mathcal{B}^3\mathcal{C}^5\mathcal{D}^3$ and $\mathcal{A}^5\mathcal{B}^4\mathcal{C}^5\mathcal{D}^4$, marked with N in Figure 6.8a,

(iii) $\mathcal{A}^5\mathcal{B}^3\mathcal{C}^5\mathcal{D}^3$ and $\mathcal{A}^6\mathcal{B}^3\mathcal{C}^6\mathcal{D}^3$, marked with O in Figure 6.8a, and

(iv) $\mathcal{A}^5\mathcal{B}^3\mathcal{C}^5\mathcal{D}^3$ and $\mathcal{A}^5\mathcal{B}^2\mathcal{C}^5\mathcal{D}^2$, marked with P in Figure 6.8a.

Figure 6.9a shows the cobweb diagram for the point M in Figure 6.8a. Here, we can see the two cycles of the two different "type A" parameter regions. The cycle $O_{\mathcal{A}^5\mathcal{B}^3\mathcal{C}^5\mathcal{D}^3}$ is shown in blue and the cycle $O_{\mathcal{A}^4\mathcal{B}^3\mathcal{C}^4\mathcal{D}^3}$ is shown in red, these colors will stay the same for other cobweb diagrams in this section. The cobweb diagram also shows the basins of attraction of both cycles. The basin of attraction of the cycle $O_{\mathcal{A}^5\mathcal{B}^3\mathcal{C}^5\mathcal{D}^3}$ is shown in blue and the basin of attraction of the cycle $O_{\mathcal{A}^4\mathcal{B}^3\mathcal{C}^4\mathcal{D}^3}$ is shown in red.

6.3.3 Only one Pair of "Type B" Cycles

Another very simple case is when a "type B" parameter region does not overlap with any other region. This causes the coexistence of two "type B" twin cycles. In this case, there are two coexisting stable cycles as discussed before in Section 2.3.3 and Section 6.1. Here, the cycles are asymmetrical. If one of the cycles is $O_{\mathcal{A}^a\mathcal{B}^b\mathcal{C}^c\mathcal{D}^d}$ where $c = a - 1$ and $d = b + 1$, the other cycle is $O_{\mathcal{A}^c\mathcal{B}^d\mathcal{C}^a\mathcal{D}^b}$. In the specific case marked with the point Q in Figure 6.8b, these cycles are $O_{\mathcal{A}^5\mathcal{B}^3\mathcal{C}^4\mathcal{D}^4}$ and $O_{\mathcal{A}^4\mathcal{B}^4\mathcal{C}^5\mathcal{D}^3}$.

Figure 6.9b shows the cobweb diagram at this point. The cycle $O_{\mathcal{A}^5\mathcal{B}^3\mathcal{C}^4\mathcal{D}^4}$ is shown in green and its basin of attraction also. Its twin cycle $O_{\mathcal{A}^4\mathcal{B}^4\mathcal{C}^5\mathcal{D}^3}$ is shown in brown and its basin of attraction is shown in yellow for better visibility. Again, for the rest of this section, the colors will stay the same when we encounter these cycles in cobweb diagrams.

6.3.4 One Pair of "Type B" Cycles and One "Type A" Cycle

We can see in Figure 6.8b that this "type B" parameter region can overlap with "type A" parameter regions. This causes the coexistence of three cycles, two "type B" cycles and one "type A" cycle. It can also happen in four different ways, as was the case with "type A" parameter regions overlapping with one another described in Section 6.3.2. Assuming the stable cycles of the parameter region in the middle are $O_{\mathcal{A}^a\mathcal{B}^b\mathcal{C}^c\mathcal{D}^d}$ and $O_{\mathcal{A}^c\mathcal{B}^d\mathcal{C}^a\mathcal{D}^b}$ with $c = a - 1$ and $d = b + 1$, it can overlap with parameter regions where either one of the following cycles is stable (i) $O_{\mathcal{A}^c\mathcal{B}^d\mathcal{C}^c\mathcal{D}^d}$, (ii) $O_{\mathcal{A}^a\mathcal{B}^d\mathcal{C}^a\mathcal{D}^d}$, (iii) $O_{\mathcal{A}^a\mathcal{B}^b\mathcal{C}^a\mathcal{D}^b}$, and (iv) $O_{\mathcal{A}^c\mathcal{B}^b\mathcal{C}^c\mathcal{D}^b}$. For the specific case pictured in Figure 6.8b, this results in the following parameter regions

(i) $\mathcal{A}^5\mathcal{B}^3\mathcal{C}^4\mathcal{D}^4$, $\mathcal{A}^4\mathcal{B}^4\mathcal{C}^5\mathcal{D}^3$, and $\mathcal{A}^4\mathcal{B}^4\mathcal{C}^4\mathcal{D}^4$, marked with R in Figure 6.8b,

(ii) $\mathcal{A}^5\mathcal{B}^3\mathcal{C}^4\mathcal{D}^4$, $\mathcal{A}^4\mathcal{B}^4\mathcal{C}^5\mathcal{D}^3$, and $\mathcal{A}^5\mathcal{B}^4\mathcal{C}^5\mathcal{D}^4$, marked with S in Figure 6.8b,

(iii) $\mathcal{A}^5\mathcal{B}^3\mathcal{C}^4\mathcal{D}^4$, $\mathcal{A}^4\mathcal{B}^4\mathcal{C}^5\mathcal{D}^3$, and $\mathcal{A}^5\mathcal{B}^3\mathcal{C}^5\mathcal{D}^3$, marked with T in Figure 6.8b, and

(iv) $\mathcal{A}^5\mathcal{B}^3\mathcal{C}^4\mathcal{D}^4$, $\mathcal{A}^4\mathcal{B}^4\mathcal{C}^5\mathcal{D}^3$, and $\mathcal{A}^4\mathcal{B}^3\mathcal{C}^4\mathcal{D}^3$, marked with U in Figure 6.8b.

Figure 6.10a shows the cobweb diagram at the point U in Figure 6.8b. This point is chosen for the cobweb diagram, since here the parameter regions $\mathcal{P}_{\mathcal{A}^4\mathcal{B}^3\mathcal{C}^4\mathcal{D}^3}$ and $\mathcal{P}_{\mathcal{A}^5\mathcal{B}^3\mathcal{C}^4\mathcal{D}^4,\mathcal{A}^4\mathcal{B}^4\mathcal{C}^5\mathcal{D}^3}$ overlap and the cycles that exist at this point were already in the previous cobweb diagrams. The colors for each cycle, as well as the color of their basins of attraction, are the same as in previous cobweb diagrams showing these cycles, Figures 6.9a and 6.9b.

6.3.5 One Pair of "Type B" Cycles And Two "Type A" Cycles

When looking closer at Figure 6.8b, we can see that the parameter regions described in the previous Section 6.3.4 can also overlap with one another. There, one "type B" parameter region overlaps with two different "type A" parameter regions. This results in parameter regions where there coexist two "type B" cycles and two "type A" cycles. It can also happen in four cases, as with previous coexistence scenarios in Sections 6.3.2 and 6.3.4. Assuming the "type B" cycles are $O_{\mathcal{A}^a\mathcal{B}^b\mathcal{C}^c\mathcal{D}^b}$ and $O_{\mathcal{A}^c\mathcal{B}^d\mathcal{C}^a\mathcal{D}^b}$ with $c = a - 1$ and $d = b + 1$, the cycles they will coexist with are the following

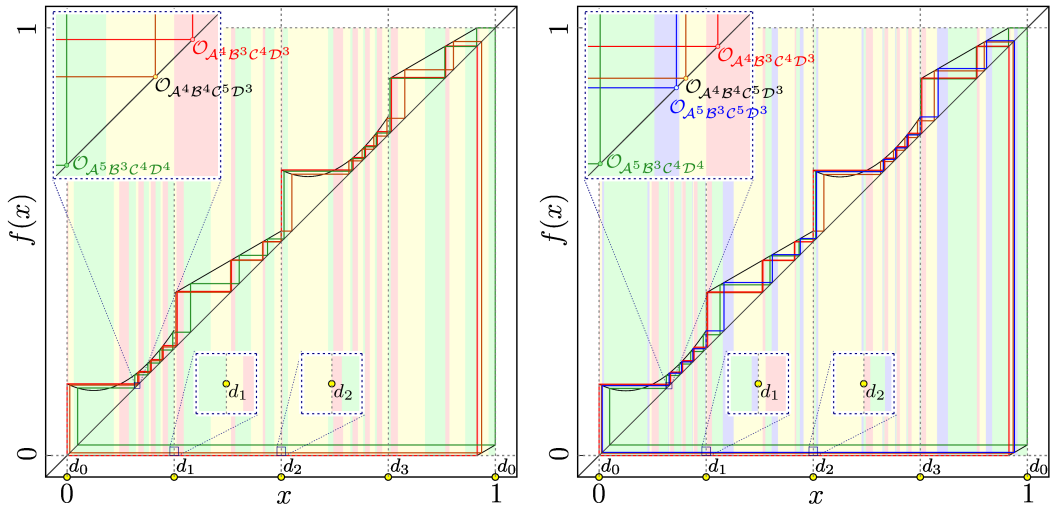

(a) U **(b)** X

Figure 6.10: Cobweb diagrams at two parameter values in the archetypal model showing coexistence of three and four stable cycles and their basins of attraction. The parameters $a_L = 4, b_L = -\frac{1}{2}$, and $g_R\left(\frac{1}{2}\right) = \frac{1}{2} + \frac{1}{40}$ are fixed. The parameters $\alpha = -g_R\left(\frac{1}{4}\right)$ and $\beta = c_L$ are differed in every diagram and are marked with points in Figure 6.8. (a) shows the cycles at the point U where $\alpha = -0.3797$ and $\beta = 0.168$. Here, two "type B" twin cycles coexist with one "type A" cycle. (b) shows the cycles at the point X where $\alpha = -0.3805$ and $\beta = 0.1672$. Here, two "type B" twin cycles coexist with two "type A" cycles.

pairs of the cycles discussed in Section 6.3.4 (i) $O_{\mathcal{A}^c\mathcal{B}^d\mathcal{C}^c\mathcal{D}^d}$ and $O_{\mathcal{A}^a\mathcal{B}^d\mathcal{C}^a\mathcal{D}^d}$, (ii) $O_{\mathcal{A}^a\mathcal{B}^d\mathcal{C}^a\mathcal{D}^d}$ and $O_{\mathcal{A}^a\mathcal{B}^b\mathcal{C}^a\mathcal{D}^b}$, (iii) $O_{\mathcal{A}^a\mathcal{B}^b\mathcal{C}^a\mathcal{D}^b}$ and $O_{\mathcal{A}^c\mathcal{B}^b\mathcal{C}^c\mathcal{D}^b}$, and (iv) $O_{\mathcal{A}^c\mathcal{B}^b\mathcal{C}^c\mathcal{D}^b}$ and $O_{\mathcal{A}^c\mathcal{B}^d\mathcal{C}^c\mathcal{D}^d}$. For the specific case pictured in Figure 6.8b, this results in the following coexistence scenarios.

(i) $\mathcal{A}^5\mathcal{B}^3\mathcal{C}^4\mathcal{D}^4, \mathcal{A}^4\mathcal{B}^4\mathcal{C}^5\mathcal{D}^3, \mathcal{A}^4\mathcal{B}^4\mathcal{C}^4\mathcal{D}^4$, and $\mathcal{A}^5\mathcal{B}^4\mathcal{C}^5\mathcal{D}^4$, marked with V in Figure 6.8b,

(ii) $\mathcal{A}^5\mathcal{B}^3\mathcal{C}^4\mathcal{D}^4, \mathcal{A}^4\mathcal{B}^4\mathcal{C}^5\mathcal{D}^3, \mathcal{A}^5\mathcal{B}^4\mathcal{C}^5\mathcal{D}^4$, and $\mathcal{A}^5\mathcal{B}^3\mathcal{C}^5\mathcal{D}^3$, marked with W in Figure 6.8b,

(iii) $\mathcal{A}^5\mathcal{B}^3\mathcal{C}^4\mathcal{D}^4, \mathcal{A}^4\mathcal{B}^4\mathcal{C}^5\mathcal{D}^3, \mathcal{A}^5\mathcal{B}^3\mathcal{C}^5\mathcal{D}^3$, and $\mathcal{A}^4\mathcal{B}^3\mathcal{C}^4\mathcal{D}^3$, marked with X in Figure 6.8b, and

(iv) $\mathcal{A}^5\mathcal{B}^3\mathcal{C}^4\mathcal{D}^4, \mathcal{A}^4\mathcal{B}^4\mathcal{C}^5\mathcal{D}^3, \mathcal{A}^4\mathcal{B}^3\mathcal{C}^4\mathcal{D}^3$, and $\mathcal{A}^4\mathcal{B}^4\mathcal{C}^4\mathcal{D}^4$, marked with Y in Figure 6.8b.

Figure 6.10b shows the cobweb diagram for the point X in Figure 6.8b. Again, this point is chosen so that the coexisting cycles were already pictured in previous cobweb diagrams in this section. The colors for each cycle as well as the color of their basins of attraction are the same as in previous cobweb diagrams. If we compare this cobweb diagram to the cobweb diagram in Figure 6.10a of point U in Figure 6.8b, we can see that the cycles $O_{\mathcal{A}^4\mathcal{B}^3\mathcal{C}^4\mathcal{D}^3}$ shown in red, $O_{\mathcal{A}^5\mathcal{B}^3\mathcal{C}^4\mathcal{D}^4}$ shown in green, and $O_{\mathcal{A}^4\mathcal{B}^4\mathcal{C}^5\mathcal{D}^3}$ shown in brown exist at almost the same point. The same is true for their basins of attraction. But there is a new cycle, $O_{A^5\mathcal{B}^3C^5\mathcal{D}^3}$ shown in blue that emerged between the basins of attraction of the two "type B" cycles, $O_{\mathcal{A}^5\mathcal{B}^3\mathcal{C}^4\mathcal{D}^4}$ shown in green and $O_{\mathcal{A}^4\mathcal{B}^4\mathcal{C}^5\mathcal{D}^3}$ shown in brown.

In this cobweb diagram, as well as in the previous ones, we can see that the borders of the function d_0, d_1, d_2, and d_3 as well as their preimages seperate basins of attraction from each other. In each diagram, the neighborhoods of the borders d_1 and d_2 are magnified. From these two borders, we can also reason about the two other borders d_0 and d_3 thanks to the symmetry of the model. The basins of attraction of the cycles of "type A" parameter regions, such as $O_{\mathcal{A}^5\mathcal{B}^3\mathcal{C}^5\mathcal{D}^3}$ shown in blue and $O_{\mathcal{A}^4\mathcal{B}^3\mathcal{C}^4\mathcal{D}^3}$ shown in red, are the same on each half of the model. For the cycles of "type B" parameter regions, such as $O_{\mathcal{A}^5\mathcal{B}^3\mathcal{C}^4\mathcal{D}^4}$ shown in green and $O_{\mathcal{A}^4\mathcal{B}^4\mathcal{C}^5\mathcal{D}^3}$ shown in brown, the cycles and their basins of attraction swap places. So at border d_3, the basin of attraction to the left will be of the cycle $\mathcal{A}^5\mathcal{B}^3\mathcal{C}^5\mathcal{D}^3$ shown in blue still, but the basin of attraction to the right will be of $O_{\mathcal{A}^5\mathcal{B}^3\mathcal{C}^4\mathcal{D}^4}$ shown in green instead of $O_{\mathcal{A}^4\mathcal{B}^4\mathcal{C}^5\mathcal{D}^3}$ shown in brown.

6.3.6 Possible Period Combinations in Coexistence Scenarios

The previous sections cover all possible coexistence scenarios in the archetypal model. We can see that only parameter regions of the same chain of parameter regions associated with the same period or parameter regions of neighboring chains can overlap. Therefore, coexisting cycles differ in their periods by two at most.

6.3.7 Coexistence Scenarios in the Original Model

Akyüz covered all these coexistence scenarios in [Aky22] with one exception. The coexistence of four cycles was not described in his preliminary investigation of the original model. This section confirms that this scenario also exists in the original model. For this, Figure 6.11a shows a 2D scan of the boundaries of parameter regions zoomed in the lower left corner of the "type B" parameter region that is associated with the twin cycles $O_{\mathcal{A}^3\mathcal{B}^2\mathcal{C}^2\mathcal{D}^3}$ and $O_{\mathcal{A}^2\mathcal{B}^3\mathcal{C}^3\mathcal{D}^2}$. Since it is magnified a lot, it has more artifacts that are not actual boundaries of parameter regions than previous scans of boundaries. Therefore, the important boundaries are marked with arrows. The lower boundary of the "type B" parameter regions is marked with $\xi_{d_3}^{\mathcal{A}^3\mathcal{B}^2\mathcal{C}^2\underline{\mathcal{D}}^3}$, $\xi_{d_1}^{\mathcal{A}^3\underline{\mathcal{B}}^2\mathcal{C}^2\mathcal{D}^3}$ and its left boundary is marked with $\xi_{d_0}^{\mathcal{A}^3\mathcal{B}^2\mathcal{C}^2\underline{\mathcal{D}}^3}$, $\xi_{d_2}^{\mathcal{A}^3\underline{\mathcal{B}}^2\mathcal{C}^2\mathcal{D}^3}$. The parameter region below the "type B" parameter region is the "type A" parameter region that is associated with the cycle $O_{\mathcal{A}^3\mathcal{B}^2\mathcal{C}^3\mathcal{D}^2}$. Its upper boundary is marked with $\xi_{d_1,d_3}^{\mathcal{A}^3\mathcal{B}^2\underline{\mathcal{C}}^3\mathcal{D}^2}$. And finally, the parameter region to the left of the "type B" parameter region is the "type A" parameter that is region associated with the cycle $\mathcal{A}^2\mathcal{B}^2\mathcal{C}^2\mathcal{D}^2$. Its right boundary is marked with $\xi_{d_0,d_2}^{\underline{\mathcal{A}}^2\mathcal{B}^2\underline{\mathcal{C}}^2\mathcal{D}^2}$. All other lines in the diagram are numerical artifacts that do not correspond to boundaries of parameter regions.

The point X marks the parameter values that are in the overlapping area of all three parameter regions mentioned above. Figure 6.11a shows the cobweb diagram at these parameter values. Here all four cycles coexist, two cycles from each "type A" parameter region and two cycles from the "type B" parameter region. This is hard to see, since the two cycles $O_{\mathcal{A}^3\mathcal{B}^2\mathcal{C}^3\mathcal{D}^2}$ shown in blue and $O_{\mathcal{A}^2\mathcal{B}^3\mathcal{C}^3\mathcal{D}^2}$ shown in brown are almost on top of each other in the blowup plot. But one can see that they are different cycles, as they are visibly separated right of the border d_3.

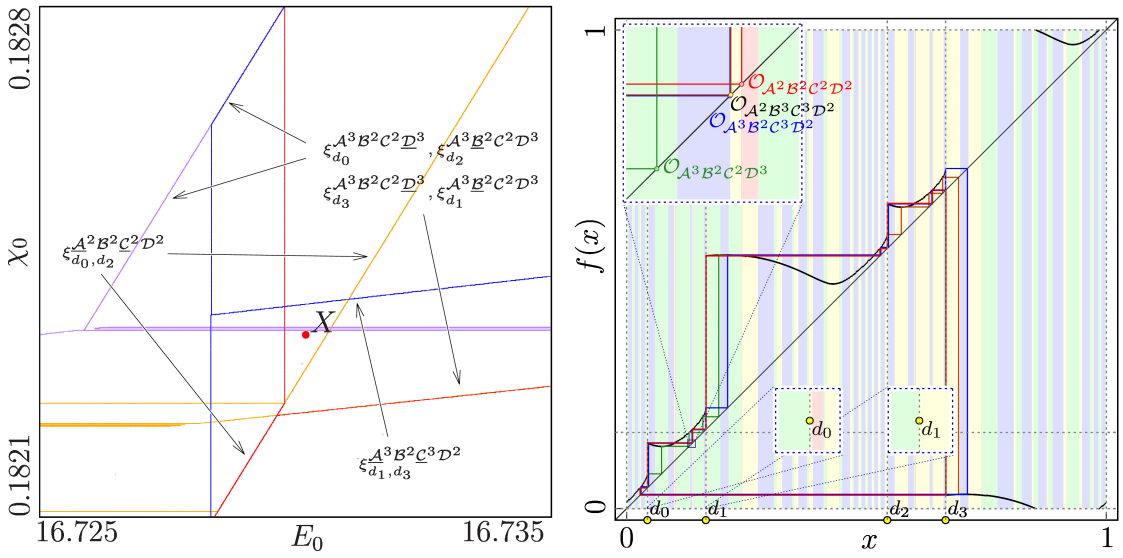

(a) 2D scan of the boundaries

(b) Cobweb diagram at point X

Figure 6.11: 2D scan of the boundaries of parameter regions with different symbolic sequences and cobweb diagram in the original model showing the coexistence of four cycles The parameters $\beta = 1, f = 150, L = 4.2 \cdot 10^{-3}, R = 2, V_m = 5$, and $\mu = 0.5$ are fixed. (a) shows the 2D scan of the boundaries of parameter regions with different symbolic sequences at a specific location where a "type B" parameter region overlaps with two "type A" parameter regions. The parameters E_0 and χ_0 are varied in the ranges $[16.725, 16.735]$ and $[0.1821, 0.1828]$. Important boundaries are marked with arrows. (b) shows the cobweb diagram at the parameter values marked with the point X in (a) where $E_0 = 16.7302$ and $\chi_0 = 0.1823$. Here, two "type B" twin cycles coexist with two "type A" cycles.

6.4 End of Chains

Thus far, the chapter only covered the parameter regions at the beginning and in the middle of chains. This section investigates how the chains develop for larger values of β.

Figure 6.12a shows a 2D scan of the periods of the halved archetypal model where the "type B" parameter regions in the chains are visible. We can see that the "type B" parameter region in Figure 6.12a between the "type A" parameter region marked with point I_{16} and the "type A" parameter region marked with point K_{16} is missing. There should have been the parameter region $\mathcal{P}_{\mathcal{A}^3\mathcal{B}^5\mathcal{C}^2\mathcal{D}^6,\mathcal{A}^2\mathcal{B}^6\mathcal{C}^3\mathcal{B}^5}$ according to the rules laid out in Section 6.1.

Furthermore, the chain is completely disconnected when looking at even higher values of β. Figure 6.12b shows this. The parameter region $\mathcal{P}_{\mathcal{A}\mathcal{B}^7\mathcal{C}\mathcal{D}^7}$ marked with M_{16} in Figure 6.12b is the predicted last "type A" parameter region of the chain with period 16. It is not connected to the second last parameter region $\mathcal{P}_{\mathcal{A}^2\mathcal{B}^6\mathcal{C}^2\mathcal{D}^6}$ marked with K_{16} in Figure 6.12b.

This violates the rules and our expectation for the archetypal model. Akyüz observed the same behavior in the original model in [Aky22]. He also looked at a chain of parameter regions with period 16. The chain behaved according to the rules up to the second last "type A" parameter region,

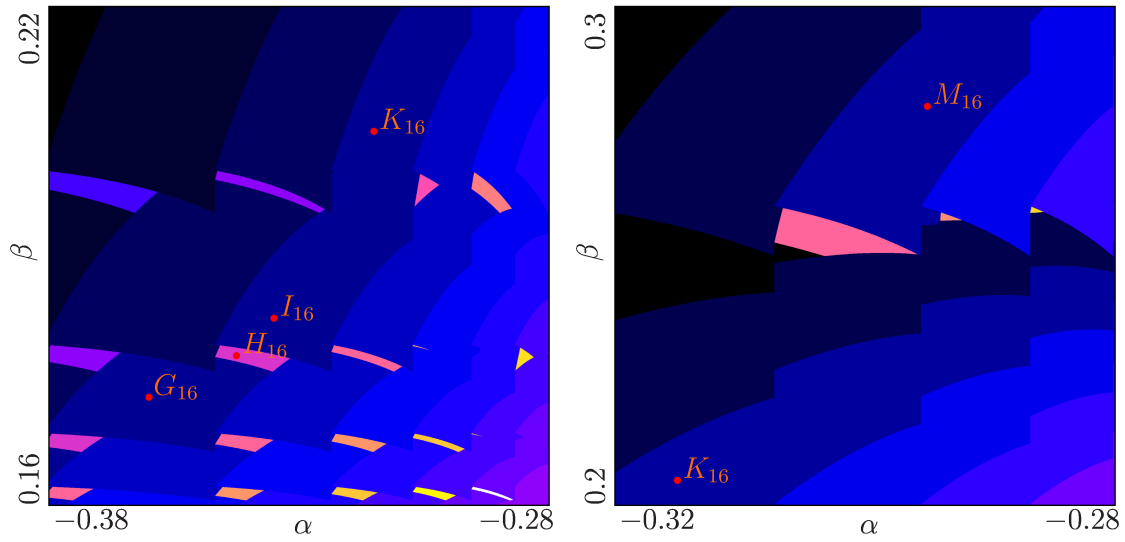

(a) Larger values for β **(b)** Even larger values for β

Figure 6.12: 2D scans of periods associated with parameter regions in the halved archetypal model showing the end of the chains of parameter regions associated of the same period. The parameters $a_L = 4, b_L = -\frac{1}{2}$, and $g_R\left(\frac{1}{2}\right) = \frac{1}{2} + \frac{1}{40}$ are fixed. The parameters $\alpha = -g_R\left(\frac{1}{4}\right)$ and $\beta = c_L$ are varied in different ranges. (a) shows the 2D scan for larger values of β where "type B" regions start missing from the chain of period 16. The parameters are varied in the ranges $[-0.38, -0.28]$ and $[0.16, 0.22]$. (b) shows the 2D scan for even larger values of β where the chain is no longer connected. The parameters are varied in the ranges $[-0.32, -0.28]$ and $[0.2, 0.3]$.

$\mathcal{P}_{\mathcal{A}^2\mathcal{B}^6\mathcal{C}^2\mathcal{D}^6}$. His hypothesis is that the scan of the periods done here is a two-dimensional one, while the model has more dimensions. So choosing a different parameter plane for the 2D scan of the periods might reveal a perfect chain with period 16 [Aky22]. This could also be the case here, since the archetypal model has 5 parameters and the period scan is done in two dimensions also. Two ways, one could perhaps obtain such complete chains are introduced next.

First, one could adjust the parameters α and β to act differently for the values at the end of the chains. For example, the parameter β influences the parameter c_L directly in the archetypal model. But it could also influence some other parameters of the model when β crosses some threshold. The same can be done for α.

Secondly, one could try to force the model to behave in such a way that the shape of the model function at some parameter values α_2 and β_2 is the same as the shape of the model function at the parameter values α_1 and β_1 shifted by $\frac{1}{4}$ where the parameter values α_1 and β_1 belong to a parameter region at the start of a chain. This can be expressed more precisely using Equation (6.1).

$$f_{\alpha_1,\beta_1}\left(x + \frac{1}{4}\right) \equiv f_{\alpha_2,\beta_2}(x) \mod 1 \tag{6.1}$$

This way, the stable cycle at the parameter values α_2 and β_2 is $O_{\mathcal{A}^{m-1}\mathcal{B}\mathcal{C}^{m-1}\mathcal{D}}$, provided the cycle at the beginning of the chain with parameter value α_1 and β_1 is $O_{\mathcal{A}\mathcal{B}^{m-1}\mathcal{C}\mathcal{D}^{m-1}}$. The newly chosen parameters should still act similar to the parameters α and β in the archetypal model. More

specifically, the new parameter α needs to still have the same effect as in the archetypal model, but also the inverse effect of β in the archetypal model to achieve the symmetry Equation (6.1). The same is true for the new parameter β. Also, the model needs to have four quadratic branches. This is therefore not possible with the archetypal model proposed in this thesis but can be achieved with the piecewise-quadratic model introduced in Section 5.2.

7 Period-adding in the Archetypal Model

This chapter explores, what else can happen in the archetypal model besides the PI structure that was described in Chapter 6. For this, the values of the fixed parameters of the archetypal model are changed. The same parameters are varied.

7.1 Adjusting the Parameters

The fixed parameters in the archetypal model are $a_L = 4, b_L = -\frac{1}{2}$, and $g_R\left(\frac{1}{2}\right) = \frac{1}{2} + \frac{1}{40}$. Only the branches $f_{\mathcal{A}}$ and f_C are not monotonously increasing. Of the three fixed parameters, a_L and b_L influence the shape of the branches $f_{\mathcal{A}}$ and f_C. These parameters are adjusted to make the branches $f_{\mathcal{A}}$ and f_C monotonously increasing. The new parameter values are $a_L = 1$ and $b_L = \frac{1}{2}$. The new shape of the function can be seen in Figure 7.2b, now all branches are monotonously increasing. We will refer to this model as the piecewise-increasing archetypal model.

Figure 7.1 shows a 2D scan of the periods associated with parameter regions in the archetypal model with these new values for the fixed parameters stated above. In this scan, we can see that the "type B" parameter regions disappeared and "type A" parameter regions of the same chain seem to start overlapping. Also, in between the chains there are now small parameter regions with much higher periods. These structures look like period-adding structures. And indeed, it is plausible for PA structures to emerge in such a map. Simpson demonstrated in his work [Sim18] that a PWS circle map with two linear and increasing branches can exhibit PA. Figure 7.2a shows this map called skew sawtooth next to the archetypal model function with increasing branches. The skew sawtooth map is continuous while the archetypal model function with increasing branches is not. And the archetypal model function with increasing branches has quadratic branches while all branches in the skew sawtooth map are linear. But they are somewhat similar as we can see in the comparison in Figure 7.2.

In the following sections these structures are explored. They are referred to as period-adding-like (PAL) structures. But first, we will take a closer look at how the bifurcations structures change when adjusting the parameters a_L and b_L to make the branches $f_{\mathcal{A}}$ and f_C increasing.

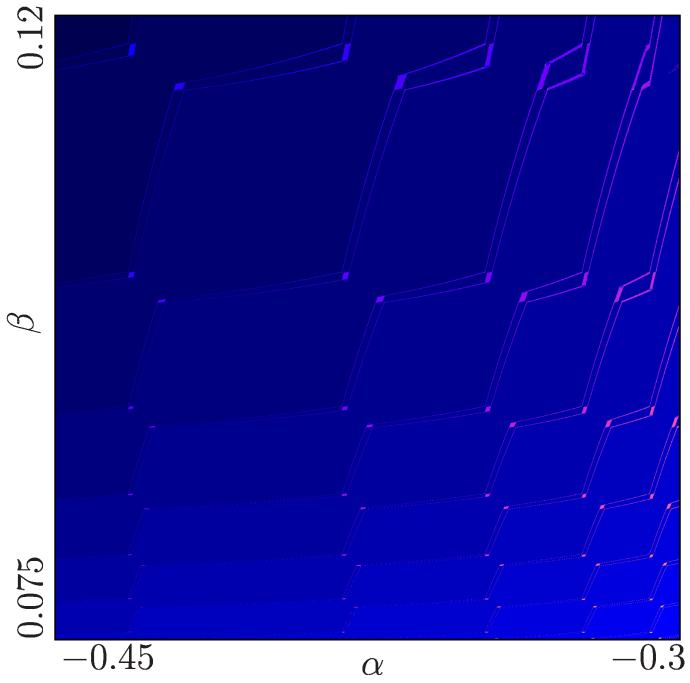

Figure 7.1: 2D scan of the periods associated with parameter regions in the archetypal model with increasing branches. The parameters $a_L = 1, b_L = \frac{1}{2}$, and $g_R\left(\frac{1}{2}\right) = \frac{1}{2} + \frac{1}{40}$ are fixed. The parameters $\alpha = -g_R\left(\frac{1}{4}\right)$ and $\beta = c_L$ are varied in the ranges $[-0.45, -0.3]$ and $[0.075, 0.12]$.

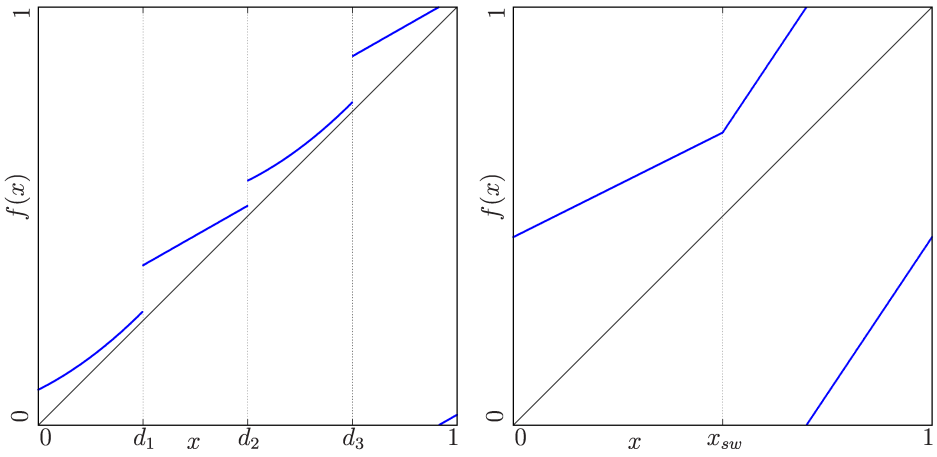

(a) Skew sawtooth map **(b)** Function shape

Figure 7.2: Comparison of the archetypal model function with increasing branches and the skew sawtooth map. (a) shows the archetypal model function with the parameters $a_L = 1, b_L = \frac{1}{2}, c_L = 0.168, g_R\left(\frac{1}{4}\right) = -0.4$, and $g_R\left(\frac{1}{2}\right) = \frac{1}{2} + \frac{1}{40}$. (b) shows the skew sawtooth map which is defined in [Sim18] with the parameters $a_L = 0.5$ and $a_R = 1.5$. The parameters happen to have similar names to the parameters of the archetypal model.

7.2 Changes to the Bifurcation Structure

This section examines how changing the parameters as described in Section 7.1 affects the bifurcation structure of the archetypal model.

7.2.1 Numerical Overview of the Changes to the Bifurcation Structure

Figure 7.3 shows diagrams depicting the borders of parameter regions with different symbolic sequences. These diagrams are used as the basis for the exploration of changes to the bifurcation structure. The lower left corner of the diagrams is always in the parameter region with the stable cycle $O_{\mathcal{A}^7\mathcal{B}^3\mathcal{C}^7\mathcal{D}^3}$. The cycles in the upper left ($O_{\mathcal{A}^6\mathcal{B}^3\mathcal{C}^6\mathcal{D}^3}$), upper right ($O_{\mathcal{A}^6\mathcal{B}^4\mathcal{C}^6\mathcal{D}^4}$), lower right ($O_{\mathcal{A}^7\mathcal{B}^4\mathcal{C}^7\mathcal{D}^4}$), and middle ($O_{\mathcal{A}^7\mathcal{B}^3\mathcal{C}^6\mathcal{D}^4}$ and $O_{\mathcal{A}^6\mathcal{B}^4\mathcal{C}^7\mathcal{D}^3}$) follow.

Here, a short notation for the symbolic sequences is introduced. "Type A" parameter regions where the cycle is associated with the symbolic sequence $\mathcal{A}^a\mathcal{B}^b\mathcal{C}^a\mathcal{D}^b$ are written as $P_b^{2\cdot(a+b)}$ "Type B" parameter regions where the coexisting twin cycles are associated with the symbolic sequences $\mathcal{A}^a\mathcal{B}^b\mathcal{C}^c\mathcal{D}^d$ and $\mathcal{A}^c\mathcal{B}^d\mathcal{C}^a\mathcal{D}^b$ where $c = a - 1$ and $d = b + 1$ are written as $P_b^{a+b+c+d}$. So for example, the "type A" parameter region in the lower left corner of every diagram in Figure 7.3 is written as P_3^{20}.

There is also a new type of parameter region that we call hybrid parameter regions with hybrid cycles. Hybrid cycles are cycles that are asymmetrical like "type B" cycles and therefore also exist in pairs. The difference to "type B" cycles is that for two hybrid twin cycles with the symbolic sequences $\mathcal{A}^a\mathcal{B}^b\mathcal{C}^c\mathcal{D}^d$ and $\mathcal{A}^c\mathcal{B}^d\mathcal{C}^a\mathcal{D}^b$ either $c \neq a - 1$ or $d \neq b + 1$ but $c \leq a$ and $d \geq b$. For example, the two hybrid twin cycles $O_{\mathcal{A}^7\mathcal{B}^4\mathcal{C}^6\mathcal{D}^4}$ and $O_{\mathcal{A}^6\mathcal{B}^4\mathcal{C}^7\mathcal{D}^4}$. The short notations for their corresponding parameter regions are P_4^{22} and P_4^{20}. The parameter region with such hybrid cycles is written as $\left[P_4^{22} \mid P_4^{20}\right]$. This notation is chosen because of an operation that is introduced in the later Section 7.3.2. Section 7.2.3 covers how these parameter regions are created. These parameter regions are connected to the PAL structures next to them, as we will see later in Section 7.3.2.

The four different diagrams in Figure 7.3 show the evolution at different points during the transition from the archetypal model to the piecewise-increasing archetypal model. For this, the parameter values for a_L and b_L are chosen along a line given by Equation (7.1).

$$a_L = \frac{5}{2} - 3 \cdot b_L \tag{7.1}$$

The disappearance of the "type B" parameter regions is examined first in the next section. The section after that examines the appearance of the PAL structures between the chains of parameter regions associated with the same period.

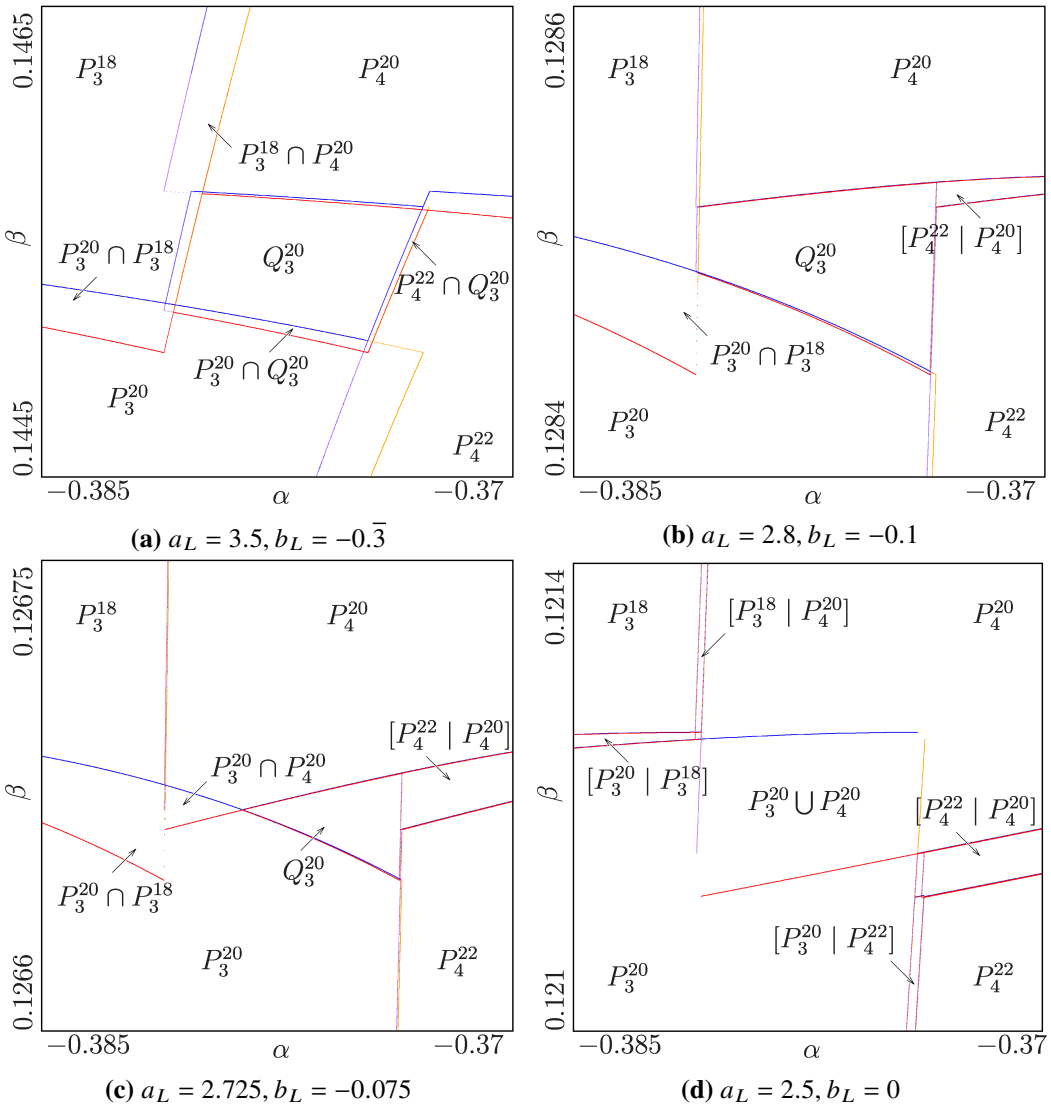

(a) $a_L = 3.5, b_L = -0.\overline{3}$ **(b)** $a_L = 2.8, b_L = -0.1$

(c) $a_L = 2.725, b_L = -0.075$ **(d)** $a_L = 2.5, b_L = 0$

Figure 7.3: 2D scans of the boundaries of parameter regions associated with different symbolic sequences in the archetypal model showing their evolution when transitioning to increasing branches. The parameter $g_R\left(\frac{1}{2}\right) = \frac{1}{2} + \frac{1}{40}$ is fixed in every diagram. The parameters a_L and b_L are fixed, but different in every diagram. Their values are on the line given by Equation (7.1). The parameter $\alpha = g_R\left(\frac{1}{4}\right)$ is varied in the range $[-0.385, -0.37]$ in every diagram. The parameter $\beta = c_L$ is varied in different ranges in every diagram such that the parameter region in the lower left corner is always P_3^{20}. (a) shows the boundaries for the fixed parameters $a_L = 3.5$ and $b_L = -0.\overline{3}$ with the parameter β being varied in the range $[0.1445, 0.1465]$, (b) shows the boundaries for the fixed parameters $a_L = 2.8$ and $b_L = -0.1$ with the parameter β being varied in the range $[0.1284, 0.1286]$, (c) shows the boundaries for the fixed parameters $a_L = 2.75$ and $b_L = -0.075$ with the parameter β being varied in the range $[0.1266, 0.12675]$, and (d) shows the boundaries for the fixed parameters $a_L = 2.5$ and $b_L = 0$ with the parameter β being varied in the range $[0.121, 0.1214]$.

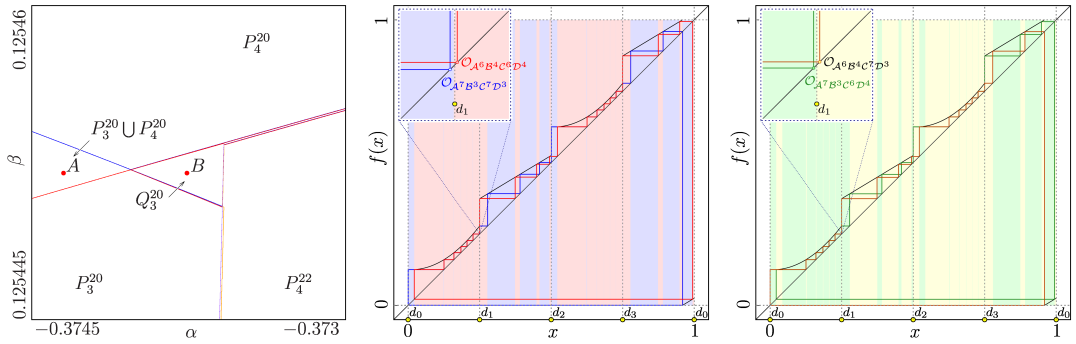

(a) Boundaries **(b)** A **(c)** B

Figure 7.4: 2D scans of the boundaries of parameter regions associated with different symbolic sequences and cobweb diagrams at two parameter values in the archetypal model showing the disappearance of "type B" parameter regions. The parameters $a_L = 2.567$, $b_L = -0.058333$, and $g_R\left(\frac{1}{2}\right) = \frac{1}{2} + \frac{1}{40}$ are fixed. The parameters $\alpha = -g_R\left(\frac{1}{4}\right)$ and $\beta = c_L$ are different in every diagram. (a) shows the 2D scan of the boundaries with the parameters α and β being varied in the ranges $[-0.3745, -0.373]$ and $[0.125445, 0.12546]$, (b) shows the cycles at the point A marked in (a) where $\alpha = -0.374348$ and $\beta = 0.125452$, and (b) shows the cycles at the point B marked in (a) where $\alpha = -0.373758$ and $\beta = 0.125452$.

7.2.2 Disappearance of "Type B" Parameter Regions

For Figures 7.3a and 7.3b, the "type B" parameter region Q_3^{20} is complete. In Figure 7.3d, it is gone completely, instead the two "type A" parameter regions P_3^{20} and P_4^{20} now overlap.

In-between those two stages, we can see how the "type B" parameter region Q_3^{20} disappears. Somewhere along the parameter line given by Equation (7.1) between Figure 7.3b and Figure 7.3c, the lower left corner of the parameter region P_4^{20} crosses the upper boundary of the parameter region P_3^{20}. This causes the "type A" parameter regions P_3^{20} and P_4^{20} to overlap in Figure 7.3c. The point, where both boundaries cross is not a codimension-2 point, since the bifurcation at the lower boundary of the overlapping parameter region We know from Section 6.2.5 that the border collision bifurcation at the upper boundary of P_3^{20} is $\xi_{d_1,d_3}^{\mathcal{A}^6\underline{\mathcal{B}}^4\mathcal{C}^6\underline{\mathcal{D}}^4}$ and the border collision bifurcation at the lower boundary of P_4^{20} is $\xi_{d_1,d_3}^{\underline{\mathcal{A}}^7\mathcal{B}^3\underline{\mathcal{C}}^7\mathcal{D}^3}$. Therefore, this point is **not** a codimension-2 point, since the bifurcations happen to different cycle. Nonetheless, this is the right corner of the overlapping parameter region of $P_3^{20} \cap P_4^{20}$.

At similar parameter values, where the lower left corner of P_4^{20} crosses the upper boundary of P_3^{20}, the upper left corner and the lower left corner of the "type B" parameter region Q_3^{20} collide causing the lower and upper boundaries of this parameter region to cross also. We know from Section 6.2.5 that the border collision bifurcations at the upper boundary of Q_3^{20} are $\xi_{d_1}^{\underline{\mathcal{A}}^7\mathcal{B}^3\mathcal{C}^6\mathcal{D}^4}$ and $\xi_{d_3}^{\mathcal{A}^6\mathcal{B}^4\underline{\mathcal{C}}^7\mathcal{D}^3}$ and the border collision bifurcations at the lower boundary of Q_3^{20} are $\xi_{d_3}^{\mathcal{A}^7\mathcal{B}^3\mathcal{C}^6\underline{\mathcal{D}}^4}$ and $\xi_{d_1}^{\mathcal{A}^6\underline{\mathcal{B}}^4\mathcal{C}^7\mathcal{D}^3}$. This is a codimension-2 point, since each of the coexisting cycles undergoes two different bifurcations

at this point. Also, this codimension-2 point is different from the codimension-2 points listed in Section 6.2.5, since those points always involve all four borders. Here, only the borders associated with vertical boundaries, namely d_1 and d_3, are involved in all four bifurcations at this point.

Along the parameter line given by Equation (7.1) for increasing values of b_L, the lower boundary of P_4^{20} and the upper boundary of Q_3^{20} move down while the upper boundary of P_3^{20} and the lower boundary of Q_3^{20} moves up. This leads to both the right corner of the overlapping region $P_3^{20} \cap P_4^{20}$ and the codimension-2 point which is the left corner of the "type B" parameter region Q_3^{20} to move right. We can observe this movement in Figure 7.4a. Here, those two corner points are near the right boundaries of Q_3^{20} and P_3^{20}. As soon as the codimension-2 point of the boundaries "type B" parameter region crosses the right boundary of the "type B" parameter region, the "type B" parameter region vanishes. And as soon as the right corner point of the overlapping parameter region $P_3^{20} \cap P_4^{20}$ collides with the upper right corner of P_3^{20}, the upper boundary of P_3^{20} stops crossing the lower boundary P_4^{20} and the overlapping parameter region $P_3^{20} \cap P_4^{20}$ has four boundaries instead of three.

Figure 7.4b shows a cobweb diagram of the coexisting "type A" cycles in the emerging overlapping parameter region $P_3^{20} \cap P_4^{20}$. We can see that the cycles are very close to colliding d_1 and d_3. The same is true for the coexisting "type B" twin cycles in the cobweb diagram in Figure 7.4c.

7.2.3 Appearance of Period-adding-like structures

This section explores the appearance of the PAL structures in between the chains of the same period. This happens at the horizontal boundaries between "type A" parameter regions of different chains, as well as at the vertical boundaries. The PAL structures in-between vertically neighboring "type A" parameter regions is examined first. After that the PAL structures in-between horizontally neighboring "type A" parameter regions is examined.

Period-adding-like Structures In-between Vertically Neighboring "Type A" Parameter Regions

In Figure 7.3a, the "type A" parameter regions P_3^{20} and P_3^{18}, as well as P_4^{22} and P_4^{20} overlap. This changes in Figure 7.3b. Here only the "type A" parameter regions P_3^{20} and P_3^{18} overlap, the parameter regions P_4^{22} and P_4^{20} stopped overlapping. Instead, in the space between the two "type A" parameter region there are now two asymmetric coexisting twin cycles $O_{\mathcal{A}^8\mathcal{B}^3\mathcal{C}^8\mathcal{D}^2}$ and $O_{\mathcal{A}^8\mathcal{B}^2\mathcal{C}^8\mathcal{D}^3}$. Those cycles are **not** "type B" cycles, because they only differ in the number of points on the branches $f_{\mathcal{B}}$ and $f_{\mathcal{D}}$. Remember that "type B" cycles are asymmetrical twin cycles $O_{\mathcal{A}^a\mathcal{B}^b\mathcal{C}^c\mathcal{D}^d}$ and $O_{\mathcal{A}^c\mathcal{B}^d\mathcal{C}^a\mathcal{D}^b}$ where $c = a - 1$ and $d = b + 1$. This is not the case here, since $a = c$. Instead, we will call them hybrid cycles and "type B" cycles are a special case of hybrid cycles. The notation $\left[P_4^{22} \mid P_4^{20}\right]$ used in the diagrams was introduced in Section 7.2.1 and is formally defined later in Section 7.3.2. Later in Figure 7.3d, the "type A" parameter regions P_3^{20} and P_3^{18} also stop overlapping. In between, there are also hybrid cycles, $O_{\mathcal{A}^7\mathcal{B}^3\mathcal{C}^6\mathcal{D}^3}$ and $O_{\mathcal{A}^6\mathcal{B}^3\mathcal{C}^7\mathcal{D}^3}$. This parameter region is therefore labeled $\left[P_3^{20} \mid P_3^{18}\right]$.

For some parameter values along the line given by Equation (7.1) between the parameter values used for Figures 7.3a and 7.3b, upper left corner of P_4^{22} crosses the lower boundary of P_4^{20}. This causes the boundaries of P_4^{22} and P_4^{20} to cross, similar to the last section where the boundaries of

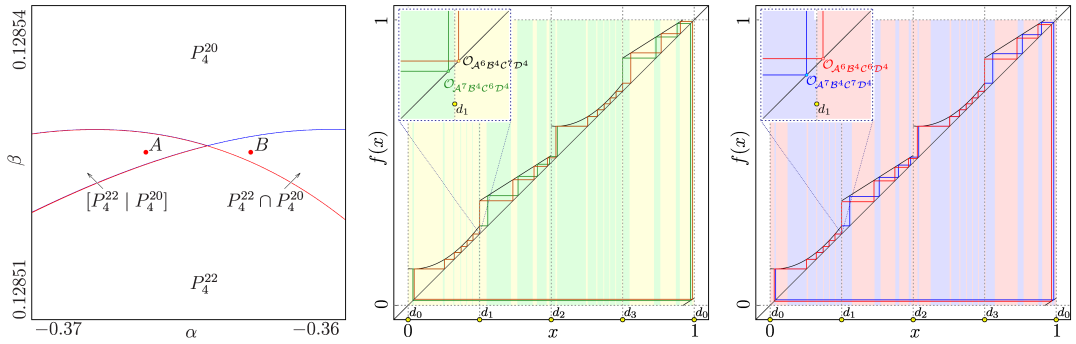

(a) Boundaries **(b)** A **(c)** B

Figure 7.5: 2D scan of the boundaries of parameter regions associated with different symbolic sequences and cobweb diagrams at two parameter values in the archetypal model showing the appearance of horizontally oriented PAL structures. The parameters $a_L = 2.8, b_L = -0.1$, and $g_R\left(\frac{1}{2}\right) = \frac{1}{2} + \frac{1}{40}$ are fixed. The parameters $\alpha = -g_R\left(\frac{1}{4}\right)$ and $\beta = c_L$ are different in every diagram. (a) shows the 2D scan of the boundaries with the parameters α and β being varied in the ranges $[-0.37, -0.36]$ and $[0.12851, 0.1254]$, (b) shows the cycles at the point A marked in (a) where $\alpha = -0.366362$ and $\beta = 0.128526$, and (b) shows the cycles at the point B marked in (a) where $\alpha = -0.363022$ and $\beta = 0.128526$.

P_3^{20} and P_4^{20} started overlapping. But in this case, the overlapping parameter region $P_4^{22} \cap P_4^{20}$ had four boundaries before and now has only three boundaries with the point where the boundaries cross moving right. The point where the boundaries cross cannot be seen in Figure 7.3b, but it is visible in Figure 7.5a. We know from Section 6.2.5 that the border collision bifurcation at the upper boundary of the "type A" parameter region P_4^{22} is $\xi_{d_1,d_3}^{\underline{\mathcal{A}^7}\mathcal{B}^4\underline{\mathcal{C}^7}\mathcal{D}^4}$. And the border collision bifurcation at the lower boundary of the "type A" parameter region P_4^{20} is $\xi_{d_1,d_3}^{\mathcal{A}^6\underline{\mathcal{B}^4}\mathcal{C}^6\underline{\mathcal{D}^4}}$. Both these border collision bifurcations are at the upper and lower boundaries of the overlapping region $P_4^{22} \cap P_4^{20}$. At the point where these boundaries cross, both these border collision bifurcations happen at the same time and both cycles vanish. We can see in Figure 7.5b that the "type A" cycles are very close to the borders d_1 and d_3, respectively.

Similarly, the hybrid parameter region $\left[P_4^{22} \mid P_4^{20}\right]$ that emerged in the opening space has a codimension-2 point as its right corner. Just as the "type B" parameter region had a codimension-2 point as its left corner. Figure 7.5b shows the coexisting hybrid cycles in this hybrid parameter region. And Figures 7.6a and 7.6b show the border collision bifurcations at the upper and lower boundaries of the hybrid parameter region, $\xi_{d_3}^{\mathcal{A}^7\mathcal{B}^4\mathcal{C}^6\underline{\mathcal{D}^4}}$ and $\xi_{d_1}^{\mathcal{A}^6\underline{\mathcal{B}^4}\mathcal{C}^7\mathcal{D}^4}$ at the lower boundary and $\xi_{d_1}^{\underline{\mathcal{A}^7}\mathcal{B}^4\mathcal{C}^6\mathcal{D}^4}$ and $\xi_{d_3}^{\mathcal{A}^6\mathcal{B}^4\underline{\mathcal{C}^7}\mathcal{D}^4}$ at the upper boundary. Those four border collision bifurcations happen at the codimension-2 point. Again, the coexisting hybrid twin cycles are very close to the borders d_1 and d_3 for the parameter values marked with the point B in Figure 7.5a. We can see this in the cobweb diagram in Figure 7.5c.

Both corner points move right for increasing values of b_L along the parameter line given by Equation (7.1). This is again caused by the movement of the boundaries of the "type A" parameter regions and the hybrid parameter region $\left[P_4^{22} \mid P_4^{20}\right]$. This time, the overlapping area disappears

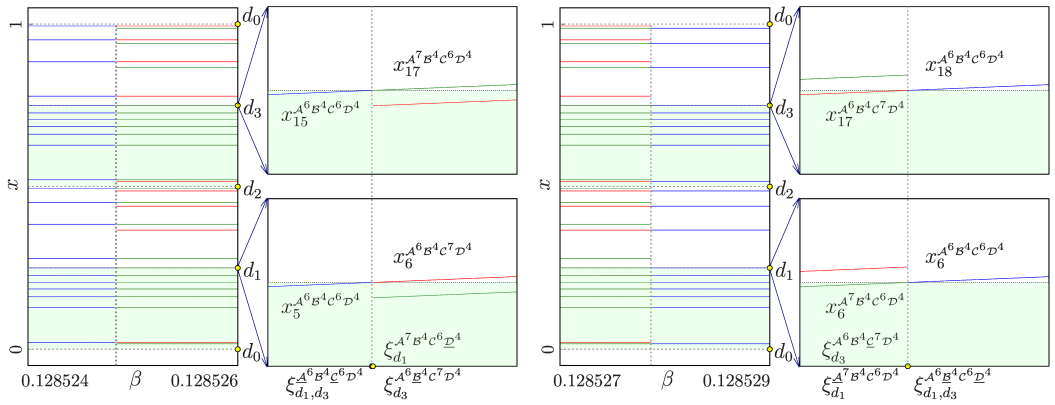

(a) Lower boundary **(b)** Upper boundary

Figure 7.6: 1D bifurcation diagrams at the upper and lower boundary of the horizontally oriented hybrid parameter region in the archetypal model. The parameters $a_L = 2.8, b_L = -0.1, g_R\left(\frac{1}{2}\right) = \frac{1}{2} + \frac{1}{40}$, and $\alpha = g_R\left(\frac{1}{4}\right) = 0.366362$ are fixed. The parameter $\beta = c_L$ is varied in different ranges. (a) shows the bifurcation diagram at the lower boundary with β being varied in the range $[0.128524, 0.128526]$ and (b) shows the bifurcation diagram at the upper boundary with β being varied in the range $[0.128527, 0.128529]$.

as soon as its left corner collides with the lower right corner of P_4^{20} and the upper right corner of P_4^{22}. And the hybrid parameter region has four boundaries as soon as its corner point reaches the theoretical right boundary. This transition can be seen for the parameter regions P_3^{20} and P_3^{18} in Figures 7.3a and 7.3d.

The appearance of the hybrid parameter region and the PAL structures in-between vertically neighboring "type A" parameter regions is very similar to the disappearance of "type B" parameter regions described in Section 7.2.2. But instead of the overlapping parameter region of two "type A" parameter regions appearing, it disappeared and a parameter region with two coexisting asymmetrical twin cycles appeared instead of disappearing.

Period-adding-like Structures In-between Horizontally Neighboring "Type A" Parameter Regions

In contrast to the PAL structures in-between vertically neighboring "type A" parameter region, no numerical evidence for a crossing of boundaries of "type A" parameter regions could be found. As far as this thesis is concerned, the opening of the space between horizontally neighboring "type A" parameter regions happens at once.

In Figures 7.3a to 7.3c, the parameter regions P_3^{20} and P_4^{22}, as well as P_3^{18} and P_4^{20} overlap. And in Figure 7.3d they do not overlap, instead there is space in-between these vertically neighboring "type A" parameter regions with hybrid parameter regions and PAL structures. The appearance of the parameter region $\left[P_3^{20} \mid P_4^{22}\right]$ in between P_3^{20} and P_4^{22} seems to happen at the same time as the appearance of the hybrid parameter region $\left[P_3^{18} \mid P_4^{20}\right]$ in between P_3^{18} and P_4^{20}, at some

parameter values on the line given by Equation (7.1) between the parameter values of Figures 7.3c and 7.3d. And with these hybrid parameter regions the vertical PAL structures between them and the neighboring "type A" parameter regions also appear.

Figures 7.7a and 7.7b show this transition again for the parameter regions P_3^{20} and P_4^{22}. As mentioned before, we assume that there is no crossing of the boundaries of the "type A" parameter regions in a point that moves up or down as in the previous section. This means that at some parameter values, the boundaries are perfectly aligned with the "type A" parameter regions overlapping for values on the parameter line for smaller values b_L and a hybrid parameter region for lager values of b_L.

Figure 7.7c shows the coexistence of the two coexisting "type A" cycles while the "type A" parameter regions still overlap. Figure 7.7d shows the coexistence of the two coexisting hybrid cycles in the newly created parameter region $\left[P_3^{20} \mid P_4^{22}\right]$. In both cases, the coexisting cycles are very close to the borders d_0 and d_2.

The border collision bifurcations at the left and right boundary of the hybrid parameter region follow the same rules as the border collision bifurcations "type B" parameter regions. At the left boundary, the hybrid cycles collide with the borders d_0 and d_2 from the left at the same time, pictured in Figure 7.8a. And at the right boundary, they collide with the same borders from the right at the same time, pictured in Figure 7.8b. Note that at the left boundary, the border collision bifurcations of the hybrid cycles are left of the border collision bifurcation of the "type A" cycle. This causes all three cycles to coexist in the parameter region between the border collision bifurcations. At the right boundary on the other hand, the border collision bifurcations of the hybrid cycles are also left of the border collision bifurcation of the "type A" cycle. This causes a space between the hybrid parameter region $\left[P_3^{20} \mid P_4^{22}\right]$ and the "type A" parameter region P_3^{20} where a period-adding-like structure emerges. The cycle of the first stage of this PAL structure is visible in purple in Figure 7.8b.

7.2.4 Summary of the Changes to the Bifurcation Structure

This section summarizes all the changes that happen to the PI structure of the archetypal model when the parameters are changed in such a way that PAL structures emerge. Furthermore, it provides an explanation for why the PI structure of the archetypal model is impossible with only increasing branches.

Schematics and Summary of the Changes

Figure 7.9 shows multiple schematics that are used in this section to summarize all changes. All schematics show some boundaries of the "type A" parameter regions P_k^m, P_{k-1}^{m-2}, P_{k+1}^m, and P_{k+1}^{m+2} and all boundaries of the "type B" parameter region Q_k^m. The "type B" parameter region is in-between all the "type A" parameter regions in the beginning. This is shown in Figure 7.9a. The corners of the parameter regions are marked as follows. The upper right corner of the "type B" parameter region in the middle is marked with the point $C_Q^{\nearrow}$. Similarly, the lower right corner is marked with the point $C_Q^{\searrow}$ and the remaining corners with the points $C_Q^{\nwarrow}$ and $C_Q^{\nwarrow}$. The corners of the "type A" parameter regions are marked analogously with $C_P^{\nearrow}$, $C_P^{\searrow}$, $C_P^{\nwarrow}$, and $C_P^{\swarrow}$. But here, the corners belong to different parameter regions.

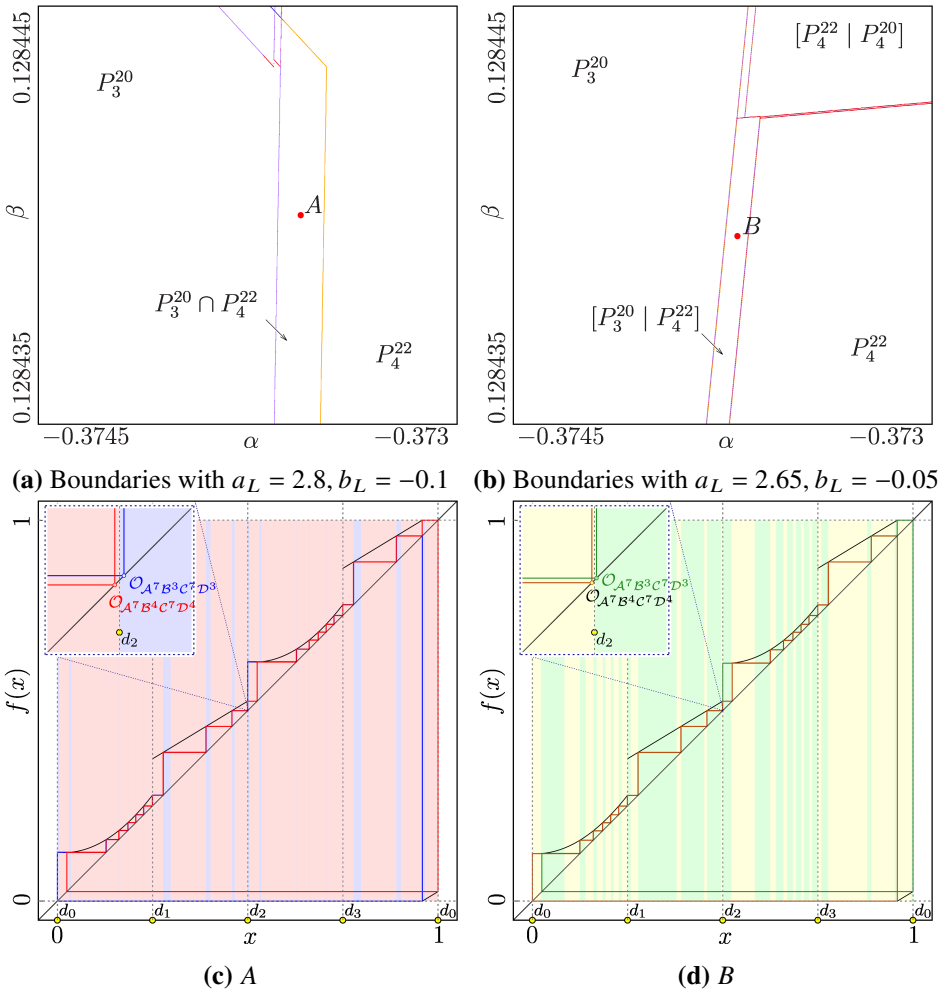

(a) Boundaries with $a_L = 2.8, b_L = -0.1$ **(b)** Boundaries with $a_L = 2.65, b_L = -0.05$

(c) A **(d)** B

Figure 7.7: 2D scans of the boundaries of parameter regions associated with different symbolic sequences and cobweb diagrams at two parameter values in the archetypal model showing the appearance of horizontally oriented PAL structures. The parameter $g_R\left(\frac{1}{2}\right) = \frac{1}{2} + \frac{1}{40}$ is fixed for all diagrams. The parameters $a_L, b_L, \alpha = -g_R\left(\frac{1}{4}\right)$, and $\beta = c_L$ are different in every diagram. In (a) and (c), the parameters $a_L = 2.8$ and $b_L = -0.1$ are fixed, and in (b) and (d), the parameters $a_L = 2.65$ and $b_L = -0.05$ are fixed. (a) and (b) show the boundaries for the aforementioned fixed parameters with α and β being varied in the ranges $[-0.3745, -0.373]$ and $[0.128435, 0.128445]$ in both diagrams, (c) shows the cycles at the point A marked in (a) where $\alpha = -0.37356$ and $\beta = 0.12844$, and (d) shows the cycles at the point B marked in (a) where $\alpha = -0.373697$ and $\beta = 0.124797$.

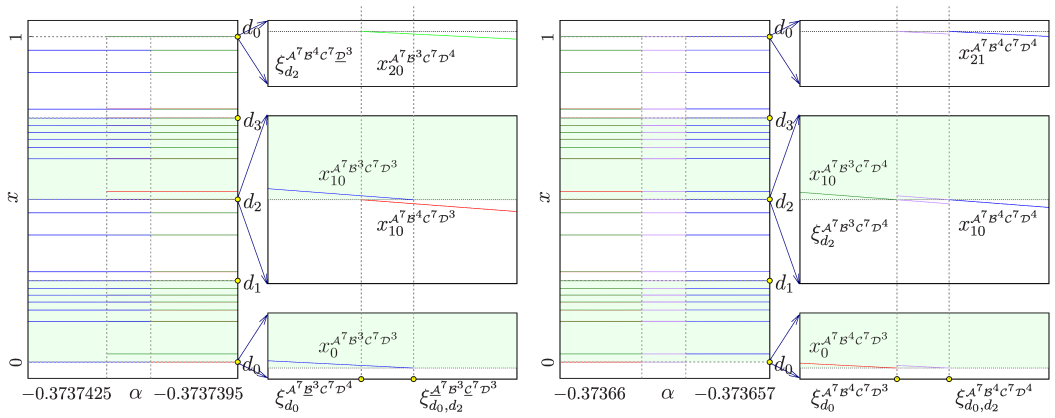

(a) Left boundary **(b)** Right boundary

Figure 7.8: 1D bifurcation diagrams at the left and right boundary of the vertically oriented hybrid parameter region in the archetypal model. The parameters $a_L = 2.65, b_L = -0.05, g_R\left(\frac{1}{2}\right) = \frac{1}{2} + \frac{1}{40}$, and $\beta = c_L = 0.124797$ are fixed. The parameter $\alpha = -g_R\left(\frac{1}{4}\right)$ is varied in different ranges. (a) shows the bifurcation diagram at the left boundary with α being varied in the range $[-0.3737425, -0.3737395]$ and (b) shows the bifurcation diagram at the right boundary with α being varied in the range $[-0.37366, -0.373657]$.

The changes are summarized in the order they happen to the parameter regions that are considered in the previous sections. This order might differ for different parameter regions.

First, the upper left corner $C_Q^{\nwarrow}$ of the lower right "type A" parameter region P_{k+1}^{m+2} moves down and crosses the lower boundary of the upper right "type A" parameter region P_{k+1}^{m}. This is visible in Figure 7.9b. The point where the two boundaries of the horizontally neighboring "type A" parameter regions cross is marked as $C_{P\cap P}^{\leftarrow}$ because this point is now the only left corner point of the overlapping parameter region $P_{k+1}^{m+2} \cap P_{k+1}^{m}$. For higher values of b_L, the point $C_Q^{\nwarrow}$ moves further down which causes the point where the boundaries cross to move right. In Figure 7.9c, this crossing point is not visible anymore, since it moved out of the domain of the picture. In Figure 7.9d, it is visible again, but on the left side of the schema. Strictly speaking, this is not the same point but the left boundary of the overlapping parameter region $P_k^m \cap P_k^{m-2}$. This point then collides with the corner point $C_P^{\nearrow}$ which then causes the two "type A" parameter regions to not overlap anymore. This final scenario can be seen in Figure 7.9e. In the spaces that opened up between the vertically neighboring "type A" parameter regions, there are big hybrid parameter regions $\left[P_{k+1}^{m+2} \mid P_{k+1}^{m}\right]$ and $\left[P_k^m \mid P_k^{m-2}\right]$, respectively. The hybrid parameter regions are not shown in the schematics but while the overlapping parameter regions have only three boundaries, they too only have three boundaries and are bounded to the right only by one codimension-2 point. At this point, their upper and lower boundaries meet.

As we can see in the schematics, this change starts first and finishes last. While the described process occurs, another change starts happening. The points $C_P^{\searrow}$ and $C_Q^{\nearrow}$ move down while the points $C_Q^{\searrow}$ and $C_P^{\nearrow}$ move up. As soon as the point $C_P^{\swarrow}$ crosses the upper boundary of P_k^m, the "type A" parameter regions P_k^m and P_{k+1}^m start to overlap. This overlapping region is bounded to the right only by the point where the horizontal boundaries of those two parameter regions cross. This point is marked as $C_{P\cap P}^{\rightarrow}$ in Figure 7.9c. Also at some parameter values the corner points $C_Q^{\nwarrow}$ and

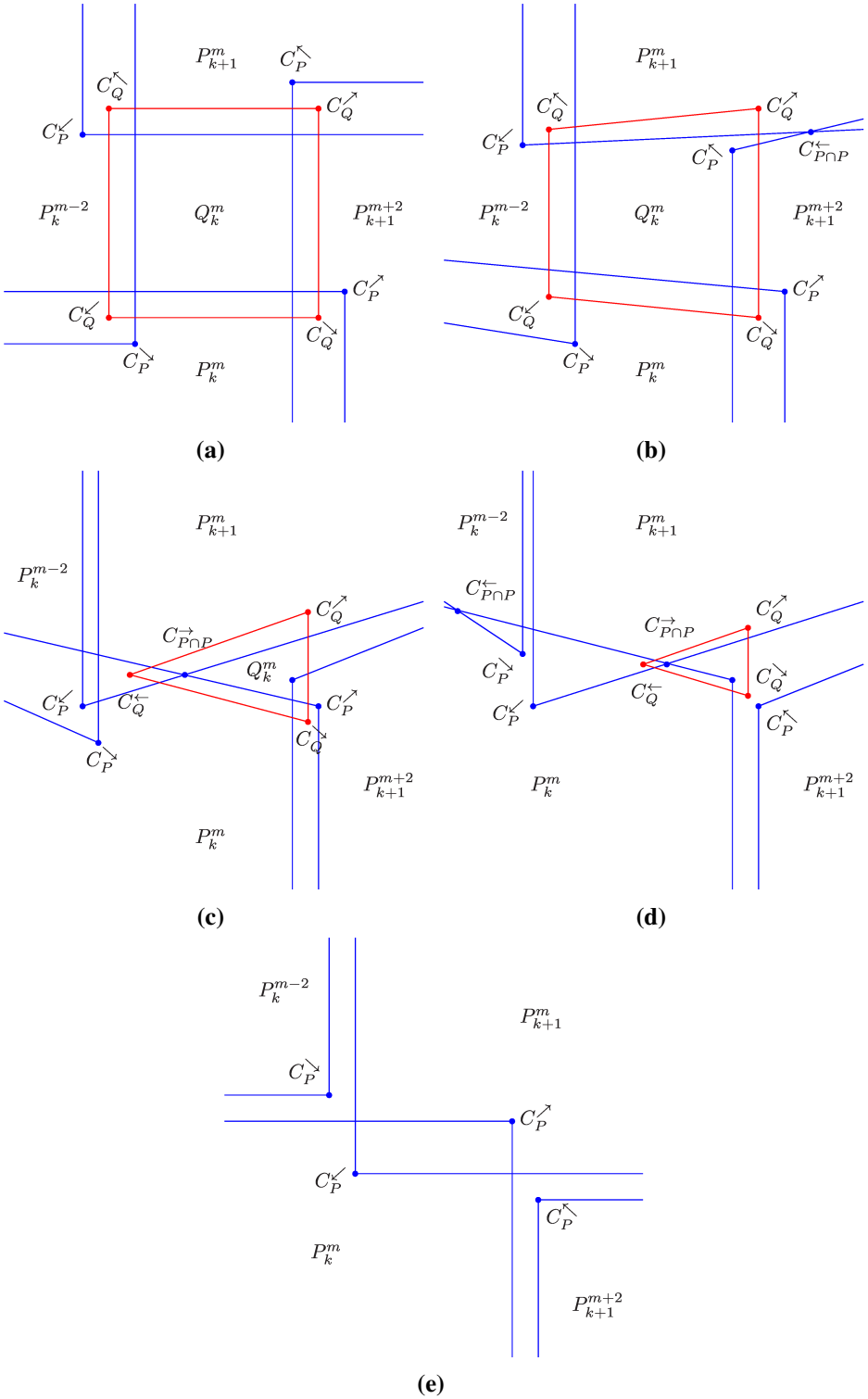

Figure 7.9: Schematics of the boundaries of parameter regions associated with different symbolic sequences during the transition of the archetypal model to increasing branches. The boundaries of "type A" parameter regions are shown in blue while the boundaries of "type B" parameter regions are shown in red. Significant points where boundaries meet or cross are marked with dots.

$C_Q^{\searrow}$ of the "type B" parameter region Q_k^m in the middle collide. This creates a codimension-2 point that bounds the parameter region Q_k^m to the left, hence it is marked as $C_Q^{\leftarrow}$. Both these newly created corner points move right, as can be seen in Figure 7.9d. Finally, the corner point $C_{P\cap P}^{\rightarrow}$ collides with the corner point $C_P^{\nearrow}$ and the two horizontal boundaries of the "type A" parameter regions stop crossing. The overlapping parameter region $P_k^m \cap P_{k+1}^m$ is now bounded by four boundaries, as can be seen in Figure 7.9e. And the corner point $C_Q^{\leftarrow}$ crosses the right boundary of the "type B" parameter region, destroying the "type B" parameter region.

While that change is happening, one more change takes place. This change does not happen by two boundaries crossing at one point like the last two changes. Instead, the numerical evidence suggests that it happens at once. The corner point $C_P^{\nwarrow}$ crosses the right boundary of P_k^m at the same time, the lower right corner point of P_k^m which is not pictured here crosses the left boundary of P_{k+1}^{m+2}. This lower corner point is not pictured, but the lower right corner point of P_k^{m-2} is pictured and marked as $C_P^{\searrow}$. Here, the equivalent happens for the horizontally neighboring "type A" parameter regions P_k^{m-2} and P_{k+1}^m. In Figure 7.9c, the horizontally neighboring "type A" parameter regions overlap and in Figure 7.9d, the parameter regions do not overlap. Instead, there is now space in-between the horizontally neighboring "type A" parameter regions. In this space there now is a big hybrid parameter region and PAL structures, similar to the vertically neighboring "type A" parameter regions.

Observations

The local minima on branches $f_{\mathcal{A}}$ and f_C seem to be important for the "type B" parameter regions. That means, parameter regions with coexisting asymmetrical cycles with the **same** period. At the same time, these minima seem to prevent period-adding structures. It will be proven next that "type B" parameter regions are impossible with only increasing branches.

Lemma 7.1 (Number and Positions of Points of two Cycles on an Increasing Branch)
Let f_χ be an increasing branch of some model function f. If two cycles σ_1 and σ_b have points on this branch, there are two possibilities for the relative number of points and relative position of the points.

(i) Both cycles have the same number of points on the branch f_χ. Let the first point of σ_1 be to the left of the first point of σ_2 on this branch w.l.o.g. Then the last point of σ_1 is also to the left of the last point of σ_2 on this branch. Figure 7.10a illustrates this case.

(ii) One cycle has one more point on the branch f_χ. Let σ_1 be the cycle with more points on this branch w.l.o.g. Then the first point of σ_1 is to the left of the first point of σ_2 on this branch and the last point of σ_1 is to the right of the last point of σ_2 on this branch. Figure 7.10b illustrates this case.

Theorem 7.2 (No "Type B" Parameter Regions with only Increasing Branches)
The "type B" parameter regions are not possible in the increasing archetypal model. The minima on the branches $f_{\mathcal{A}}$ and f_C are essential for the bifurcation structure.

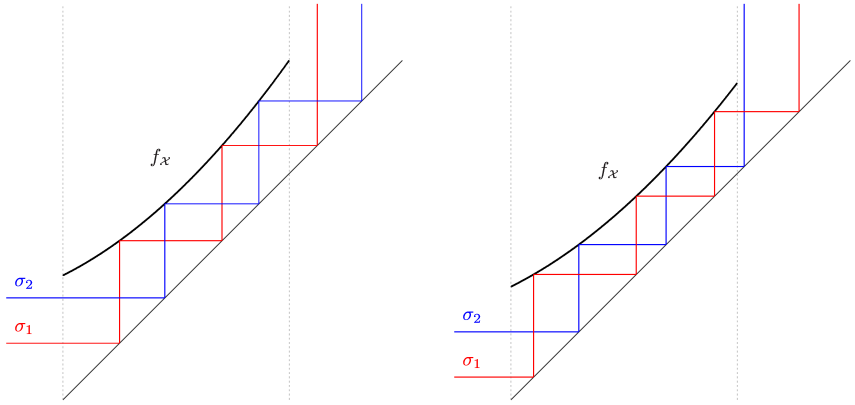

(a) Same number of points **(b)** Number of points differing by one

Figure 7.10: Illustration of the relative number and positions of the points of two cycles on an increasing branch. Both figures show a function branch $f_\mathcal{X}$ and parts of two cycles, σ_1 shown in red and σ_2 shown in blue. (a) shows the case where both cycles have the same number of points on the branch $f_\mathcal{X}$ and the first point of σ_1 is to the left of the first point of σ_2 on this branch. (a) shows the case where the cycle σ_1 has one point more on the branch $f_\mathcal{X}$ than σ_2 and the first point of σ_1 is to the left of the first point of σ_2 on this branch.

Proof

Let's assume that all branches of the archetypal model $f_\mathcal{A}$, $f_\mathcal{B}$, f_C, and $f_\mathcal{D}$ are increasing. And let σ_1 and σ_2 be "type B" twin cycles. The following conditions are true for such cycles.

$$|\sigma_1|_\mathcal{A} - 1 = |\sigma_2|_\mathcal{A} \tag{7.2a}$$
$$|\sigma_1|_\mathcal{B} + 1 = |\sigma_2|_\mathcal{B} \tag{7.2b}$$
$$|\sigma_1|_C + 1 = |\sigma_2|_C \tag{7.2c}$$
$$|\sigma_1|_\mathcal{D} - 1 = |\sigma_2|_\mathcal{D} \tag{7.2d}$$

For Equation (7.2a) *to hold, the first point of σ_1 needs to be to the left of first point of σ_2 on the branch $f_\mathcal{A}$, because σ_1 has one point more on this branch than σ_2 and this branch is increasing. At the same time, the last point of σ_1 must be to the right of the last point of σ_2 on this branch.*

The order of the first points on the next branch, $f_\mathcal{B}$, is the same as for the last points on the branch $f_\mathcal{A}$. So the first point of σ_2 is to the left of the first point of σ_1 on this branch. For Equation (7.2b) *to hold, the last point of σ_2 must be to the right of the last point of σ_1 on this branch per the same logic as before.*

The order of the first points on the next branch, f_C, is the same as for the last points on the branch $f_\mathcal{B}$. So the first point of σ_1 is to the left of the first point of σ_2 on this branch. This is a contradiction, since the first point of σ_1 on the branch $f_\mathcal{A}$ is also to the left of the first point of σ_2 on that branch. This violates the symmetry. Also, Equation (7.2c) *cannot be fulfilled if the first point of σ_1 is to the left of the first point of σ_2 on the branch f_C, since the first point of with more points, σ_2 in this case, on the branch must be to the left of the first point of the other cycle on that branch if the branch is increasing.*

■

7.3 Investigation of the Period-adding-like Structures

Now we know, how the PAL structures develop. This section investigates the PAL structures. First, there will be a description of the structures. Here we will see why they are called period-adding-like structures and not period-adding structures.

7.3.1 Description of the Structures in the Increasing Archetypal Model

The first step in the description of the PAL structures is plotting a 2D scan of the periods of such a structure. Here, b_L is changed to 0.8, and a_L and $g_R\left(\frac{1}{2}\right)$ are kept as described before, because the PAL structures are more pronounced at these parameter values. Figure 7.11 shows a 2D period scan with these parameters at a corner of the space between chains. Here, the parameter region P_2^{12} is in the lower left corner and the parameter region P_3^{12} of the same chain is in the upper right corner. In the lower right corner is the parameter region P_3^{14}.

Next, this section takes a closer look at the horizontally PAL structures between the parameter regions P_3^{14} and P_3^{12}. After that, it examines the vertically oriented PAL structures between the parameter regions P_2^{12} and P_3^{14}. And lastly, it examines the complex looking structure in the corner between all three "type A" parameter regions.

Period-adding-like Structures In-between Vertically Neighboring "Type A" Parameter Regions

Figure 7.12a shows a 2D scan of the horizontally oriented PAL structures between the parameter regions P_3^{14} and P_3^{12}. We can see two PAL structures, one between the "type A" parameter region P_3^{14} and the hybrid parameter region $\left[P_3^{14} \mid P_3^{12}\right]$ and one in between the hybrid parameter region $\left[P_3^{14} \mid P_3^{12}\right]$ and the "type A" parameter region P_3^{12}. There is a red arrow in the 2D period scan that indicates the parameter range for the 1D period scan in Figure 7.12b.

Looking at the 1D period scan, one can see why the section is called period-adding-like. In the middle between the parameter regions associated with the periods 14 and 13, we would expect the most pronounced parameter region to be associated with the period 27. Instead, the most pronounced parameter region in-between those parameter regions is associated with the period 40. And the most pronounced parameter region between this parameter region and the parameter region associated with the period 14, has period 27 where we would expect period 54. We can see that the periods do not add in our case.

The structure is not just a skewed PA structure, as one might think since the period 27 is associated with another parameter region that is not the most pronounced between the parameter regions associated with the periods 14 and 13, respectively. And also 27 + 13 = 40 which is associated with the parameter region between the parameter regions associated with the periods 27 and 13, respectively. We can see that when examining the symbolic sequences associated with the parameter regions in that structure. Figure 7.13 shows the Farey-tree with the symbolic sequences of this structure. The starting nodes are associated with the symbolic sequences associated with the parameter regions P_3^{14} and $\left[P_3^{14} \mid P_3^{12}\right]$, respectively. The parameter region associated with the period 27 is the lowest node in level 2, which is associated with two coexisting cycles.

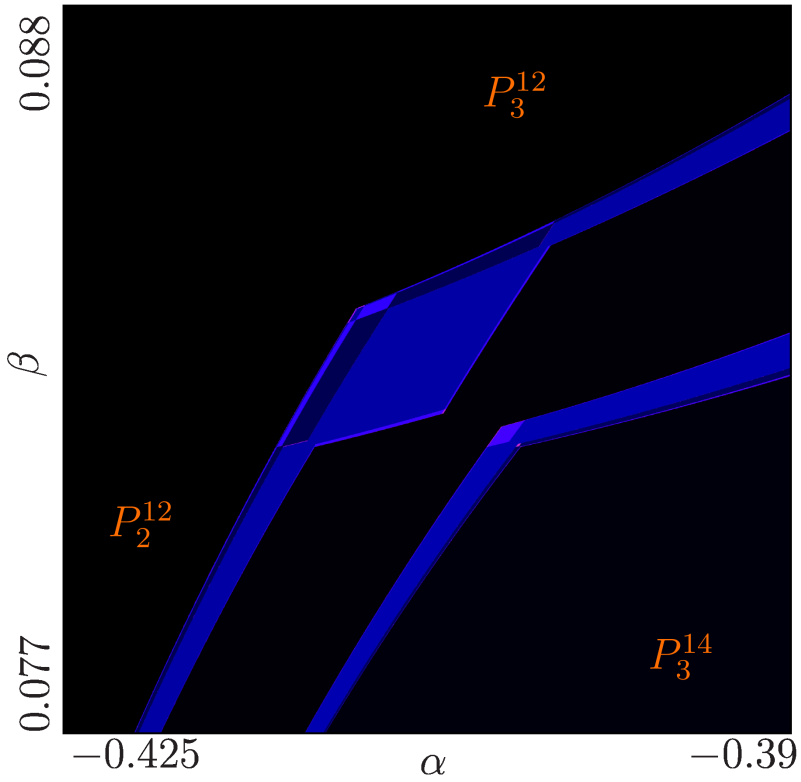

Figure 7.11: 2D scan of the periods associated with parameter regions in the archetypal model with increasing branches showing an overview of all three kinds of PAL structures. The parameters $a_L = 1, b_L = 0.8$, and $g_R\left(\frac{1}{2}\right) = \frac{1}{2} + \frac{1}{40}$ are fixed. The parameters $\alpha = -g_R\left(\frac{1}{4}\right)$ and $\beta = c_L$ are varied in the ranges $[-0.425, -0.39]$ and $[0.077, 0.088]$.

These two cycles, $\mathcal{A}^4\mathcal{B}^3C^4\mathcal{D}^3\mathcal{A}^4\mathcal{B}^3C^3\mathcal{D}^3$ and $\mathcal{A}^4\mathcal{B}^3C^4\mathcal{D}^3\mathcal{A}^3\mathcal{B}^3C^4\mathcal{D}^3$ could be the result of concatenating the symbolic sequences $A^4\mathcal{B}^3C^4\mathcal{D}^3$ and $\mathcal{A}^4\mathcal{B}^3C^3\mathcal{D}^3$, as well as $\mathcal{A}^4\mathcal{B}^3\mathcal{B}^4\mathcal{D}^3$ and $\mathcal{A}^3\mathcal{B}^3C^4\mathcal{D}^3$ of the parameter regions associated with the periods 14 and 13, respectively. But the cycle $\mathcal{A}^4\mathcal{B}^3C^4\mathcal{D}^3\mathcal{A}^3\mathcal{B}^3\mathcal{B}^4\mathcal{D}^3\mathcal{A}^4\mathcal{B}^3C^3\mathcal{D}^3$ of the parameter region associated with the period 40 cannot be a result of concatenating any pair of symbolic sequences $\mathcal{A}^4\mathcal{B}^3C^3\mathcal{D}^3$ and $\mathcal{A}^3\mathcal{B}^3C^4\mathcal{D}^3$ of the parameter region associated with the period 13 and $\mathcal{A}^4\mathcal{B}^3C^4\mathcal{D}^3\mathcal{A}^4\mathcal{B}^3C^3\mathcal{D}^3$ and $\mathcal{A}^4\mathcal{B}^3C^4\mathcal{D}^3\mathcal{A}^3\mathcal{B}^3C^4\mathcal{D}^3$ of the parameter region associated with the period 27. One can see that this is truly no PA structure.

Period-adding-like Structures In-between Horizontally Neighboring "Type A" Parameter Regions

Next, vertically oriented PAL structures are examined. Figure 7.14a shows a 2D period scan of this structure. Here, we can also see two PAL structures, one in-between the parameter regions P_2^{12} and $\left[P_2^{12} \mid P_3^{14}\right]$ and one in-between the parameter regions $\left[P_2^{12} \mid P_3^{14}\right]$ and P_3^{14}. The PAL structure in-between the parameter regions P_2^{12} and $\left[P_2^{12} \mid P_3^{14}\right]$ is chosen for closer investigation. Again, a red arrow marks the parameter range for the 1D period scan of this PAL structure in Figure 7.14b.

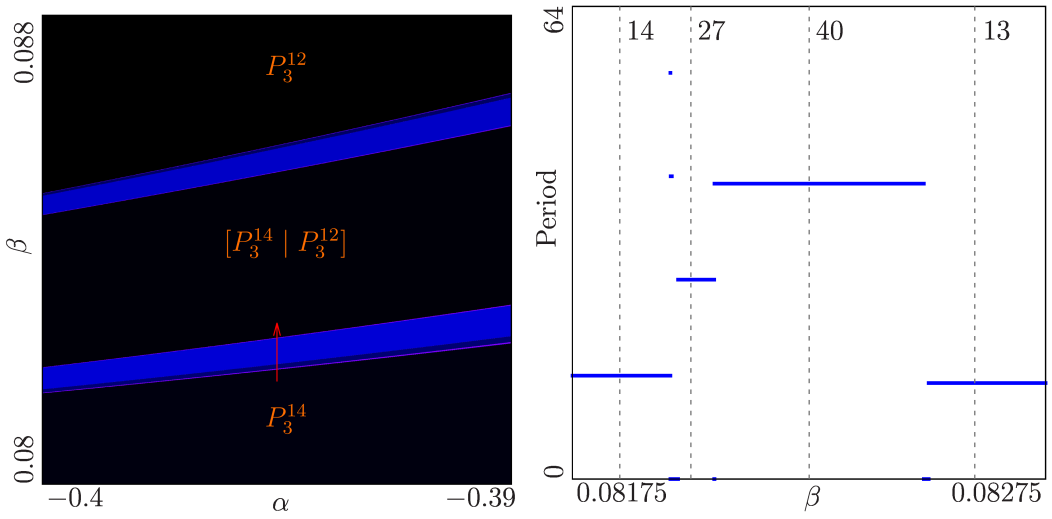

(a) 2D period scan **(b)** 1D period scan

Figure 7.12: 2D and 1D scans of the periods associated with parameter regions in the archetypal model with increasing branches showing horizontally oriented PAL structures. The parameters $a_L = 1, b_L = 0.8$, and $g_R\left(\frac{1}{2}\right) = \frac{1}{2} + \frac{1}{40}$ are fixed. The parameters $\alpha = g_R\left(\frac{1}{4}\right)$ and $\beta = c_L$ are different in each diagram. (a) shows the 2D scan where the parameters α and β are varied in the ranges $[-0.4, -0.39]$ and $[0.08, 0.088]$ and (b) shows the 1D scan where the parameter $\alpha = -0.395$ is fixed and β is varied in the range $[0.08175, 0.08275]$ which is marked with a red arrow in (a).

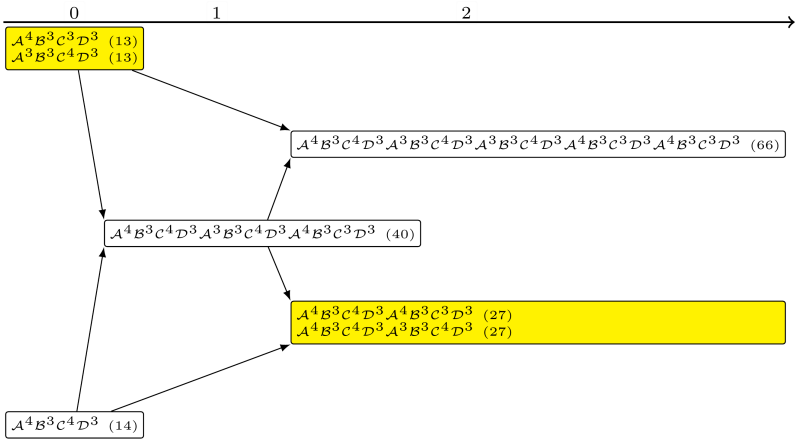

Figure 7.13: Farey-tree showing the symbolic sequences associated with the parameter regions of the lower horizontally oriented PAL structure marked with a red arrow in Figure 7.12a up to two levels. Nodes of parameter regions associated with two coexisting cycles are colored yellow and the periods associated with the parameter regions are in parentheses.

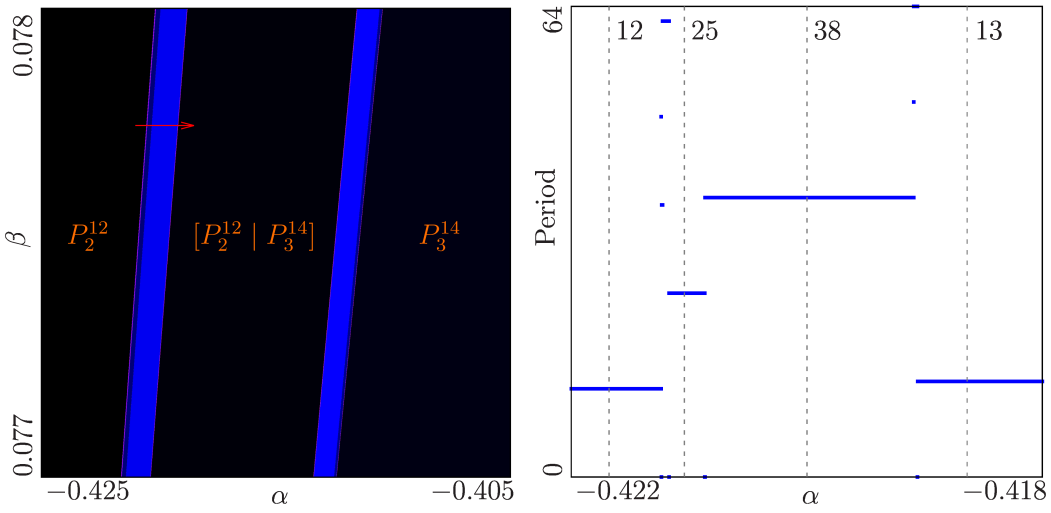

(a) 2D period scan **(b)** 1D period scan

Figure 7.14: 2D and 1D scans of the periods associated with parameter regions in the archetypal model with increasing branches showing vertically oriented PAL structures. The parameters $a_L = 1, b_L = 0.8$, and $g_R\left(\frac{1}{2}\right) = \frac{1}{2} + \frac{1}{40}$ are fixed. The parameters $\alpha = g_R\left(\frac{1}{4}\right)$ and $\beta = c_L$ are different in each diagram. (a) shows the 2D scan where the parameters α and β are varied in the ranges $[-0.425, -0.405]$ and $[0.077, 0.078]$ and (b) shows the 1D scan where the parameter $\beta = 0.07775$ is fixed and α is varied in the range $[-0.422, -0.418]$ which is marked with a red arrow in (a).

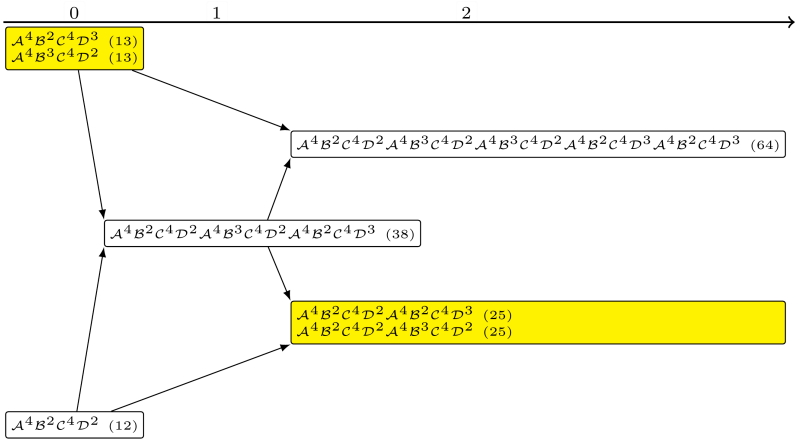

Figure 7.15: Farey-tree showing the symbolic sequences associated with the parameter regions of the left vertically oriented PAL structure marked with a red arrow in Figure 7.14a up to two levels. Nodes of parameter regions associated with two coexisting cycles are colored yellow and the periods associated with the parameter regions are in parentheses.

As before, the periods do not add as we would expect from a PA structure. The most pronounced parameter region between the parameter regions associated with the periods 12 and 13 is associated with the period 38. And the most pronounced parameter region between this parameter region and the parameter region associated with the period 12 is associated with the period 25, which should have been the most pronounced parameter region between the parameter regions associated with the periods 12 and 13, respectively.

Again, a Frey-tree with the symbolic sequences associated with the parameter regions in this PAL structure is provided in Figure 7.15. One can see that the expected concatenation of the symbolic sequence does not work. Nor does the concatenation of the symbolic sequence of the parameter region associated with the period 25, which is the lowest node in level 2, with the symbolic sequences of the parameter region associated with the period 13, which is the upper starting node, to get the symbolic sequences of the parameter region of the parameter region associated with the period 38, which is the only node in level 1. Therefore, this is no PA structure either.

Period-adding-like Structures in the Corners

Finally, the structure in the corner which Figure 7.16a shows a 2D period scan of is examined. Here, we see many PAL structures. These are organized as follows. There is one horizontally oriented PAL structure between the parameter regions $\left[P_2^{12} \mid P_3^{14}\right]$ and P_3^{12}. And one horizontally oriented PAL structure between the parameter region P_3^{12} and every parameter region in the vertically oriented PAL structure between the parameter regions P_2^{12} and $\left[P_2^{12} \mid P_3^{14}\right]$. Analogously, there is one vertically oriented PAL structure between the parameter regions P_2^{12} and $\left[P_3^{14} \mid P_3^{12}\right]$. And one vertically oriented PAL structure between the parameter region P_2^{12} and every parameter region in the horizontally oriented PAL structure between the parameter regions P_3^{14} and $\left[P_3^{14} \mid P_3^{12}\right]$. Similarly, there is also one horizontally oriented PAL structure between the parameter region $\left[P_3^{14} \mid P_3^{12}\right]$ and every parameter region in the vertically oriented PAL structure between the parameter regions $\left[P_2^{12} \mid P_3^{14}\right]$ and P_3^{14}. And one vertically oriented PAL structure between the parameter region $\left[P_2^{12} \mid P_3^{14}\right]$ and every parameter region in the horizontally oriented PAL structure between the parameter regions P_3^{14} and $\left[P_3^{14} \mid P_3^{12}\right]$. A very similar phenomenon was discovered by Tramontana et al. where there are many PA structures between some parameter region and every parameter region of a PA structure [TGAS12].

The 1D period scan in Figure 7.16b shows a 1D period scan of one of the simpler PAL structures. It is the PAL structure between the parameter regions P_2^{12} and $\left[P_3^{14} \mid P_3^{12}\right]$ marked with a red arrow in Figure 7.16a. The diagram looks exactly like the 1D period scan for the vertical PAL structure in Figure 7.14b. Here, the periods also do not add up as we expect them to in PA structures.

The symbolic sequences are different from the vertical PAL structure in Figure 7.14a. Still the same argument as before works that this structure is not a skewed PA structure. Since there are infinitely many PAL structures in this corner it is very hard to describe each one and construct rules for the periods and symbolic sequences in the structures. Luckily there is an easier way to describe the PAL structures in the increasing archetypal model and construct the wanted rules. This involves the halved archetypal model, which is introduced in the next section.

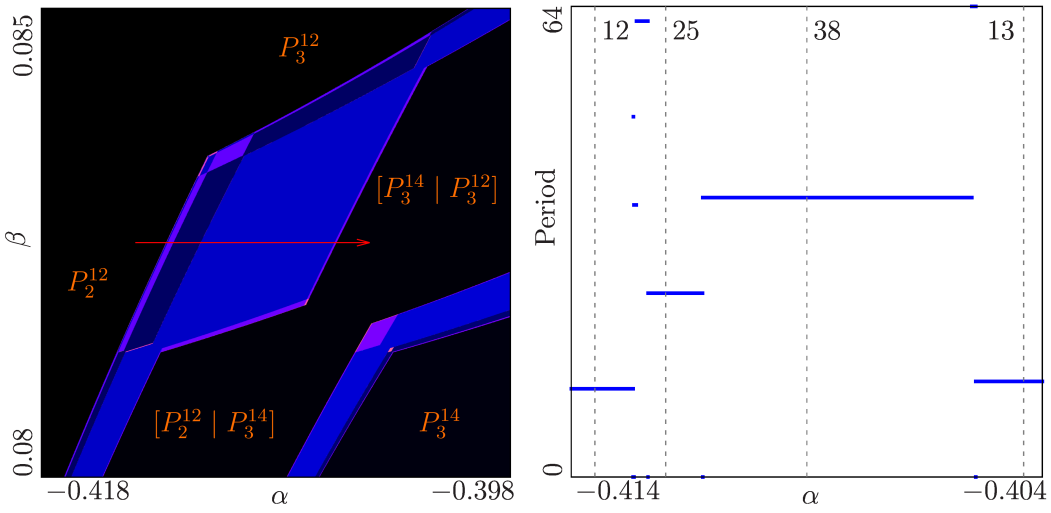

(a) 2D period scan **(b)** 1D period scan

Figure 7.16: 2D and 1D scans of the periods associated with parameter regions in the archetypal model with increasing branches showing diamond-shaped PAL structures. The parameters $a_L = 1, b_L = 0.8$, and $g_R\left(\frac{1}{2}\right) = \frac{1}{2} + \frac{1}{40}$ are fixed. The parameters $\alpha = -g_R\left(\frac{1}{4}\right)$ and $\beta = c_L$ are different in each diagram. (a) shows the 2D scan where the parameters α and β are varied in the ranges $[-0.418, -0.398]$ and $[0.08, 0.085]$ and (b) shows the 1D scan where the parameter $\beta = 0.0825$ is fixed and α is varied in the range $[-0.414, -0.404]$ which is marked with a red arrow in (a).

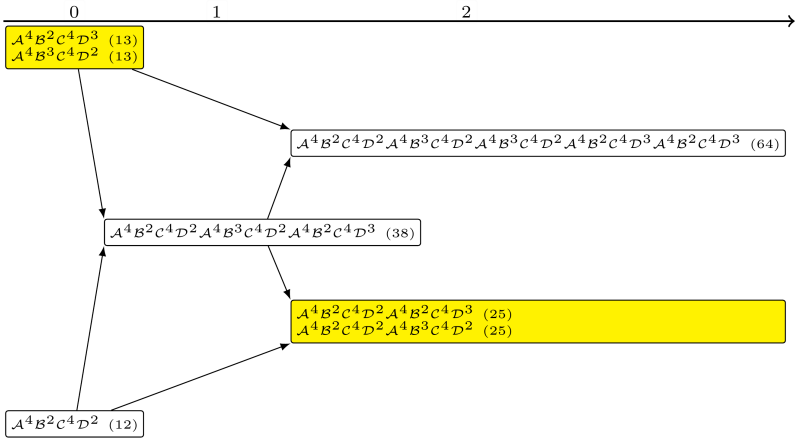

Figure 7.17: Farey-tree showing the symbolic sequences associated with the parameter regions of the diamond-shaped PAL structure marked with a red arrow in Figure 7.14a up to two levels. Nodes of parameter regions associated with two coexisting cycles are colored yellow and the periods associated with the parameter regions are in parentheses.

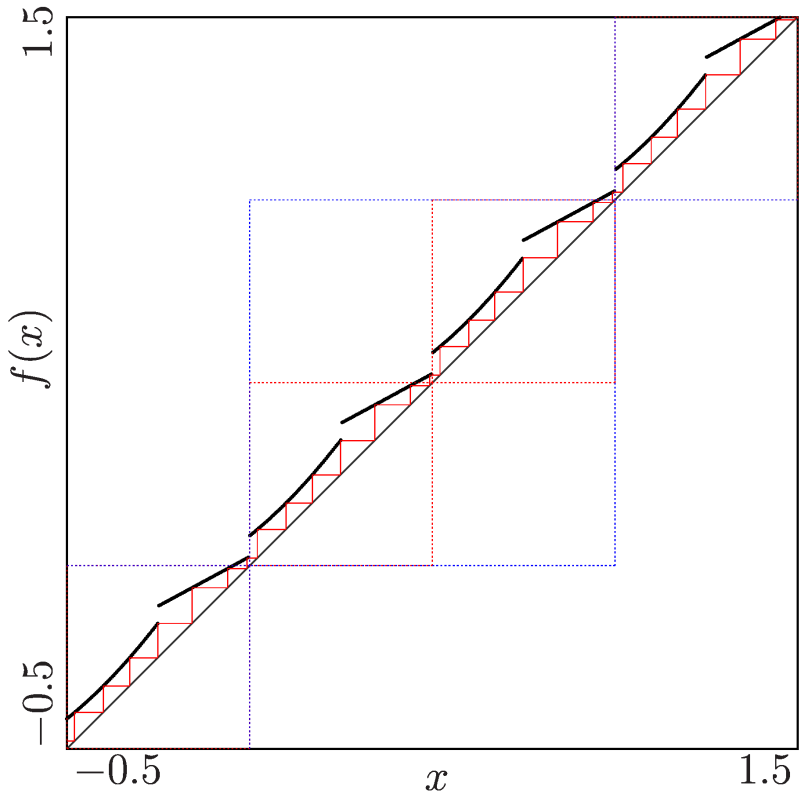

Figure 7.18: Illustration of the lifted archetypal model.

7.3.2 Halved Archetypal Model

This section introduces the halved archetypal model. First, the motivation and a definition is given. After that, this section explains how this halved archetypal model is used to describe the PAL structures in the archetypal model.

Motivation and Definition

Since the archetypal model is a circle map, it can also be looked at as an infinite map. Let m be the archetypal model. We know the model m maps an input x to $f(x) \mod 1$, meaning that if the output $f(x)$ is greater or equal to 1 we subtract 1 from it until it is in the range $[0, 1)$. Similarly, we add 1 to it if it is smaller than 0 until it is in the desired range. Now instead of confining the model to the domain of $[0, 1)$, we think of it repeating infinitely in both directions. This process is called lifting of circle maps and is described by Devaney in his book [Dev89]. We can achieve this by mapping $T^m : x \mapsto f(x - \lfloor x \rfloor)$. This trick maps any input $x \in \mathbb{R}$ into the domain $[0, 1)$ of the archetypal model m and causes T^m to repeat infinitely. T^m is now a lift of the model m in the domain of all real numbers $\mathbb{R}$. Figure 7.18 illustrates this concept for the cycle in the parameter region P_3^{14}. The archetypal model in the lifted archetypal model is marked with a blue square. These blue squares repeat infinitely in each direction. One can see that the branch $f_{\mathcal{D}}$ is outside the blue square at its right edge. This is because it was cut off and continued at the bottom of the square in the archetypal model, due to the $\mod 1$ operation.

In this model, there are no cycles that have multiple rotations. Instead, the cycles that had multiple rotations in the archetypal model, manifest as a sequence of different blocks of the archetypal model. Meaning, for the example P_3^{14}, the same blocks of $\mathcal{A}^4\mathcal{B}^3\mathcal{C}^4\mathcal{D}^3$ are repeating infinitely. But for an example with multiple rotations, such as $\mathcal{ABCDA}^2\mathcal{B}^2\mathcal{C}^2\mathcal{D}^2$, the blocks will not all be the same. Instead, the blocks $\mathcal{ABCD}$ and $\mathcal{A}^2\mathcal{B}^2\mathcal{C}^2\mathcal{D}^2$ will be alternating.

Now we will take advantage of the symmetry in the model function f of the archetypal model. Since $f\left(x+\frac{1}{2}\right) \equiv f(x)+\frac{1}{2} \mod 1$, we can split the lifted model T^m into smaller blocks of size $\frac{1}{2}$. The function of the infinite model repeats in these smaller blocks. These blocks are marked red in Figure 7.18. The red blocks represent the halved model, it is the smallest repeating part of the lifted model T^m. Basically we choose the smallest model, of which T^m is a lift. This happens to be exactly our model m folded in half. So the halved archetypal model is defined as $x_{n+1} = g(x_n) \mod \frac{1}{2}$, where $g(x)$ is the same as in the archetypal model defined in Section 5.4.1.

Application of the Halved Archetypal Model to Explain the Period-adding-like Structures

Figure 7.19a shows a 2D scan of the periods associated with parameter regions in the halved archetypal model in the same parameter ranges used for the 2D period scan of the horizontally oriented PAL structures in Figure 7.12a. The red arrow indicates the parameter range for the 1D period scan in Figure 7.19b. The 1D scan shows that the periods in this structure add up as we would expect in PA structures.

As in the previous sections, the symbolic sequences of the cycles associated with the parameter regions in this structures are examined. Figure 7.20 shows the Farey-tree with the symbolic sequences associated with the parameter regions of this structure. One can see that the symbolic sequence of a child node is the concatenation of the symbolic sequences of the parent nodes, as we would expect from PA structures. It turns out that the hybrid parameter region $\left[P_3^{14} \mid P_3^{12}\right]$ was also part of the horizontal PAL structure described in Section 7.3.1. And the PAL structures in the archetypal model are consequences of the PA structures in the halved archetypal model.

The numerical evidence shows that the PA structures in the halved archetypal model manifest as PAL structures in the archetypal model. And the rules for the symbolic sequences of parameter regions in PA structures are well known. By formulating an algorithm that can translate symbolic sequences between the halved archetypal model and the archetypal model, one can generate the symbolic sequences of any PAL structure without the need for simlulating the archetypal model in every parameter region of the PAL structure. Furthermore, with such an algorithm, one can derive rules for the PAL structures in the archetypal model from the rules for PA structures. The rules include rules for the periods, symbolic sequences, multistability, and even rotation numbers of the cycles associated with the parameter regions.

The next section introduces such algorithms and formulates some regularities in the translation of symbolic sequences. With these algorithms and regularities, the rules for PAL structures in the archetypal model are derived later.

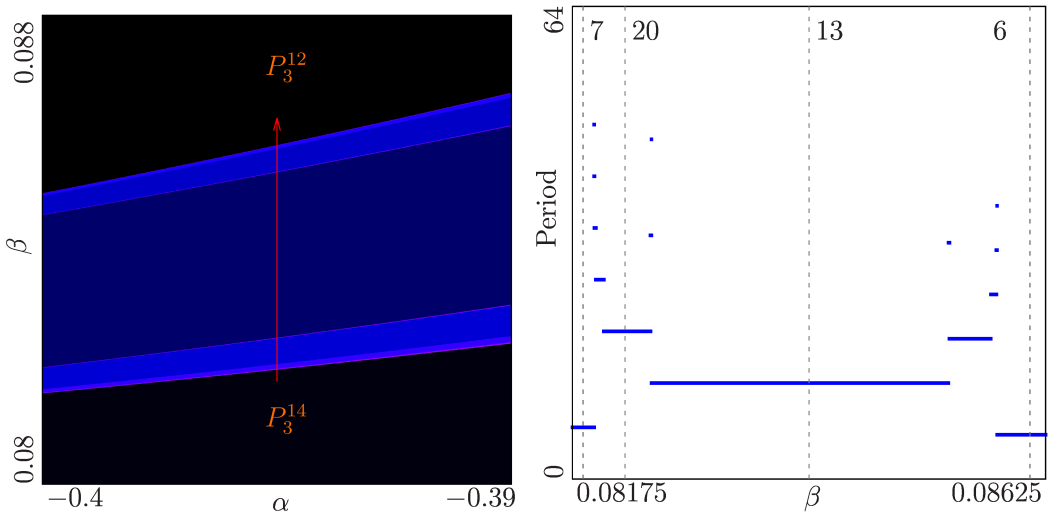

(a) 2D period scan **(b)** 1D period scan

Figure 7.19: 2D and 1D scans of the periods associated with parameter regions in the archetypal model with increasing branches showing a horizontally oriented PA structure. The parameters $a_L = 1, b_L = 0.8$, and $g_R\left(\frac{1}{2}\right) = \frac{1}{2} + \frac{1}{40}$ are fixed. The parameters $\alpha = g_R\left(\frac{1}{4}\right)$ and $\beta = c_L$ are different in each diagram. (a) shows the 2D scan where the parameters α and β are varied in the ranges $[-0.4, -0.39]$ and $[0.08, 0.088]$ and (b) shows the 1D scan where the parameter $\alpha = -0.395$ is fixed and β is varied in the range $[0.08175, 0.08275]$ which is marked with a red arrow in (a).

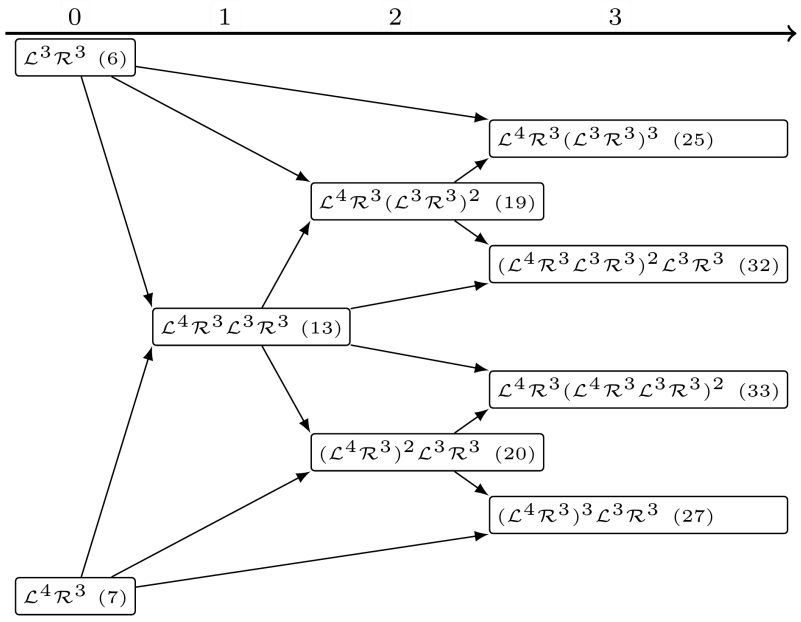

Figure 7.20: Farey-tree showing the symbolic sequences associated with the parameter regions of the horizontal PA structure marked with a red arrow in Figure 7.19a up to three levels. The periods associated with the parameter regions the cycles are in parentheses.

7.3.3 Translating Symbolic Sequences

First, we define naïve algorithms for translating symbolic sequences between the archetypal and the halved archetypal model based on the idea of the lifted model. Then, we derive regularities for translated symbolic sequences in the archetypal model. Finally, we refine the algorithms using the regularities of translated symbolic sequences.

In the following, cycles of the archetypal model get the symbols ϕ, ψ, and π. Cycles of the halved archetypal model get the symbols σ, ρ, and τ. If there are two coexisting twin cycles, they are written as ϕ^a and ϕ^b. Also, the symbols for the symbolic sequences in the halved archetypal model are $\mathcal{L}$ and $\mathcal{R}$ instead of $\mathcal{A}, \mathcal{B}, C$, and $\mathcal{D}$ to avoid confusion.

Naïve Algorithms

We start by formulating a naïve algorithm for translating symbolic sequences from the archetypal model to the halved archetypal model. This is the easier direction. From this algorithm we don't learn much about the nature of the PAL structures in the archetypal model. The algorithm for translating symbolic sequences in the other direction, from the halved archetypal model to the archetypal model, will be more important for that.

To translate a symbolic sequence of the archetypal model we start by writing it down. For example, let $\phi = \mathcal{A}^4\mathcal{B}^3C^4\mathcal{D}^3$. Then we replace the symbols $\mathcal{A}$ and C by $\mathcal{L}$ and the symbols $\mathcal{B}$ and $\mathcal{D}$ by $\mathcal{R}$. Now we have $\mathcal{L}^4\mathcal{R}^3\mathcal{L}^4\mathcal{R}^3$. Finally, we have to check for redundancy in the resulting cycle. In our example, the cycle $\mathcal{L}^4\mathcal{R}^3$ repeats twice in $\mathcal{L}^4\mathcal{R}^3\mathcal{L}^4\mathcal{R}^3$, so we just keep $\mathcal{L}^4\mathcal{R}^3$.

The opposite direction is trickier. We start by writing down the symbolic sequence in the halved archetypal model. For example $\sigma = \mathcal{L}^4\mathcal{R}^3\mathcal{L}4\mathcal{R}^3\mathcal{L}^3\mathcal{R}^3$. Now we need to build pairs of rotations since each blue block fits exactly two red blocks. If there is one rotation left over at the end, we wrap around or equivalently write down the original sequence again. We repeat this until all rotations we have written down are paired up.

Lemma 7.3 (How Often to Write Down the Symbolic Sequence)
In order to translate a cycle from the halved archetypal model σ with an even number of rotations n, we only need to write the original cycle down once. In order to translate a cycle from the halved archetypal model σ with an odd number of rotations n, we need to write the original cycle down exactly twice.

Proof

(i) Let $n = 2i$. Then, we can build i pairs of rotations and fit all $2i$ rotations of the original model.

(ii) Let $n = 2i + 1$. We start by building i pairs of rotations, fitting $2i$ rotations. This will leave the last rotation unpaired, so we write down the sequence of $2i + 1$ rotations again. Now we can pair up the last rotation of the first sequence we wrote down with the first rotation of the sequence we just wrote down. $2i$ rotations remain, which we can fit into i pairs.

■

Notice that our example symbolic sequence has 3 rotations. This means we have to write down the original sequence twice $\sigma^2 = \left(\mathcal{L}^4\mathcal{R}^3\mathcal{L}^4\mathcal{R}^3\mathcal{L}^3\mathcal{R}^3\right)^2 = \mathcal{L}^4\mathcal{R}^3\mathcal{L}^4\mathcal{R}^3\mathcal{L}^3\mathcal{R}^3\mathcal{L}^4\mathcal{R}^3\mathcal{L}^4\mathcal{R}^3\mathcal{L}^3\mathcal{R}^3$.

Then we pair up the rotations, this corresponds to drawing blue boxes around the red boxes in the lifted model. In our example, we get the pairs $\left(\mathcal{L}^4\mathcal{R}^3\mathcal{L}^4\mathcal{R}^3\right)\left(\mathcal{L}^3\mathcal{R}^3\mathcal{L}^4\mathcal{R}^3\right)\left(\mathcal{L}^4\mathcal{R}^3\mathcal{L}^3\mathcal{R}^3\right)$. The pairs then have to be translated using the function t defined below in Definition 7.2. The resulting symbolic sequence is $T(h) = \mathcal{A}^4\mathcal{B}^3\mathcal{C}^4\mathcal{D}^3\mathcal{A}^3\mathcal{B}^3\mathcal{C}^4\mathcal{D}^3\mathcal{A}^4\mathcal{B}^3\mathcal{C}^3\mathcal{D}^3$. The formal definition of T is below in Definition 7.3. But we first need to define the notion of syllables which is needed for the Definitions 7.2 and 7.3.

Definition 7.1 (Syllables)
A syllable of a symbolic sequence is a subsequence of maximal length consisting of only one symbol. A 2-syllable is a pair of syllables that are next to each other. And a 4-syllable is a pair of 2-syllables that are next to each other.

So for example, the symbolic sequence $\mathcal{L}^4\mathcal{R}^3\mathcal{L}^3\mathcal{R}^3$ has 4 syllables. Its syllables are $\mathcal{L}^4$, $\mathcal{L}^3$, and two times $\mathcal{R}^3$. And a 2-syllable of the cycle is $\mathcal{L}^4\mathcal{R}^3$. In the halved archetypal model, a 2-syllable corresponds to one rotation. The 2-syllables of a symbolic sequence σ of a cycle in the halved archetypal model are written as σ_i. In the archetypal model, a 4-syllable corresponds to one rotation. The 4-syllables of a symbolic sequence ϕ of a cycle in the archetypal model are written as ϕ_i. These terms are used interchangeably in the rest of this chapter.

Definition 7.2 (Translating 4-syllables from the Halved to the Full Archetypal Model)
The function t maps two rotations, or a 4-syllable that starts with the symbol $\mathcal{L}$ of a symbolic sequence in the halved archetypal model to a single rotation in the archetypal model. It is defined in the following way.

$$t:\ \mathcal{L}^a\mathcal{R}^b\mathcal{L}^c\mathcal{R}^d \mapsto \mathcal{A}^a\mathcal{B}^b\mathcal{C}^c\mathcal{D}^d \tag{7.3}$$

Definition 7.3 (Translating Symbolic Sequences from the Halved to the Full Archetypal Model)
The function T translates a symbolic sequence $\sigma = \sigma_1\sigma_2\ldots\sigma_n$ in the halved archetypal model to the archetypal model. Where σ_i are the 2-syllables of σ. From Theorem 7.3 we know how often we need to write down σ, and therefore also which 4-syllables to translate with t.

$$T:\ \sigma \mapsto \begin{cases} t(\sigma_1\sigma_2)\ldots t(\sigma_{n-1}\sigma_n) & \text{if } n \text{ is even} \\ t(\sigma_1\sigma_2)\ldots t(\sigma_n\sigma_1)\ldots t(\sigma_{n-1}\sigma_n) & \text{else} \end{cases} \tag{7.4}$$

Now we have a way to translate full symbolic sequences. But this is not enough, since a cycle in the halved archetypal model might manifest as multiple coexisting cycles in the archetypal model. Let $\varrho = \mathcal{L}^4\mathcal{R}^3\mathcal{L}^3\mathcal{R}^3$ be another cycle in the halved archetypal model. Since this cycle has an even number of rotations, the 2-syllables $\varrho_1 = \mathcal{L}^4\mathcal{R}^3$ and $\varrho_2 = \mathcal{L}^3\mathcal{R}^3$, we only need to write it down once. And the translation of this cycle is $T(\varrho) = T(\varrho_1\varrho_2) = T\left(\mathcal{L}^4\mathcal{R}^3\mathcal{L}^3\mathcal{R}^3\right) = \mathcal{A}^4\mathcal{B}^3\mathcal{C}^3\mathcal{D}^3$. But when we translate the cycle $\varrho' = \varrho_2\varrho_1$, which is indistinguishable from the cycle ϱ, we get $T(\varrho') = T(\varrho_2\varrho_1) = T\left(\mathcal{L}^3\mathcal{R}^3\mathcal{L}^4\mathcal{R}^3\right) = \mathcal{A}^3\mathcal{B}^3\mathcal{C}^4\mathcal{D}^3$. This is a different cycle from $T(\varrho)$. So we need to first obtain all indistinguishable cycles of the original cycle in the halved archetypal model, then translate each one, and finally check for indistinguishable results in order to not have any duplicate cycles in the archetypal model. The concepts needed for this are defined below in Definitions 7.4 and 7.5.

Definition 7.4 (Shifting Symbolic Sequences)
The function s_2 shifts a symbolic sequence σ in the halved archetypal model by a single rotation, or equivalently by a 2-syllable. Let $\sigma = \sigma_1\sigma_2 \dots \sigma_n$. Then s_2 is defined in the following way:

$$s_2 : \sigma_1\sigma_2 \dots \sigma_n \mapsto \sigma_2 \dots \sigma_n\sigma_1 \tag{7.5}$$

In the archetypal model, there is a similar function, s_4 that shifts a symbolic sequence ϕ in the archetypal model by a single rotation. Let $\phi = \phi_1\phi_2 \dots \phi_n$. Then s_4 is defined in the following way:

$$s_4 : \phi_1\phi_2 \dots \phi_n \mapsto \phi_2 \dots \phi_n\phi_1 \tag{7.6}$$

Definition 7.5 (Shift-equivalence)
Two symbolic sequences σ and ϱ in the halved archetypal model are shift-equivalent $\sigma \equiv_2 \varrho$, if they both have the same number of rotations n and there is a number $0 \leq i < n$, such that $\sigma = s_2^i(\varrho)$, where $s_2^i(\varrho)$ is defined as $s_2^{i-1}(s_2(\varrho))$ and $s_2^1(\varrho) = s_2(\varrho)$.

Two symbolic sequences ϕ and ψ in the archetypal model are shift-equivalent $\phi \equiv_4 \psi$, if they both have the same number of rotations n and there is a number $0 \leq i < n$, such that $\phi = s_4^i(\psi)$, where $s_4^i(\psi)$ is defined as $s_4^{i-1}(s_4(\psi))$ and $s_4^1(\psi) = s_4(\psi)$.

Note that the symbols for shift-equivalence are different for the halved archetypal model and the archetypal model. We use $\equiv_2$ for the shift-equivalence in the halved archetypal model to express that the symbolic sequences are equivalent by shifting them by a multiple of two syllables with s_2^i. Similarly, we use $\equiv_4$ for the shift-equivalence in the archetypal model to express that the symbolic sequences are equivalent by shifting them by a multiple of four syllables with s_4^i.

Since the halved archetypal model has two branches, any cycles that have shift-equivalent ($\equiv_2$) symbolic sequences are indistinguishable in the halved archetypal model. Similarly, since the archetypal model has four branches, any cycles that have shift-equivalent ($\equiv_4$) symbolic sequences are indistinguishable in the archetypal model. We obtain all symbolic sequences of cycles that are indistinguishable from the original cycle by shifting the symbolic sequence of the original cycle with s_2. If the symbolic sequence τ of a cycle in the halved archetypal model has n 2-syllables, the cycle has n indistinguishable cycles with the symbolic sequences $\left\{s_2^i(\tau) \mid 0 \leq i < n\right\}$, since $s_2^n(\tau) = \tau$. Returning to our initial example with the symbolic sequence $\sigma = \mathcal{L}^4\mathcal{R}^3\mathcal{L}^4\mathcal{R}^3\mathcal{L}^3\mathcal{R}^3$, there are three indistinguishable cycles with the symbolic sequences $\sigma = \mathcal{L}^4\mathcal{R}^3\mathcal{L}^4\mathcal{R}^3\mathcal{L}^3\mathcal{R}^3$, $s_2(\sigma) = \mathcal{L}^4\mathcal{R}^3\mathcal{L}^3\mathcal{R}^3\mathcal{L}^4\mathcal{R}^3$, and $s_2^2(\sigma) = \mathcal{L}^3\mathcal{R}^3\mathcal{L}^4\mathcal{R}^3\mathcal{L}^4\mathcal{R}^3$.

Now we translate each symbolic sequence of the indistinguishable cycles. We already know that the translation of σ is $T(\sigma) = \mathcal{A}^4\mathcal{B}^3\mathcal{C}^4\mathcal{D}^3\mathcal{A}^3\mathcal{B}^3\mathcal{C}^4\mathcal{D}^3\mathcal{A}^4\mathcal{B}^3\mathcal{C}^3\mathcal{D}^3$ from before. The translation of $s_2(\sigma)$ is

$$\begin{aligned} T\left(s_2(\sigma)\right) &= T\left(\mathcal{L}^4\mathcal{R}^3\mathcal{L}^3\mathcal{R}^3\mathcal{L}^4\mathcal{R}^3\right) \\ &= t\left(\mathcal{L}^4\mathcal{R}^3\mathcal{L}^3\mathcal{R}^3\right) t\left(\mathcal{L}^4\mathcal{R}^3\mathcal{L}^4\mathcal{R}^3\right) t\left(\mathcal{L}^3\mathcal{R}^3\mathcal{L}^4\mathcal{R}^3\right) \\ &= \mathcal{A}^4\mathcal{B}^3\mathcal{C}^3\mathcal{D}^3\mathcal{A}^4\mathcal{B}^3\mathcal{C}^4\mathcal{D}^3\mathcal{A}^3\mathcal{B}^3\mathcal{C}^4\mathcal{D}^3 \end{aligned}$$

And finally, the translation of $s_2^2(\sigma)$ is

$$\begin{aligned} T\left(s_2(\sigma)\right) &= T\left(\mathcal{L}^3\mathcal{R}^3\mathcal{L}^4\mathcal{R}^3\mathcal{L}^4\mathcal{R}^3\right) \\ &= t\left(\mathcal{L}^3\mathcal{R}^3\mathcal{L}^4\mathcal{R}^3\right) t\left(\mathcal{L}^4\mathcal{R}^3\mathcal{L}^3\mathcal{R}^3\right) t\left(\mathcal{L}^4\mathcal{R}^3\mathcal{L}^4\mathcal{R}^3\right) \\ &= \mathcal{A}^3\mathcal{B}^3\mathcal{C}^4\mathcal{D}^3\mathcal{A}^4\mathcal{B}^3\mathcal{C}^3\mathcal{D}^3\mathcal{A}^4\mathcal{B}^3\mathcal{C}^4\mathcal{D}^3 \end{aligned}$$

Looking closely, we can see that $T(\sigma) = s_4^2\left(T\left(s_2(\sigma)\right)\right) = s_4\left(T\left(s_2^2(\sigma)\right)\right)$. So the symbolic sequences of the cycles are shift-equivalent $T(\sigma) \equiv_4 T\left(s_2(\sigma)\right) \equiv_4 T\left(s_2^2(\sigma)\right)$ and therefore the cycles are indistinguishable. This means that the cycle σ manifests as a single cycle in the archetypal model. The final result of the translation process is a set and, it is defined as the function F which is formally defined in Definition 7.6.

Definition 7.6 (Translating Cycles from the Halved to the Archetypal Model)
The function F translates a cycle in the halved archetypal model with the symbolic sequence σ that has n 2-syllables to the archetypal model. The result is a set of the symbolic sequences of all the cycles that the original cycle manifests as in the archetypal model.

$$F:\ \sigma \mapsto \left\{ {}_i\phi = T\left(s_2^i(\sigma)\right)\ \middle|\ 0 \le i < n \wedge \nexists 0 \le j < i :\ {}_i\phi \equiv_4 {}_j\phi \right\} \tag{7.7}$$

Note that here, the left index is used for ${}_i\phi$, since the right index is reserved for the 2-syllables of symbolic sequences in the halved archetypal model and 4-syllables of symbolic sequences in the archetypal model.

Properties of Translated Symbolic Sequences in the Full Model

With this naïve algorithm, we can start to investigate rules for the PAL structures in the archetypal model.

Lemma 7.4 (Shif-equivalence of Translated Symbolic Sequences in the Archetypal Model)
The translations of the two cycles σ and $\rho = s_2^{2i}(\sigma)$ in the halved archetypal model are shift-equivalent $T(\sigma) \equiv_4 T(\rho)$ in the archetypal model for all integers i.

Proof
Let $\sigma = \sigma_1\sigma_2\ldots\sigma_n$, therefore $\rho = \sigma_{2i+1}\ldots\sigma_n\sigma_1\ldots\sigma_{2i}$. The translations are $T(\sigma) = t(\sigma_1\sigma_2)t(\sigma_3\sigma_4)\ldots t(\sigma_{n-1}\sigma_n)$ and $T(\rho) = t(\sigma_{2i+1}\sigma_{2i+2})\ldots t(\sigma_{n-1}\sigma_n)t(\sigma_1\sigma_2)\ldots t(\sigma_{2i-i}\sigma_{2i})$. We can see that $T(\rho) = s_4^i(T(\sigma))$ and therefore $T(\sigma) \equiv_4 T(\rho)$.

■

Theorem 7.5 (Coexistence of Translated Symbolic Sequences in the Archetypal Model)
The manifestations of a cycle σ in the halved archetypal model is either $F(\sigma) = \{T(\sigma), T(s_2(\sigma))\}$ or $F(\sigma) = \{T(\sigma)\}$. Specifically,

(i) $F(\sigma) = \{T(\sigma), T(s_2(\sigma))\}$ if the number of rotations of the sequence σ is even.

(ii) $F(\sigma) = \{T(\sigma)\}$ if the number of rotations of the sequence σ is odd.

Proof
Let $\sigma = \sigma_1\sigma_2 \ldots \sigma_n$ be a symbolic sequence in the halved archetypal model with n rotations. We know from Theorem 7.4 that the only possible candidates for $F(\sigma)$ are $T(\sigma)$ and $T(s_2(\sigma))$. These are the first two possibilities we check in the algorithm and the translations of all other shifts of the original cycle, $T(s_2^i(\sigma))$ with $2 \leq i < n$, are shift-equivalent to either $T(\sigma)$ or $T(s_2(\sigma))$. This follows directly from Theorem 7.4. So, in the following, we only check for the shift-equivalence of these two candidates.

(i) Let $n = 2i$.

$$\begin{aligned} T(h) &= t(\sigma_1\sigma_2)t(\sigma_3\sigma_4)\ldots t(\sigma_{n-1}\sigma_n) \\ \not\equiv_4\ T(s_2(h)) &= t(\sigma_2\sigma_3)t(\sigma_4\sigma_5)\ldots t(\sigma_n\sigma_1) \end{aligned}$$

The two candidates are not shift-equivalent because the pair $t(\sigma_1\sigma_2)$ in $T(\sigma)$ is not included in the other candidate $T(s_2(\sigma))$. The same is true for any other pair, and therefore $F(\sigma) = \{T(\sigma), T(s_2(\sigma))\}$.

(ii) Let $n = 2i + 1$.

$$\begin{aligned} T(h) &= t(\sigma_1\sigma_2)t(\sigma_3\sigma_4)\ldots t(\sigma_n\sigma_1)t(\sigma_2\sigma_3)\ldots t(\sigma_{n-1}\sigma_n) \\ \equiv_4\ T(s_2(h)) &= t(\sigma_2\sigma_3)\ldots t(\sigma_{n-1}\sigma_n)t(\sigma_1\sigma_2)t(\sigma_3\sigma_4)\ldots t(\sigma_n\sigma_1) \end{aligned}$$

The two candidates are shift-equivalent. By shifting the second candidate $T(s_2(\sigma))$ $2i$ times, we get the first candidate $T(\sigma)$. Therefore, the second candidate is discarded and $F(\sigma) = \{T(\sigma)\}$.

■

Revised Algorithms

With all these properties and functions we now can formulate a more compact algorithm, Algorithm 7.1, for translating symbolic sequences from the halved archetypal model to the archetypal model. This revised algorithm is used in the following to construct the rules for the PAL structures in the archetypal model.

Algorithm 7.1 Algorithm for the Translation of Symbolic Sequences from the Halved Archetypal Model to the Archetypal Model

Require: $\sigma = \sigma_1\sigma_2 \ldots \sigma_n$ with $n > 0$
  if n is even **then**
    return $\{t(\sigma_1\sigma_2)t(\sigma_3\sigma_4)\ldots t(\sigma_{n-1}\sigma_n), t(\sigma_2\sigma_3)t(\sigma_4\sigma_5)\ldots t(\sigma_n\sigma_1)\}$
  else
    return $\{t(\sigma_1\sigma_2)\ldots t(\sigma_n\sigma_1)\ldots t(\sigma_{n-1}\sigma_n)\}$
  end if

Algorithm 7.2 shows the inverse algorithm for translating symbolic sequences from the archetypal model to the halved archetypal model for completeness. It uses the inverse t^{-1} of the function t.

Definition 7.7 (Translating 4-syllables from Archetypal to Halved Archetypal)
The function t^{-1} maps a 4-syllable of a symbolic sequence in the archetypal model to the halved archetypal model. It is defined in the following way:

$$t^{-1}: \quad \mathcal{A}^a\mathcal{B}^b\mathcal{C}^c\mathcal{D}^d \mapsto \mathcal{L}^a\mathcal{R}^b\mathcal{L}^c\mathcal{R}^d \tag{7.8}$$

Algorithm 7.2 Algorithm for the Translation of Symbolic Sequences from the Archetypal Model to the Halved Archetypal Model

Require: $\phi = \phi_1\phi_2 \dots \phi_n$ with $n > 0$
  $d \leftarrow t^{-1}(\phi_1)t^{-1}(\phi_2) \dots t^{-1}(\phi_n) = \sigma_1\sigma_2 \dots \sigma_m$ // $m = 2n$ is even
  $\tau \leftarrow \sigma_1\sigma_2 \dots \sigma_{\frac{m}{2}}$
  if $\sigma = \tau^2$ **then**
    return τ
  else
    return σ
  end if

7.3.4 Properties of the Period-adding-like Structures in the Archetypal Model

With the revised algorithms we can now explain the PAL structures in the archetypal model. We start by explaining why some cycles have a much higher period than expected in the PAL structures. After that, we construct rules for the symbolic sequences in the PAL structures in the archetypal model. And finally, we construct rules for the rotation-like numbers in the PAL structures in the archetypal model.

Periods in the Period-adding-like Structures

First, we state that the function t that translates 4-syllables from the halved archetypal model to the archetypal model preserves the period of the 4-syllable. The function is defined in Section 7.3.3.

Lemma 7.6 (t Preserves Period)
The function t preserves the period.

$$|\sigma_1\sigma_2| = |t(\sigma_1\sigma_2)| \tag{7.9}$$

Proof *Let $\sigma_1\sigma_2 = \mathcal{L}^a\mathcal{R}^b\mathcal{L}^c\mathcal{R}^d$.*

$$|\sigma_1\sigma_2| = |\mathcal{L}^a\mathcal{R}^b\mathcal{L}^c\mathcal{R}^d| = a + b + c + d = |\mathcal{A}^a\mathcal{B}^b\mathcal{C}^c\mathcal{D}^d| = |t(\mathcal{L}^a\mathcal{R}^b\mathcal{L}^c\mathcal{R}^d)| = |t(\sigma_1\sigma_2)|$$

■

Theorem 7.7 (Periods Associated with Parameter Regions in the PAL Structures)

(i) If a cycle in the halved archetypal model manifests as two coexisting cycles in the archetypal model, the period of either cycle is the same as the period of the cycle in the halved archetypal model.

$$|T(\sigma)| = |T(s_2(\sigma))| = |\sigma| \tag{7.10}$$

(ii) If a cycle in the halved archetypal model manifests as a single cycle in the archetypal model, the period of this cycle is double the period of the cycle in the halved archetypal model.

$$|T(\sigma)| = 2|\sigma| \tag{7.11}$$

Proof

(i) We know from Theorem 7.5 that if the cycle σ in the halved archetypal model manifests as two coexisting cycles in the archetypal model, σ has an even number of rotations n. And its translation is $T(\sigma) = t(\sigma_1\sigma_2)t(\sigma_3\sigma_4)\dots t(\sigma_{n-1}\sigma_n)$. Combining this with the fact that t preserves the period of its input as described in Theorem 7.6, we can calculate the period of $T(\sigma)$ in the following way.

$$\begin{aligned}
|T(\sigma)| &= |t(\sigma_1\sigma_2)t(\sigma_3\sigma_4)\dots t(\sigma_{n-1}\sigma_n)| \\
&= |t(\sigma_1\sigma_2)| + |t(\sigma_3\sigma_4)| + \dots + |t(\sigma_{n-1}\sigma_n)| \\
&= |\sigma_1\sigma_2| + |\sigma_3\sigma_4| + \dots + |\sigma_{n-1}\sigma_n| \\
&= |\sigma_1\sigma_2\dots\sigma_n| = |\sigma|
\end{aligned}$$

So the period of the cycle $T(\sigma)$ in the archetypal model is the same as the period of the cycle σ in the halved archetypal model. The same calculation can be done for $T(s(\sigma))$ and is omitted here.

(ii) Similarly, we know that if the cycle σ in the halved archetypal model manifests as a single cycle in the archetypal model, σ has an odd number of rotations n. And its translation is $T(\sigma) = t(\sigma_1\sigma_2)\dots t(\sigma_n\sigma_1)\dots t(\sigma_{n-1}\sigma_n)$. Its period can be calculated in the following way.

$$\begin{aligned}
|T(\sigma)| &= |t(\sigma_1\sigma_2)\dots t(\sigma_n\sigma_1)\dots t(\sigma_{n-1}\sigma_n)| \\
&= |t(\sigma_1\sigma_2)| + \dots + |t(\sigma_n\sigma_1)| + \dots + |t(\sigma_{n-1}\sigma_n)| \\
&= |\sigma_1\sigma_2| + \dots + |\sigma_n\sigma_1| + \dots + |\sigma_{n-1}\sigma_n| \\
&= |\sigma_1\sigma_2\dots\sigma_n\sigma_1\dots\sigma_{n-1}\sigma_n| = |\sigma\sigma| = 2|\sigma|
\end{aligned}$$

So the period of the cycle $T(\sigma)$ in the archetypal model is twice the period of the cycle σ in the halved archetypal model.

■

With this property we can also explain the regularities for coexistence of two cycles in the Farey-trees of PAL structures.

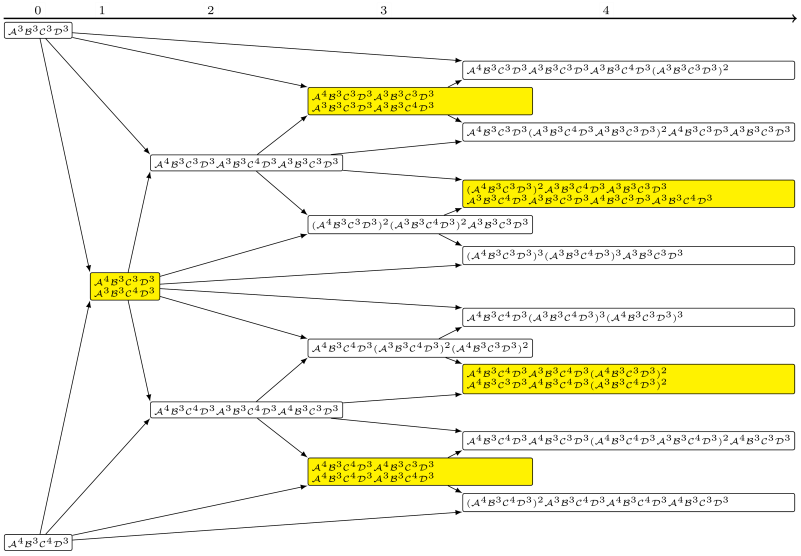

Figure 7.21: Farey-tree showing the symbolic sequences associated with the parameter regions of the horizontally oriented PAL structure marked with a red arrow in Figure 7.19a up to four levels. Nodes of parameter regions associated with two coexisting cycles are colored yellow and the periods are omitted here.

Theorem 7.8 (Coexistence in Child Nodes)

(i) The child of two nodes that are both associated with a single cycle each is associated with two coexisting cycles.

(ii) The child of a node that is associated with a single cycle and a node that is associated with two coexisting cycles is associated with a single cycle.

(iii) The child of two nodes that are both associated with two coexisting cycles each is associated with two coexisting cycles.

Proof

(i) Let ϕ and ψ be the cycles that the parent nodes are associated with. Since they both are associated with a single cycle each in the archetypal model, there are two cycles σ and ϱ with odd period in the halved archetypal model, such that $T(\sigma) = \phi$ and $T(\varrho) = \psi$. The child node of both nodes is therefore associated with the cycles $F(\sigma\varrho)$. $|\sigma\varrho| = |\sigma| + |\varrho|$ is even, because $|\sigma|$ and $|\rho|$ are odd. Therefore, we know that $|F(\sigma\varrho)| = 2$.

(ii) Let ϕ be the cycle that one parent node is associated with and ψ^a and ψ^b the twin cycles that the other parent node is associated with. Then there are two cycles σ and ϱ in the halved archetypal model where the period of σ is odd, the period of ϱ is even, $T(\sigma) = \phi$, and $T(\varrho) = \psi^a$. The child node of both nodes is therefore associated with the cycles $F(\sigma\varrho)$. $|\sigma\varrho| = |\sigma| + |\varrho|$ is odd, because $|\sigma|$ is odd and $|\rho|$ is even. Therefore, we know that $|F(\sigma\varrho)| = 1$.

(iii) Let ϕ^a, ϕ^b, ψ^a, and ψ^b be the pairs of twin cycles that each parent node is associated with. Then there are two cycles σ and ϱ with even period in the halved archetypal model, such that $T(\sigma) = \phi^a$ and $T(\varrho) = \psi^a$. The child node of both nodes is therefore associated with the cycles $F(\sigma\varrho)$. $|\sigma\varrho| = |\sigma| + |\varrho|$ is even, because $|\sigma|$ and $|\rho|$ are even. Therefore, we know that $|F(\sigma\varrho)| = 2$.

■

This explains the pattern we can observe in the periods of the PAL structures in Section 7.3.1. We take another look at the 1D period scan of the horizontal PAL structure between the parameter regions P_3^{14} and $\left[P_3^{14} \mid P_3^{12}\right]$ in Figure 7.12b. We get the information, whether a parameter region in the structure was associated with two coexisting cycles from the Farey-tree in Figure 7.21. The parameter region associated with the period 14 is not associated with coexisting cycles, therefore the corresponding cycle in the halved archetypal model has an odd number of revolutions and its period is twice as high as the period associated with the same parameter region in the halved archetypal model, which is 7. The parameter region associated with the period 13 is associated with coexisting cycles, therefore the corresponding cycle in the halved archetypal model has an even number of revolutions its period is the same as the period associated with the same parameter region in the halved archetypal mode. The parameter region in between those two parameter regions is associated with the period $7 + 13 = 20$ in the halved archetypal model. Also, its cycle has an odd number of revolutions, since it is the concatenation of one cycle with an even and one cycle with an odd number of revolutions. We know from Theorem 7.7 that this parameter region is associated with the period 40 in the archetypal model. This is true as we can observer this in the 1D period scan in Figure 7.12b. Also, we know from Theorem 7.8 that this parameter region is associated with two coexisting cycles. This is true as we can see in the Farey-tree in Figure 7.21.

The third case of Theorem 7.8 cannot be seen in the Farey-tree. It is actually not possible in the PAL structures we are investigating here. We will prove this next.

Theorem 7.9 (No Coexistence in both Parent Nodes)
*In the PAL structures we are investigating, no node has two parent nodes that are **both** associated with two coexisting cycles each.*

Proof
The Farey-trees for the symbolic sequences of PA structures can be constructed similarly to the original rule for creation of Farey-sequences for fractions. We write down both starting nodes in a list. Then, for each iteration we combine every pair of neighboring nodes according to the rules. The result is inserted between the two nodes that are combined. And the nodes created at each iteration are the nodes of the next level.

We now construct a Farey-tree where the content of the nodes is just whether the node is associated with coexistence, c, or not, n. The rules for combining nodes are from Theorem 7.8. We reformulate the statement in Theorem 7.9 to a concrete statement about the lists at each iteration.

In all lists, there will be no neighboring nodes that both have the content c. This implies no two nodes that both have the content c are combined to have a child node. So no node has two parent nodes that are both associated with two coexisting cycles. We now prove this by induction.

$n = 0$ The starting nodes are both associated with two coexisting cycles, so the initial list is $\{n, n\}$. We can see, there are no two nodes with both content c next to each other. ✓

$n + 1$ We assume that the current list of 2^n nodes has no two nodes with both content c next to each other. We take a look at each possible pair of neighboring nodes.

- $\{\ldots, n, n, \ldots\}$: *We combine both nodes with content n, the resulting node has content c. The resulting list is the list $\{\ldots, n, c, n, \ldots\}$. This rule will therefore never cause two neighboring nodes to both have the content c.*
- $\{\ldots, n, c, \ldots\}$: *We combine the node with content n with the node with content c, the resulting node has content n. The resulting list is the list $\{\ldots, n, n, c, \ldots\}$. This rule will therefore also never cause two neighboring nodes to both have the content c.*
- $\{\ldots, c, n, \ldots\}$: *We combine the node with content c with the node with content n, the resulting node has content n. The resulting list is the list $\{\ldots, c, n, n, \ldots\}$. This rule will therefore also never cause two neighboring nodes to both have the content c.*

■

Symbolic Sequences in the Period-adding-like Structures

So far, we have derived rules for the periods and multistability of cycles that are associated with parameter regions of PAL structures in the archetypal model based on the corresponding PA structure in the halved archetypal model. Let us now derive rules for the symbolic sequences that child nodes are associated with based on the symbolic sequences their parent nodes are associated with. For this, we first need to introduce a new operator. It is defined in Definition 7.8.

Definition 7.8 (Merging two 4-syllables)
The operation $\left[\phi_i \mid \psi_j\right]$ merges two 4-syllables ϕ_i and ψ_j. Let $\phi_i = \mathcal{A}^a\mathcal{B}^b\mathcal{C}^c\mathcal{D}^d$ and $\psi_j = \mathcal{A}^e\mathcal{B}^f\mathcal{C}^g\mathcal{D}^h$. Then $\left[\phi_i \mid \psi_j\right] = \mathcal{A}^a\mathcal{B}^b\mathcal{C}^g\mathcal{D}^h$. It concatenates the first 2-syllable of ϕ_i with the second 2-syllable of ψ_j.

Theorem 7.10 (Symbolic Sequences in Child Nodes I)
The child node of two nodes that are both associated with a singular cycle each with the symbolic sequences $\phi = \phi_1 \ldots \phi_n$ and $\psi = \psi_1 \ldots \psi_m$ is associated with two coexisting cycles with the following symbolic sequences.

$$\pi^a = \phi_1 \ldots \phi_{\frac{n-1}{2}} \left[\phi_{\frac{n+1}{2}} \mid \psi_{\frac{m+1}{2}}\right] \psi_{\frac{m+3}{2}} \ldots \psi_m \tag{7.12}$$

and

$$\pi^b = \phi_{\frac{n+3}{2}} \ldots \phi_n \psi_1 \ldots \psi_{\frac{m-1}{2}} \left[\psi_{\frac{m+1}{2}} \mid \phi_{\frac{n+1}{2}}\right] \tag{7.13}$$

Proof
Let $\sigma = \sigma_1\sigma_2\ldots\sigma_i$ with odd i, $\varrho = \varrho_1\varrho_2\ldots\varrho_j$ with odd j, $T(\sigma) = \phi$, and $T(\varrho) = \psi$. The child of both nodes in the halved archetypal model is associated with the symbolic sequence $\sigma\varrho = \sigma_1\ldots\sigma_i\varrho_1\ldots\varrho_j$. This manifests as two coexisting cycles in the archetypal model with the following symbolic sequences.

$$\begin{aligned}\pi^a &= T(\sigma\varrho) = T(\sigma_1\ldots\sigma_i\varrho_1\ldots\varrho_j)\\ &= t(\sigma_1\sigma_2)\ldots t(\sigma_i\varrho_1)\ldots t(\varrho_{j-1}\varrho_j)\\ &= \phi_1\ldots\phi_{\frac{n-1}{2}}t(\sigma_i\varrho_1)\psi_{\frac{m+3}{2}}\ldots\psi_j\\ &= \phi_1\ldots\phi_{\frac{n-1}{2}}\left[\phi_{\frac{n+1}{2}} \mid \psi_{\frac{m+1}{2}}\right]\psi_{\frac{m+3}{2}}\ldots\psi_j\end{aligned}$$

and

$$\begin{aligned}\pi^b &= T(s_2(\sigma\varrho)) = T(\sigma_2\ldots\sigma_i\varrho_1\ldots\varrho_j\sigma_1)\\ &= t(\sigma_2\sigma_3)\ldots t(\sigma_{i-1}\sigma_i)t(\varrho_1\varrho_2)\ldots t(\varrho_j\sigma_1)\\ &= \phi_{\frac{n+3}{2}}\ldots\phi_n\psi_1\ldots\psi_{\frac{m-1}{2}}t(\varrho_j\sigma_1)\\ &= \phi_{\frac{n+3}{2}}\ldots\phi_n\psi_1\ldots\psi_{\frac{m-1}{2}}\left[\psi_{\frac{m+1}{2}} \mid \phi_{\frac{n+1}{2}}\right]\end{aligned}$$

■

Theorem 7.11 (Symbolic Sequences in Child Nodes II)
The child node of a node that is associated with a singular cycle with the symbolic sequence $\phi = \phi_1\phi_2\ldots\phi_n$ and a node that is associated with two coexisting cycles with the symbolic sequences $\phi^a = \phi_1^a\phi_2^a\ldots\phi_m^a$ and $\phi_1^b\phi_2^b\ldots\phi_m^b$ is associated with one of the following symbolic sequences.

(i) If ϕ is associated with the left parent.

$$\pi = \phi_1\ldots\phi_{\frac{n-1}{2}}\left[\phi_{\frac{n+1}{2}} \mid \psi_m^b\right]\psi_1^b\ldots\psi_{m-1}^b\left[\psi_m^b \mid \phi_{\frac{n+1}{2}}\right]\phi_{\frac{n+3}{2}}\ldots\phi_n\psi^a \tag{7.14}$$

(ii) If ϕ is associated with the right parent.

$$\pi = \psi^a\phi_1\ldots\phi_{\frac{n-1}{2}}\left[\phi_{\frac{n+1}{2}} \mid \psi_m^b\right]\psi_1^b\ldots\psi_{m-1}^b\left[\psi_m^b \mid \phi_{\frac{n+1}{2}}\right]\phi_{\frac{n+3}{2}}\ldots\phi_n \tag{7.15}$$

Both cases are shift-equivalent to each other, but we must distinguish them in order to guarantee the correctness of the symbolic sequences in subsequent child nodes.

Proof

(i) Let $\sigma = \sigma_1\sigma_2\ldots\sigma_i$ with odd i, $\varrho = \varrho_1\varrho_2\ldots\varrho_j$ with even j, $T(\sigma) = \phi, T(\varrho) = \psi^a$, and $T(s_2(\varrho)) = \psi^b$. The child of both nodes in the halved archetypal model is associated with the symbolic sequence $\sigma\varrho = \sigma_1\sigma_2\ldots\sigma_i\varrho_1\varrho_2\ldots\varrho_j$. This will manifest as the following symbolic sequence in the archetypal model.

$$\begin{aligned}\pi &= T(\sigma\varrho) = T(\sigma_1\ldots\sigma_i\varrho_1\ldots\varrho_j)\\ &= t(\sigma_1\sigma_2)\ldots t(\sigma_i\varrho_1)\ldots t(\varrho_j\sigma_1)\ldots t(\sigma_{i-1}\sigma_i)t(\varrho_1\varrho_2)\ldots t(\varrho_{j-1}\varrho_j)\\ &= \phi_1\ldots\phi_{\frac{n-1}{2}}t(\sigma_i\varrho_1)\psi_1^b\ldots\varrho_{m-1}^b t(\varrho_j\sigma_1)\phi_{\frac{n+3}{2}}\ldots\phi_n\psi_1^a\ldots\psi_m^a\\ &= \phi_1\ldots\sigma_{\frac{n-1}{2}}\left[\sigma_{\frac{n+1}{2}} \mid \varrho_m^b\right]\psi_1^b\ldots\psi_{m-1}^b\left[\varrho_m^b \mid \sigma_{\frac{n+1}{2}}\right]\phi_{\frac{n+3}{2}}\ldots\phi_n\psi^a\end{aligned}$$

(ii) Let $\sigma = \sigma_1\sigma_2\ldots\sigma_i$ with even i and $\varrho = \varrho_1\varrho_2\ldots\varrho_j$ with odd j and $T(\sigma) = \psi^a, T(s_2(\sigma)) = \psi^b$, and $T(\varrho) = \phi$. The child of both nodes in the halved archetypal model is associated with the symbolic sequence $\sigma\varrho = \sigma_1 l_2\ldots\sigma_i\varrho_1\varrho_2\ldots\varrho_j$. This will manifest as the following symbolic sequence in the archetypal model.

$$\begin{aligned}\pi &= T(\sigma\varrho) = T(\sigma_1\ldots\sigma_i\varrho_1\ldots\varrho_j)\\ &= t(\sigma_1\sigma_2)\ldots t(\sigma_{i-1}\sigma_i)t(\varrho_1\varrho_2)\ldots t(\varrho_j\sigma_1)\ldots t(\sigma_i\varrho_1)\ldots t(\varrho_j\sigma_1)\ldots t(\sigma_i)\\ &= \psi_1^a\ldots\psi_m^a\phi_1\ldots\phi_{\frac{n-1}{2}}t(\sigma_i\varrho_1)\psi_1^b\ldots\psi_{m-1}^b t(\varrho_j\sigma_1)\phi_{\frac{n+3}{2}}\ldots\phi_n\\ &= \psi^a\phi_1\ldots\phi_{\frac{n-1}{2}}\left[\phi_{\frac{n+1}{2}} \mid \psi_m^b\right]\psi_1^b\ldots\psi_{m-1}^b\left[\psi_m^b \mid \phi_{\frac{n+1}{2}}\right]\phi_{\frac{n+3}{2}}\ldots\phi_n\end{aligned}$$

■

As mentioned before, the next case does not appear in the PAL structures we investigate. But we will include it here for completeness.

Theorem 7.12 (Symbolic Sequences in Child Nodes III)
The child node of two nodes that are both associated with two coexisting cycles each with the symbolic sequences $\phi^a = \phi_1^a\phi_2^a\ldots\phi_n^a, \phi^b = \phi_1^b\phi_2^b\ldots\phi_n^b, \psi^a = \psi_1^a\psi_2^a\ldots\psi_m^a$, and $\psi^b = \psi_1^b\psi_2^b\ldots\psi_m^b$ is associated with two coexisting cycles with the following symbolic sequences.

$$\pi^a = \phi^a\psi^a \tag{7.16}$$

and

$$\pi^b = \phi_1^b\ldots\phi_{n-1}^b\left[\phi_n^b \mid \psi_m^b\right]\psi_1^b\ldots\psi_{m-1}^b\left[\psi_m^b \mid \phi_n^b\right] \tag{7.17}$$

Proof
Let $\sigma = \sigma_1\ldots\sigma_i$ with even i, $\varrho = \varrho_1\ldots\varrho_j$ with even j, $T(\sigma) = \phi^a, T(s_2(\sigma)) = \phi^b, T(\varrho) = \phi^a$, and $T(s_2(\varrho)) = \phi^b$. The child of both nodes in the halved archetypal model is associated with the symbolic sequence $\sigma\varrho$. This manifests as two coexisting cycles with the following symbolic sequences in the archetypal model.

$$\begin{aligned}\pi^a &= T(\sigma\varrho) = T(\sigma_1\ldots\sigma_i\varrho_1\ldots\varrho_j)\\ &= t(\sigma_1\sigma_2)\ldots t(\sigma_{i-i}\sigma_i)t(\varrho_1\varrho_2)\ldots t(\varrho_{j-1}\varrho_j)\\ &= \phi_1^a\ldots\phi_n^a\psi_1^a\ldots\psi_m^a = \phi^a\psi^a\end{aligned}$$

and

$$\begin{aligned}\pi^b &= T(s_2(\sigma\varrho)) = T(\sigma_2\ldots\sigma_i\varrho_1\ldots\varrho_j\sigma_1)\\ &= t(\sigma_2\sigma_3)\ldots t(\sigma_i\varrho_1)\ldots t(\varrho_j\sigma_1)\\ &= \phi_1^b\ldots\phi_{n-1}^b t(\sigma_i\varrho_1)\phi_1^b\ldots\phi_{m-1}^b t(\varrho_j\sigma_1)\\ &= \phi_1^b\ldots\phi_{n-1}^b\left[\phi_n^b \mid \phi_m^b\right]\phi_1^b\ldots\phi_{m-1}^b\left[\phi_m^b \mid \phi_n^b\right]\end{aligned}$$

■

Rotation-numbers in the Period-adding-like Structures

Next, we derive rules for the rotation-numbers in the Farey-trees of the PAL structures. Note that we don't have two branches in the archetypal model, instead we have four. This means that the definition Definition 2.10 does not work for our case. Instead, we define rotation-tuples. Figure 7.22 shows as Farey-tree with rotation-tuples.

Definition 7.9 (Rotation Tuples)
The rotation tuple of a cycle with the symbolic sequence ϕ in the archetypal model is defined as the following.

$$\rho(\phi) = (\rho_{\mathcal{A}}(\phi), \rho_{\mathcal{B}}(\phi), \rho_{C}(\phi), \rho_{\mathcal{D}}(\phi)) = \left(\frac{|\phi|_{\mathcal{A}}}{|\phi|}, \frac{|\phi|_{\mathcal{B}}}{|\phi|}, \frac{|\phi|_{C}}{|\phi|}, \frac{|\phi|_{\mathcal{D}}}{|\phi|} \right) \tag{7.18}$$

Where $|\phi|_{\mathcal{A}}$ is the number of symbols $\mathcal{A}$ in the sequence. Analogous for the symbols $\mathcal{B}$, C, and $\mathcal{D}$.

Theorem 7.13 (Rotation Tuples in Child Nodes I)
The child node of two nodes that are both associated with a single cycle each with the symbolic sequences ϕ and ψ is associated with the following period. In the following, we call the symbolic sequences of the two twin cycles associated with the child node π^a and π^b.

$$|\pi^a| = |\pi^b| = \frac{|\phi| + |\psi|}{2} = |\pi| \tag{7.19}$$

And its associated rotation tuples are:

$$\rho(\pi^a) = (\rho_{\mathcal{A}}(\pi^a), \rho_{\mathcal{B}}(\pi^a), \rho_{C}(\pi^a), \rho_{\mathcal{D}}(\pi^a)) \tag{7.20}$$

and

$$\rho(\pi^b) = (\rho_{\mathcal{A}}(\pi^b), \rho_{\mathcal{B}}(\pi^b), \rho_{C}(\pi^b), \rho_{\mathcal{D}}(\pi^b)) \tag{7.21}$$

Where the elements of each tuple are defined by the following equations.

$$\rho_{\mathcal{A}}(\pi^a) = \frac{\left|\phi_1 \dots \phi_{\frac{n+1}{2}}\right|_{\mathcal{A}} + \left|\psi_{\frac{m+3}{2}} \dots \psi_m\right|_{\mathcal{A}}}{|\pi|} \tag{7.22a}$$

$$\rho_{\mathcal{B}}(\pi^a) = \frac{\left|\phi_1 \dots \phi_{\frac{n+1}{2}}\right|_{\mathcal{B}} + \left|\psi_{\frac{m+3}{2}} \dots \psi_m\right|_{\mathcal{B}}}{|\pi|} \tag{7.22b}$$

$$\rho_{C}(\pi^a) = \frac{\left|\phi_1 \dots \phi_{\frac{n-1}{2}}\right|_{C} + \left|\psi_{\frac{m+1}{2}} \dots \psi_m\right|_{C}}{|\pi|} \tag{7.22c}$$

$$\rho_{\mathcal{D}}(\pi^a) = \frac{\left|\phi_1 \dots \phi_{\frac{n-1}{2}}\right|_{\mathcal{D}} + \left|\psi_{\frac{m+1}{2}} \dots \psi_m\right|_{\mathcal{D}}}{|\pi|} \tag{7.22d}$$

and

$$\rho_{\mathcal{A}}(\pi^b) = \frac{\left|\psi_1 \dots \psi_{\frac{m+1}{2}}\right|_{\mathcal{A}} + \left|\phi_{\frac{n+3}{2}} \dots \phi_n\right|_{\mathcal{A}}}{|\pi|} \tag{7.23a}$$

$$\rho_{\mathcal{B}}(\pi^b) = \frac{\left|\psi_1 \dots \psi_{\frac{m+1}{2}}\right|_{\mathcal{B}} + \left|\phi_{\frac{n+3}{2}} \dots \phi_n\right|_{\mathcal{B}}}{|\pi|} \tag{7.23b}$$

$$\rho_{\mathcal{C}}(\pi^b) = \frac{\left|\psi_1 \dots \psi_{\frac{m-1}{2}}\right|_{\mathcal{C}} + \left|\phi_{\frac{n+1}{2}} \dots \phi_n\right|_{\mathcal{C}}}{|\pi|} \tag{7.23c}$$

$$\rho_{\mathcal{D}}(\pi^b) = \frac{\left|\psi_1 \dots \psi_{\frac{m-1}{2}}\right|_{\mathcal{D}} + \left|\phi_{\frac{n+1}{2}} \dots \phi_n\right|_{\mathcal{D}}}{|\pi|} \tag{7.23d}$$

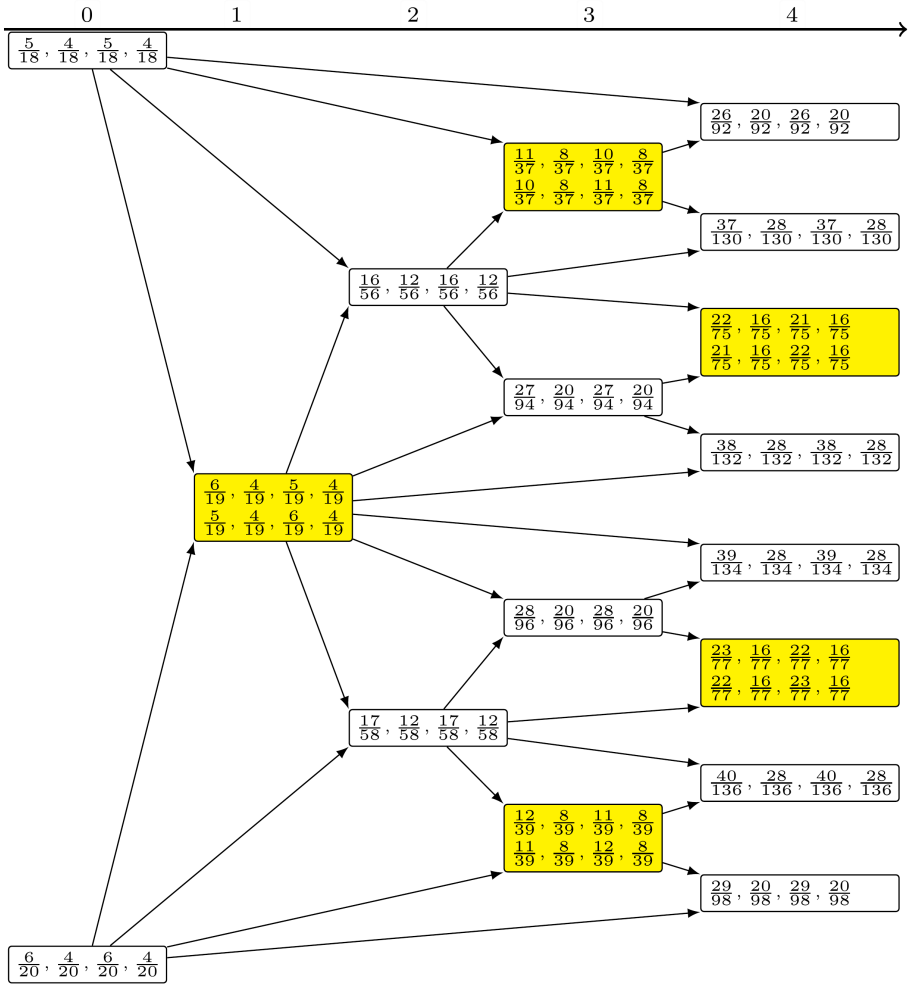

Figure 7.22: Farey-tree showing the rotation tuples associated with the parameter regions of the horizontally oriented PAL structure marked with a red arrow in Figure 7.19a up to four levels. Nodes of parameter regions associated with two coexisting cycles are colored yellow.

Proof

Let $\sigma = \sigma_1\sigma_2\ldots\sigma_i$ with odd i, $\varrho = \varrho_1\varrho_2\ldots\varrho_j$ with odd j, $T(\sigma) = \phi$, and $T(\varrho) = \psi$. The child of both nodes in the halved archetypal model is associated with the symbolic sequence $\sigma\varrho = \sigma_1\ldots\sigma_i\varrho_1\ldots\varrho_j$. This manifests as two coexisting cycles in the archetypal model with the symbolic sequences π^a and π^b following the rules in Theorem 7.10.

We start by proving the period of the cycles with symbolic sequences π^a and π^b.

$$\begin{aligned}
|\pi^a| &= |T(\sigma\varrho)| \\
&= |T(\sigma_1\ldots\sigma_i\varrho_1\ldots\varrho_j)| \\
&= |t(\sigma_1\sigma_2)\ldots t(\sigma_i\varrho_1)\ldots t(\varrho_{j-1}\varrho_j)| \\
&= |\sigma_1\sigma_2\ldots\sigma_i\varrho_1\ldots\varrho_{j-1}\varrho_j| \\
&= |\sigma\varrho| = \frac{|\phi|}{2} + \frac{|\psi|}{2} = \frac{|\phi| + |\psi|}{2}
\end{aligned}$$

Note that the last step takes advantage of the fact about the periods of cycles in the archetypal model described in Theorem 7.7. The proof for π^b is similar and leads to the same result.

$$\begin{aligned}
|\pi^b| &= |T(s_2(\sigma\varrho))| \\
&= |T(\sigma_2\ldots\sigma_i\varrho_1\ldots\varrho_j\sigma_1)| \\
&= |t(\sigma_2\sigma_3)\ldots t(\sigma_{i-1}\sigma_i)t(\varrho_1\varrho_2)\ldots t(\varrho_j\sigma_1)| \\
&= |\sigma_2\sigma_3\ldots\sigma_i\varrho_1\ldots\varrho_j\sigma_1| \\
&= |\sigma_1\sigma_2\ldots\sigma_i\varrho_1\ldots\varrho_j| \\
&= |\sigma\varrho| = \frac{|\phi|}{2} + \frac{|\psi|}{2} = \frac{|\phi| + |\psi|}{2}
\end{aligned}$$

This gives us the denominators of all elements of both rotation tuples. For the numerators, we have to count the symbols in the symbolic sequences of the cycles associated with each child node. We start with π^a and the symbol $\mathcal{A}$.

$$\begin{aligned}
|\pi^a|_{\mathcal{A}} &= \left|\phi_1\ldots\phi_{\frac{n-1}{2}}\left[\phi_{\frac{n+1}{2}} \mid \psi_{\frac{m+1}{2}}\right]\psi_{\frac{m+3}{2}}\ldots\psi_m\right|_{\mathcal{A}} \\
&= |\phi_1|_{\mathcal{A}} + \cdots + \left|\left[\phi_{\frac{n+1}{2}} \mid \psi_{\frac{n+1}{2}}\right]\right|_{\mathcal{A}} + \left|\psi_{\frac{m+3}{2}}\right|_{\mathcal{A}} + \cdots + |\psi_m|_{\mathcal{A}} \\
&= |\phi_1|_{\mathcal{A}} + \cdots + \left|\phi_{\frac{n+1}{2}}\right|_{\mathcal{A}} + \left|\psi_{\frac{m+3}{2}}\right|_{\mathcal{A}} + \cdots + |\psi_m|_{\mathcal{A}} \\
&= \left|\phi_1\ldots\phi_{\frac{n+1}{2}}\right|_{\mathcal{A}} + \left|\psi_{\frac{m+3}{2}}\ldots\psi_m\right|_{\mathcal{A}}
\end{aligned}$$

We can do the second to last step, since the symbol $\mathcal{A}$ is in the first 2-syllable of $\phi_{\frac{n+1}{2}}$. The same is true for the symbol $\mathcal{B}$ and the proof works exactly the same for $|\pi^a|_{\mathcal{B}}$, so we will omit it here. For the symbols C and $\mathcal{D}$ the last step does not work, instead we have to choose $\psi_{\frac{n+1}{2}}$. We demonstrate it for $|\pi^a|_C$, the proof for $|\pi^a|_{\mathcal{D}}$ works exactly the same.

$$\begin{aligned}
|\pi^a|_C &= \left|\phi_1\ldots\phi_{\frac{n-1}{2}}\left[\phi_{\frac{n+1}{2}} \mid \psi_{\frac{m+1}{2}}\right]\psi_{\frac{m+3}{2}}\ldots\psi_m\right|_C \\
&= |\phi_1|_C + \cdots + \left|\left[\phi_{\frac{n+1}{2}} \mid \psi_{\frac{n+1}{2}}\right]\right|_C + \left|\psi_{\frac{m+3}{2}}\right|_C + \cdots + |\psi_m|_C \\
&= |\phi_1|_C + \cdots + \left|\psi_{\frac{n+1}{2}}\right|_C + \left|\psi_{\frac{m+3}{2}}\right|_C + \cdots + |\psi_m|_C \\
&= \left|\phi_1\ldots\psi_{\frac{n+1}{2}}\right|_C + \left|\psi_{\frac{m+3}{2}}\ldots\psi_m\right|_C
\end{aligned}$$

Now we will take a look at the numerators of the elements in the rotation tuple of π^b. We start with the symbol $\mathcal{A}$.

$$\begin{aligned}
|\pi^b|_{\mathcal{A}} &= \left|\phi_{\frac{n+3}{2}} \dots \phi_n \psi_1 \dots \psi_{\frac{m-1}{2}} \left[\psi_{\frac{m+1}{2}} \mid \phi_{\frac{n+1}{2}}\right]\right|_{\mathcal{A}} \\
&= \left|\phi_{\frac{n+3}{2}}\right|_{\mathcal{A}} + \dots + |\phi_n|_{\mathcal{A}} + |\psi_1|_{\mathcal{A}} + \dots + \left|\psi_{\frac{m-1}{2}}\right|_{\mathcal{A}} + \left|\left[\psi_{\frac{m+1}{2}} \mid \phi_{\frac{n+1}{2}}\right]\right|_{\mathcal{A}} \\
&= \left|\phi_{\frac{n+3}{2}}\right|_{\mathcal{A}} + \dots + |\phi_n|_{\mathcal{A}} + |\psi_1|_{\mathcal{A}} + \dots + \left|\psi_{\frac{m-1}{2}}\right|_{\mathcal{A}} + \left|\psi_{\frac{m+1}{2}}\right|_{\mathcal{A}} \\
&= \left|\phi_{\frac{n+3}{2}} \dots \phi_n\right|_{\mathcal{A}} + \left|\psi_1 \dots \psi_{\frac{m-1}{2}}\right|_{\mathcal{A}} + \left|\psi_{\frac{m+1}{2}}\right|_{\mathcal{A}}
\end{aligned}$$

Again, we can do the second to last step, since the symbol $\mathcal{A}$ is in the first 2-syllable of $\psi_{\frac{n+1}{2}}$. The same is true for the symbol $\mathcal{B}$ and the proof works exactly the same for $|\pi^b|_{\mathcal{B}}$. We will omit it here. For the symbols C and $\mathcal{D}$ the last step does not work, instead we have to choose $\phi_{\frac{n+1}{2}}$. We demonstrate it for $|\pi^b|_C$, the proof for $|\pi^b|_{\mathcal{D}}$ works exactly the same.

$$\begin{aligned}
|\pi^b|_C &= \left|\phi_{\frac{n+3}{2}} \dots \phi_n \psi_1 \dots \psi_{\frac{m-1}{2}} \left[\psi_{\frac{m+1}{2}} \mid \phi_{\frac{n+1}{2}}\right]\right|_C \\
&= \left|\phi_{\frac{n+3}{2}}\right|_C + \dots + |\phi_n|_{\mathcal{A}} + |\psi_1|_C + \dots + \left|\psi_{\frac{m-1}{2}}\right|_C + \left|\left[\psi_{\frac{m+1}{2}} \mid \phi_{\frac{n+1}{2}}\right]\right|_C \\
&= \left|\phi_{\frac{n+3}{2}}\right|_C + \dots + |\phi_n|_C + |\psi_1|_C + \dots + \left|\psi_{\frac{m-1}{2}}\right|_C + \left|\psi_{\frac{m+1}{2}}\right|_C \\
&= \left|\phi_{\frac{n+3}{2}} \dots \phi_n\right|_C + \left|\psi_1 \dots \psi_{\frac{m-1}{2}} \psi_{\frac{m+1}{2}}\right|_C
\end{aligned}$$

■

Theorem 7.14 (Rotation Tuples in Child Nodes II)
The child node of a node that is associated with a single cycle ϕ and a node that is associated with two coexisting cycles with the symbolic sequences ψ^a and ψ^b is associated with the following rotation tuple. We use element-wise Farey-addition here, since it is the same for each symbol.

$$\rho(\pi) = \rho(\phi) \oplus \rho(\psi^a) \oplus \rho(\psi^b) \tag{7.24}$$

Proof
We prove this again in two parts. First, we prove that the denominator of each element of the rotation tuples add up.

$$\begin{aligned}
|\pi| &= \left|\phi_1 \dots \phi_{\frac{n-1}{2}} \left[\phi_{\frac{n+1}{2}} \mid \psi^b_m\right] \psi^b_1 \dots \psi^b_{m-1} \left[\psi^b_m \mid \phi_{\frac{n+1}{2}}\right] \phi_{\frac{n+3}{2}} \dots \phi_n \psi^a\right| \\
&= \left|\phi_1 \dots \phi_{\frac{n-1}{2}} \left[\phi_{\frac{n+1}{2}} \mid \phi_{\frac{n+1}{2}}\right] \phi_{\frac{n+3}{2}} \dots \phi_n \psi^b_1 \dots \psi^b_{m-1} \left[\psi^b_m \mid \psi^b_m\right] \psi^a\right| \\
&= |\phi\psi^b\psi^a| = |\phi| + |\psi^a| + |\psi^b|
\end{aligned}$$

Note that the first step is achieved by simply reordering some 4-syllables and two 2-syllables in the symbolic sequences. This does not change the period. It does also not change the number of symbols, since we only swapped the second 2-syllable of $\left[\phi_{\frac{n+1}{2}} \mid \psi^b_m\right]$ and $\left[\psi^b_m \mid \phi_{\frac{n+1}{2}}\right]$. Therefore, the proof for works the same for the number of any symbol. We will demonstrate this for symbol $\mathcal{A}$.

$$\begin{aligned}
|\pi|_{\mathcal{A}} &= \left|\phi_1 \dots \phi_{\frac{n-1}{2}} \left[\phi_{\frac{n+1}{2}} \mid \psi^b_m\right] \psi^b_1 \dots \psi^b_{m-1} \left[\psi^b_m \mid \phi_{\frac{n+1}{2}}\right] \phi_{\frac{n+3}{2}} \dots \phi_n \psi^a\right|_{\mathcal{A}} \\
&= \left|\phi_1 \dots \phi_{\frac{n-1}{2}} \left[\phi_{\frac{n+1}{2}} \mid \phi_{\frac{n+1}{2}}\right] \phi_{\frac{n+3}{2}} \dots \phi_n \psi^b_1 \dots \psi^b_{m-1} \left[\psi^b_m \mid \psi^b_m\right] \psi^a\right|_{\mathcal{A}} \\
&= |\phi\psi^b\psi^a|_{\mathcal{A}} = |\phi|_{\mathcal{A}} + |\psi^a|_{\mathcal{A}} + |\psi^b|_{\mathcal{A}}
\end{aligned}$$

Therefore, the numerators of each element in the rotation tuples add up too.

One might criticize that we only proved it for the case where the left parent node is associated with a single cycle. In that case

$$\pi = \phi_1 \dots \phi_{\frac{n-1}{2}} \left[\phi_{\frac{n+1}{2}} \mid \psi_m^b\right] \psi_1^b \dots \psi_{m-1}^b \left[\psi_m^b \mid \phi_{\frac{n+1}{2}}\right] \phi_{\frac{n+3}{2}} \dots \phi_n \psi^a$$

If the right parent node is associated with a single cycle, then

$$\pi = \psi^a \phi_1 \dots \phi_{\frac{n-1}{2}} \left[\phi_{\frac{n+1}{2}} \mid \psi_m^b\right] \psi_1^b \dots \psi_{m-1}^b \left[\psi_m^b \mid \phi_{\frac{n+1}{2}}\right] \phi_{\frac{n+3}{2}} \dots \phi_n$$

The only difference in both cases is that the symbols of ψ^a are at the end of the symbolic sequence in the first case and at the beginning of the symbolic sequence in the second case. Since reordering of 4-syllables does not change the period nor the number of individual symbols, this proof works for both cases.

■

As mentioned before, the next case does not appear in the PAL structures we investigate. But we will include it here again for completeness.

Theorem 7.15 (Rotation Tuples in Child Nodes III)
The child node of two nodes that are both associated with two coexisting cycles each with symbolic sequences ϕ^a, ϕ^b, ψ^a, and ψ^b is associated with two coexisting cycles. Their rotation tuples are the defined by the following equations. Note that we use element-wise Farey-addition here again.

$$\rho(\pi^a) = \rho(\phi^a) \oplus \rho(\psi^a) \tag{7.25}$$

and

$$\rho(\pi^b) = \rho(\phi^b) \oplus \rho(\psi^b) \tag{7.26}$$

Proof
We start with the cycle with symbolic sequence π^a. Again, we first prove that the denominators, i.e. the periods, add up.

$$|\pi^a| = |\phi^a \psi^a| = |\phi^a| + |\psi^a|$$

This is straightforward and can be done for each symbol exactly like this. We will demonstrate it for the symbol $\mathcal{A}$.

$$|\pi^a|_{\mathcal{A}} = |\phi^a \psi^a|_{\mathcal{A}} = |\phi^a|_{\mathcal{A}} + |\psi^a|_{\mathcal{A}}$$

Therefore, the numerators also add up.

Now we prove the same thing for the cycle with symbolic sequence π^b.

$$\begin{aligned} |\pi^b| &= \left|\phi_1^b \dots \phi_{n-1}^b \left[\phi_n^b \mid \psi_m^b\right] \psi_1^b \dots \psi_{m-1}^b \left[\psi_m^b \mid \phi_n^b\right]\right| \\ &= \left|\phi_1^b \dots \phi_{n-1}^b \left[\phi_n^b \mid \phi_n^b\right] \psi_1^b \dots \psi_{m-1}^b \left[\psi_m^b \mid \psi_m^b\right]\right| \\ &= |\phi^b \psi^b| = |\phi^b| + |\psi^b| \end{aligned}$$

Here we simply swapped the second 2-syllables of $\left[\phi_n^b \mid \psi_m^b\right]$ *and* $\left[\psi_m^b \mid \phi_n^b\right]$*. This does not change the period. It also does not change the number of any symbol. Therefore, we can use the same proof for any symbol and show that the numerators also add up. We demonstrate it for the symbol* $\mathcal{A}$ *in the following.*

$$\begin{aligned}|\pi^b|_{\mathcal{A}} &= \left|\phi_1^b \dots \phi_{n-1}^b \left[\phi_n^b \mid \psi_m^b\right] \psi_1^b \dots \psi_{m-1}^b \left[\psi_m^b \mid \phi_n^b\right]\right|_{\mathcal{A}} \\ &= \left|\phi_1^b \dots \phi_{n-1}^b \left[\phi_n^b \mid \phi_n^b\right] \psi_1^b \dots \psi_{m-1}^b \left[\psi_m^b \mid \psi_m^b\right]\right|_{\mathcal{A}} \\ &= |\phi^b \psi^b|_{\mathcal{A}} = |\phi^b|_{\mathcal{A}} + |\psi^b|_{\mathcal{A}}\end{aligned}$$

■

In the usual case with two symbols, the rotation numbers are monotone. In our case we have rotation tuples instead of numbers, and we will consider the monotonicity of the single elements. Also, we sometimes have coexistence of two cycles. We will consider the rotation tuples of each of the coexisting twin cycles independently. The monotonicity does not hold up for our case, unfortunately. We can see a counter example in Figure 7.22. Let's consider the rotation numbers for the symbol $\mathcal{A}$ which are the first element in each rotation tuple. The right starting node, the upper node of level 0, is associated with the rotation number $\frac{5}{18}$ for the symbol $\mathcal{A}$. And the left starting node is associated with the rotation number $\frac{6}{20}$ for the symbol $\mathcal{A}$. And $\frac{6}{20} > \frac{5}{18}$, so each rotation number for the symbol $\mathcal{A}$ of the coexisting cycles associated with the child node should be in-between those two numbers. But the rotation numbers for the symbol $\mathcal{A}$ in the child node are $\frac{6}{19} > \frac{6}{20}$ and $\frac{5}{19} < \frac{5}{18}$. If we instead consider the element-wise Farey-sum of both rotation tuples in the case of coexisting cycles, the monotonicity holds.

Theorem 7.16 (Monotonicity of Rotation Tuples in PAL Structures)
Let the rotation tuple of the left starting node be element-wise smaller than the rotation tuple of the right starting node w.l.o.g. Then the rotation tuple of a node that is associated with a cycle ϕ *is element-wise smaller than the rotation tuple of a node that is associated with a cycle* ψ*, if the node associated with* ϕ *is to left of the node associated with* ψ *in the Farey-tree.*

Proof
This is a proof by induction, and it will rely heavily on the following fact. If $\frac{a_1}{b_1} < \frac{a_2}{b_2}$*, then*

$$\frac{a_1}{b_1} < \frac{a_1}{b_1} \oplus \frac{a_2}{b_2} < \frac{a_2}{b_2} \tag{7.27}$$

We consider the structure of the Farey-tree like in the proof for Theorem 7.9. First, we write down the starting nodes. Here, the only content is the rotation tuples and the left starting node is element-wise smaller than the right starting node w.l.o.g. Note that for coexisting twin cycles π^a *and* π^b*, we consider the element-wise Farey-sum of their rotation tuples* $\rho(\pi) = \rho(\pi^a) \oplus \rho(\pi^b)$*. For each iteration we combine each pair of rotation tuples in the list and insert the result in the middle of each pair. We again reformulate the statement of Theorem 7.16 to a statement about the lists at each iteration.*

In all lists, the node $\rho(\phi)$ *will be element-wise smaller than the next node* $\rho(\psi)$*. This implies global monotonicity at each iteration for the lists. And therefore also global monotonicity in the Farey-tree across all levels.*

$n = 0$ *The left starting node is element-wise smaller than the right starting node by construction.*

$n + 1$ *We assume that the above statement is true for the current list of* 2^n*. And we proof that for each neighboring nodes* $\{\ldots, \rho(\phi), \rho(\psi), ...\}$ *the values of their child node* $\rho(\pi)$ *is in-between the values of its two parent nodes.*

$$\rho(\phi) < \rho(\pi) < \rho(\psi)$$

We need to consider four cases. First, let's assume that the node associated with $\rho(\phi)$ *is associated with a single cycle when considering the Farey-tree with symbolic sequences and the node associated with* $\rho(\psi)$ *is also associated with a single cycle. Then for symbol* $\mathcal{A}$

$$\begin{aligned}
\rho_{\mathcal{A}}(\pi) &= \rho_{\mathcal{A}}(\pi^a) \oplus \rho_{\mathcal{A}}(\pi^b) \\
&= \frac{\left|\phi_1 \ldots \phi_{\frac{n+1}{2}}\right|_{\mathcal{A}} + \left|\psi_{\frac{m+3}{2}} \ldots \psi_m\right|_{\mathcal{A}}}{|\pi|} \oplus \frac{\left|\psi_1 \ldots \psi_{\frac{m+1}{2}}\right|_{\mathcal{A}} + \left|\phi_{\frac{n+3}{2}} \ldots \phi_n\right|_{\mathcal{A}}}{|\pi|} \\
&= \frac{\left|\phi_1 \ldots \phi_{\frac{n+1}{2}}\right|_{\mathcal{A}} + \left|\psi_{\frac{m+3}{2}} \ldots \psi_m\right|_{\mathcal{A}} + \left|\psi_1 \ldots \psi_{\frac{m+1}{2}}\right|_{\mathcal{A}} + \left|\phi_{\frac{n+3}{2}} \ldots \phi_n\right|_{\mathcal{A}}}{2 \cdot |\pi|} \\
&= \frac{\left|\phi_1 \ldots \phi_{\frac{n+1}{2}} \psi_{\frac{m+3}{2}} \ldots \psi_m \psi_1 \ldots \psi_{\frac{m+1}{2}} \phi_{\frac{n+3}{2}} \ldots \phi_n\right|_{\mathcal{A}}}{2 \cdot \frac{|\phi|+|\psi|}{2}} \\
&= \frac{\left|\phi_1 \ldots \phi_{\frac{n+1}{2}} \phi_{\frac{n+3}{2}} \ldots \phi_n \psi_1 \ldots \psi_{\frac{m+1}{2}} \psi_{\frac{m+3}{2}} \ldots \psi_m\right|_{\mathcal{A}}}{|\phi| + |\psi|} \\
&= \frac{|\phi\psi|_{\mathcal{A}}}{|\phi| + |\psi|} = \frac{|\phi|_{\mathcal{A}} + |\psi|_{\mathcal{A}}}{|\phi| + |\psi|} = \rho_{\mathcal{A}}(\phi) \oplus \rho_{\mathcal{A}}(\psi)
\end{aligned}$$

And since $\rho_{\mathcal{A}}(\phi) < \rho_{\mathcal{A}}(\psi) \implies \rho_{\mathcal{A}}(\phi) < \rho_{\mathcal{A}}(\phi) \oplus \rho_{\mathcal{A}}(\psi) < \rho_{\mathcal{A}}(\psi)$*, it also implies that* $\rho_{\mathcal{A}}(\phi) < \rho_{\mathcal{A}}(\pi) = \rho_{\mathcal{A}}(\pi^a) \oplus \rho_{\mathcal{A}}(\pi^h) < \rho_{\mathcal{A}}(\psi)$*.*

This works exactly the same for the symbol $\mathcal{B}$*, and we will omit it here. For the symbols* C *and* $\mathcal{D}$ *it is slightly different. We will demonstrate it for the symbol* C *in the following.*

$$\begin{aligned}
\rho_C(\pi) &= \rho_C(\pi^a) \oplus \rho_C(\pi^b) \\
&= \frac{\left|\phi_1 \ldots \phi_{\frac{n-1}{2}}\right|_C + \left|\psi_{\frac{m+1}{2}} \ldots \psi_m\right|_C}{|\pi|} \oplus \frac{\left|\psi_1 \ldots \psi_{\frac{m-1}{2}}\right|_C + \left|\phi_{\frac{n+1}{2}} \ldots \phi_n\right|_C}{|\pi|} \\
&= \frac{\left|\phi_1 \ldots \phi_{\frac{n-1}{2}}\right|_C + \left|\psi_{\frac{m+1}{2}} \ldots \psi_m\right|_C + \left|\psi_1 \ldots \psi_{\frac{m-1}{2}}\right|_C + \left|\phi_{\frac{n+1}{2}} \ldots \phi_n\right|_C}{2 \cdot |\pi|} \\
&= \frac{\left|\phi_1 \ldots \phi_{\frac{n-1}{2}} \psi_{\frac{m+1}{2}} \ldots \psi_m \psi_1 \ldots \psi_{\frac{m-1}{2}} \phi_{\frac{n+1}{2}} \ldots \phi_n\right|_C}{2 \cdot \frac{|\phi|+|\psi|}{2}} \\
&= \frac{\left|\phi_1 \ldots \phi_{\frac{n-1}{2}} \phi_{\frac{n+1}{2}} \ldots \phi_n \psi_1 \ldots \psi_{\frac{m-1}{2}} \psi_{\frac{m+1}{2}} \ldots \psi_m\right|_C}{|\phi| + |\psi|} \\
&= \frac{|\phi\psi|_C}{|\phi| + |\psi|} = \frac{|\phi|_C + |\psi|_C}{|\phi| + |\psi|} = \rho_{\mathcal{A}}(\phi) \oplus \rho_C(\psi)
\end{aligned}$$

And since $\rho_C(\phi) < \rho_C(\psi) \implies \rho_C(\phi) < \rho_C(\phi) \oplus \rho_C(\psi) < \rho_C(\psi)$*, it also implies that* $\rho_C(\phi) < \rho_C(\pi) = \rho_C(\pi^a) \oplus \rho_C(\pi^h) < \rho_C(\psi)$.

Next, let's consider the case where the node associated with $\rho(\phi)$ *is associated with a single cycle when considering the Farey-tree with symbolic sequences and the node associated with* $\rho(\psi) = \rho(\psi^a) \oplus \rho(\psi^b)$ *is also associated with two coexisting cycles. Here, we can use the element-wise Farey-sum and prove it simultaneously for all symbols.*

$$\begin{aligned}\rho(\pi) &= \rho(\phi) \oplus \rho(\psi^a) \oplus \rho(\psi^b) \\ &= \rho(\phi) \oplus \rho(\psi)\end{aligned}$$

Since $\rho(\phi) < \rho(\psi) \implies \rho(\phi) < \rho(\phi) \oplus \rho(\psi) < \rho(\psi)$*, it also implies that* $\rho(\phi) < \rho(\pi) = \rho(\phi) \oplus \rho(\psi) < \rho(\psi)$.

The proof works similar for the third case, where the node associated with $\rho(\phi) = \rho(\phi^a) \oplus \rho(\phi^b)$ *is also associated with two coexisting cycles and the node associated with* $\rho(\psi)$ *is associated with a single cycle.*

$$\begin{aligned}\rho(\pi) &= \rho(\phi^a) \oplus \rho(\phi^b) \oplus \rho(\psi) \\ &= \rho(\phi) \oplus \rho(\psi)\end{aligned}$$

Since $\rho(\phi) < \rho(\psi) \implies \rho(\phi) < \rho(\phi) \oplus \rho(\psi) < \rho(\psi)$*, it also implies that* $\rho(\phi) < \rho(\pi) = \rho(\phi) \oplus \rho(\psi) < \rho(\psi)$.

The last case does not occur in the PAL structures that we are investigating, but we will include a proof for this case also. Both the left node that is associated with $\rho(\phi) = \rho(\phi^a) \oplus \rho(\phi^b)$ *and the right node that is associated with* $\rho(\psi) = \rho(\psi^a) \oplus \rho(\psi^b)$ *are associated with two coexisting cycles. Again we can use element-wise Farey-addition.*

$$\begin{aligned}\rho(\pi) &= \rho(\pi^a) \oplus \rho(\pi^b) \\ &= (\rho(\phi^a) \oplus \rho(\psi^a)) \oplus \left(\rho(\phi^b) \oplus \rho(\psi^b)\right) \\ &= \rho(\phi^a) \oplus \rho(\psi^a) \oplus \rho(\phi^b) \oplus \rho(\psi^b) \\ &= \rho(\phi^a) \oplus \rho(\phi^a) \oplus \rho(\psi^a) \oplus \rho(\psi^b) \\ &= \rho(\phi) \oplus \rho(\psi)\end{aligned}$$

And $\rho(\phi) < \rho(\psi) \implies \rho(\phi) < \rho(\pi) = \rho(\phi) \oplus \rho(\psi) < \rho(\psi)$.

■

This concludes the derived properties and rules for the PAL structures in the archetypal model.

8 Conclusion

This chapter summarizes all findings of this thesis and touches on some topics that can be investigated next based on the findings of this thesis.

8.1 Summary

This section contains the summary of all findings. It is divided into two logical parts

First, the original model function and the parameter effects on the model function in the original model were analyzed. Then, the characteristics of the model function and parameter effects that are needed for the PI structure of interest were identified. This is achieved by developing the archetypal model, a model that is simpler than the original model and exhibits the same behavior. This model is defined by four branches $f_{\mathcal{A}}$, $f_{\mathcal{B}}$, f_C, and $f_{\mathcal{D}}$ like the original model. And it is symmetric like the original model. The branches $f_{\mathcal{A}}$ and f_C are quadratic and both governed by a function $g_L(x) = a_L \cdot x^2 + b_L \cdot x + c_L$, while the branches $f_{\mathcal{B}}$ and $f_{\mathcal{D}}$ are linear and governed by a function $g_R(x) = b_L \cdot x + c_L$. The parameters of the function g_L are altered directly, while the parameters of the function g_R are altered indirectly via two composite parameters $g_R\left(\frac{1}{4}\right)$ and $g_R\left(\frac{1}{2}\right)$ influencing the value of the branches $f_{\mathcal{B}}$ and $f_{\mathcal{D}}$ at their borders. Two parameters are varied in the archetypal model. The first one is $\alpha = -g_R\left(\frac{1}{4}\right)$, and it has negative sign to orient the PI structure in the archetypal model like in the original model. The other parameter is $\beta = c_L$, it influences the offset of the branches $f_{\mathcal{A}}$ and $f_{\mathcal{D}}$.

Then the PI structure in the archetypal model was described. All possible bifurcations and coexistence scenarios were identified. This lead to a deeper understanding of the role of the symmetry in the archetypal model. It causes the coexistence of two asymmetric cycles in the "type B" parameter regions. Also, it causes the border collision bifurcations bounding "type A" parameter regions to always involve two borders and the border collision bifurcations bounding "type B" parameter regions to always occur in pairs.

After that, it was confirmed numerically that this archetypal model exhibits the same behavior as the original model. While doing so, the previously undiscovered coexistence of four cycles was found, and its existence in the original model was confirmed. The numerical evidence that the archetypal model exhibits the same behavior as the original model confirms that the approach of constructing an archetypal model is feasible in PWS discontinuous models where normal forms do not exist.

Second, it was demonstrated that the archetypal model proposed in this thesis can exhibit behavior leading to bifurcation structures that are related to PA structures. For this, the shape of the branches $f_{\mathcal{A}}$ and f_C was altered, making them increasing. This leads to a piecewise-increasing model, since the branches $f_{\mathcal{B}}$ and $f_{\mathcal{D}}$ are already increasing. The appearance of these structures were found to be tied to the disappearance of the local minima on the branches $f_{\mathcal{A}}$ and f_C and the disappearance of the "type B" prameter regions in the chains. It was also proven that the local minima are necessary for the "type B" parameter regions in the chains.

It was found that these structures defy the expectations for PA structures, since the periods associated with the parameter regions in those structures do not add up as they normally would in PA structures. Also, there are no obvious regularities in the symbolic sequences associated with the parameter regions in these structures. Hence, they are called PAL structures. Some parameter regions in these PAL structures are also affected by multistability similar to the "type B" parameter regions in the original and the archetypal model. Then the organizing principles of the PAL structures were explained. To this end, the halved archetypal model was introduced. It was created by taking advantage of the symmetry in the archetypal model. The same structures in the halved archetypal model exhibit the expected behavior of PA structures and no parameter regions of these structures are affected by multistability.

Algorithms for translating cycles in-between the halved archetypal model and the archetypal model were developed. With their help, rules for the periods, symbolic sequences, multistability, and rotation tuples associated with the parameter regions of the PAL structures in the archetypal model were derived.

8.2 Future Work

This section touches on topics that were not covered extensively in this thesis or may be explained with results of this thesis. It is divided into three logical parts.

First, the theory of the halved archetypal model was fully developed in the later part of this thesis. It may be possible to explain the regularities of the bifurcations at the boundaries of "type B" parameter regions as they are described in Section 6.2.5. The regularities being that at the upper boundary of a "type A" parameter region, the border collision bifurcation is $\xi_{d1,d_2}^{\overline{\mathcal{A}}^a \mathcal{B}^b \underline{C}^a \mathcal{D}^b}$ while at the upper boundary of a "type B" parameter region, there are two border collision bifurcations $\xi_{d_1}^{\overline{\mathcal{A}}^a \mathcal{B}^b C^c \mathcal{D}^d}$ and $\xi_{d_3}^{\mathcal{A}^c \mathcal{B}^d \underline{C}^a \mathcal{D}^d}$. Note that in the "type A" parameter boundary border collision bifurcation, two points of the branches $f_{\mathcal{A}}$ and f_C collide with the borders d_1 and d_3 respectively. While in the "type B" border collision bifurcations this distributes onto both border collision bifurcations. Here, the point of the branch $f_{\mathcal{A}}$ collides with the border d_1 for the cycle $O_{\mathcal{A}^a \mathcal{B}^b C^c \mathcal{D}^d}$ and the point of the branch f_C collides with d_3 for the cycle $O_{\mathcal{A}^c \mathcal{B}^d C^a \mathcal{D}^b}$. The interesting part is that this distribution inverts for the lower boundary. At the lower boundary, the point of the branch $f_{\mathcal{D}}$ collides with the border d_3 for the cycle $O_{\mathcal{A}^a \mathcal{B}^b C^c \mathcal{D}^d}$ and the point of the branch $f_{\mathcal{B}}$ collides with the border d_1 for the cycle $O_{\mathcal{A}^c \mathcal{B}^d C^a \mathcal{D}^b}$. And for the right and left boundaries of the parameter regions this distribution of border collisions onto two bifurcations in the case of "type B" parameter regions is similar.

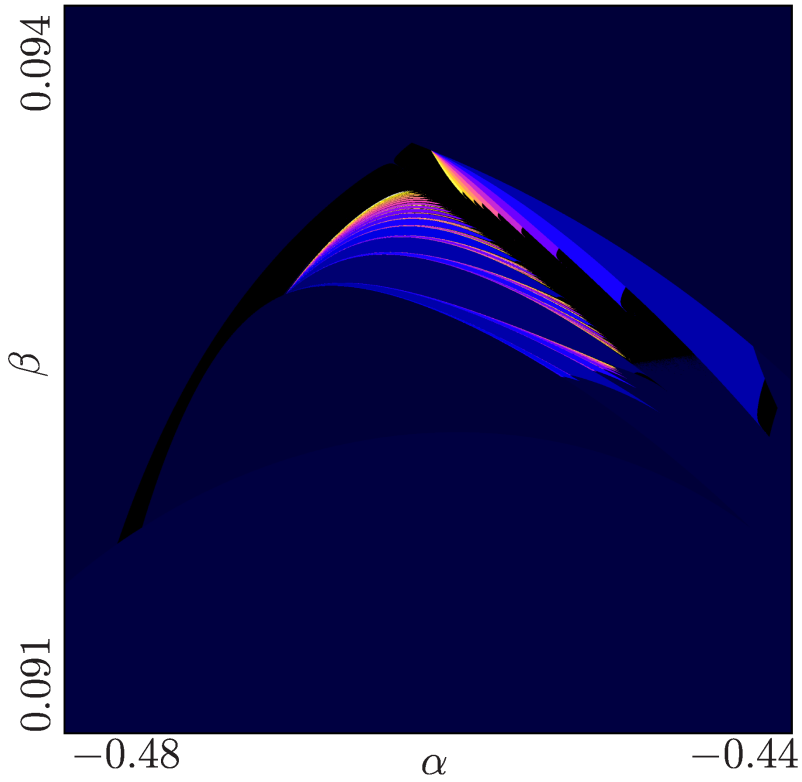

Figure 8.1: 2D scan of the periods associated with parameter regions in the archetypal model with steep branches showing an interesting bifurcation structure. The parameters $a_L = 8, b_L = -\frac{1}{2}$, and $g_R\left(\frac{1}{2}\right) = \frac{1}{2} + \frac{1}{40}$ are fixed. The parameters $\alpha = g_R\left(\frac{1}{4}\right)$ and $\beta = c_L$ are varied in the ranges $[-0.48, -0.44]$ and $[0.091, 0.094]$.

Second, Section 6.4 describes how the chains of parameter regions associated with the same period start falling apart for larger values of $\beta = c_L$. This agrees with the behavior of the original model where the chains also start falling apart for larger values of χ_0. Nonetheless, this thesis proposes ways to obtain full chains with the archetypal model or a similar model. These could be investigated in future work.

Third, there is another kind of bifurcation structure that the archetypal model can exhibit. It is possible if the parameter a_L is increased. Figure 8.1 shows this bifurcation structure. In this figure we can see PA and PI incrementing behavior close to each other. On the left side there is PA and on the right side there is PI. A similar bifurcation structure was observed in [ASB06]. It would be interesting to investigate, how this bifurcation structure is affected by the symmetry in the archetypal model. And if it is affected similarly to the PAL structures in this thesis, the algorithms developed here may be used to derive rules for this bifurcation structure as well.

Bibliography

[AGST19] V. Avrutin, L. Gardini, I. Sushko, F. Tramontana. *Continuous and discontinuous piecewise-smooth one-dimensional maps: invariant sets and bifurcation structures*. World Scientific, 2019. DOI: 10.1142/8285 (cit. on p. 18).

[Aky22] Y. Akyüz. *Investigation of Bifurcation Phenomena in a Model of Power Converter with Hysteresis*. 2022 (cit. on pp. 22, 24, 26, 55, 64, 71–73, 133).

[ALSW99] V. Avrutin, R. Lammert, M. Schanz, G. Wackenhut. *AnT*. 1999. URL: https://github.com/cloudsftp/AnT (visited on 08/26/2023) (cit. on p. 133).

[ASB06] V. Avrutin, M. Schanz, S. Banerjee. "Multi-parametric bifurcations in a piecewise-linear discontinuous map". In: *Nonlinearity* 19 (2006), pp. 1875–1906. DOI: 10.1088/0951-7715/19/8/007 (cit. on p. 121).

[BBCK08] M. Bernardo, C. Budd, A. R. Champneys, P. Kowalczyk. *Piecewise-smooth dynamical systems: theory and applications*. Vol. 163. Springer Science & Business Media, 2008 (cit. on p. 15).

[Dev89] R. L. Devaney. *An introduction to chaotic dynamical systems*. Addison-Wesley, 1989 (cit. on p. 95).

[GAK14] A. Granados, L. Alsedà, M. Krupa. "Period adding and incrementing gluing bifurcations in one-dimensional piecewise-smooth maps: theory and applications". In: (July 2014) (cit. on pp. 19, 20).

[GAK17] A. Granados, L. Alsedà, M. Krupa. "The period adding and incrementing bifurcations: from rotation theory to applications". In: *SIAM Review* 59.2 (2017), pp. 225–292 (cit. on p. 21).

[Kee80] J. P. Keener. "Chaotic Behavior in Piecewise Continuous Difference Equations". In: *Trans. Am. Math. Soc.* 261.2 (1980), pp. 589–604 (cit. on p. 20).

[Sim10] D. J. W. Simpson. "Bifurcations in Piecewise-smooth Continuous Systems". In: *World Scientific Series on Nonlinear Science*. Ed. by L. O. Chua. 2010 (cit. on p. 15).

[Sim16] D. Simpson. "Border-collision bifurcations in R^n". In: *SIAM Review* 58.2 (2016), pp. 177–226 (cit. on p. 18).

[Sim18] D. J. Simpson. "The structure of mode-locking regions of piecewise-linear continuous maps: II. Skew sawtooth maps". In: *Nonlinearity* 31.5 (2018), p. 1905 (cit. on pp. 75, 76).

[TGAS12] F. Tramontana, L. Gardini, V. Avrutin, M. Schanz. "Period adding in piecewise linear maps with two discontinuities". In: *International Journal of Bifurcation and Chaos* 22.03 (2012), p. 1250068 (cit. on p. 93).

[Wei23] F. Weik. *translating-symbolic*. 2023. URL: https://crates.io/crates/translating-symbolic (visited on 08/26/2023) (cit. on p. 143).

[ZM03] Z. T. Zhusubaliyev, E. Mosekilde. *Bifurcations and Chaos in piecewise-smooth dynamical systems*. Vol. 44. Nonlinear Science A. World Scientific, 2003 (cit. on p. 18).

A Other Constructed Models

This chapter is a collection of interesting looking 2D period scans of different constructed models that are not covered in the main part in Chapter 5. It does not cover all constructed models, but only those with interesting looking 2D period scans. Also, most of the detailed analysis, such as cobweb diagrams and symbolic sequences, is omitted in this chapter.

A.1 Piecewise-linear Model

The first model in this chapter and also the first constructed model is the piecewise-linear model. It has 4 linear branches and is defined as the map $x_{n+1} = f(x_n) \mod 1$ where the following set of equations defines f.

$$f(x) = \begin{cases} g(x) & \text{if } x < \frac{1}{2} \\ g\left(x - \frac{1}{2}\right) + \frac{1}{2} & \text{else} \end{cases} \tag{A.1}$$

$$g(x) = \begin{cases} g_L(x) = \alpha \cdot x + \beta & \text{if } x < \frac{1}{4} \\ g_R(x) = \alpha \cdot x - \frac{\alpha}{4} & \text{else} \end{cases} \tag{A.2}$$

One can see that this model definition is a little different from the model definitions in the main part of the thesis. For example, Equation (A.2) also enforces the symmetry that is found in the original model in this model explicitly. And Equation (A.2) then breaks each half of the model function into two smaller parts. One difference is that α influences the slope of all four branches and also influences the offset of the function g_R. g_R governs the branches $f_{\mathcal{B}}$ and $f_{\mathcal{D}}$ and its offset causes the branch $f_{\mathcal{B}}$ to start at 0 and the branch $f_{\mathcal{D}}$ to start at $\frac{1}{2}$.

Figure A.1a shows a 2D scan of the periods associated with parameter regions in this model. The structures look a lot like PA structures. Scanning the periods in 1D, results in Figure A.1b. This indeed shows a pattern that is typical for PA structures.

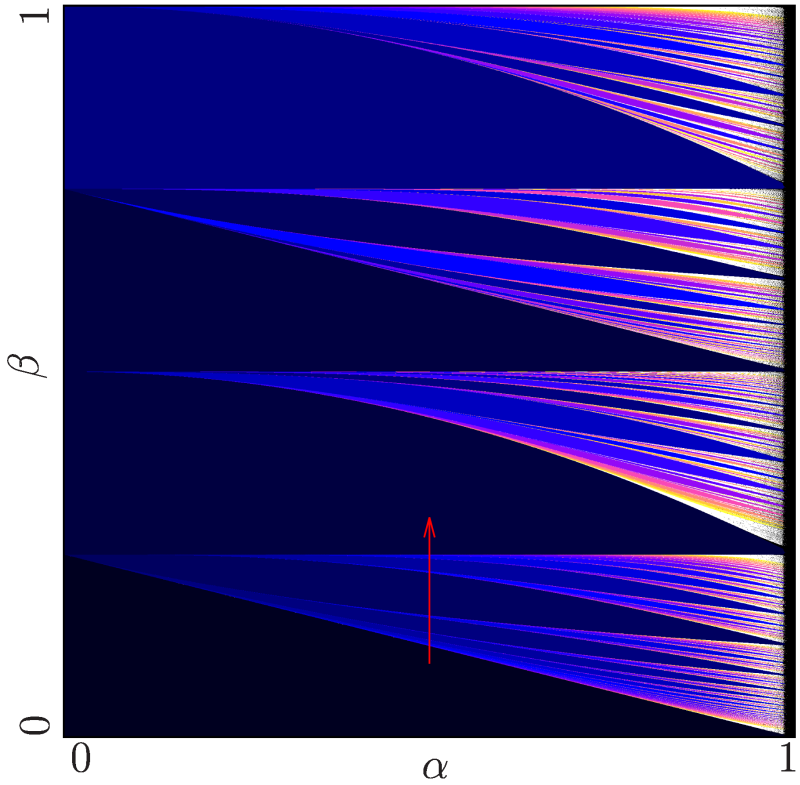

(a) 2D scan

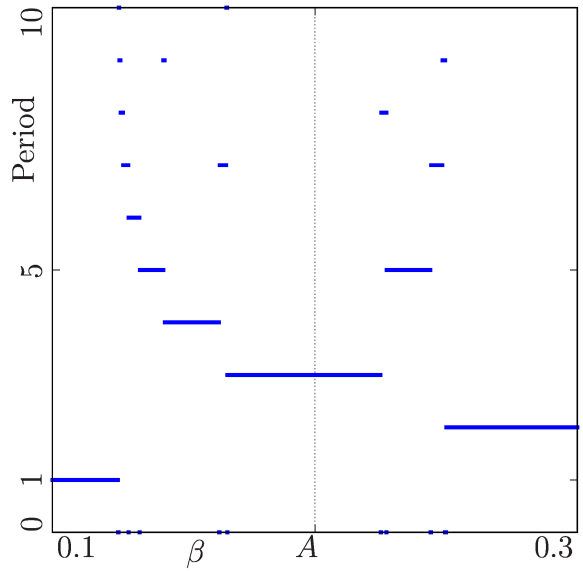

(b) 1D scan

Figure A.1: 2D and 1D scans of the periods associated with parameter regions in the piecewise-linear model The parameters α and β are different in every diagram. (a) shows the 2D scan with the parameters α and β both being varied in the range $[0, 1]$, (b) shows the 1D scan with the parameter $\alpha = \frac{1}{2}$ fixed and β varied in the range $[0.1, 0.3]$,

A.2 Piecewise-quadratic Model

The piecewise-quadratic model was covered extensively in Sections 5.2 and 5.3. This section will cover choices of the varied parameters α and β that are similar to the approach of Section 5.3. Instead of defining the composite parameters as values of the model function, the parameters multiple parameters of the parameters a_L, b_L, c_L, a_R, b_R, and c_R are chosen to be influenced by the parameter α.

Note that the definition of the piecewise-quadratic model is a little different in this section. The domain is $[0, 6]$ and the borders are at $d_0 = 0, d_1 = \frac{3}{2}, d_2 = 3$, and $d_3 = \frac{9}{2}$.

A.2.1 First Choice of Composite Parameters

The parameters $a_R = 1 + \alpha$ and $b_R = 2 \cdot \alpha$ are chosen. The parameter $\beta = c_R$ is chosen like throughout Sections 5.2 and 5.3, since it is already a very good choice for emulating the parameter χ_0 of the original model.

Figure A.2a shows a 2D scan of the periods of cycles associated with parameter regions in the piecewise-quadratic model with the parameter choices above. We can see wing-shaped parameter regions. The big parameter regions form a PI cascade, while there is something that looks like PA in-between the big wings.

Figure A.2b shows an exemplary cobweb diagram where we can see the shape of the model function. The parameter values used for this diagram are marked with the point A in Figure A.2a.

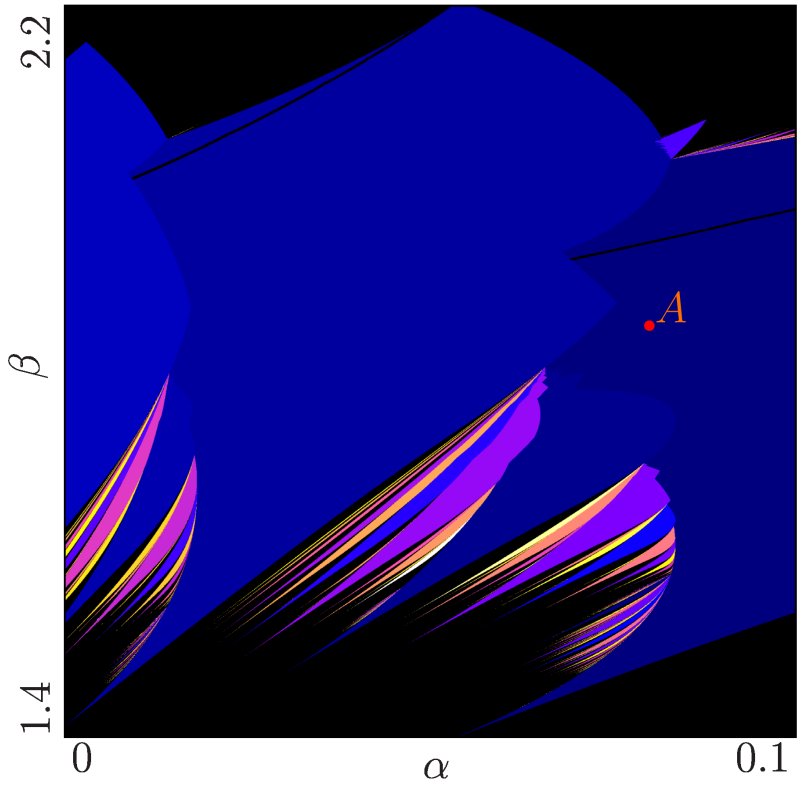

(a) 2D scan

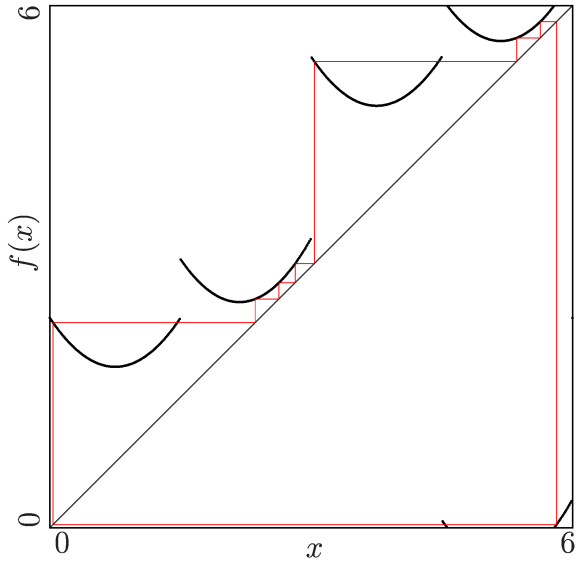

(b) Cobweb diagram

Figure A.2: 2D scan of the periods associated with parameter regions in the piecewise-quadratic model with composite parameters and an exemplary cobweb diagram. The parameters $a_L = 1, b_L = 0$, and $c_R = 2.6$ are fixed. The parameters $a_R = 1 + \alpha$ and $b_R = 2 \cdot \alpha$ depend on the varied parameter α. And the parameters α and β are different in each diagram. (a) shows the 2D scan with the parameters α and β being varied in the ranges $[0, 0.1]$ and $[1.4, 2.2]$, (b) shows the exemplary cobweb diagram of the cycle at the point A marked in (a) where $\alpha = 0.08$ and $\beta = 1.85$.

A.2.2 Second Choice of Composite Parameters

The parameters $a_R = 1 + 2 \cdot \alpha$ and $b_R = \alpha$ are chosen. This is similar to the first choice of composite parameters, but this time α influences the parameter a_R more and b_R less. The other varied parameter is still $\beta = c_L$.

Figure A.3a shows a 2D scan of the periods of cycles associated with parameter regions in the piecewise-quadratic model with the parameter choices above. Again, we can see wing-shaped parameter regions. The big parameter regions are now oriented horizontally, but they still seem to form a PI cascade. Also, there are smaller parameter regions between the bigger ones that seem to form PA structures.

Something, we did not see before that is present here are hybrid parameter regions. Figure A.3b shows a cobweb diagram at the parameter values marked with the point A in Figure A.3a. It shows the twin cycles $O_{A^4\mathcal{B}C^2\mathcal{D}}$ and $O_{A^2\mathcal{B}C^4\mathcal{D}}$ coexisting.

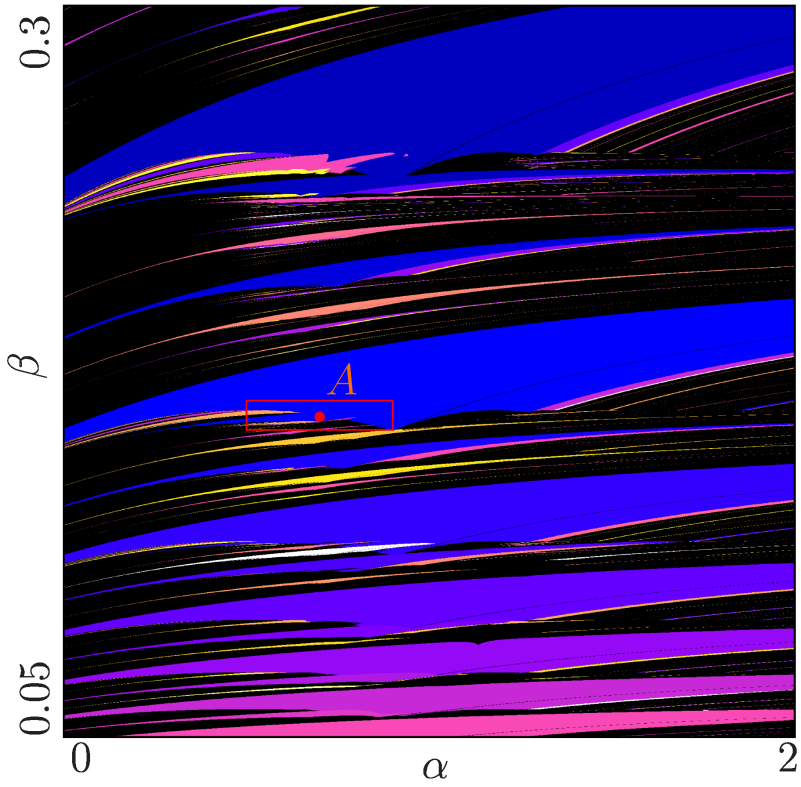

(a) 2D scan

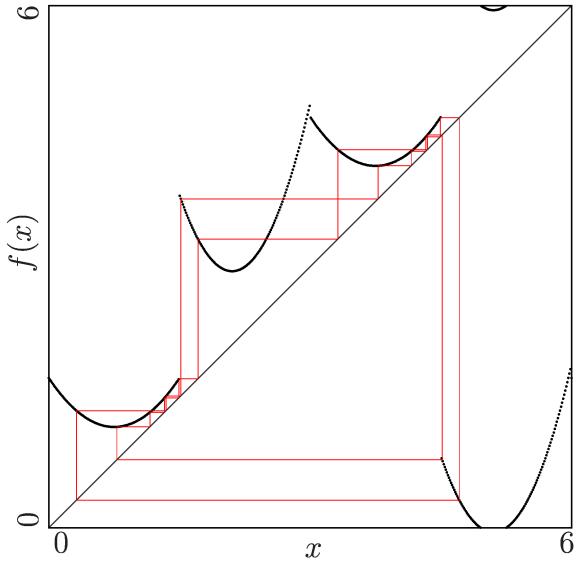

(b) Cobweb diagram

Figure A.3: 2D scan of the periods associated with parameter regions in the piecewise-quadratic model with composite parameters and an exemplary cobweb diagram. The parameters $a_L = 1, b_L = 0$, and $c_R = 2.6$ are fixed. The parameters $a_R = 1 + \alpha$ and $b_R = 2 \cdot \alpha$ depend on the varied parameter α. And the parameters α and β are different in each diagram. (a) shows the 2D scan with the parameters α and β being varied in the ranges $[0, 0.1]$ and $[1.4, 2.2]$, (b) shows the exemplary cobweb diagram of the cycle at the point A marked in (a) where $\alpha = 0.08$ and $\beta = 1.85$.

A.2.3 Mirrored Configuration Based on the Second Choice of Composite Parameters

The marked parameter range in Figure A.3a is interesting, because here two wing-shaped parameter regions overlap. The lower parameter region is a hybrid parameter region that is associated with the twin cycles $O_{A^4\mathcal{B}C^2\mathcal{D}}$ and $O_{A^2\mathcal{B}C^4\mathcal{D}}$ while the upper parameter region is associated with the cycle $O_{\mathcal{A}^4\mathcal{B}C^4\mathcal{D}}$.

Now the parameters α and β are chosen very differently. The parameters are chosen in such a way that for $\alpha = \beta = 0$, the parameter values are precisely the same as the parameter values that are marked with the point A in Figure A.4a. And for $\alpha = \beta = 1$, the parameter values are precisely the same but a_L is swapped with a_R, b_L with b_R, and c_L with c_R. The goal is to force the model to form a chain from a parameter region associated with two coexisting twin cycles $O_{A^4\mathcal{B}C^2\mathcal{D}}$ and $O_{A^2\mathcal{B}C^4\mathcal{D}}$ to a parameter regions associated with two twin cycles $O_{A\mathcal{B}^4C\mathcal{D}^2}$ and $O_{A\mathcal{B}^2C\mathcal{D}^4}$. Ideally with "type A" parameter regions and one point after the other moving from the branches $\mathcal{A}$ and C to $\mathcal{B}$ and $\mathcal{D}$.

α should only influence the parameters a_L, b_L, a_R, and b_r, while β should only influence c_L and c_R. With these constraints, we arrive at the following values for a_L, b_L, c_L, a_R, b_R, and c_R in dependence of α and β.

$$a_L = 1 + \frac{3}{2} \cdot \alpha \tag{A.3a}$$

$$b_L = \frac{3}{4} \cdot \alpha \tag{A.3b}$$

$$c_L = 1.1605 + 0.3395 \cdot \beta \tag{A.3c}$$

$$a_R = 2.5 - \frac{3}{2} \cdot \alpha \tag{A.3d}$$

$$b_R = \frac{3}{4} - \frac{3}{4} \cdot \alpha \tag{A.3e}$$

$$c_R = 3 - 0.3395 \cdot \beta \tag{A.3f}$$

Figure A.4b shows a 2D scan of the periods of the cycles associated with the parameter regions in the piecewise-quadratic model with the parameter values chosen above. We see that it is symmetric, which we would expect, since we chose the parameters α and β were chosen with that goal in mind. Unfortunately there are no chains with this choice of parameters either.

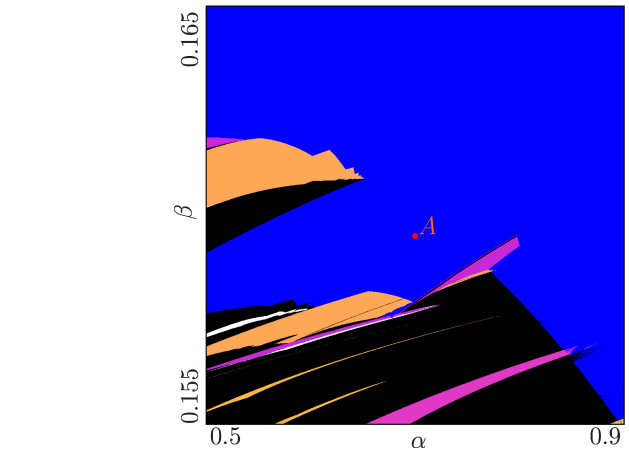

(a)

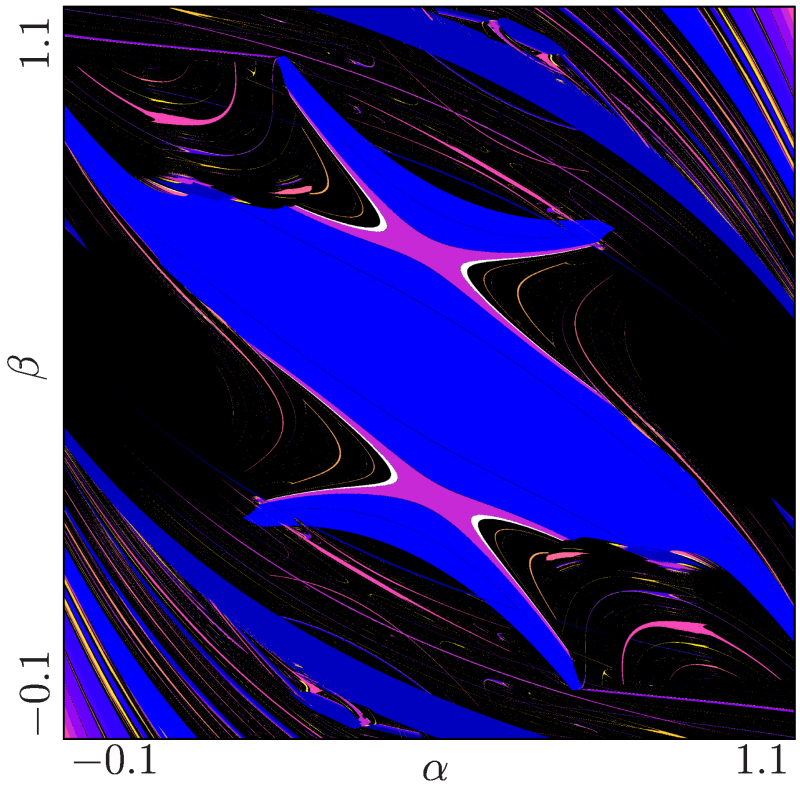

(b)

Figure A.4: 2D scan of the periods associated with parameter regions in the mirrored piecewise-quadratic model (a) show a magnified version of Figure A.3a with parameters α and β varied in the ranges $[0.5, 0.9]$ and $[0.155, 0.165]$ which is marked with a red rectangle in Figure A.3a. (b) shows the 2D scan of another model that has the same parameters as the model above at the point marked with A in (a) at $\alpha = 0$ and $\beta = 0$ but has the configuration where the parameters of g_L and g_R are swapped for $\alpha = 1$ and $\beta = 1$ as explained above.

B Implementations

This chapter contains code for the most important models of this thesis. It also contains an implementation of the naïve algorithm used to translate symbolic sequences from the halved archetypal model to the archetypal model introduced in Section 7.3.3.

B.1 Model Implementations

The models are implemented in C++. They are compiled to shared libraries to be then executed with `AnT`. The source code for `AnT` can be obtained at the GitHub repository [ALSW99].

B.1.1 Original Model

Listing B.1 shows the code used for the simulations of the original model. The majority of the code is copied from Akyüz thesis [Aky22]. But the function `invertor` is simplified drastically. This also improved the performance a little. The modified function `invertor` was copied and modified again to implement the function `symbolic` for the symbolic analysis of the original model.

```
1  #include "AnT.hpp"

3  #define mod(a,b) ((a)-(floor((a)/(b))*(b)))

5  #define E0 parameters[0]
6  #define hi parameters[1]
7  #define mu parameters[2]

9  #define R (2.0)
10 #define L 4.2E-3
11 #define Vref 5.0
12 #define bt 1

14 #define Lr1 (-R/L)
15 #define T (1.0/150)
16 #define q (R*Vref/bt/E0)
17 #define omega (2*Pi/T)
18 #define Lr (Lr1/omega)

20 #define chi (R*hi/bt/E0)

22 real_t F(real_t xk, real_t z, real_t Kp, int StepAlg, const Array<real_t>& parameters)
23 {
24   if (StepAlg == 1)
```

```
25    {
26      return q*cos(xk+z)-Kp*chi-(q*cos(xk)-Kp*mu*chi)*exp(Lr*z);
27    }
28    else if (StepAlg == 2)
29    {
30      return q*cos(xk+z)+Kp*chi-(q*cos(xk)-Kp*mu*chi)*exp(Lr*z);
31    }
32    else
33    {
34      return Kp+(q*cos(xk)-Kp*chi-Kp)*exp(Lr*z)-q*cos(xk+z)+Kp*chi*mu;
35    }
36  }

38  real_t half(real_t xk, real_t Kp, int StepAlg, const Array<real_t>& parameters)
39  {
40    real_t zk, za, zb, z, fk, fa, fb;
41    zk = 0;

43    do {
44      za = zk;
45      fa = F(xk, za, Kp, StepAlg, parameters);
46      zk += 0.02;
47      fk = F(xk, zk, Kp, StepAlg, parameters);
48    } while (fa*fk > 0);

50    zb = zk;
51    fa = F(xk, za, Kp, StepAlg, parameters);
52    fb = F(xk, zb, Kp, StepAlg, parameters);

54    do {
55      z = 0.5*(za+zb);

57      fk = F(xk, z, Kp, StepAlg, parameters);

59      if (fa*fk < 0) {
60        zb = z;
61      } else {
62        za = z;
63        fa = fk;
64      }
65    } while (fabs(za-zb)>1E-15);

67    z = 0.5*(za+zb);

69    return z;
70  }

72  bool invertor (const Array<real_t>& currentState,
73    const Array<real_t>& parameters,
74    Array<real_t>& RHS)
75  {
76    real_t xk, Kp = 1;
77    real_t et;
```

```
78    real_t tk, tk1, tk2;
79    real_t z, z_0, z_k;
80    int StepAlg;

82    xk = currentState[0];

84    if (xk < 3.0 / 2 * Pi and xk > Pi / 2) {
85      Kp = -1;
86    }

88    z_k = half(xk, Kp, 1, parameters);
89    z_0 = half(xk, Kp, 2, parameters);

91    if (Kp == 1) {
92      if (z_k < z_0) {
93        xk = xk+z_k;
94      } else {
95        Kp = -1;
96        xk = xk+z_0;
97      }
98    } else {
99      if (z_k < z_0) {
100       Kp = -1;
101       xk = xk+z_k;
102     } else {
103       Kp = +1;
104       xk = xk+z_0;
105     }
106   }

108   z_k = half(xk, Kp, 3, parameters);
109   xk = mod(xk+z_k, 2*Pi);

111   RHS[0] = xk;
112   return true;
113 }

115 bool symbolic(
116     const Array<real_t>& currentState,
117     const Array<real_t>& parameters,
118     string& RHS
119 ) {
120   real_t xk, Kp = 1;
121   real_t et;
122   real_t tk, tk1, tk2;
123   real_t z, z_0, z_k;
124   int StepAlg;

126   xk = currentState[0];

128   if (xk < 3.0 / 2 * Pi and xk > Pi / 2) {
129     Kp = -1;
130   }
```

```
132   z_k = half(xk, Kp, 1, parameters);
133   z_0 = half(xk, Kp, 2, parameters);

135   if (Kp == 1) {
136     if (z_k < z_0) {
137       RHS = "D";
138     } else {
139       RHS = "A";
140     }
141   } else {
142     if (z_k < z_0) {
143       RHS = "B";
144     } else {
145       RHS = "C";
146     }
147   }

149   return true;
150 }

152 extern "C"
153 {
154   void connectSystem ()
155   {
156     MapProxy::systemFunction = invertor;
157     MapProxy::symbolicFunction = symbolic;
158   }

160 }
```

Listing B.1: Implementation of the Original Model

Listing B.2 shows the original implementation of the function `invertor` for comparison. The `for`-loop in lines 33-38 is very inefficient and also duplicated in lines 57-62 in Listing B.2. It was pulled out of the `if`-statement and inlined into lines 88 and 89 in Listing B.1.

```
1  bool invertor (const Array<real_t>& currentState,
2    const Array<real_t>& parameters,
3    Array<real_t>& RHS)
4  {
5    real_t xk, Kp;
6    real_t et;
7    real_t tk, tk1, tk2;
8    real_t z, z_0, z_k;
9    int StepAlg;

11   xk = currentState[0];

13   static long K = 0;
14   static bool finish = false;

16   if ((xk>=0) and (xk<Pi/2))
```

```
17    {
18      Kp = 1;
19    }
20    else
21    {
22      if ((xk>=3.0/2*Pi) and (xk<=2*Pi))
23      {
24        Kp = 1;
25      }
26      else
27      {
28        Kp = -1;
29      }
30    }
31    if (Kp == 1)
32    {
33      for (StepAlg = 1; StepAlg <=2; ++StepAlg)
34      {
35        z = half(xk, Kp, StepAlg, parameters);
36        if (StepAlg == 1) z_k = z;
37        else z_0 = z;
38      }
39      if (z_k<z_0)
40      {
41        xk = mod(xk+z_k, 2*Pi);
42        StepAlg = 3;
43        z_k = half(xk, Kp, StepAlg, parameters);
44        xk = mod(xk+z_k, 2*Pi);
45      }
46      else
47      {
48        Kp = -1;
49        xk = mod(xk+z_0, 2*Pi);
50        StepAlg = 3;
51        z_k = half(xk, Kp, StepAlg, parameters);
52        xk = mod(xk+z_k, 2*Pi);
53      }
54    }
55    else
56    {
57      for (StepAlg = 1; StepAlg <=2; ++StepAlg)
58      {
59        z = half(xk, Kp, StepAlg, parameters);
60        if (StepAlg == 1) z_k = z;
61        else z_0 = z;
62      }
63      if (z_k < z_0)
64      {
65        Kp = -1;
66        xk = mod(xk+z_k, 2*Pi);
67        StepAlg = 3;
68        z_k = half(xk, Kp, StepAlg, parameters);
69        xk = mod(xk+z_k, 2*Pi);
```

```
70      }
71      else
72      {
73        Kp = +1;
74        xk = mod(xk+z_0, 2*Pi);
75        StepAlg = 3;
76        z_k = half(xk, Kp, StepAlg, parameters);
77        xk = mod(xk+z_k, 2*Pi);
78      }
79    }

81    RHS[0] = xk;
82    return true;
83  }
```

Listing B.2: Original Implementation of the Function `invertor`

And for completeness, Listing B.3 shows the python implementation of the original model. It was used to generate data for the cobweb diagrams of the original model to draw the model function.

```
1  #!/usr/bin/env python

3  from math import cos, exp, floor, pi
4  import argparse

6  R = 2.
7  L = 4.2e-3
8  Vref = 5.0
9  bt = 1

11 Lr1 = -R / L
12 T = 1. / 150

14 omega = 2 * pi / T
15 Lr = Lr1 / omega

17 def mod(a, b):
18     return a - floor(a/b) * b

20 def F(xk, z, Kp, stepAlg, E0, hi, q, chi, mu):
21     if stepAlg == 1:
22         return q*cos(xk+z)-Kp*chi-(q*cos(xk)-Kp*mu*chi)*exp(Lr*z)
23     elif stepAlg == 2:
24         return q*cos(xk+z)+Kp*chi-(q*cos(xk)-Kp*mu*chi)*exp(Lr*z)
25     elif stepAlg == 3:
26         return Kp+(q*cos(xk)-Kp*chi-Kp)*exp(Lr*z)-q*cos(xk+z)+Kp*chi*mu

28 def half(xk, Kp, stepAlg, E0, hi, q, chi, mu):
29     za = 0

31     # Find 0.02 interval where 0point is

33     fb = F(xk, za, Kp, stepAlg, E0, hi, q, chi, mu)
34     while True:
```

```
35          fa = fb
36          zb = za + 0.02
37          fb = F(xk, zb, Kp, stepAlg, E0, hi, q, chi, mu)

39          if fa * fb <= 0:
40              break

42          za = zb

44      # Find exactly, where 0point is

46      while True:
47          z = (za + zb) / 2
48          fb = F(xk, z, Kp, stepAlg, E0, hi, q, chi, mu)

50          if fa * fb < 0:
51              zb = z
52          else:
53              za = z
54              fa = fb

56          if za - zb <= 1e-15:
57              break

59      return (za + zb) / 2

61  def invert(xk, E0, hi, q, chi, mu):
62      if cos(xk) > 0:
63          Kp = 1
64      else:
65          Kp = -1

67      z_k = half(xk, Kp, 1, E0, hi, q, chi, mu)
68      z_0 = half(xk, Kp, 2, E0, hi, q, chi, mu)

70      if Kp == 1:
71          if z_k < z_0:
72              xk = mod(xk + z_k, 2 * pi)
73          else:
74              Kp = -1
75              xk = mod(xk + z_0, 2 * pi)

77      else:
78          if z_k < z_0:
79              Kp = -1
80              xk = mod(xk + z_k, 2 * pi)
81          else:
82              Kp = 1
83              xk = mod(xk + z_0, 2 * pi)

85      z_k = half(xk, Kp, 3, E0, hi, q, chi, mu)
86      xk = mod(xk + z_k, 2 * pi)
```

```
88      return xk

90  def function(x: float, E0: float, hi: float, mu: float) -> float:
91      q = R * Vref / bt / E0
92      chi = R * hi / bt / E0

94      return invert(x, E0, hi, q, chi, mu)

96  def symbolic(xk: float, E0: float, hi: float, mu: float) -> str:
97      q = R * Vref / bt / E0
98      chi = R * hi / bt / E0

100     if cos(xk) > 0:
101         Kp = 1
102     else:
103         Kp = -1

105     z_k = half(xk, Kp, 1, E0, hi, q, chi, mu)
106     z_0 = half(xk, Kp, 2, E0, hi, q, chi, mu)

108     if Kp == 1:
109         if z_k < z_0:
110             return "D"
111         else:
112             return "A"

114     else:
115         if z_k < z_0:
116             return "B"
117         else:
118             return "C"

120 if __name__ == "__main__":
121     parser = argparse.ArgumentParser()

123     parser.add_argument('--start', type=float, required=True)
124     parser.add_argument('--end', type=float, required=True)
125     parser.add_argument('--resolution', type=int, required=True)

127     parser.add_argument('--E0', type=float, required=True)
128     parser.add_argument('--hi', type=float, required=True)
129     parser.add_argument('--mu', type=float, required=True)

131     parser.add_argument('--branch', type=bool, required=False)

133     args = parser.parse_args()

135     for i in range(args.resolution):
136         x = args.start + ((args.end - args.start) / args.resolution) * i
137         y = function(x, args.E0, args.hi, args.mu)

139         if not args.branch:
140             print(f'{x} {y}')
```

```
141         else:
142             print(f'{symbolic(x, args.E0, args.hi, args.mu)}, {x}, {y}')
```

Listing B.3: Python Implementation of the Original Model

B.1.2 Archetypal Model

Listing B.4 shows the code used for the simulations of the archetypal model. As one can see, this code is a lot shorter than the implementation of the original model in Listing B.1. To simulate the halved archetypal model, one simply changes the lines 47 and 48 to use `n` instead of `2 * n`.

```
1  #include "AnT.hpp"

3  // External parameters
4  #define aL parameters[0]
5  #define bL parameters[1]
6  #define cL parameters[2]
7  #define px parameters[3] // Only the last two are varied
8  #define py parameters[4]

10 // Internal parameters for computing branches A and C
11 #define _aL (aL)
12 #define _bL (bL)
13 #define _cL (cL + py)

15 // Internal parameters for fitting branches B and D
16 #define A (-px)
17 #define B (0.525)

19 // Internal parameters for computing branches B and D
20 #define _bR (4. * (B - A))
21 #define _cR ((2. * A) - B)

23 #define n       0.5     // Discontinuity in the middle
24 #define border  0.25    // Discontinuity in the middle of the left half

26 bool f(
27     const Array<real_t>& currentState,
28     const Array<real_t>& parameters,
29     Array<real_t>& RHS
30 ) {
31     real_t y = 0;

33     real_t x = currentState[0];
34     // Enforce symmetry f(x + n) = f(x) + n
35     if (x >= n) {
36         x -= n;
37         y += n;
38     }

40     if (x < border) {   // "Left" branch (branches A and C)
41         y += _aL * x * x + _bL * x + _cL;
```

```
42      } else {            // "Right" branch (branches B and D)
43          y += _bR * x + _cR;
44      }

46      // Normalize
47      if (y >= 2 * n) {
48          y -= 2 * n;
49      }

51      RHS[0] = y;
52      return true;
53  }

55  bool symbolic(
56      const Array<real_t>& currentState,
57      const Array<real_t>& parameters,
58      string& RHS
59  ) {
60      real_t x = currentState[0];

62      if (x < n) {
63          if (x < border) {
64              RHS = "A";
65          } else {
66              RHS = "B";
67          }
68      } else {
69          if (x < n + border) {
70              RHS = "C";
71          } else {
72              RHS = "D";
73          }
74      }

76      return true;
77  }

79  extern "C" {
80      void connectSystem() {
81          MapProxy::systemFunction = f;
82          MapProxy::symbolicFunction = symbolic;
83      }
84  }
```

Listing B.4: Implementation of the Archetypal Model

And for completeness, Listing B.5 shows the gnuplot implementation of the archetypal model. It was used for the cobweb diagrams.

```
A = -px
B = 0.525

_aL = aL
_bL = bL
_cL = cL + py

_bR = 4. * (B - A)
_cR = (2. * A) - B

mod(a, b) = a - (floor(a/b) * b)

l(x) =  _aL * x * x + _bL * x + _cL
r(x) =  _bR * x + _cR
h(x) =  (x < 0.25) ? l(x) : r(x)

g(x) =  (x < 0.5) ? h(x) : h(x - 0.5) + 0.5
f(x) =  mod(g(x), 1)
```

Listing B.5: Gnuplot Implementation of the Archetypal Model

B.2 Translating Symbolic Sequences

This section covers the implementation of the naïve algorithm for translating symbolic sequences from the halved archetypal model into the archetypal model. It is implemented in the programming language Rust. The program can be obtained via `cargo` at the crate [Wei23]. Listing B.6 shows the implementation of `HalvedCycle` and `FullCycle`. Both structs use the type `Sequence` for representing the symbolic sequence in memory with different symbols each, `SYMBOLS_FULL` and `SYMBOLS_HALVED`. From line 52, the trait `RotationEquivalence` is defined and implemented for the type `Sequence`. It is used to implement equality via the `PartialEq` trait for both structs `HalvedCycle` and `FullCycle`. As far as the program is concerned, two cycles that are rotation invariant are thus equal. The implementations for displaying the cycles to the user are omitted.

```
use std::fmt::{Display, Write};

pub const SYMBOLS_FULL: [char; 4] = ['A', 'B', 'C', 'D'];
pub const SYMBOLS_HALVED: [char; 2] = ['L', 'R'];

#[derive(Debug, Eq)]
pub struct FullCycle {
    pub sequence: Sequence,
}

impl FullCycle {
    fn period(&self) -> usize {
        self.sequence.iter().map(|p| p.1).sum()
    }
```

```
16      fn rnum(&self, sym: usize) -> usize {
17          self.sequence
18              .iter()
19              .filter(|p| p.0 == sym)
20              .map(|p| p.1)
21              .sum()
22      }
23  }

25  impl PartialEq for FullCycle {
26      fn eq(&self, other: &Self) -> bool {
27          self.sequence.rotation_equals(&other.sequence)
28      }
29  }

31  impl Display for FullCycle {
32      /* ... */
33  }

35  #[derive(Debug, Eq)]
36  pub struct HalvedCycle {
37      pub sequence: Sequence,
38  }

40  impl PartialEq for HalvedCycle {
41      fn eq(&self, other: &Self) -> bool {
42          self.sequence.rotation_equals(&other.sequence)
43      }
44  }

46  impl Display for HalvedCycle {
47      /* ... */
48  }

50  pub type Sequence = Vec<(usize, usize)>;

52  trait RotationEquivalence {
53      fn rotation_equals(&self, other: &Self) -> bool;
54  }

56  impl RotationEquivalence for Sequence {
57      fn rotation_equals(&self, other: &Self) -> bool {
58          (0..self.len()).any(|rot| {
59              let mut s = self.clone();
60              s.rotate_left(rot);
61              &s == other
62          })
63      }
64  }
```

Listing B.6: Implementation of Cycles for the Naïve Translating Algorithm

Listing B.7 shows the implementation of the naïve algorithm for translating symbolic sequences. It uses the definitions of `HalvedCycle` and `FullCycle` from Listing B.7. The algorithm is implemented as the `TryFrom` trait. This implementation returns a `Vec` of `FullCycles`, since the cycle in the halved archetypal model may manifest as multiple cycles in the archetypal model. It takes the symbolic sequence from the `HalvedCycle` and duplicates it such that the original symbolic sequence is now three times in the symbolic sequence in the variable `seq`. Then it translates the symbolic sequences starting at different 2-syllables. This translation step is wrapped in the function `translate_to_full_from_index`. That function is basically the implementation of the function T defined in Section 7.3.3. Then the translated symbolic sequences are used to create `FullCycles`. Finally, the implementation filters rotation equivalent `FullCycles`. This is done with the `for`-loop that starts on line 20. The detection of rotation equivalent cycles is easy, since the program considers rotation equivalent `FullCycles` as equal.

```
1  use anyhow::{anyhow, Error};
2
3  use crate::cycles::{FullCycle, HalvedCycle, Sequence};
4
5  impl TryFrom<HalvedCycle> for Vec<FullCycle> {
6      type Error = Error;
7      fn try_from(value: HalvedCycle) -> Result<Self, Self::Error> {
8          let og_len = value.sequence.len();
9          let mut seq = value.sequence.clone();
10         seq.extend_from_within(..);
11         seq.extend_from_within(..seq.len() / 2);
12
13         let sequences: Result<Vec<Sequence>, Error> = (0..og_len)
14             .filter(|i| i % 2 == 0)
15             .map(|i| translate_to_full_from_index(&seq, i, og_len))
16             .collect();
17
18         let cycles = sequences?.into_iter().map(|s| FullCycle { sequence: s });
19         let mut unique_cycles = Vec::with_capacity(cycles.len());
20         for cycle in cycles {
21             let unique = &unique_cycles.iter().all(|u| u != &cycle);
22             if *unique {
23                 unique_cycles.push(cycle);
24             }
25         }
26
27         Ok(unique_cycles)
28     }
29 }
30
31 fn translate_to_full_from_index(
32     seq: &Sequence,
33     start: usize,
34     og_len: usize,
35 ) -> Result<Sequence, Error> {
36     let mut seq = seq[start..start + 2 * og_len].to_vec();
37
38     for i in 0..seq.len() {
39         let c = i % 4;
```

```
        if c < 2 && seq[i].0 != c {
            return Err(anyhow!("expected symbol {}, got {}", c, seq[i].0));
        }
        if c >= 2 {
            if seq[i].0 + 2 != c {
                return Err(anyhow!("expected symbol {}, got {}", c - 2, seq[i].0));
            }
            seq[i].0 = c;
        }
    }

    Ok(smallest_cycle(seq))
}

fn smallest_cycle(seq: Sequence) -> Sequence {
    let length = (1..(seq.len() / 2) + 1)
        .filter(|i| {
            if seq.len() % i != 0 {
                return false;
            }

            let chunks: Vec<&[(usize, usize)]> = seq.chunks(*i).collect();
            (1..chunks.len()).all(|j| chunks[j] == chunks[0])
        })
        .next();

    match length {
        None => seq,
        Some(length) => seq[..length].to_vec(),
    }
}
```

Listing B.7: Implementation of the Naïve Translating Algorithm

Declaration

I hereby declare that the work presented in this thesis is entirely my own and that I did not use any other sources and references than the listed ones. I have marked all direct or indirect statements from other sources contained therein as quotations. Neither this work nor significant parts of it were part of another examination procedure. I have not published this work in whole or in part before. The electronic copy is consistent with all submitted copies.

---

place, date, signature